Assessment of Fatigue in Robot-Mediated Upper Limb Interactions Using EEG

Udeshika Chaturangee Dissanayake

School of Physics, Engineering and Computer Science
University of Hertfordshire

submitted to the University of Hertfordshire in partial fulfilment of the requirements for the degree of Doctor of Philosophy

September 2021

This thesis is dedicated to my beloved parents,
brother-in-law Sajitha, sister Maheshi, and nephew Thareen
for their endless love, support and encouragement ...

Acknowledgements

First and foremost, I wish to express my sincere gratitude to my supervisors, Professor Farshid Amirabdollahian and Professor Volker Steuber, for their endless guidance and encouragement throughout my PhD journey. Their thoughtful comments and recommendations put me in the right direction and helped me in successfully completing this research work. Without their continuous support, knowledge, and patience this research might not have been possible.

My sincere thanks also go to the research degrees administrators, Mrs Lorraine Nicholls, Ms Emma Thorogood, Ms Lynette Spelman, Ms Michaella Guarnieri, Ms Kathy Head, and Ms Elizabeth Day for their friendly gestures and support from the very beginning of my PhD journey. I am also grateful to the members of the staff at the University of Hertfordshire, particularly to Dr Mariana Lilley, Dr Martina Doolan, and Dr Nathan Baddoo for their tremendous support in developing my professional skills during my PhD.

A special thanks go to my friends Vijitha Jayasundara, Preeti Kandwal, Srila Satoh, Beatriz León, Weam Binjumah, Alessandra Rossi, Piyamas Choochalerm, and Sylvia Beka for making my life in the UK a wonderful time. I would also like to thank my colleague from the Adaptive Systems Research Group, Angelo Basteris, Azeemsha Thacham Poyil, Adeline Chenasu, Shadiya Alingal-Meethal, Vignesh Velmurugan and Mohammad Abadi for sharing their knowledge with me and providing a pleasant working atmosphere during my time at the University of Hertfordshire.

I would like to thank the University of Hertfordshire for granting me the UH Research Studentship and providing the financial support during my studies. I am also thankful to all the participants who contributed their time and effort to this research work.

Finally yet importantly, I am thankful to my father, mother, brother-in-law Dr Sajitha Weerasinghe, sister Dr Maheshi Dissanayake, and nephew Thareen Weerasinghe for their endless love, support and encouragement. This journey would not have been possible without their tremendous understanding and encouragement in the past few years. Thank you for always being there for me.

Abstract

Fatigue experienced during post-stroke rehabilitation and its implications for the therapy outcome are often overlooked in existing rehabilitation programmes. Past studies have shown that intensive and repetitive robot-mediated upper limb therapies improve the neuroplasticity of stroke survivors. However, it is more likely that the increased motor/cognitive processing demands required during post-stroke motor retraining exercises may exacerbate stroke patients' fatigue levels. The elevated fatigue levels may impair motivation and compliance to effectively perform the rehabilitation tasks and the long-term commitment towards it. Hence, it is highly questionable whether continuing a stroke therapy while or beyond fatigue would impede motor performance and motor skill relearning during the session.

While robot-mediated rehabilitation has been gaining traction over the past 40 years, EEG feature modulations associated with fatigue induced by robot-mediated interactions has not yet been comprehensively explored. Personalised rehabilitation sessions that incorporate the knowledge of patient fatigue levels and the effects of fatigue on brain activity are thought to improve the intervention's efficiency. Moreover, EEG-based fatigue indices could also be used to mitigate fatigue accumulated during human-robot collaboration tasks, thereby managing the fatigue-related risks in the automotive industry. Therefore, the present research aims to investigate the modulations in spectral and nonlinear EEG features due to fatigue in a range of robot-mediated interactions involving gross motor, fine motor and visuomotor tracking tasks.

This research work analysed and evaluated EEG correlations of fatigue induced by three different robot-mediated interactions using two experimental studies. A comparison of EEG spectral feature modulations following robot-mediated gross motor and fine motor interactions was conducted in experiment 1. An in-depth analysis of spectral and nonlinear EEG feature modulations during a robot-mediated visuomotor tracking task was conducted in experiment 2. Healthy participants were considered since this is an early-stage investigation. The two experiments have shown that fatigue was induced during robot-mediated interactions and has differently changed the EEG features and cortical sites depending on the type of

interaction. Experiment 1 revealed that the robot-mediated gross motor interactions most likely change the EEG activity around the central and parietal brain regions. In contrast, this experiment found that the robot-mediated fine motor interactions most likely change the EEG activity around the frontopolar and central brain regions. Experiment 2 revealed that the robot-mediated visuomotor tracking tasks most likely change the EEG activity around the central, parietal and occipital brain regions. These observations were supported by the subjective measures of the level of fatigue. The correlation analysis performed in experiment 2 also revealed that the participants who maintained increased tracking accuracies during the robot-mediated visuomotor tracking task experienced an increase in their physical fatigue level, thereby contributing to a greater change in EEG features. Taken together, the findings presented in this thesis suggest that the modulations in EEG features and the cortical regions that are mostly affected due to fatigue induced by the robot-mediated interactions are specific to the physical and cognitive nature of the task performed. Therefore, the findings presented in this thesis confirm the hypothesis of this research *"EEG correlates of fatigue during robot-mediated interactions are specific to the physical or cognitive nature of the task and the differences in the usage of proximal or distal upper limb"*.

Table of Contents

List of Figures

List of Tables

Nomenclature

Greek Symbols

α alpha

β beta

δ delta

θ theta

Other Symbols

α_{absolute} Absolute alpha band power

β_{absolute} Absolute beta band power

δ_{absolute} Absolute delta band power

θ_{absolute} Absolute theta band power

α_{relative} Relative alpha band power

β_{relative} Relative beta band power

δ_{relative} Relative delta band power

θ_{relative} Relative theta band power

Acronyms / Abbreviations

AMI Average Mutual Information

ANOVA Analysis of Variance

API Application Programming Interface

AppEN Approximate entropy

BCI Brain-Computer Interface

BSS Blind Source Separation

CI Confidence Interval

DIP Distal Interphalangeal

df Degree of freedom

DOF Degree of Freedom

ECG Electrocardiogram

EEG Electroencephalogram

EMG Electromyogram

EOG Electrooculogram

FFT Fast Fourier transform

FIR Finite Impulse Response

fMRI Functional Magnetic Resonance Imaging

fNIRS Functional Near Infra-Red Spectroscopy

FNN False Nearest Neighbour

ICA Independent Component Analysis

IIR Infinite Impulse Response

LLyapExp Largest Lyapunov Exponent

LSD Least Significant Difference

MAD Mean Absolute values of the Distance

MCP Metacarpophalangeal

MI Motor Imagery

OpenGL Open Graphics Library

PIP Proximal Interphalangeal

QEEG Quantitative Electroencephalography

RMSD Root Mean Square Distance

SCRIPT Supervised Care and Rehabilitation Involving Personal Tele-robotics

std Standard Deviation

Chapter 1

Introduction

Fatigue experienced during post-stroke upper limb rehabilitation and its implications for the therapy outcome are often overlooked in existing post-stroke rehabilitation programmes. Many stroke survivors (about 30% to 70%) have reported persistence of fatigue as a debilitating symptom (Lerdal et al., 2009; Staub and Bogousslavsky, 2001). For instance, up to 85% of stroke patients show some degree of upper limb deficits following a stroke (Feys et al., 1998; Lawrence et al., 2001), thereby may find profoundly challenging to perform activities of daily living independently without getting help from others. Many studies have shown that intensive and repetitive robot-mediated upper-limb therapies improve neuroplasticity of stroke survivors (Bütefisch et al., 1995; Fasoli et al., 2003; Kwakkel, 2006; Lohse et al., 2014; Oujamaa et al., 2009; Veerbeek et al., 2014). However, since stroke survivors experience significant musculoskeletal and cardiorespiratory deterioration, there is a higher possibility that the intensive therapeutic interactions may accelerate the depletion of skeletal muscle energy reserves. Consequently, the force production capabilities may rapidly decrease and cause fatigue (Sterr and Furlan, 2015). Therefore, repetitive and sustained upper limb movements practised during a therapeutic session with the intention of performance improvement over time may eventually exacerbate the patient's fatigue level. The elevated fatigue levels may impair motivation and compliance to effectively perform the rehabilitation tasks and the long-term commitment towards it. Hence, it is highly questionable whether continuing a stroke therapy while or beyond fatigue levels would impede motor performance and motor skill relearning during the session and beyond. However, the evidence is still lacking in the domain of stroke rehabilitation.

During the past years, many researchers investigated the relationship of fatigue to motor performance and/or learning (Alderman, 1965; Aune et al., 2008; Branscheidt et al., 2019;

Carron, 1972, 1969; Cotten et al., 1972; Gates and Dingwell, 2008; Godwin and Schmidt, 1971; Smith et al., 2016; Thomas et al., 1975; Van Cutsem et al., 2017; Williams and Singer, 1975), but the findings were diverse and not conclusive. Most studies have reported that fatigue is detrimental to motor performance (Alderman, 1965; Branscheidt et al., 2019; Carron, 1972, 1969; Cotten et al., 1972; Godwin and Schmidt, 1971; Smith et al., 2016; Thomas et al., 1975; Van Cutsem et al., 2017; Williams and Singer, 1975). However, some findings have shown that participants preserved the task performance by altering their movement patterns with fatigue progression, thereby suggesting a potential adaptive role for fatigue (Aune et al., 2008; Gates and Dingwell, 2008). Furthermore, several investigators have found that practice under fatigued conditions impaired motor skill learning efficiency (Branscheidt et al., 2019; Carron, 1972; Godwin and Schmidt, 1971; Thomas et al., 1975; Williams and Singer, 1975), whereas the others have found that the learning was unaffected by fatigue (Alderman, 1965; Carron, 1969; Cotten et al., 1972). The relationship between exercise-induced fatigue and motor performance and learning in motor skill learning tasks has suggested showing an inverted-U or inverted-J shape behaviour (Carron, 1972; Thomas et al., 1975; Williams and Singer, 1975). Thus, the minimal exercise that would result in little or no fatigue has little or no effect upon motor performance. As the exercise intensity increases, a facilitative effect on performance and learning is visible until a certain intensity (optimal point) is reached. If the intensity is increased beyond this point, fatigue build-up will have detrimental effects on task performance. Furthermore, at the extreme levels of physical exertion, the performance would deteriorate, thereby impairing motor skill learning. The optimal exercise intensity may vary between tasks performed.

There is some, but limited evidence on fatigue's effects on motor task performance and learning following post-stroke therapies. Sterr and Furlan (2015) argued that the relationship between training intensity and motor outcomes of constraint-induced therapy in chronic hemiparetic stroke is modulated by residual motor ability (i.e. the stage of recovery) and fatigue. As shown in Figure 1.1, the authors hypothesised that the motor task performance increases with the increasing training intensity, until the optimal point is reached. When the therapy intensity is further increased, the performance is deteriorated, which presumably reflects the impact of fatigue. Thus, this optimal point could be the fatigue threshold. Moreover, the optimum training intensity is comparatively different between the stroke survivors with high-functioning hemiparesis and those with low-functioning hemiparesis. Low-functioning chronic stroke survivors, in general, show reduced performance and reach the optimum training intensity earlier than the stroke patients with high-functioning hemiparesis. Thus, when determining the optimal therapy intensity, the individual fatigue levels should be taken into consideration in addition to the residual motor ability. Furthermore,

Foong et al. (2019) also suggested that the poor performance in the nBETTER (neurostyle brain exercise therapy towards enhanced recovery) system which is an EEG-based motor imagery (MI) brain-computer interface (BCI) employing visual feedback for upper limb stroke rehabilitation, could be due to the mental fatigue progressed during the therapy. In Prasad et al. (2010)'s study where chronic hemiplegic stroke patients performed both physical practice and MI, a trend of more considerable variability in the BCI performance was observed with the rise in individual fatigue levels measured via the visual analogue scale. Fatigue was also reported to be associated with the concentration of attention after about 20-30 min of training by most stroke patients, and an increase in inter-trial or inter-session intervals was visible during MI-based BCI training due to fatigue build-up (Frolov et al., 2017). Therefore, the aforementioned findings in the literature emphasise that continuing a stroke rehabilitation program while fatigued may degrade the task performance and learning. Furthermore, the optimal therapy intensity level that each individual should practise to get performance enhancements may vary between patients, depending on their level of fatigue. Therefore, to get optimal recovery rates, it is essential to monitor fatigue progression during the therapy session and provide feedback or adapt the session while addressing individual fatigue levels. Since the advancements in technology have enabled the use of robotic interfaces to assist with physiotherapy, adapting the delivered therapy intensity and task difficulty in real-time according to the patients' fatigue level is possible when reliable physiological fatigue biomarkers are known. However, the neurophysiological biomarkers that can best describe the effects of fatigue during stroke rehabilitation are relatively unknown.

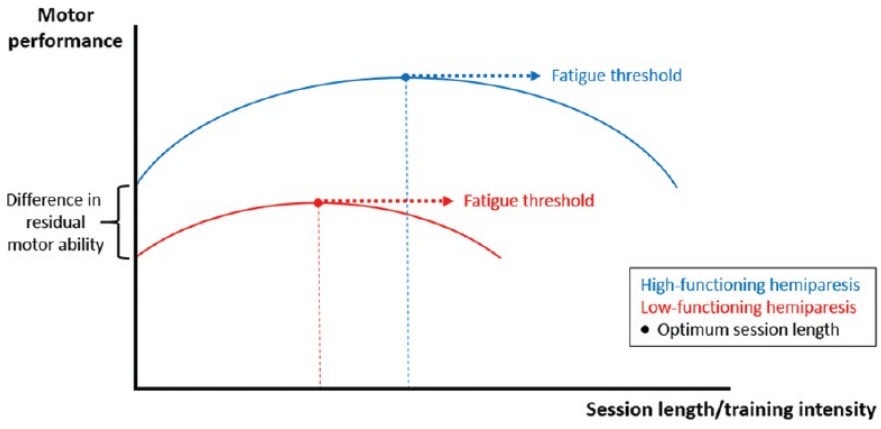

Figure 1.1: Hypothetical relationship between training intensity and outcomes in chronic hemiparetic stroke (Sterr and Furlan, 2015).

Despite its clinical importance, there exists no unambiguous and universally agreed definition for the term fatigue. In general, fatigue is defined as a sensation of tiredness, weariness or lack of energy experienced following or during prolonged physical or mental activity, and is broadly categorised as mental fatigue and physical (or muscular) fatigue. Mental fatigue is characterised by a subjective feeling of tiredness, and a lack of energy during prolonged periods of demanding cognitive activity (Lorist et al., 2005; Marcora et al., 2009). In contrast, physical fatigue is defined as a failure to maintain physical force (or power output) during prolonged voluntary, and rhythmic contractions of muscles (Gibson and Edwards, 1985). Physical fatigue also impairs coordination and increases errors and the risk of injuries (Grandjean, 1979).

Electroencephalogram (EEG) has shown to be the most predictive and promising biomarker of fatigue (Lal and Craig, 2001; Tran et al., 2020). EEG is a recording of the electrical activity originated by the brain that is obtained using electrodes placed on the surface of the human scalp. It reflects the resultant excitatory and inhibitory cortical postsynaptic potentials of the pyramidal cell membrane. The electrodes establish contact between the recording system's input terminal and the electrical source(s) that generates the electrical activities of interest (Schomer and Da Silva, 2012). To date, many studies have investigated the alterations in EEG activity associated with fatigue, including fatigue induced by driving tasks (Borghini et al., 2014; Craig et al., 2012; Eoh et al., 2005; Jap et al., 2009; Lal and Craig, 2001, 2002; Tran et al., 2008; Zhao et al., 2012), voluntary motor tasks (Wang et al., 2017; Yao et al., 2009), cognitive tasks (Tanaka et al., 2012; Trejo et al., 2015), brain-computer interfaces (Käthner et al., 2014), exercises and sports related activities (Bailey et al., 2008; Barwick et al., 2012; Baumeister et al., 2012; Xu et al., 2018), visual display terminal tasks (Cheng and Hsu, 2011; Fan et al., 2015), visual tasks in 3D displays (Chen et al., 2013; Zou et al., 2015). However, the influence of fatigue induced by robot-mediated interactions on EEG activity has not yet been comprehensively explored to the author's knowledge. The main aim of this research is to compare and contrast the modulations in spectral and nonlinear EEG features caused by fatigue accumulated during robot-mediated interactions. Also, this research aims to determine the EEG feature(s) and electrode location(s) that best describe the underlying changes in the processing capacity of sensory information and motor output, and the complexity of the brain with the progression of fatigue.

Healthy participants were considered for this study due to several reasons. Firstly, the fatigue caused by the experiments is unknown; therefore, stroke patients cannot be directly employed. There is evidence that over-exhaustion can adversely affect the rehabilitation process (Sterr and Furlan, 2015). Secondly, stroke patients may exhibit different initial fatigue levels and motor function impairments due to the nature of their brain injury. Therefore, including stroke

patients would increase the experiment's complexity and extent by introducing more control variables. Furthermore, because this study is an early-stage investigation, it is customary to employ healthy participants, and in future investigations, stroke patients can be considered with care and attention paid to their health and rehabilitation status.

1.1 Research Hypothesis

The hypothesis of this research work was that the ***"EEG correlates of fatigue during robot-mediated interactions are specific to the physical or cognitive nature of the task and the differences in the usage of proximal or distal upper limb"***. Therefore, the following two research questions were considered as the main focal points of this research work.

1.1.1 Research Question 1

Are the EEG spectral feature modulations associated with fatigue localised to different brain regions depending on the type of robotic interaction and the underlying physical and mental workload?

A. Rationale

EEG consists of a wide frequency spectrum, and the EEG spectral features are frequently used as indicators of fatigue. The systematic review conducted as part of this research (Table 2.1) found that many researchers study the modulations in EEG delta (δ), theta (θ), alpha (α), and beta (β) band power associated with fatigue. Although findings in literature are equivocal, it was evident that in the majority of studies, theta and alpha band power significantly increased with the progression of fatigue, whereas the beta band power decreased significantly (Barwick et al., 2012; Chen et al., 2013; Cheng and Hsu, 2011; Craig et al., 2012; Eoh et al., 2005; Fan et al., 2015; Jap et al., 2009; Käthner et al., 2014; Lal and Craig, 2002; Tanaka et al., 2012; Trejo et al., 2015; Wang et al., 2017; Xu et al., 2018; Zhao et al., 2012; Zou et al., 2015) . Some studies investigated the variations in delta band power as well; however, not many studies were able to identify significant variations with fatigue (Caldwell et al., 2002; Chen et al., 2013; Craig et al., 2012; Fan et al., 2015; Jap et al., 2009; Lal and Craig, 2002; Tanaka et al., 2012; Zhao et al., 2012). In these studies, the EEG band power is given either in terms of absolute band power or relative band power. Furthermore, variations in the power ratio between slow and fast wave activities were also examined since the basic band power indices can be insufficient to observe the shift of brain activity from fast waves to slow waves during the transition to fatigue (Cheng and Hsu, 2011; Eoh et al., 2005; Fan et al., 2015; Jap

et al., 2009; Tanaka et al., 2012; Xu et al., 2018; Zou et al., 2015). The most commonly used power ratios were $(\theta+\alpha)/\beta$, α/β, $(\theta+\alpha)/(\alpha+\beta)$, and θ/β and a significant increase in the ratio power indices were mostly reported (Chen et al., 2013; Eoh et al., 2005; Fan et al., 2015; Jap et al., 2009; Tanaka et al., 2012; Xu et al., 2018). Eoh et al. (2005) stated that the index $(\theta+\alpha)/\beta$ was a more reliable fatigue indicator during a simulated driving task due to the mutual addition of α and θ activity during the repetitive phase transition between wakefulness and microsleep. Jap et al. (2009) also reported a greater increase in the index $(\theta+\alpha)/\beta$, in comparison to the other power ratios, when a person experienced a fatigued state at the end of a monotonous simulated driving task. Modulations in EEG spectral features exhibited a widespread topographical distribution in the majority of the studies. Variations in methodological approaches, including differences in the fatiguing study protocol, low sample size, differences in the number of electrodes used, the electrode placement and the feature definition could explain the discrepancies present across the studies.

The literature does not comprehensively explore how the fatigue induced by robot-mediated exercises affect brain activities. The type of fatigue experienced during visuomotor exercises performed with the assistance of robotic interventions may depend on the exercise mode, intensity, and the condition of the patient. For instance, in physiotherapy, the upper limb joints and muscles involved in an exercise may differ from one therapy to another, depending on the severity in the loss of fine or gross motor skills. Gross motor skills retraining exercises such as the arm reach/return exercises are mostly involved in movement and coordination of the upper limb's proximal joints and muscles (shoulder and arm). Fine motor skills retraining exercises, on the other hand, involve coordination of the distal joints and muscles of the upper limb (hand, wrist, and fingers). Cowley and Gates (2017) found that proximal fatigue in a repetitive, timed movement task, significantly changes the movement in trunk shoulder, and elbow kinematics, whereas the changes were mainly in wrist and hand movement due to distal muscle fatigue. Therefore, in general, repetitive gross motor skill retraining exercises may induce a higher physical fatigue level than fine motor skill retraining exercises. Moreover, most therapeutic fine motor activities require considerable attention and decision-making skills combined with hand, wrist and finger movements; therefore, could induce more significant mental fatigue than most gross motor activities. As the type of prominent fatigue developed during a robot-mediated interaction may vary depending on the physical and mental workload associated with the task, the cortical sites that show significant variations in EEG spectral features following fatigue may differ between interactions. However, these differences between gross and fine motor robot-mediated interactions are not systematically investigated. The above research question was formulated to address this, and an experiment

was conducted to compare and contrast the modulations in EEG spectral features caused by the fatigue induced by robot-mediated gross motor and fine motor interactions.

B. Experiment Design in Summary

In this preliminary experiment, an arm reach/return task performed with the assistance of the HapticMASTER (Motekforce Link, The Netherland) (Amirabdollahian et al., 2007; Chemuturi et al., 2013*a*) was considered as the robot-mediated gross motor task. A hand open/close task that was performed by wearing the SCRIPT passive orthosis (Amirabdollahian et al., 2014) was considered as the robot-mediated fine motor task. EEG data were recorded from FP1, F3, FC3, C3, C4, P3, O1, and T7 electrode locations using an eight-channel EEG data acquisition system, g.MOBIlab+ (g.tec medical engineering GmbH, Austria). The EEG spectral features obtained from EEG data recorded before and after the robotic interactions were compared to evaluate how the type of robotic interaction and the underlying physical and mental workload affect fatigue progression. Given the differences in the two tasks, it could be expected that the gross motor task might induce more physical fatigue than the fine motor task, in which more mental fatigue may be visible. Therefore, it was anticipated that the resulting statistically significant differences in the EEG spectral features might show varying topographical distributions between the two robot-mediated interactions. Following the robot-mediated gross movements, significant changes to the EEG spectral features localised around the motor cortex were expected, as fatigue may affect motor coordination skills. In the fine motor robot-mediated interaction that requires more attention and decision making, significant changes to the frontopolar brain activities were expected in addition to the attenuation in the motor cortex.

C. Summary of Main Findings

- A significant increase in relative alpha band power (α_{relative}), $(\theta+\alpha)/\beta$, α/β and a significant decrease in relative delta band power ($\delta_{relative}$) following the robot-mediated gross motor interaction.
- A significant increase in α_{relative} and a significant decrease in $\delta_{relative}$ following the robot-mediated fine motor interaction.
- The gross motor task mostly changed the EEG activity around central and parietal brain regions whereas the fine motor task mostly changed the EEG activity around frontopolar and central brain regions, thereby suggesting that the effects of fatigue in robot-mediated interactions are specific to the physical or cognitive nature of the task performed using the proximal or distal upper limb.

- More physical fatigue was reported following the gross motor task performed using the HapticMASTER, whereas more mental fatigue was reported following the fine motor task performed using the SCRIPT passive orthosis.

1.1.2 Research Question 2

Which spectral and nonlinear EEG features and which EEG electrode locations are most capable and reliable in estimating the progression of fatigue during a robot-mediated visuomotor tracking task?

A. Rationale

The findings of the preliminary experiment showed that the modulations in EEG spectral features with fatigue were specific to the physical or cognitive nature of the task performed using the proximal or distal upper limb. This experiment's major drawback was the use of a limited number of electrodes since the EEG data acquisition system used in this experiment only had eight EEG channels. Therefore, the association of the regional changes in the EEG features with fatigue were not fully understood. The GENTLE/EEG robot-mediated system which included a higher number of EEG electrode locations was implemented to perform a visuomotor tracking task using HapticMASTER and to further explore the regional variations in EEG features caused by fatigue in robot-mediated interactions.

The human brain is known to be composed of more than 86 billion neurons, interacting with other neurons via synapses. The transfer characteristic of neurons is essentially deterministic and inherently nonlinear (Galka, 2000). Therefore, the EEG signals recorded from the scalp via electrodes can be in general considered as the output of a nonlinear system (Sanei and Chambers, 2013). The recent investigations also stated that the linear analysis methods such as frequency domain analysis, movement-related cortical potential, and coherence analysis could not fully describe the underlying complex dynamics of EEG. The nonlinear dynamics of the EEG are often studied to detect and predict epileptic seizures (Acharya et al., 2012; Kannathal et al., 2005; Osowski et al., 2007), to analyse sleep stages (Fell et al., 1993; Pradhan and Sadasivan, 1996; Röschke et al., 1993; Zhao et al., 2019), to measure the depth of anaesthesia (Bruhn et al., 2000; Ferenets et al., 2007; Jordan et al., 2006), to predicting the prognosis of unconscious subjects in a persistent vegetative state or minimally conscious state (Wu et al., 2011), to diagnose and get a deeper understanding of the brain functionality of Alzheimer's disease, depression, autism spectrum conditions, Parkinson's disease, dementia, and schizophrenia (Abásolo et al., 2005; Ahmadlou et al., 2010; Hosseinifard et al., 2013; Stam et al., 1994).

Some researchers have recently applied nonlinear time series analysis methods to detect fatigue, but there are only a few studies conducted to date. For example, Yao et al. (2009) found that the largest Lyapunov exponent decreased significantly with muscle fatigue induced by handgrip maximal voluntary contractions. Liu et al. (2010) reported a significant decrease in two complexity parameters: approximate entropy and Kolmogorov complexity of EEG with increasing mental fatigue levels. Driver fatigue also caused a decrease in approximate entropy (Xiong et al., 2016), sample entropy (Tran et al., 2007, 2008; Xiong et al., 2016) and correlation dimension (Wang et al., 2014), indicating the brain's reduced complexity due to fatigue. Furthermore, Kar et al. (2010) evaluated the variations in five types of entropies, i.e. Shannon's entropy, Rényi entropy of order 2 and 3, Tsallis wavelet entropy and Generalised Escort-Tsallis entropy with driver fatigue. Min et al. (2017) suggested that the multiple entropy fusion features (spectral entropy, approximate entropy, sample entropy and fuzzy entropy) can be used to characterise driver fatigue. Wang et al. (2019) also proposed a method to classify driver fatigue based on fusion entropy analysis (spectral entropy, sample entropy, and approximate entropy) combining EOG and EEG. The driver fatigue detection method implemented by Wang et al. (2020) considered the alterations in the spectral entropy, sample entropy, approximate entropy, fuzzy entropy, correlation dimension, and largest Lyapunov exponent with the fatigue progression.

The second research question further evaluates the association of modulations in EEG relative band powers, band power ratios, largest Lyapunov exponent and approximate entropy with fatigue induced by a robot-mediated visuomotor tracking task. Therefore, this investigation will identify the EEG feature(s) that can best describe the underlying changes in the processing capacity of sensory information and motor output, and the complex dynamics of the brain during the transition to fatigue. Also, the optimal number and placement of EEG electrodes will be suggested since using a larger set of EEG channels will include noisy and redundant channels that may reduce the classification accuracy and system performance (Shan et al., 2015). Moreover, the use of a minimum number of EEG electrodes may facilitate faster processing of EEG signals, thereby reducing the computational complexity (Lahiri et al., 2017). The preparation time and the cost of hardware can also be reduced. Given that the findings will be used in future to facilitate robot-mediated post-stroke therapies that adapt to individual fatigue levels, the use of a lower number of EEG electrodes may be more convenient to stroke patients.

B. Experiment Design in Summary

A robot-mediated visuomotor tracking task performed using the HapticMASTER was developed by the author to gradually build a fatigued state during the experiment. The participants were instructed to move the HapticMASTER robot arm between target points presented in the virtual reality environment, while tracking the trajectory of a guide point that moves at a constant speed. The robotic interaction lasted for 25 minutes or until volitional fatigue. Also, it consisted of five levels with gradually increasing difficulty. The damping coefficient of the HapticMASTER was increased at each level, thereby increased tracking accuracies maintained during the task may induce more fatigue on the participants. The EEG data were recorded from a 32-channel EEG data acquisition system, g.GAMMAbox (g.tec medical engineering GmbH, Austria). The EEG electrode locations: FP1, FP2, F3, Fz, F4, FC3, FCz, FC4, C5, C3, C1, Cz, C2, C4, C6, CP3, CPz, CP4, P3, P1, Pz, P2, P4, PO3, PO4, O1, Oz, O2, T7, T8, P7, and P8 were selected so that a wider brain region could be explored. This implementation will be referred to as the 'GENTLE/EEG robot-mediated system' in this thesis.

C. Summary of Main Findings

- A significant increase in α_{relative} and a significant decrease in δ_{relative}, $(\theta+\alpha)/(\alpha+\beta)$, δ/α, largest Lyapunov exponent during the robot-mediated visuomotor tracking task.
- A significant decrease in the new EEG feature, LLyapExp$/\alpha_{\text{relative}}$ proposed in this investigation.
- Significant differences were mostly localised around the central, parietal and occipital brain regions.
- A significant increase in the subjective measures of physical and mental fatigue levels, thereby confirming transition to fatigue following the robot-mediated visuomotor tracking task.
- The greater change in the substantive EEG features was mostly associated with a greater increase in the physical fatigue level, and either a decrease or a smaller increase in the mean absolute distance, thereby suggesting that the more attention, focus, and physical energy drawn to maintain increased tracking accuracies during the robot-mediated visuomotor tracking task may have gradually increased the individual fatigue levels.
- The $(\theta+\alpha)/(\alpha+\beta)$ is the most reliable EEG feature that can be used to quantify the progression of fatigue during a robot-mediated visuomotor tracking task. The α_{relative}, largest Lyapunov exponent and LLyapExp$/\alpha_{\text{relative}}$ could also be used to estimate fatigue in robot-mediated visuomotor tracking tasks.

1.2 Thesis Layout

Chapter 1: Introduction

Chapter 1, firstly, introduces the importance of measuring the level of fatigue during robot-mediated interactions, followed by the research hypothesis and research questions explored in the present work to find EEG correlates of fatigue in robot-mediated interactions.

Chapter 2: Background

Background information on EEG, previous work related to EEG-based fatigue measures, and robot-mediated stroke rehabilitation are discussed in this chapter. A detailed review of the operational mechanisms of two robotic interfaces: HapticMASTER and SCRIPT passive orthosis used in the present work is also presented.

Chapter 3: EEG data processing pipeline

The EEG data processing pipeline followed to analyse the EEG data recorded from each participant in the two experiments conducted as part of the present research work is described in this chapter. The chapter provides information on the EEG data preprocessing methods, including DC correction, filtering, and blind source separation by independent component analysis (ICA), used to remove the artifacts contaminated with the recorded EEG data. Also, a detailed description of the EEG features evaluated in this research is given. Finally, the statistical analysis methods and the general interpretations used to compare and contrast the modulations in EEG features due to fatigue in robot-mediated interactions are discussed.

Chapter 4: Experiment 1: EEG spectral feature modulations associated with fatigue in robot-mediated upper limb gross motor and fine motor interactions

The experimental protocol conducted to address the research question 1 is given in Chapter 4. The chapter also presents the modulations in spectral EEG features including relative delta, theta, alpha and beta band powers, and $(\theta+\alpha)/\beta$, α/β, $(\theta+\alpha)/(\alpha+\beta)$, and θ/β band power ratios during transition to fatigue following robot-mediated upper limb gross motor and fine motor interactions. Regional differences in EEG features that may have caused by the differences in the underlying physical and mental workload of the two tasks and the association with the subjective measures of fatigue are also further explored in this chapter.

Chapter 5: Experiment 2 - Part I: Modulations in spectral and nonlinear EEG features associated with fatigue in a visuomotor tracking task performed using the GENTLE/EEG robot-mediated system

This chapter describes the GENTLE/EEG robot-mediated system implemented by the author to gradually build a fatiguing state on the user while performing a visuomotor tracking task using HapticMASTER. The GENTLE/EEG robot-mediated system is used to address research question 2 and investigate the effects of fatigue on sensory information and motor output processing capacity and the complexity of the brain. The modulations in both spectral (relative delta, theta, alpha and beta band powers, $(\theta+\alpha)/\beta$, α/β, $(\theta+\alpha)/(\alpha+\beta)$, and θ/β band power ratios) and nonlinear (largest Lyapunov exponent and approximate entropy) EEG features during transition to fatigue following the robot-mediated visuomotor tracking task is described in this chapter. Also, a new EEG feature, LLyapExp$/\alpha_{\text{relative}}$ is proposed, and its variations due to fatigue are evaluated.

Chapter 6: Experiment 2 - Part II: Association of the modulations in EEG features with subjective measures of the level of fatigue and movement variability measures

This chapter discusses the changes in subjective measures of the level of fatigue following the robot-mediated visuomotor tracking task, and the mean absolute distance and root mean square distance between control and guide points during the task. Also, the association between the modulations in substantive EEG features with the change in subjective measures of the level of fatigue and movement variability measures are discussed. Therefore, findings in this chapter reveal the EEG features and electrode locations that are most capable and reliable in estimating fatigue progressed during a robot-mediated visuomotor tracking task.

Chapter 7: Conclusions and Future Works

In this chapter, the conclusions on assessing fatigue in robot-mediated interactions using EEG and the contributions to knowledge are discussed. The shortcomings of the present research work are outlined, and the possible applications of the findings presented in this thesis are suggested as future works.

Chapter 2

Background

In this chapter, background information on electroencephalogram (EEG) such as the physiological basis of EEG, external anatomy of the brain, standard EEG frequency bands, EEG recording techniques, electrode placement, montages and artifacts are firstly introduced. This chapter also gives a detailed literature review on EEG-based measures of fatigue including spectral and nonlinear EEG features, self-administered questionnaires, and the movement variability associated with fatigue. The chapter concludes by introducing the therapeutic strategies used for stroke rehabilitation and providing a detailed review of the operational mechanism of two robotic interfaces: HapticMASTER and SCRIPT passive orthosis used in the present work.

2.1 Electroencephalogram (EEG)

Electroencephalogram (EEG) is a non-invasive method used to record electrical activity of the brain with electrodes placed on the human scalp. EEG data recorded at each electrode channel is a linear mixture of underlying electrical signals which originated from the cortex or from other physiologic or nonphysiologic sources that overlap with cerebral activity. EEG has a high temporal resolution and is relatively low cost.

Richard Caton (1842-1926), a physician practising in Liverpool, explored electrical phenomena of the exposed cerebral hemispheres of rabbits and monkeys in 1875 using a galvanometer. The first human EEG was recorded by Hans Berger (1873–1941), a German neuropsychiatrist in 1924 (Haas, 2003). His first report published in 1929 features alpha rhythm and alpha blocking response (Schomer and Da Silva, 2012). The British scientists, Edgar Douglas Adrian and Brian Matthews has confirmed the Berger‘s observations (Adrian and Matthews,

1934). Since then, EEG is widely used in medicine, neuro-, phycho-, physiological measures and in many other brain-related research to identify human brain functionality.

2.1.1 Physiological Basis of EEG

EEG reflects the resultant excitatory and inhibitory cortical postsynaptic potentials of the pyramidal cell membrane. Neurons (nerve cells) transmit impulses from one neuron to another via a synapse. Sequence of events involved in transmission at a typical chemical synapse is shown in Figure 2.1. The presynaptic neuron is the neuron where the impulse is initiated while the postsynaptic neuron is the neuron that receives the impulse. Synapse is the junction between the pre-and postsynaptic neuron that allows a neuron to pass an electrical or chemical signal to another cell. The cell membrane separates the interior of the cell from the outside environment. The electrical potential difference between the interior of the cell and the surrounding extracellular space is known as the membrane potential of the cell. Like all other neurons, while at rest (i.e., unstimulated), cortical neurons also have a resting membrane potential of about -65 mV (typically -40 to -90 mV) (Fisch and Spehlmann, 1999). The membrane potential changes when the impulse reaches the axon terminal of the presynaptic neuron. Consequently, the voltage-gated calcium channels in the presynaptic membrane open and Ca^{2+} influxes into the presynaptic terminal. The increase in Ca^{2+} concentration, in turn, allows synaptic vesicles which contain neurotransmitters (chemical agents acting as messengers between the communicating neurons) to fuse with the cell membrane. This fusion releases neurotransmitters into the synaptic cleft (a small space adjacent to another neuron) (Purves et al., 2004).

Neurotransmitters that diffuse across the synaptic cleft then bind with the postsynaptic receptors thereby opening (or sometimes closing) the ion channels in the postsynaptic membrane. Ions flowing through these channels change the postsynaptic conductance, thus leading to ionic current flow, the postsynaptic current and a change in the membrane potential of the receiving cell, the postsynaptic potential. The postsynaptic potentials can be categorised into two types: the excitatory and inhibitory postsynaptic potentials. The positively charged sodium ion flow into the postsynaptic membrane leads to local increment in the positivity inside the cell (depolarisation), thus increasing the likelihood of a postsynaptic action potential occurring. Hence, this local reduction in the membrane potential is termed excitatory postsynaptic potential. On the other hand, when negatively charged chloride ions flow into the cell or potassium ions exit the cell, the intracellular negativity is increased (hyperpolarisation), thereby inhibiting the firing of an action potential. Hence, this transient increment in the intracellular negativity is called inhibitory postsynaptic potential (Fisch and

Spehlmann, 1999; Kirschstein and Köhling, 2009). These postsynaptic potentials induce currents that flow within and around the neuron. The summation of these excitatory and inhibitory postsynaptic potentials of the pyramidal neuron in the cortex is recorded as the EEG from the scalp (Kirschstein and Köhling, 2009).

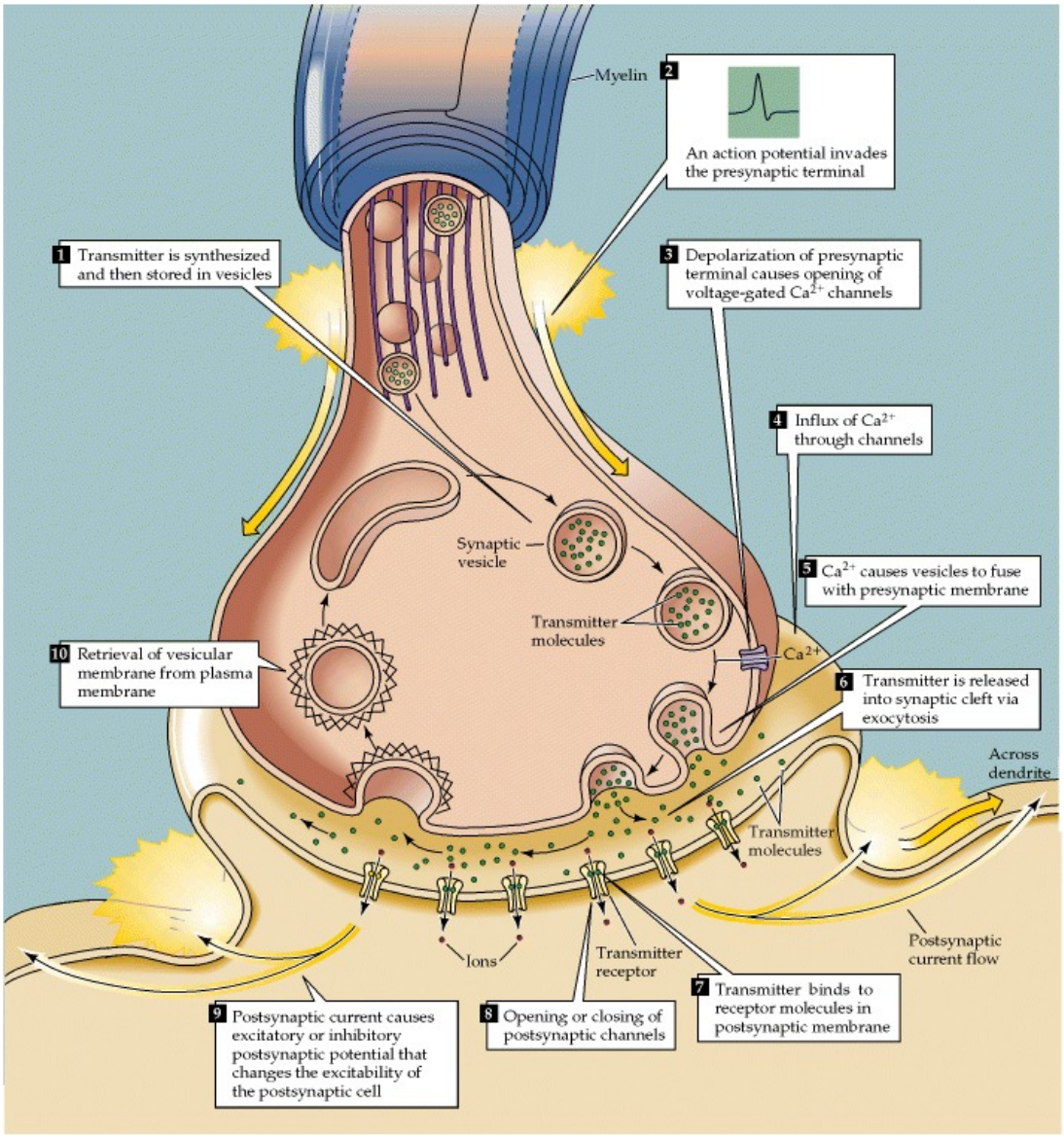

Figure 2.1: Sequence of events involved in transmission at a typical chemical synapse (Purves et al., 2004).

2.1.2 Neuroanatomical Terminology

An understanding of anatomical terminology is required to describe the organisation of any neural system. The anatomical terms used to specify the location in the central nervous system are same as the terms used to describe the anatomy of the rest of the body. Figure 2.2 gives a pictorial representation of these neuroanatomical terminology (Purves et al., 2004). The terms *anterior*, *posterior*, *superior*, and *inferior* refer to the long axis of the body, which is straight and indicate the same direction for both the forebrain and the brainstem. The terms *anterior* and *posterior* indicate front and back (head and tail); *superior* and *inferior* indicate above and below. The terms *dorsal*, *ventral*, *rostral*, and *caudal*, in contrast, refer to the long axis of the central nervous system, which has a bend in it. Therefore, the *dorsal* direction is toward the back for the brainstem and spinal cord, but toward the top of the head for the forebrain; the *ventral* is the opposite direction. The *rostral* direction, on the other hand, is toward the top of the head for the brainstem and spinal cord, but toward the face for the forebrain; the opposite direction is *caudal*.

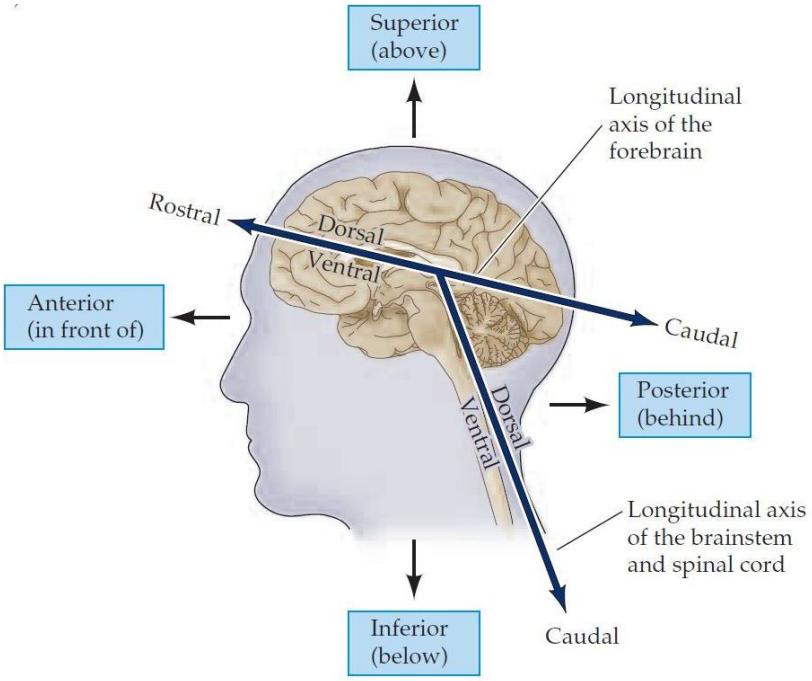

Figure 2.2: Anatomical terminology (Purves et al., 2004).

2.1.3 The External Anatomy of the Brain

The human brain is made up of the cerebrum, cerebellum, and brainstem. The cerebrum is the largest part of the brain and has a highly convoluted surface. The ridges of these convolutions

are known as gyri, and the valleys (grooves) between them are called sulci. The outermost layer of the cerebrum is known as the cerebral cortex. The cerebrum is divided into right and left hemispheres by a longitudinal fissure (a deep groove) (Jones Jr et al., 2013). The left hemisphere controls the right side of the body, while the right hemisphere controls the left side of the body. Hence, any damage or lesion to one hemisphere will affect the functionality of the contralateral side of the body. The brainstem is collectively composed of the midbrain, pons, and medulla. The cerebral hemispheres and diencephalon are collectively called the forebrain. The cerebellum is essential for coordination and planning of movements, balance, posture, learning motor tasks and storing that information (Purves et al., 2004). Each cerebral hemisphere is further subdivided into four lobes, namely the frontal lobe, the parietal lobe, the temporal lobe, and the occipital lobe (Figure 2.3), each with a multitude of functions. The names of the lobes are derived from the cranial bones that overlie them. The central sulcus divides the frontal lobe at the rostral end of the hemisphere from the more caudal parietal lobe (Purves et al., 2004). The Sylvian fissure divides the temporal lobe from the frontal and parietal lobe while the parieto-occipital fissure divides the parietal and occipital lobes (Javed and Lui, 2019).

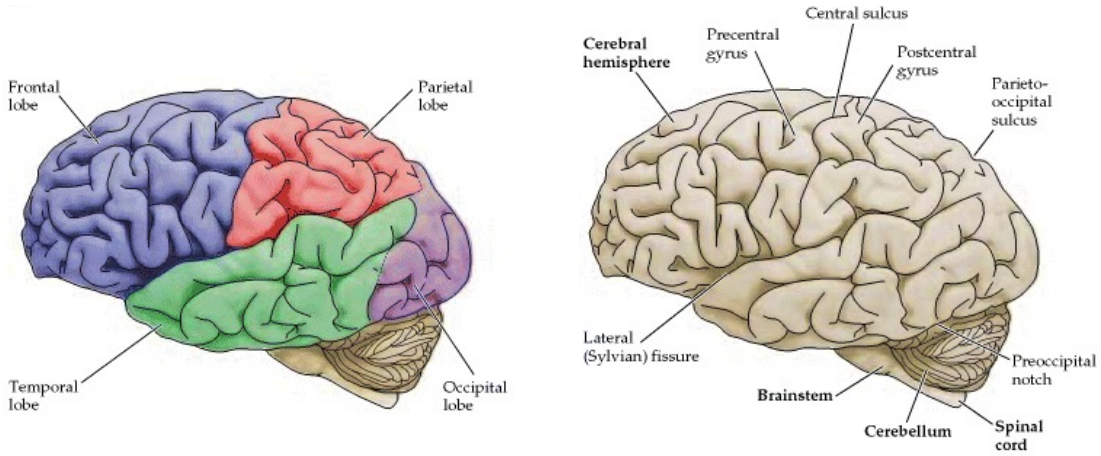

(a) The four lobes of the brain.

(b) Some of the major sulci and gyri.

Figure 2.3: Lateral view of the human brain. (a) The four lobes of the brain, and (b) some of the major sulci and gyri (Purves et al., 2004).

A. Frontal Lobe

The frontal lobe is the largest lobe of the brain and extends from the frontal pole posteriorly to the central sulcus. It controls the complex behaviours related to social functioning and individual personality, expressive speech, cognition skills, and motor functions (Watson et al., 2010).The prefrontal cortex and motor cortex resides in the frontal lobe. The prefrontal

cortex is composed of the anterior portion of the frontal lobes and plays vital roles in memory, judgment, planning, decision making, emotional responses, mood regulation, personal and social behaviour, categorisation, error detection, and empathy (Borden et al., 2015). The motor cortex is responsible for planning, initiating, and directing sequences of voluntary movements. The motor cortex can be divided into three areas, namely the premotor cortex, primary motor cortex, and supplementary motor area. The premotor cortex uses information from other cortical regions to select a specific movement or a sequence of movements from the repertoire of possible movements that are appropriate to the context of the action (Purves et al., 2004). Therefore, the premotor cortices are in general responsible for planning and selecting movements. The primary motor cortex, which is located in the precentral gyrus, on the other hand, is responsible for the voluntary control and execution of movement. The German physiologists, G. Theodor Fritsch and Eduard Hitzig, had shown that the electrical stimulation of the motor cortex in animal studies cause contractions in the muscles on the contralateral side of the body. The motor homunculus (*'little man'*) (Figure 2.4) visualises the primary motor cortex areas and proportions that are dedicated to processing motor functions of different anatomical divisions of the body. The most medial parts of the motor cortex are responsible for controlling muscles in the legs, whereas the most lateral portions are responsible for controlling muscles in the face. The supplementary motor area mediates the initiation and programming of body movements (Ramachandran, 2002). Broca's area is involved in the generation of speech (Borden et al., 2015) Damages to the frontal lobe may lead to weakness and impaired planning, control and execution of motor tasks of the contralateral side, a variety of language deficits, personality changes, deficits and disinhibition in orientation, concentration, and judgment (Javed and Lui, 2019; Ramachandran, 2002).

B. Parietal Lobe

The parietal lobe is positioned in between frontal and occipital lobes. This area is responsible for perception, sensation, and integration of sensory information such as touch, pressure, determination of texture, weight, size and shape. The primary somatic sensory (or somatosensory) cortex, which is located in the postcentral gyrus of the parietal lobe responds to stimulation of proprioceptors, cutaneous stimuli, and process both tactile and proprioceptive stimuli (Purves et al., 2004). The somatosensory homunculus shown in Figure 2.4 visualises the brain areas that are dedicated to sensory processing of different anatomical divisions of the body. A larger amount of somatic sensory cortex is dedicated to the face and hand since facial expression, manipulation, and speaking are essential to humans. The visual areas in the parietal lobe are concerned with motion and are critical for understanding the spatial relations between objects in the visual field (Purves et al., 2004). Lesions of the parietal lobe

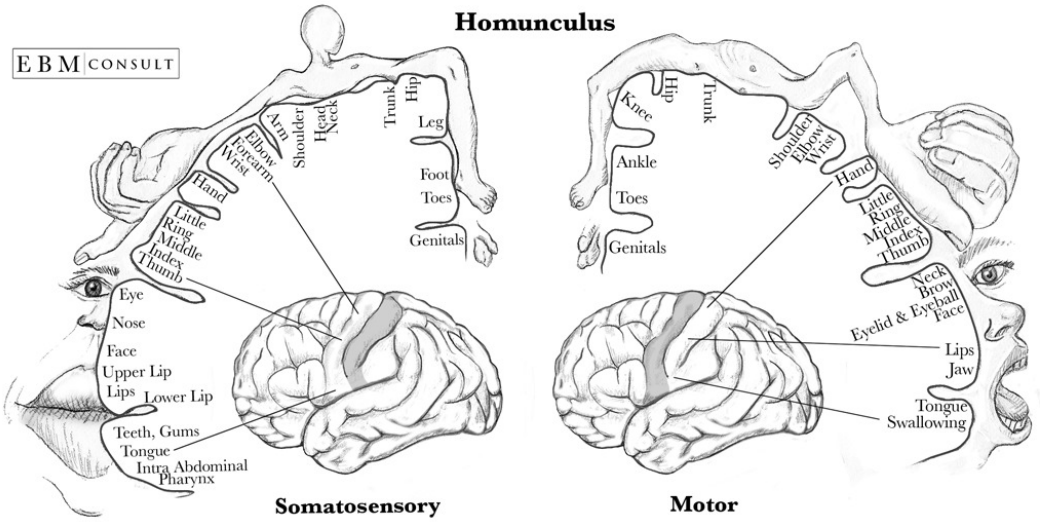

Figure 2.4: Somatosensory and motor homunculus. *"Image Provided by EBM Consult"*

result in sensory ataxia (loss of coordination), defective recognition of sensory impulses, a lack of interpretation of spatial relationships, and a loss of general awareness (Jones Jr et al., 2013).

C. Occipital Lobe

The occipital lobe, located at the posterior portion of the human cerebral cortex is primarily responsible for interpreting visual stimuli and information. The primary visual cortex resides in the occipital lobe. Hence, lesion of the occipital lobe results in either complete or partial blindness and other vision-related problems. For example, tracking an object moving from right to left will be difficult when the left parieto-occipital region is damaged (Purves et al., 2004).

D. Temporal Lobe

The temporal lobe is located under the parietal and frontal lobes just above the ear. The temporal lobe is concerned with the reception and interpretation of auditory information, language reception, understanding and recognising different categories of objects. The primary auditory cortex is located on the superior temporal gyrus in the temporal lobe. Also, the hippocampus and the amygdala that lies in the temporal lobe are involved in the acquisition of declarative memories and emotional behaviour, respectively. Visual areas in the temporal lobe are responsible for object recognition. Lesion of the temporal lobe causes

difficulty in understanding spoken language and an inability to recognise and identify faces and objects (Purves et al., 2004).

2.1.4 EEG Frequency Bands and Amplitudes

The EEG contains a wide frequency spectrum, and the predominant frequencies vary from one state (e.g., alert, wakefulness, drowsiness, sleep) to another in healthy adults and reflect various aspects of cognitive activity. In the normal adult EEG, medium (8 to 13 Hz) and fast (14 to 30 Hz) frequency ranges predominate, whereas the slow (0.3 to 7 Hz) and the very fast (above 30 Hz) ranges are sparsely represented (Schomer and Da Silva, 2012). The frequency range of the EEG is often divided into five frequency bands, namely delta (δ), theta (θ), alpha (α), beta (β), and gamma (γ). EEG amplitude, usually measured in microvolts (μV) is a measure of the change of EEG signals with respect to the mean value. It is often expressed as the difference between the maximum and minimum deviation (i.e. peak-to-peak) or in rectified EEG from baseline-to-peak (Kane et al., 2017). The amplitude of normative EEG oscillations lies between 10 and 100 μV (in adults, more commonly between 10 and 50 μV) (Schomer and Da Silva, 2012). In general, there exists a negative correlation between the frequency of brain oscillations and the amplitudes; i.e., the amplitude of the brain oscillations decreases with the increasing frequency. Thus, the slow frequency waves (e.g., δ and θ) show large synchronised amplitudes, whereas high frequencies (e.g., β and γ) show small amplitudes. The term EEG activity refers to an EEG wave or sequence of waves of cerebral origin (Kane et al., 2017).

A. Delta frequency band (0.5 - <4 Hz)

Delta frequency band lies within the frequency range 0.1 Hz to <4 Hz and has a higher amplitude value between 20 μV to 200 μV in comparison to the other frequency bands. The lower frequency limit of the delta band is set to 0.5 Hz for practical purposes. In adults, delta activity is particularly prominent during light and deep sleep stages (i.e., sleep stages 2 to 4), during anaesthesia and in neurological pathology (Schomer and Da Silva, 2012).

B. Theta frequency band (4 - <8 Hz)

Theta rhythm occurring in the frequency range from 4 to <8 Hz, has an amplitude ranging from 20 μV to 100 μV. The normal adult waking EEG recordings show a small amount of theta frequencies (Schomer and Da Silva, 2012) and a predominant rise in the theta activity is visible during the transition from waking to sleeping (Klimesch, 1999). The theta activity is linked to the reduction in the alertness, which results in impaired processing of

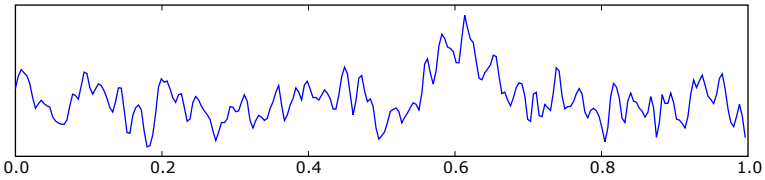

(a) Raw EEG waveform.

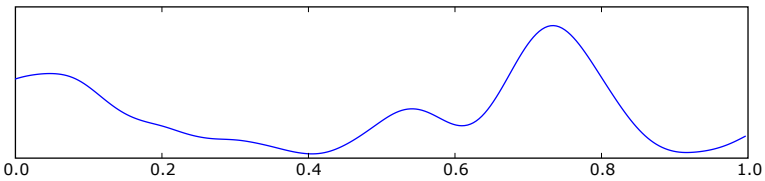

(b) Delta (δ) waveform.

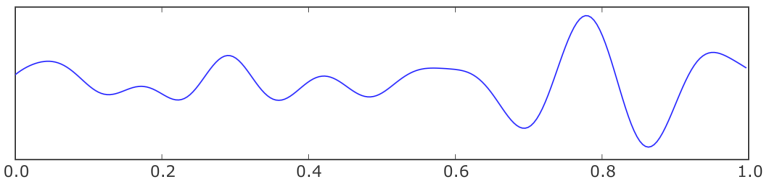

(c) Theta (θ) waveform.

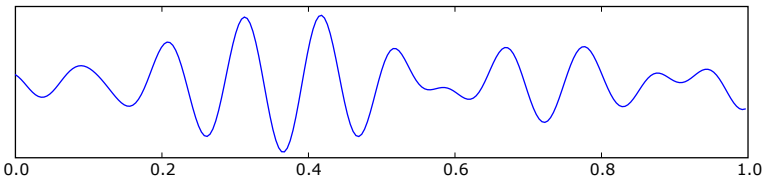

(d) Alpha (α) waveform.

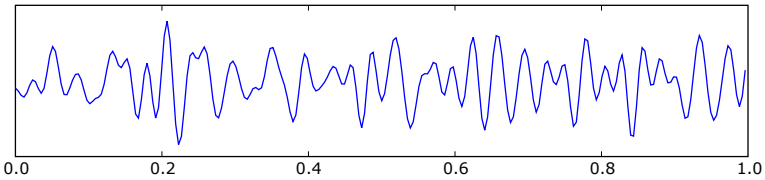

(e) Beta (β) waveform.

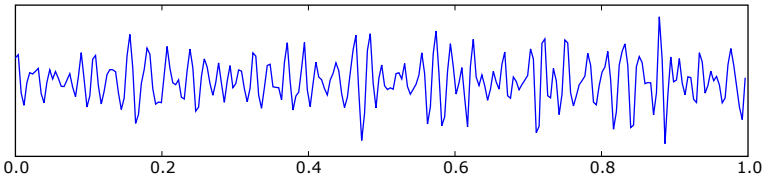

(f) Gamma (γ) waveform.

Figure 2.5: EEG frequency bands (Hz) and amplitudes (μV). (a) Raw EEG waveform recorded from Oz electrode at a sampling frequency of 256 Hz. (b) delta, (c) theta, (d) alpha, (e) beta, and (f) gamma waveforms. (created by Hugo Gambo, CC BY-SA 3.0, https://commons.wikimedia.org/wiki/User:Hgamboa)

various kinds of information (Schacter, 1977). Theta oscillations were more evident during problem solving and perceptual processing tasks with focused attention (Schacter, 1977) and showed a significant rise with the increase in the working-memory load (Jensen and Tesche, 2002). Theta oscillations have also been associated with sensorimotor processing; for example, during the onset of fast ballistic movements an increase in theta band activity in the contralateral motor area was found in Ofori et al. (2015). Furthermore, the theta band power increases during the transition from waking to sleeping (i.e., hypnagogic state) (Klimesch, 1999; Williams and Gruzelier, 2001), Theta activity has also been associated with meditation (Lagopoulos et al., 2009). Finally, a rise in the theta activity was also observed during the state of fatigue induced by graded cycle exercise (Bailey et al., 2008), and simulated driving (Craig et al., 2012; Lal and Craig, 2002).

C. Alpha frequency band (8 - 13 Hz)

Alpha rhythm spans within the frequency range 8 to 13 Hz (inclusive). Alpha rhythm over the posterior regions of the head is visible during wakefulness (Kane et al., 2017; Schomer and Da Silva, 2012). Alpha frequency varies inter- and intraindividually as a function of processing capacity. From early childhood to adulthood, the alpha frequency increases and then decreases with increasing age or age-related neurological diseases. Also, a variety of neurological disorders lowers the alpha frequency. Although most research use a fixed range (e.g. 8-13 Hz), due to interindividual differences in alpha frequency, parts of alpha power distribution may fall outside the fixed range for some individuals (Klimesch, 1997). The amplitude of the EEG alpha rhythm varies considerably from individual to individual as well as from moment to moment in a given person (Schomer and Da Silva, 2012). In adults, the alpha rhythm amplitude is mostly below 50 μV (Kane et al., 2017) and higher alpha amplitudes are mostly associated with slow alpha frequencies (Schomer and Da Silva, 2012). The phenomenon of increased alpha power is termed as alpha synchronisation, whereas the decrease in alpha power is termed as alpha desynchronisation. In terms of alpha desynchronisation, a decrease in alpha frequency indicates that the upper alpha band shows a more pronounced reduction than the lower alpha band.

Alpha frequency is a sensitive measure for cognitive and memory processing capacity and shows a positive correlation with the speed of processing information (Klimesch, 1996, 1999). Klimesch (1996, 1997) states that the upper alpha band is sensitive to semantic memory demands and the lower alpha band is sensitive to to attentional demands. For instance, the upper alpha power decreases after sustained wakefulness and during the transition from waking to sleeping (i.e., during the hypnagogic state) when the ability to respond to

external stimuli ceases (Klimesch, 1999). In contrast, an increase in the lower alpha band power is visible in old people and people with difficulties in maintaining a state of alert wakefulness (i.e., fatigued or drowsy individuals) as well as during a state of sustained wakefulness (Klimesch, 1999; Torsvall and Others, 1987). Thus, this increase in lower alpha band power may reflect the increased efforts (and probable difficulties) taken by old or drowsy individuals to maintain their attention and alertness particularly under less favourable conditions. Moreover, the increase in lower alpha band power is visible only when an individual is forced to stay awake without falling sleep; a decrease in alpha power is visible if the fatigued individual is allowed to fall asleep (Klimesch, 1999).

Alpha activity is most visible during physical relaxation and relative mental inactivity with the eyes closed and is greatly attenuated or blocked by eye opening, mental effort and attention (Schomer and Da Silva, 2012). Alpha synchronisation serves as an indicator of cortical idling as well as is associated with active internal processing and creative thinking (Benedek et al., 2011). The event-related desynchronisation of alpha band presumably reflects arousal and activated cortical areas with an increased excitability level of neurons (Neuper and Pfurtscheller, 2001). For example auditory, tactile, and other somatosensory stimuli, or increased mental activity such as solving difficult arithmetical problems, usually decreases the alpha band power, but is less pronounced than the blocking effect of eye opening (Schomer and Da Silva, 2012). Many studies have observed an inverse relationship between task difficulty and alpha power: i.e., alpha band tend to be attenuated in the high-load task relative to the low-load task. Thus, it is hypothesised that the magnitude of alpha activity during cognitive tasks are inversely proportional to the fraction of cortical neurons recruited into a transient functional network for purposes of task performance (Gevins and Smith, 2007; Mulholland, 1995)

According to the cortical areas involved with the sensory perception, three independent alpha rhythms have been reported. The occipitoparietal alpha associated with the visual system generally shows the maximum amplitude and is suppressed (reduced) with visual attention. The central alpha, also called mu rhythm, is associated with the sensorimotor areas and is reactive to sensorimotor stimuli. The mu rhythm occurs during a state of muscular relaxation and attenuates or blocks with contralateral movement, thought of movement, readiness to move or tactile stimulation (Kane et al., 2017). The temporal alpha (also known as the tau rhythm) localised in the auditory cortex desynchronises following auditory stimuli.

D. Beta frequency band (<13 - 30 Hz)

The high-frequency and low-amplitude beta waves are found in almost every healthy adult. The frequency range of the beta rhythm spans from 13 to 30 Hz. Rhythmical beta activity is mainly visible over the frontal and central regions during wakefulness, with a variable amplitude but mostly below 30 μV. (Okogbaa et al., 1994) pointed out that beta wave is associated with states of excitement or arousal, and the presence of high components of beta rhythm is associated with increased alertness. Contralateral movement or tactile stimulation attenuates or blocks the EEG beta activity (Kane et al., 2017).

E. Gamma band (>30 - 80)

The gamma frequency band spans from >30 to 80 Hz, is not often used in literature on EEG fatigue studies. Thus, this frequency band was not considered in this thesis.

2.1.5 EEG Recording Techniques

The first ink-writing biological amplifies to record brain potentials was developed by Toennies (1902–1970). Rockefeller Foundation (1932) later introduced a differential amplifier for recording EEGs. Kornmüller recognised the importance of recording EEG from multiple brain regions, thereby giving rise to more discoveries on multichannel EEG recording technologies (Sanei and Chambers, 2013; Schomer and Da Silva, 2012). The advances in technology have brought different EEG recording devices to the market, with varying technologies used for the data recording, processing and display. The non-invasive EEG acquisition systems commercially available today for research purposes mainly consists of several surface electrodes, a set of differential amplifiers (one for each EEG channel) with filters, analogue-to-digital converter, and a personal computer or other relevant data storage and processing device.

The summated electrical changes of the underlying cortex are recorded using electrodes placed on the skull (Fisch and Spehlmann, 1999). The electrodes establish contact between the input terminal of the recording system and the electrical source(s) that generates the electrical activities of interest (Schomer and Da Silva, 2012). The electrical conductive properties of the tissues in between the electrical source(s) and the recording electrode(s) (e.g., skull, scalp, brain parenchyma (the functional tissue in the brain), cerebrospinal fluid), the electrode size, electrical properties of the electrode material, skin impedance, and the orientation of the electrical generator to the recording electrode modifies the amplitude and

the morphology (shape) of the cortical signal before it reaches the recording electrodes (Fisch and Spehlmann, 1999).

EEG electrodes are mainly categorised into two types, namely 'wet' and 'dry' electrodes, depending on whether there is a liquid junction between the scalp and the electrode or metal contact. The electrodes that use a conductive gel (also known as electrode or electrolyte gel) in between the electrode and the skin to form an electrolyte bridge are termed wet electrodes. Wet electrodes are the most frequently used and are also considered as the gold standard (Lopez-Gordo et al., 2014). Most of the wet electrodes also require rubbing the skin below the electrode contact with an abrasive paste before applying the electrode gel so that the skin-electrode interface impedance is lowered (Lin et al., 2011), typically to a value less than 5 kΩ (g.tec medical engineering GmbH, 2014*a*). Hence, the setting up for an EEG recording using wet electrodes is a time consuming and laborious process. The electrode gel should be applied with great care, especially if the electrodes in the close proximity are used for the studies, as the excess gel could cause electrical bridges between electrodes, thus affecting the quality of the recording. The conductive gel dries when the recording last for several hours, thus deteriorating the impedance value (Lopez-Gordo et al., 2014) and reducing the signal quality (Lin et al., 2011). Moreover, the skin preparation and the application of the electrode gel cause an uncomfortable situation to the subject under test and may leave its residue on the scalp, thus reducing the interest and preventing most people from taking part in EEG related studies. These aforementioned difficulties can be overcome with the use of dry electrodes that create direct contact with the skin without any electrolyte bridge in between. However, the dry electrodes result in higher skin-electrode impedance than the wet electrodes; thus, the recordings are susceptible to distortions due to electrodes and cable movement artifacts (Guger et al., 2011; Pinegger et al., 2016). Hence, the accuracy and the reliability of EEG signals acquired from dry electrodes are yet questionable and more studies are needed before using them as an alternative to the standard wet electrodes (Guger et al., 2011; Lopez-Gordo et al., 2014; Pinegger et al., 2016). Therefore, gel-based electrodes were used in this research.

The EEG signal of interest is susceptible for distortions as the electrode cable that transmit the signal to the amplification unit of the recording system pick up an ambient electrical activity such as 50/60 Hz line noise, electrical noise created by nearby electrical equipments, artifacts caused by electrode or cable movement. These distortions can be avoided or reduced by amplifying the signal directly at the electrode before the signal enters the electrode lead. This method is named as active amplification (Laszlo et al., 2014), and the electrodes that have inbuilt circuitry to provide active amplification are termed active electrodes. Moreover, the use of active electrodes eliminates the need for skin preparation using abrasive gel, as

they provide a cleaner signal than that is acquired via passive electrodes (electrodes that have no inbuilt pre-amplification circuitry) at higher skin-electrode interface impedance (Laszlo et al., 2014). Ag/AgCl active electrodes (g.LADYbird active and g.GAMMAearclip) are used in the EEG data recordings related to this research, except for the ground electrode.

The differential amplifiers of the recording system (one per each EEG channel) amplifies the potential difference between an active electrode and a referential electrode in referential or monopolar recordings or the potential difference between two active electrodes in bipolar recordings. Analogue anti-aliasing, high-pass and notch filtering are applied to the amplified signal, before digitisation. The anti-aliasing filter is a low pass filter (pass low frequency while attenuating high frequency signals) that is designed to pass frequencies below the Nyquist frequency and to attenuate the frequencies above it. A high-pass filter can be used to attenuate the DC offset and low-frequency noise components. A notch filter can be used to eliminate 50/60 Hz power line noise. The analogue-to-digital converter converts the analogue EEG signal into a digital format. The acquisition system is connected to a personal computer or other relevant data storage and processing device to record, store, process and display the signals. Most commercial EEG data acquisition systems enable users to customise the filter parameters and sampling frequencies according to the task at hand. Two EEG data acquisition systems developed by Guger Technologies OG (g.tec), Austria was used to record EEG data in the present research work.

2.1.6 Electrode Placement

With the increased investigations on simultaneous EEG recordings from multiple brain locations, an urge to standardise the placement of electrodes on the head to facilitate comparison of different patient recordings taken in different laboratories over different time durations. Hence, the International Federation of Societies for Electroencephalography and Clinical Neurophysiology recommended a standard electrode placement method to be used in all laboratory settings (Jasper, 1958). This recommendation is currently known as the International 10-20 system (Figure 2.6). In this system, 21 electrodes are positioned based on measurements from standard landmarks on the skull, namely nasion, inion, and left and right preauricular points. Nasion is the depressed area at the top of the nose. Inion is the bony lump at the lowest point of the skull on the midline, at the back of the head (g.tec medical engineering GmbH, 2014*a*; Malmivuo and Plonsey, 1995). The preauricular points are felt as depressions at the root of the zygoma (a bone of the human skull commonly referred to as the cheekbone), just anterior to the tragus (a small pointed eminence of the external ear) (Klem et al., 1999). The name *'10-20'* is given as the distances between adjacent

electrodes are either 10% or 20% of the total measurement from nasion to inion or from left preauricular point to the right preauricular point as illustrated in Figures 2.6a and 2.6b. This system is applicable for different head sizes and shapes as the electrodes are places in proportional measurements.

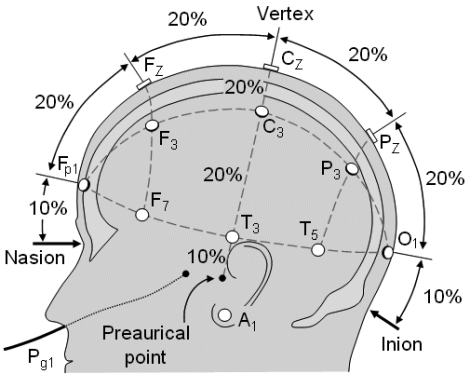

(a) Lateral view of the skull illustrating the measurements from nasion to inion at the mid-line.

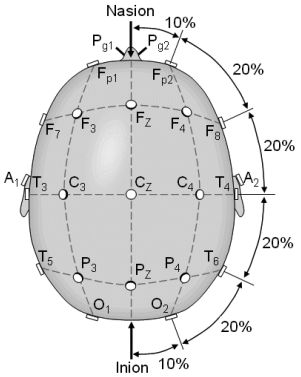

(b) Superior view with cross section of skull through the temporal line of electrodes.

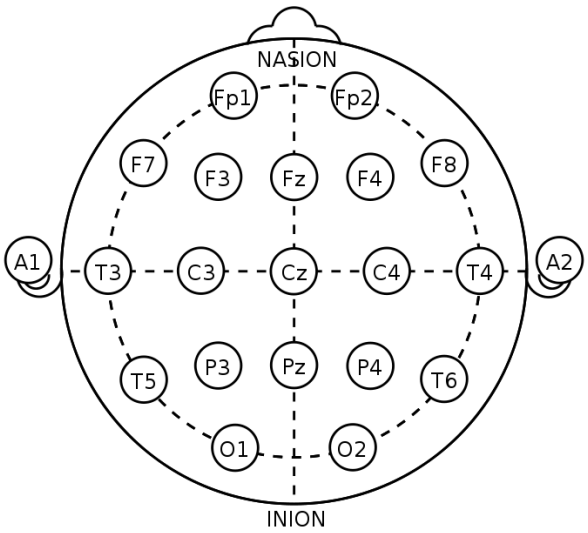

(c) A single plane projection of the head showing all 21 electrode positions.

Figure 2.6: The International 10-20 EEG electrode positioning system for the placement of 21 electrodes. Fp = frontal polar, F = frontal, C = central, P = parietal, O = occipital, T = temporal, and A = ear lobe (Malmivuo and Plonsey, 1995).

The electrode position designations are named in anatomical terms of the underlying brain areas except for the central region electrodes. Central region partly belongs to the frontal lobe

and partly to the parietal lobe as it represents the cortex in the vicinity of the central sulcus, both pre and post-central and is sometimes known as the sensory-motor area (Jasper, 1958). Therefore, the expressions FP (or Fp), F, C, P, O and T represent the frontopolar, frontal, central, parietal, occipital and temporal areas, respectively. In order to differentiate between homologous positions over the right and left hemispheres, even number (2, 4, 6, 8) subscripts are used for the right hemisphere electrode locations, and odd number (1, 3, 5, 7) subscripts are used for the left hemisphere locations. The numbers increase with distance from the midline. Also, the electrodes at the midline are designated with a subscript of letter 'z' (z for zero). The electrodes placed at the left and right earlobes are called A1 and A2, respectively. The complete International 10-20 system of electrode placements with designations is shown in Figure 2.6c.

The International 10-10 system of electrode placement (Epstein, 2006) illustrated in Figure 2.7 is an extension of the International 10-20 system, with additional electrode positions designated over the four 10% intermediate coronal lines lying between the five standard coronal lines of the 10-20 system, thereby giving rise to 81 electrode positions altogether. The electrode positions in the intermediate coronal lines are named by the expressions FT, FC, TP, CP, PO, AF representing frontotemporal, frontocentral, temporal-posterior temporal, centroparietal, posterior temporo-occipital/parieto-occipital, and anterior frontal positions, respectively. In addition, the modified combinatorial terminology replaces the T3/T4 and T5/T6 designations with T7/T8 and P7/P8 terms so that except for FP1/FP2 and O1/O2 positions, all electrode positions along the same coronal line have the same letter(s) and all electrode positions along the same sagittal line have the same postscript number. However, the electrode locations designated with the letter 'P' and a numeral value of 7 or greater represent posterior temporal, whereas the letter P with numeral values of 6 or less represent the parietal region.

2.1.7 Electrode Montage

The term *electrode montage* refers to the logical and orderly arrangements of electrode pairs over the scalp (Society and Others, 2006). In referential montage or monopolar montage, the EEG signal of each channel is represented as the voltage difference between an active electrode and a designated reference electrodes. The vertex (Cz), ipsilateral or contralateral ear lobe, linked-ear, and linked mastoid can be used as the reference electrode position for referential montage (Sanei and Chambers, 2013). In the bipolar montage, each channel represent the voltage difference between the two active electrodes is recorded. A common reference which is calculated by summing and averaging the voltage of the channel-wise

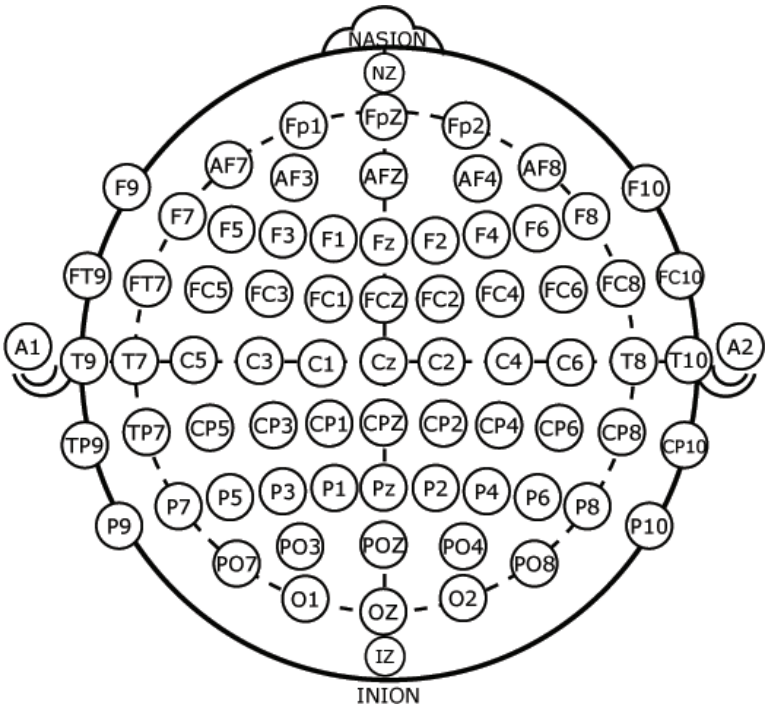

Figure 2.7: The International 10-10 EEG electrode positioning system for the placement of 81 electrodes. Fp = frontal polar, F = frontal, C = central, P = parietal, O = occipital, T = temporal, FT = frontotemporal, FC = frontocentral, TP = temporal-posterior temporal, CP = centroparietal, PO = posterior temporo-occipital/parieto-occipital, AF = anterior frontal, and A = ear lobe.

EEG data is used in the average reference montage. Each channel in the Laplacian montage on the other hand represents the voltage difference between an electrode and a weighted average of the surrounding electrodes. In this research, EEG was recorded in reference to the right earlobe (A2).

2.1.8 EEG Artifacts

EEG recordings are highly susceptible to extracerebral interferences or 'artifacts'. EEG artifacts can obscure the EEG signal of interest and may lead to misinterpretation of the EEG. These artifacts can be of physiologic and nonphysiologic origins (Schomer and Da Silva, 2012). The physiologic artifacts are generated by the biological activities of participant's eyes, heart, muscles of the head and face, respiration and movement, which are typically not of interest. The nonphysiologic artifacts, on the other hand, are generated by the EEG recording system due to the electrode and lead movement or from the environment. The physiologic artifacts, in general, show characteristic waveform morphologies and electric

fields. Therefore, the artifactual components can be identified easily by observing the EEG data recording manually. The nonphysiologic artifacts, on the other hand, show a wide variety of morphologies.

A. Ocular Artifacts

Ocular artifacts, including eye blinks and movement, is visible in every awake and conscious individual during EEG recording sessions. These artifacts distort the low-frequency EEG activity with maximal frequencies below 4 Hz and are easy to recognize. The eye blinks generate abrupt amplitude changes (250 - 490 μV) in frontal electrodes with maximal deflections at frontopolar electrodes (FP1 and FP2) relative to more posteriorly placed electrodes (Iwasaki et al., 2005). Eye blinks occur with an approximate frequency of 20 blinks per minute with a 50 - 500 ms duration in between (Halder et al., 2007). The horizontal and verticle eye movements, also known as saccades, are visible in frontal electrodes (F7 and F8) (Schomer and Da Silva, 2012). The eye movements can be slow or quite rapid and show a characteristic deflection that includes a rapid rise and more gradual fall with the corrective movement (Schomer and Da Silva, 2012). The strength of the interference depends on the proximity of the electrodes to the eyes and the direction of the eye movement (Urigüen and Garcia-Zapirain, 2015). Figure 2.8 shows the waveform morphologies of the eye blink and eye movement artifacts. Ocular artifacts can be minimized by instructing the subject to avoid unnecessary eye blinks and movements.

B. Muscle Artifacts

Muscle or myogenic artifact is a high-frequency activity often visible in EEG data taken from awake participants. Muscle artifacts have a wider spectral distribution (from 0 to $>$200 Hz (Goncharova et al., 2003)), thereby obscuring the EEG signal frequencies of critical importance. The frontalis and temporalis muscles are major contributors to muscle artifacts. Frontalis muscles become active with forced eye closure and photic stimulation, and the frontalis muscle activity peaks around 20 - 30 Hz (Muthukumaraswamy, 2013). Temporalis muscles, on the other hand, involved with jaw clenching, chewing, or bruxism are also major contributors for artifacts (Schomer and Da Silva, 2012). The temporalis activity has a board plateau around 40 - 80 Hz with an amplitude of $\sim$100 μV (Muthukumaraswamy, 2013) visible over temporal region electrodes. Figure 2.9 shows the waveform morphologies of the jaw clenching artifact visible in the EEG data recorded in experiment 2. In order to reduce this artifact during an EEG recording session, participants can be asked to open the mouth so that the jaws are relaxed.

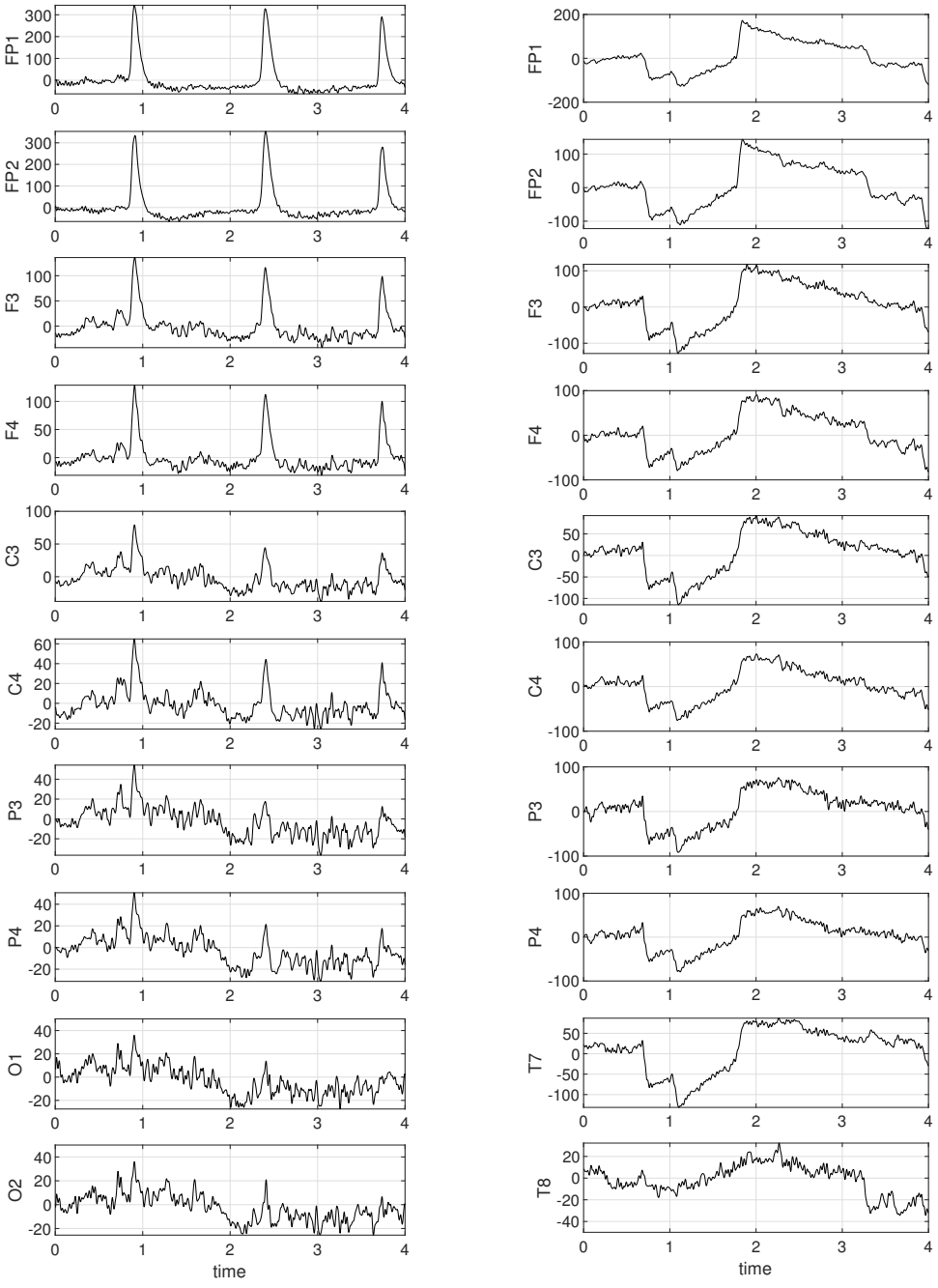

(a) Eye blink artifact

(b) Eye movement artifact

Figure 2.8: Ocular artifacts visible in the EEG data recorded in experiment 2. (a) eye blink artifact. (b) eye movement artifact. EEG data was sampled at 256 Hz and was referenced to the right earlobe (A1).

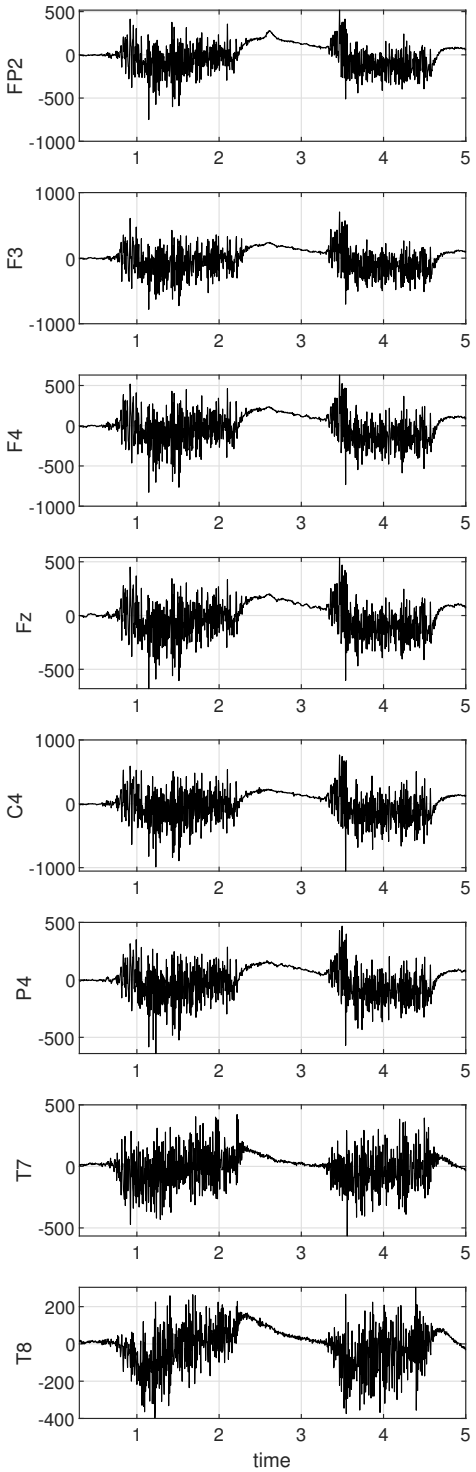

Figure 2.9: Jaw clenching artifact visible in the EEG data recorded in experiment 2. EEG data was sampled at 256 Hz and was referenced to the right earlobe (A1).

C. Cardiac Artifacts

The cardiac artifact or electrocardiogram (ECG) artifact is also visible in EEG recordings depending on the size of the participant and the montage used. It is often visible when using a referential montage, especially on EEG data recorded with ipsilateral ear reference due to the greater inter-electrode distances. It can be reduced by using linked ears montage or with a common average reference montage. EEG data recorded from overweight patients with short, stocky necks may also be contaminated with cardiac artifacts since the dipole is situated closer to the recording electrodes and better able to transmit the current, and this may be reduced by altering the head position (Schomer and Da Silva, 2012). ECG interference will be visible as a periodic slow-wave with a regular interval that follows a small spike with a 1 Hz frequency. Furthermore, if an EEG electrode is positioned over an artery, pulse artifact will appear approximately 200 ms after the QRS complex. This artifact can be eliminated by moving the electrode away from the artery (Schomer and Da Silva, 2012). Figure 2.10 shows the waveform morphologies of the cardiac (ECG) and pulse artifacts.

D. Perspiration Artifacts

Perspiration artifact is caused by the changes in the DC electrode potential from scalp perspiration. It appears as a very low frequency ($<$0.5 Hz) and low-amplitude waveform. Perspiration artifact is mostly visible in multiple adjacent channels or over the entire scalp and can be reduced by drying the skull and reapplying the gel or by increasing the high pass filter cut-off frequency (Schomer and Da Silva, 2012).

E. Participant Movements

The movements of the participant during the EEG recording session causes electrode or lead movement, thus result in a physiologic artifact. This artifact can be identified using synchronous video recordings taken during the EEG recording session.

F. Nonphysiologic Artifacts

Electrode and input lead artifacts, electric interference from mains power supplies (50/60 Hz), malfunction of some parts of the EEG data acquisition system, electrostatic and electromagnetic artifacts are the most common nonphysiologic artifacts visible in EEG recordings. Poor electrode contact, loose electrode or a movement in an electrode, drying of the electrode gel, broken lead wires, poor connection of the electrode to the electrode wire or faulty connection may result in an unusual waveform that is restricted to a single electrode (Schomer and Da Silva, 2012). Figure 2.11 shows the 60 Hz power line noise obscuring the EEG recording.

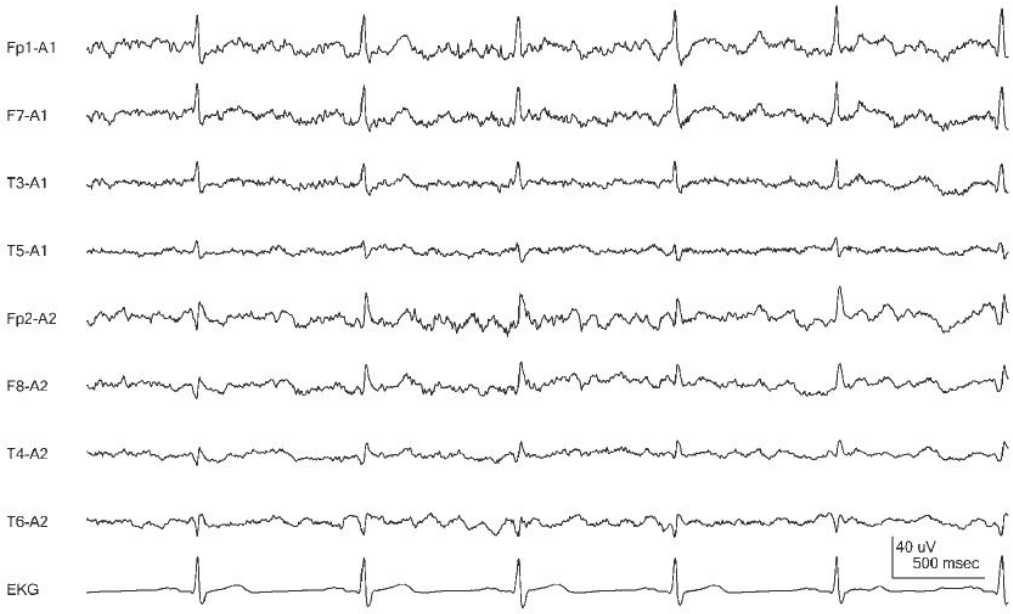

(a) Cardiac artifact

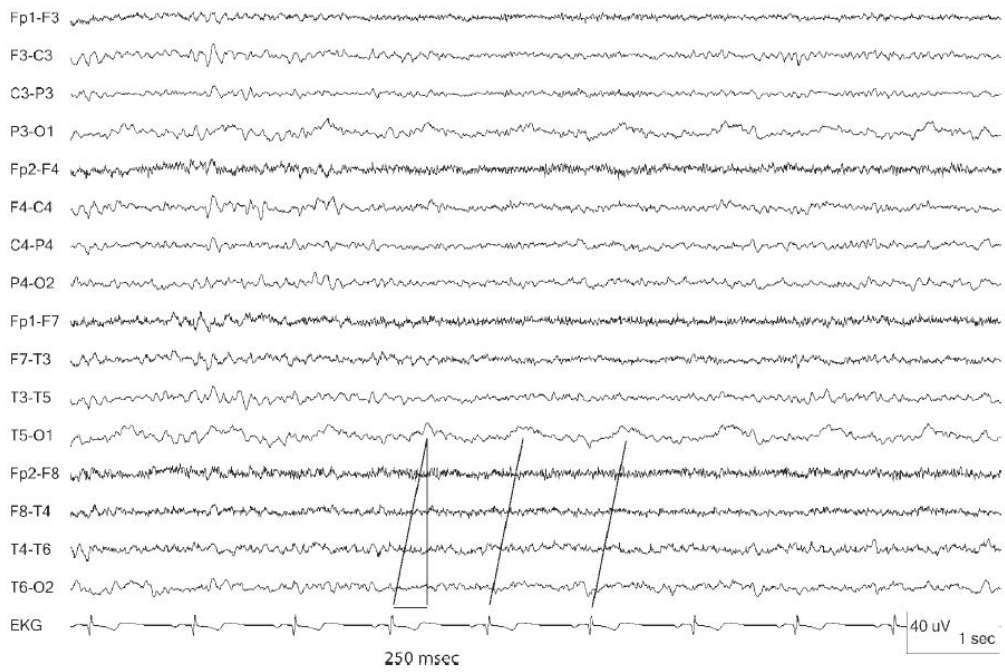

(b) Pulse artifact

Figure 2.10: Cardiac and pulse artifacts visible in the EEG recording. (a) ECG artifact accentuated when using an ipsilateral ear reference. (b) pulse artifact is visible at O1 time-locked to the ECG, but occurring 250 ms after the QRS (Schomer and Da Silva, 2012).

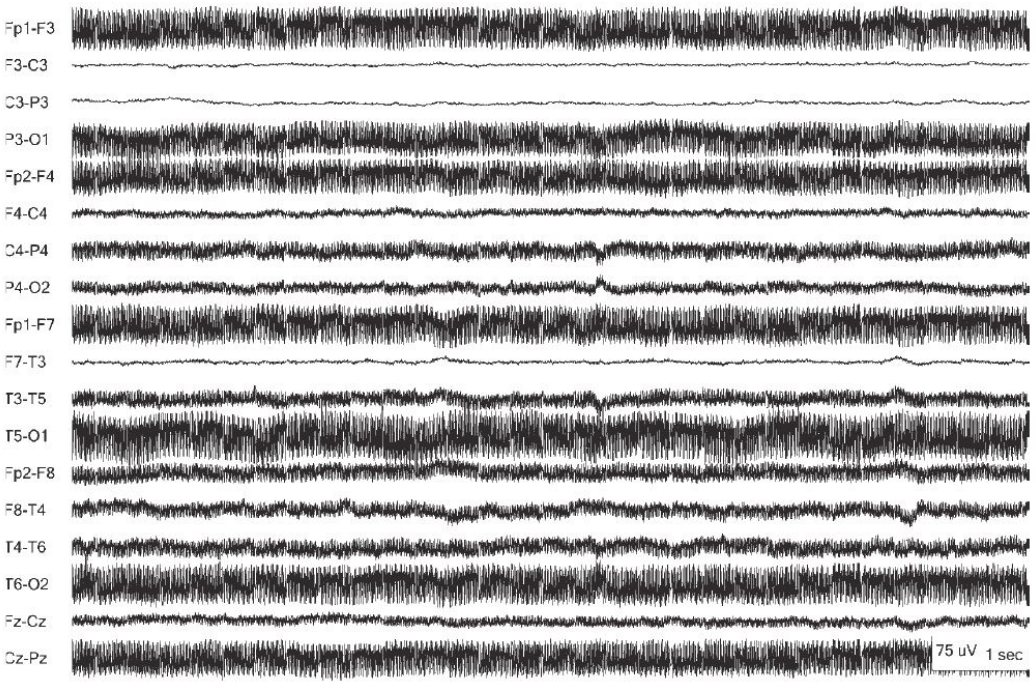

Figure 2.11: The 60 Hz power line noise obscuring the EEG recording (Schomer and Da Silva, 2012).

G. Artifact Detection and Rejection

The literature on EEG artifact detection and rejection is extensive and is yet evolving. Most physiologic and nonphysiologic artifacts can be identified by visual inspection, remontaging, an digital filtering (Schomer and Da Silva, 2012). The removal of EEG channels, time segments, or epochs that are contaminated with artifacts may result in a loss of data if only limited data is available. Low-pass, high-pass or band-pass filters can be applied to the raw EEG data if the analysis is restricted to certain frequency bands. However, alternative techniques are needed if the EEG data of interest and interferences are with spectral overlap. Blind source separation (BSS) (Delorme et al., 2001; Jung et al., 1998, 2000; Sahonero-Alvarez and Calderón, 2017), regression (Waser and Garn, 2013; Woestenburg et al., 1983), EOG correction (Croft and Barry, 2000), the wavelet transform method (Krishnaveni et al., 2006; Safieddine et al., 2012), empirical mode decomposition (Molla et al., 2010; Safieddine et al., 2012) are some of methods that can be used to remove artifacts in EEG recordings. Independent component analysis (ICA) is one of the most widely BSS technique to separate artifactual EEG components (Jung et al., 1998, 2000; Makeig et al., 1996). An extensive review on the artifact removal algorithms can be found in (Croft and Barry, 2000; Jiang et al., 2019; Mannan et al., 2018; Urigüen and Garcia-Zapirain, 2015). A detailed description of the artifact removal methods used in this thesis is given in Chapter 3.

H. Automatic Artifact Removal Methods

It is of great interest to separate and remove artifactual EEG components in real-time with the increase in the use of EEG in real-time applications. Many studies have explored methods to automate the identification and removal of artifactual EEG components using ICA (ICA is explained in Section 3.1.4). Bian et al. (2006) proposed an automatic artifact removal method for EEG data, by analysing three exponents, largest Lyapunov exponent (LLE), kurtosis and Hurst exponent (HE) of each independent component (IC). Delorme et al. (2001) developed a semi-automated method that jointly uses kurtosis and Shannon's entropy variations of ICs as a measure of artifactual ICs. The joint use of kurtosis and Reny's entropy proposed by Mammone and Morabito (2008) outperforms the method introduced by Delorme et al. (2001). An automatic method for removing the eye blink artifact is proposed by Li et al. (2006) based on a spatial template matching of the eye blink artifact. Zhu et al. (2008) used sample entropy as a measure of artifactual ICs. Kong et al. (2013) automatically detects eye blink component based on correlation index and power topography characteristics. Modified multiscale sample entropy and kurtosis have been used by Mahajan and Morshed (2014) to distinguish eye blink artifactual ICs. Moreover, probability density, the central moment of frequency, spectral entropy, and fractal dimension are also used to identify artifacts from ICA decomposition (Phothisonothai et al., 2012). A fully automated and on-line artifact removal method based on ICA, wavelet decomposition and thresholding was proposed by Daly et al. (2014), and it can remove ocular and electromyographic artifacts. ADJUST (Automatic EEG artifact Detection based on the Joint Use of Spatial and Temporal features) algorithm proposed by Mognon et al. (2011) classifies eye blinks, eye movements, and generic discontinuities. It is based on the joint use of artifact-specific spatial and temporal features of ICA components, and the threshold value for features is calculated by using automatic image processing thresholding algorithm based on the Expectation-Maximization (EM) technique. FASTER (Fully Automated Statistical Thresholding for EEG artifact Rejection) applies a statistical thresholding method to ICA data and uses ICA to subtract the EOG contribution to the EEG data (Nolan et al., 2010). The IClabel classifier recently developed by Pion-Tonachini et al. (2019) computes IC class probabilities across seven IC categories: brain, eye, muscle, heart, line noise, channel noise and other.

2.1.9 Applications of EEG

In recent years, there has been significant growth in the study of cerebral activity using EEG. EEG has been mostly used to study the physiological and psychological brain states, such as sleep (Fell et al., 1993; Pradhan and Sadasivan, 1996; Röschke et al., 1993; Zhao et al., 2019),

attention (Harmony et al., 1996; Klimesch et al., 1998), anaesthesia (Bruhn et al., 2000; Murphy et al., 2011), drowsiness (Eoh et al., 2005; Santamaria and Chiappa, 1987; Vuckovic et al., 2002), alertness (Vuckovic et al., 2002), fatigue (Barwick et al., 2012; Baumeister et al., 2012; Borghini et al., 2014; Chen et al., 2013; Craig et al., 2012; Eoh et al., 2005; Fan et al., 2015; Käthner et al., 2014; Tran et al., 2020; Trejo et al., 2015; Yao et al., 2009; Zhao et al., 2012), pain (Chen, 2001; Sarnthein et al., 2006), anxiety (Blackhart et al., 2006), and emotions (Liu et al., 2011). Diagnose and study of various neural diseases and brain disorders such as epilepsy (Acharya et al., 2012; Osowski et al., 2007), attention deficit hyperactivity disorder (Arns et al., 2013; Snyder and Hall, 2006), depression (Blackhart et al., 2006; Bruder et al., 1997), Parkinson's disease (Oh et al., 2018; Stam et al., 1995), schizophrenia (Boutros et al., 2008; Li et al., 2008), and Alzheimer's disease (Abásolo et al., 2005). EEG is also extensively used to identify the neural mechanisms critical for enhancing sports performance (Cheron et al., 2016; Haufler et al., 2000). Brain-computer interface (BCI) is a *"a communication system that does not depend on the brain's normal output pathways of peripheral nerves and muscles."* (Wolpaw et al., 2000). BCIs could provide a new augmentative communication option for many people with severe motor disabilities. Therefore, a growing number of studies have been conducted on implementation and application of EEG-based BCI systems and evaluation of translation algorithms and signal processing methods to achieve greater speed and accuracy (Hoffmann et al., 2008; Schalk et al., 2004; Wolpaw et al., 2000, 1991). EEG-neurofeedback (also known as biofeedback) is a promising non-invasive technique where the participants learn to self-regulate their brain activity. EEG-neurofeedback is used to treat many neurological and physiological disorders such as attention deficit hyperactivity disorder, depression, epilepsy, anxiety, and learning disorders (Hammond, 2005; Hurt et al., 2014). It is also used to enhance the cognitive performance of healthy individuals (Gruzelier, 2014; Zoefel et al., 2011).

2.2 Fatigue

Fatigue is a common sensation that confronts everyone in their day-to-day activities as well as in many clinical and rehabilitation settings, yet, there exists no unambiguous and universally agreed definition for the term fatigue, nor the underlying mechanisms involved in causing a fatigued status are clearly understood. The definitions used for 'fatigue' may vary depending on the experimental context. Fatigue, in general, is a sensation of tiredness, weariness or lack of energy that is associated with a reduction in alertness and task performance that develops during prolonged physical or mental activity and can be relieved by rest. Psychological, physical and physiological factors may induce fatigue. It is a complex and

highly subjective phenomenon, that impairs reaction and response time (Boksem et al., 2005), muscle strength (Enoka and Stuart, 1992), and proprioception (Myers et al., 1999) leading towards a decrement in the mental and physical task performance. Grandjean (1979) defined fatigue as a reduction in efficiency and a disinclination for effort. Fatigue can be broadly categorised into two types: physical (or muscular) fatigue and mental fatigue.

2.2.1 Physical Fatigue

Physical fatigue is defined as a failure to maintain force (or power output) during sustained muscle contractions (Gibson and Edwards, 1985). Physical fatigue also impairs coordination and may lead towards changes in the human movement patterns, thus increasing the liability to errors, accidents and acute or overuse injuries (Cowley and Gates, 2017; Grandjean, 1979). Underlying causes of physical fatigue are manifold, and may not only relate to processes of peripheral (i.e. outside of the central nervous system (CNS)) origin but also processes of central (i.e. within the CNS) origin. Peripheral fatigue occurs as a result of impairments in the function of the peripheral nerves, neuromuscular junction transmission, electrical activity of muscle fibres or the processes of activation within the fibre. Factors contributing towards central fatigue are motivation, impaired recruitment of motor neurons, and impaired transmission down the spinal cord (Gibson and Edwards, 1985). In comparison to the physical fatigue that is widespread over several muscles, fatigue that is localised to a specific group of muscles may cause greater changes in the muscle coordination, movement amplitude and speed (Cowley and Gates, 2017). Furthermore, the effects of physical fatigue may also vary depending on the joints and muscles extensively used by the task. For instance, tasks that heavily use the proximal joints and muscles (e.g., overhead lifting, reaching tasks) may lead to fatigue in proximal muscles whereas the tasks that use the distal joints and muscles (e.g., assembly tasks) may lead to fatigue in distal muscles; tasks that use both proximal and distal joints and muscles may lead to fatigue in both proximal and distal joints (e.g., ball-throwing task). Studies have also shown that the distal and proximal muscle fatigue differentially affect the kinematic and movement variability (Côté et al., 2005; Cowley and Gates, 2017; Huffenus et al., 2006; Qin, Lin, Faber, Buchholz and Xu, 2014). Moreover, exercise-induced acute muscle fatigue will be experienced shortly after the onset of exercise and delayed exercise-induced fatigue will be experienced following a constant, high-intensity exercise for a prolonged period (Finsterer, 2012).

2.2.2 Mental Fatigue

Mental fatigue can be conceptualised as a feeling that an individual may experience during or after a prolonged period of cognitive activity (Boksem et al., 2005). Mental fatigue is a functional state which grades in one direction into sleep and in the opposite direction into a relaxed and restful condition. The functional state of a person at any moment is determined by the level of activity of the cerebral cortex ranging from a deep sleep, light sleep, drowsy, weary, hardly awake, relaxed, resting, fresh, alert, very alert, stimulated and a state of alarm (Grandjean, 1979). Mental fatigue is generally associated with a sensation of weariness, feelings of inhibition, heaviness, and drowsiness, reduced alertness, and impaired performance leaving an individual with no desire for either mental or physical effort. The effects of mental fatigue on cognitive performance (Boksem et al., 2005; Lorist et al., 2000; Tanaka et al., 2015; Van der Linden et al., 2003) and vehicle driving and pilot performance (Caldwell, 2005; Ting et al., 2008; Wang et al., 2006) is extensively studied in the past. Recent studies have also shown that mental fatigue impairs physical performance, especially in sports (Marcora et al., 2009; Mehta and Parasuraman, 2014; Van Cutsem et al., 2017).

2.2.3 Measurement of Fatigue

There are various subjective and objective measurements of fatigue that have been described in the literature. Many self-administered questionnaires have been used to evaluate fatigue in general practice settings and a variety of medical and neurologic disorders (Neuberger, 2003; Shahid et al., 2010). The Chalder fatigue scale (CFQ 11) (Chalder et al., 1993), Fatigue Assessment Scale (FAS) (Michielsen et al., 2003), fatigue severity scale (FSS) (Krupp et al., 1989), multidimensional assessment of fatigue (MAF) (Belza, 1995), checklist individual strength (CIS) (Vercoulen et al., 1994), fatigue assessment inventory (FAI) (Schwartz et al., 1993), and fatigue impact scale (FIS) (Fisk et al., 1994) are some of these subjective rating scales. Furthermore, behavioural indices such as reaction time (Cao et al., 2017), percentage of eyelid closure (PERCLOS) (Mandal et al., 2016; Sommer and Golz, 2010), movement variability (Cortes et al., 2014; Cowley and Gates, 2017), and error ratio are widely used to characterise the subjective experience of fatigue and related changes in the day-to-day activity. With the recent advancements in neuroergonomics, neurophysiological changes caused by fatigue were extensively investigated using electroencephalogram (EEG) (Bailey et al., 2008; Barwick et al., 2012; Baumeister et al., 2012; Borghini et al., 2014; Craig et al., 2012; Jap et al., 2009; Lal and Craig, 2002; Tanaka et al., 2012; Tran et al., 2020; Trejo et al., 2015; Yao et al., 2009), electrooculogram (EOG) (Hu and Zheng, 2009; Morris and Miller, 1996; Zhao et al., 2012), electromyogram (EMG) (Bigland-Ritchie, 1981; Bigland-Ritchie

et al., 1983; Cifrek et al., 2009), electrocardiogram (ECG) (Wang et al., 2018; Zhao et al., 2012), functional magnetic resonance imaging (fMRI) (Bakshi et al., 1999; DeLuca et al., 2008; Liu et al., 2002), functional near infra-red spectroscopy (fNIRS) (Ahn et al., 2016). These measures provide an objective measure of the level of fatigue. Among these fatigue indicators, EEG recordings have shown to be the most predictive and reliable measure of fatigue (Lal and Craig, 2001, 2002; Tran et al., 2020). Therefore the following section summarises the findings in the literature on quantitative EEG feature modulations with fatigue.

2.2.4 Quantitative EEG Measures of Fatigue

To date, many studies have investigated the variations in quantitative EEG features associated with the fatigue induced by driving tasks (Borghini et al., 2014; Craig et al., 2012; Eoh et al., 2005; Jap et al., 2009; Lal and Craig, 2001, 2002; Zhao et al., 2012), voluntary motor tasks (Wang et al., 2017; Yao et al., 2009), cognitive tasks (Tanaka et al., 2012; Trejo et al., 2015), brain-computer interactions (Käthner et al., 2014), exercises and sports related activities and conditions (Bailey et al., 2008; Barwick et al., 2012; Baumeister et al., 2012; Xu et al., 2018), visual display terminal tasks (Cheng and Hsu, 2011; Fan et al., 2015), visual tasks in 3D displays (Chen et al., 2013; Zou et al., 2015), and many more. Modulations in the EEG spectral features were mostly studies in the literature (Table 2.1). With the recent advancement in the nonlinear time series analysis methods, current research is also focused on evaluating the variations in nonlinear EEG features such as largest Lyapunov exponent (Wang et al., 2020; Yao et al., 2009), approximate entropy (Min et al., 2017; Wang et al., 2020, 2019; Xiong et al., 2016), sample entropy (Tran et al., 2007, 2008; Wang et al., 2020, 2019; Xiong et al., 2016), fuzzy entropy (Min et al., 2017), spectral entropy (Wang et al., 2019) and correlation dimension (Wang et al., 2020, 2014) with the development of fatigue.

To the author's knowledge, the influence of fatigue induced by robot-mediated exercises on EEG activity has not been yet fully explored. Therefore, in this thesis, variations in the EEG spectral features (band power and power ratios), largest Lyapunov exponent and approximate entropy with fatigue induced by robot-mediated upper limb interactions were further analysed. A systematic literature review on the EEG features considered in this thesis is given below.

A. Spectral EEG Features as Fatigue Indices

Over the past years, many researchers have focused on decomposing the recorded EEG data into its frequency bands, and evaluating the variations in the absolute or relative band power

or band power ratios with fatigue. In a neurophysiological sense, EEG power represents the sum of neurons discharging synchronously (Kanda et al., 2009). A greater proportion of fast frequency activity reflects decreased neural synchrony; i.e., many different neural circuits in the brain are actively processing information. Desynchronised activity occurs when a person is actively thinking or at an alert and attentive state. Conversely, a higher proportion of slow frequency activity reflects increased neural synchrony; i.e., decreased brain activation (Carlson, 1994). Many studies have reported that when a person is fatigued, EEG power shifts towards the lower frequency bands; i.e., the proportion of low-frequency EEG waves such as theta and alpha increase with fatigue whereas high-frequency EEG waves such as beta decrease with fatigue (Barwick et al., 2012; Craig et al., 2012). Modulations in both absolute and relative band power measures are considered in the literature. In addition, band power ratios such as $(\theta+\alpha)/\beta$, α/β, $(\theta+\alpha)/(\alpha+\beta)$, and θ/β are also used in the literature since the basic band power measures can be insufficient to observe the shift of brain activity from fast waves to slow waves (Eoh et al., 2005; Fan et al., 2015; Jap et al., 2009).

Table 2.1 summarises 16 studies identified by a systematic review on the association between EEG spectral features and fatigue over the last two decades. The majority of the studies (15/16 studies) evaluated the variations in alpha activity with fatigue and a significant increase in in alpha band power was observed in 10 studies. Alpha synchronization was associated with mental, physical and visual fatigue. Theta activity (evaluated by 13 studies) was found to be significantly increasing in 8 studies and significantly decreasing in 1 study. The increase in the theta band power was mostly associated with mental fatigue, whereas the decrease was observed during a fatiguing knee joint reproduction task. The majority of the studies (8/12 studies) showed a significant reduction in beta activity with fatigue. However, the variation associated with driver fatigue is equivocal since both significant increment (Craig et al., 2012; Lal and Craig, 2002) and decrement (Eoh et al., 2005; Jap et al., 2009) in beta band power was reported. Delta activity was only explored in seven studies, where two studies showed a significant increase delta activity while four studies showed no significant difference with fatigue. The changes in the relative band power was considered in eight studies. Furthermore, the ratio between slow and fast frequency activities was reported in eight studies, where a majority of studies (6/8 studies) showed a significant increase in band power ratios with fatigue. Eoh et al. (2005) stated that the index $(\theta+\alpha)/\beta$ was a more reliable fatigue indicator during a simulated driving task due to the mutual addition effect of alpha waves and theta waves during the repetitive phase transition between wakefulness and microsleep. Jap et al. (2009) also reported a greater increase in the index $(\theta+\alpha)/\beta$, in comparison to the other power ratios, when a person experienced a fatigued state at the end of a monotonous simulated driving task. Moreover, the modulations in EEG spectral features exhibited a widespread

Table 2.1: Literature summary on modulations in the spectral features with fatigue.

Reference	Description	No of participants	No of electrodes	δ	θ	α	β	$\frac{(\theta+\alpha)}{\beta}$	$\frac{\alpha}{\beta}$	$\frac{(\theta+\alpha)}{(\alpha+\beta)}$	$\frac{\theta}{\beta}$
Barwick et al. (2012)	Fatigue during administration of a neuropsychological test batter	14 M=70%, F=30%	42	-	$\uparrow^{R}$ F, C, P	$\uparrow^{R}$ F, C, P, O	$\downarrow^{R}$ C, P	-	-	-	-
Baumeister et al. (2012)	Effects of fatigue induced by a cycling exercise on knee joint reproduction task	12 M=12	22	-	$\downarrow$ F, FC	$\downarrow^{L,U}$ F, FC, T, P, O	-	-	-	-	-
Chen et al. (2013)	Fatigue induced by watching 3DTV	10	16	$\uparrow^{R}$ FP1, FP2, C4, F8	NS	$\downarrow^{R}$ FP1, FP2, F8	$\downarrow^{R}$ FP1, FP2, F3, C3, F7, T5	$\uparrow$ FP1, F3, C3	$\uparrow$ FP1, F3, C3	$\uparrow$ FP1	$\uparrow$ FP1, FP2
Cheng and Hsu (2011)	Mental fatigue induced by visual display terminal tasks	20 M=20	7	-	$\uparrow^{R}$ F3, Fz, F4, Cz, Pz, O1, O2	$\downarrow^{R}$ F3, Fz, F4, Cz, Pz, O1, O2	NS	$\downarrow$ O1, O2	NS[a]	-	-
Craig et al. (2012)	Fatigue induced by monotonous simulated driving task	48 M=25, F=23	32	NS	$\uparrow$ F, C, PO	$\uparrow^{L,U}$ F, C, PO	$\uparrow$ F, C, PO	-	-	-	-
Eoh et al. (2005)	Fatigue during a simulated driving task	8 M=8	8	-	NS	$\uparrow^{R}$	$\downarrow^{R}$	$\uparrow$	$\uparrow^{a}$	-	-
Fan et al. (2015)	Mental fatigue in visual search task	10 M=10	64	NS	NS	$\uparrow^{R}$ F, C, P, O, PT	$\downarrow^{R}$ FP, IF, O, PT	$\uparrow$ FP, IF, F, C, P, O, PT	$\uparrow$ FP, IF, F, C, P, O, T, PT	$\uparrow$ FP, IF, F, C, P, O, PT	$\uparrow$ FP, IF, F, C, P, O, PT
Jap et al. (2009)	Fatigue induced during a monotonous driving session	52 M=36, F=16	30	* F, EB	* F, C, P, EB	$\downarrow$ T	$\downarrow$ T	$\uparrow$ T	$\uparrow$ T	$\uparrow$ T	$\uparrow$ T
Käthner et al. (2014)	Mental fatigue during P300 brain computer interface	12 F=12	31	-	$\uparrow$ Fz, FC5, FC6, C5, CP5, P3, O1, O2, PO8	$\uparrow$ F3, Fz, F4, FC5,FC3, FCz, FC4, FC6, C5, C3, Cz, C4, C6, CP5, CP3, CPz, CP4, CP6, P3, P1, Pz, P2, P4,PO7, PO3, POz, PO4, PO8	-	-	-	-	-
Lal and Craig (2002)	Fatigue during simulated driving task	35 M=26, F=9	19	$\uparrow$ EB	$\uparrow$ EB	$\uparrow$ EB	$\uparrow$ EB	-	-	-	-
Tanaka et al. (2012)	Mental fatigue induced by $0^{(NS)}$ or 2-back test	18 M=18	11	NS	$\uparrow$ Fz	$\downarrow$ P3, O2	$\downarrow$ Pz	-	-	-	$\uparrow$ Fz, Pz, O1
Trejo et al. (2015)	Mental fatigue induced by a sustained low-workload mental arithmetic task	16 M=12, F=4	2	-	$\uparrow$ Fz	$\uparrow$ Pz	-	-	-	-	-
Wang et al. (2017)	Muscle fatigue during right arm side lateral raise task with loads	18 M=18	2	-	-	$\uparrow$ C3, C4	NS	-	-	-	-
Xu et al. (2018)	Fatigue in mental$^{(NS)}$ and physical-mental task	14 M=5, F=9	16	-	-	-	$\downarrow^{R}$ C3, P3, Pz, Oz, T3, T5	-	$\uparrow$ C3, P3, T4	-	-
Zhao et al. (2012)	Mental fatigue in simulated driving task	13 M=13	32	NS	$\uparrow^{R}$ F, C, O	$\uparrow^{R}$ C, P, O, T	$\downarrow^{R}$ F, C, T	-	-	-	-
Zou et al. (2015)	Stereoscopic 3D visual fatigue caused by vergence-accommodation conflict	11 M=5, F=6	30	-	NS	$\uparrow^{R}$ F, C, P, EB	$\downarrow^{R}$	*	* F, C	NS	NS

Notes. $\uparrow$ = significant increase; $\downarrow$ = significant decrease; * = significant, but the direction of change is not specified; NS = no significant change; - = not reported; R = relative band power measures were considered; L, U = lower and upper bands were considered; a = β/α was reported; The brain regions denoted by FP, IF, F, FL, FM, FR, FC, C, CL, CM, CR, P, PO, O, T, PT, POL, POM, POR, and EB corresponds to frontopolar (or pre-frontal), inferior frontal, frontal, left frontal, midline frontal, right frontal, fronto-central, central, central left, midline central, central right, parietal, parieto-occipital, occipital, temporal, posterior temporal, posterior left, midline posterior, posterior right and entire brain average.

topographical distribution in the majority of the studies. Although it is evident that fatigue significantly alters the EEG spectral features, some findings are equivocal and needs further exploration (Baumeister et al., 2012; Chen et al., 2013; Cheng and Hsu, 2011; Jap et al., 2009; Tanaka et al., 2012). Variations in methodological approaches, including differences in the fatiguing study protocol, low sample size, gender bias, differences in the number of electrodes used, the electrode placement and the feature definition could be a possible explanation for the discrepancies present across the studies. However, changes in brain activities due to fatigue induced by robot-mediated exercises have not been yet fully explored. Moreover, the current studies do not systematically investigate whether the modulations in EEG spectral features are specific to the physical or cognitive nature of the task performed using the proximal or distal upper limb.

B. Largest Lyapunov Exponent of EEG as a Fatigue Index

In recent years, there has been an increasing interest in the modulations in largest Lyapunov exponents of EEG to investigate the chaotic behaviour of the brain. Lyapunov exponents provide a qualitative and quantitative characterization of dynamical behaviour and are related to the exponentially fast divergence and convergence of nearby orbits in phase space (Section 3.2.2). Although many studies have used largest Lyapunov exponents of EEG to analyse different sleep stages (Acharya et al., 2005; Fell et al., 1993, 1996; Röschke et al., 1995*a*,*b*), mental stages (Natarajan et al., 2004), and emotion functioning (Aftanas et al., 1997) or to test for differences among healthy and diseased subjects (Osowski et al., 2007; Röschke et al., 1995*a*,*b*; Stam et al., 1995), only a few studies have investigated the association of largest Lyapunov exponent with fatigue (Wang et al., 2020; Yao et al., 2009). Yao et al. (2009) reported a significant decrease in largest Lyapunov exponent with muscle fatigue induced by intermittent handgrip maximal voluntary contractions. They showed that the largest Lyapunov exponent values were lower under severe fatigue conditions than those under minimal and moderate fatigue conditions. Also, higher largest Lyapunov exponent values were visible in the frontal lobe and contralateral (left) hemisphere under minimal and moderate fatigue conditions. A significant positive correlation was also observed between the largest Lyapunov exponent values and force. Therefore, the largest Lyapunov exponent may be used to classify fatigue stages of the brain and to measure motor control-related cortical signal adaptations. Table 2.2 summarises the study Yao et al. (2009) that found an association between the largest Lyapunov exponent and fatigue.

Table 2.2: Literature summary on modulations in the largest Lyapunov exponent with fatigue.

Reference	Description	No of participants	No of electrodes	Parameters Used		Largest Lyapunov exponent
				Dimension	Time lag	
Yao et al. (2009)	Intermittent handgrip maximal voluntary contractions that resulted in significant fatigue	8 M=6, F=2	63	5	4 ms	↓

Notes. ↓ = significant decrease.

C. Approximate Entropy of EEG as a Fatigue Index

Approximate entropy, introduced by Pincus (Pincus, 1995), measures the complexity of a time series (Section 3.2.3). Approximate entropy was also considered when designing automated driver fatigue detection system (Hu, 2017; Hu and Min, 2018; Min et al., 2017; Mu et al., 2017; Xiong et al., 2016; Zhang et al., 2013). Xiong et al. (2016) observed a significant decrease in approximate entropy with fatigue induced by a simulated driving task on P4, Pz, P3, and Oz electrodes. Liu et al. (2010) investigated the modulations in approximate entropy with mental fatigue induced by three types of simple cognitive tasks: vigilance task, arithmetic calculation task, and simple switch task. They extracted the EEG components of the delta, theta, alpha, beta and total frequency bands and evaluated the variations in approximate entropy of the five frequency bands with fatigue. In general, the findings of this study showed a significant decrease in approximate entropy values with the increase in mental fatigue level. The decrement in the mean values of the approximate entropy was visible on Fp2, Fp1, F4, Fz, F3, C4, Cz, C3, P4, Pz, and P3 electrodes for total frequency band; on prefrontal electrodes for alpha frequency band, on parietal electrodes for beta frequency band. However, no significant difference was visible on mean value of approximate entropy in delta and theta frequency band on all electrodes. Wang et al. (2019) also reported a decrease in the approximate entropy in occipital area due to fatigue induced by a simulated driving task. Table 2.3 summarises the significant variations in the EEG approximate entropy values with fatigue found in the literature.

Table 2.3: Literature summary on modulations in the approximate entropy with fatigue.

Reference	Description	No of participants	No of electrodes	Parameters Used		Approximate entropy
				m	r	
Liu et al. (2010)	Mental fatigue induced by a cognitive tasks (vigilance task, arithketic calculation task, simple switch task)	50 M=50	11	2	0.2	↓
Xiong et al. (2016)	Fatigue during simulated driving task	50 M=25, F=25	12	1	0.2	↓

Notes. ↓ = significant decrease.

2.2.5 Movement Variability Associated With Fatigue

Human movement variability addresses the natural variations observed in the motor performance by an individual under repetitive tasks over time (Stergiou and Decker, 2011; Stergiou et al., 2006). It is defined as the variability in kinematic properties of movements (Yang et al., 2018). Linear statistical tools such as mean, standard deviation, coefficient of variation and root mean square distance, quantify the amount or magnitude of the variability around a central point (mean) (Colombo et al., 2005; Cortes et al., 2014; MacKenzie et al., 2001; Madeleine and Madsen, 2009; Selen et al., 2007). The non-linear dynamics tools, such as approximate entropy, sample entropy , Lyapunov exponent, correlation dimension, canonical correlation analysis evaluate the structure or organization of variability and uncover the underlying complexity (Cortes et al., 2014; Madeleine and Madsen, 2009; Stergiou et al., 2006). A substantial increase in the measures of movement variability indicates a higher variability (Cignetti et al., 2009).

Several studies have explored the association between movement variability and fatigue, but the findings are still unclear. Some studies have reported that the increase in movement variability with fatigue was associated with a decrement in task performance (Singh et al., 2010; Srinivasan and Mathiassen, 2012). A higher movement variability may also reflect adaptation strategies followed by an individual to lower the load on fatiguing tissues such that task performance is preserved (Cignetti et al., 2009; Fuller et al., 2009; Huysmans et al., 2008; Selen et al., 2007; Yang et al., 2018). For example, Huysmans et al. (2008) reported a significant increase in the mean and standard deviation of the distance to target following the fatigue protocol and suggested that the higher variability of the distance to target may indicate larger corrective movements that have been made at the expense of a higher muscular effort to meet the task requirements. Similarly, Yang et al. (2018) showed that fatigue during a repetitive pointing task increased the shoulder and elbow angle variability and the shoulder-elbow coordination variability; the increase in the shoulder-elbow coordination variability may indicate the greater use of motor abundance to preserve the global task performance. Selen et al. (2007) also reported a change in the target tracking control strategy with increasing fatigue; thus, despite the increase in overall kinematic variability, task performance was retained by staying closer to the centre of the target when fatigued. It was also stated that the increases in movement variability in athletes when fatigued can act as a protective mechanism to counteract the negative effects of fatigue that may lead to the risk of injury (Edwards et al., 2012). The theoretical model of movement variability developed by Stergiou et al. (2006) assumes that the neuromuscular system becomes noisier and less adaptable when the variability is increased beyond its optimal value. Cignetti et al. (2009) observed increased

and more random fluctuations of the limb movements of the skiers with fatigue, thereby, supporting the theoretical model of movement variability developed by Stergiou et al. (2006). As discussed in Cortes et al. (2014), fatigue can also have a differential effect on movement variability during a side-step cutting task, thereby causing both an increase and a decrease in the different indices of variability. Thus, the authors argue that the fatigue not only decreases the force producing capacity of an individual, but also limits the ability of an individual to perform a smooth and controlled action.

2.3 Robot-Mediated Upper Limb Stroke Rehabilitation

2.3.1 Stroke

A. Pathophysiology of Stroke

Stroke, clinically known as *cerebrovascular accident*, yet remains as a leading cause of morbidity and mortality worldwide, despite the advances in diagnosis and treatment of stroke risk factors. It is a clinical syndrome that is caused due to an interruption in the blood flow to the brain. Blood supply interruption deprives the oxygen and nutrients flow to the brain cells and leads to a brain cell death. There are two main types of stroke: ischemic and hemorrhagic. Ischemic stroke results from a blockage in a brain artery or a small blood vessel deep within the brain, due to a blood clot or fatty deposit buildup within the walls of the arteries. These plaques narrow the inside diameter of the arteries and inhibit normal blood supply to parts of the brain. Ischemic stroke can occur in two ways, namely thrombotic and embolic. In a thrombotic stroke, a blood clot is formed inside one of the arteries supplying blood to the brain. In contrast, an embolic stroke occurs if a blood clot or fatty deposits are migrated from a distant location and blocks the cerebral vessel (Bendok et al., 2011). Haemorrhagic stroke occurs due to rupture or leaking of an artery within or on the surface of the brain, which will result in a seeping of blood into or around the brain. Accumulation of blood creates pressure and swelling and damages brain cells and tissues. Haemorrhagic stroke encompasses both intracerebral haemorrhage and subarachnoid haemorrhage. Intracerebral haemorrhage is caused by bleeding within an artery inside the brain, whereas subarachnoid haemorrhage is caused by bleeding into the space surrounding the brain.

B. Epidemiology of Stroke

Annually, 15 million people around the world experience a stroke; 5 million of these instances are fatal, and an equal amount is left with long-term disabilities (Mackay et al., 2004). In the

United Kingdom, more than 100,000 strokes occur each year (i.e. on average, one stroke per every 5 minutes) and over 1.2 million stroke survivors are living in the United Kingdom. In 2016, almost 38,000 lives were lost in the United Kingdom due to stroke, making it the fourth leading cause of death (Stroke Association, 2018). Epidemiologic studies show that of all strokes, 85% are ischemic, and 13% are haemorrhagic. Approximately, 60% of ischemic strokes are caused by a thrombus, and an embolus causes 25%. Intracerebral haemorrhage strokes account for nearly 8% of all haemorrhagic strokes, whereas 5.4% are subarachnoid haemorrhage strokes (Bendok et al., 2011). The mortality rates of stroke patients have significantly decreased over the past few years due to the improvements in acute treatment and supportive care. However, the number of first-time strokes (stroke incidence) and the number of stroke survivors (stroke prevalence) are expected to rise in future with the increase in the ageing population (Bendok et al., 2011).

C. Stroke Related Disability

Stroke impairs the physical, psychological or anatomical structures and functions of the human body and the severity of the impairment depend on the location and size of the lesion in the brain. For example, people who have experienced a stroke will face partial or complete paralysis, limited movement coordination, spasticity, hemispatial neglect, muscle weakness, memory and attention deficits, sensory loss, aphasia, chronic fatigue, depression, behavioural changes and many more health issues (Molier et al., 2011). Almost two-thirds of stroke survivors have a disability leading towards long-term difficulties in independently performing activities of daily living. Hence, stroke survivors have to depend on carers or personal assistants as well as need to undergo inpatient and outpatient rehabilitation to regain control and independence to perform daily living activities. Therefore, the burden on health care systems and the economic impact of stroke and rehabilitation is a pressing concern worldwide.

D. Risk Factors of Stroke

Owing to the economic and social burden of stroke patient rehabilitation, it is essential to recognise, control, and treat risk factors in advance to prevent a stroke. Although some of the stroke risk factors such as age, gender, race/ethnicity, and genetics are non-modifiable, many are easily modifiable by adjusting to an active, healthy lifestyle and by following proper medical advice. For example, lifestyle and behavioural factors such as physical inactivity, obesity, excessive alcohol intake, smoking/tobacco usage, sleep apnea and unhealthy diet increase the risk of stroke and can be prevented by adopting healthy lifestyle choices. In

2012, the governmental organisations and charities in the United Kingdom spent £56 million on stroke research (Luengo-Fernandez et al., 2015), on helping patients and understanding treatment methods and rehabilitation programs.

E. Fatigue After a Stroke

Fatigue after a stroke is a common and persistent, yet often overlooked consequence of stroke (Staub and Bogousslavsky, 2001). Many stroke survivors (about 30% to 70%) have reported persistence of fatigue as a debilitating symptom (Lerdal et al., 2009; Staub and Bogousslavsky, 2001). The presence of fatigue in patients with upper limb deficit following a stroke may severely impair their functional capabilities, thereby impeding their motivation and commitment to actively participate in rehabilitation sessions. Also, the physical inability to exert the desired forces required during repetitive and sustained upper limb movements may impair patient's motivation to actively participate in the training exercises. Fatigue conditions may also affect the precision of sensorimotor control, thereby leading to a decrease in performance and an increase in the risk of injury (Baumeister et al., 2012). However, the existing rehabilitation programs often neglect the adverse effects of fatigue on therapy outcome.

2.3.2 Therapeutic Strategies and Stroke Rehabilitation

As a direct consequence of the stroke, patients will suffer from a variety of sensory, cognitive, motor, and psychological impairments. Some degree of upper limb deficits is mostly experienced by stroke survivors, occurring in about 77% of patients with a first-in-a-lifetime stroke (Lawrence et al., 2001). However, since the human brain has a potential capability to compensate for lesions, it is possible to regain these lost functions partially or entirely (Johansson, 2000). Following a brain injury, the human brain can change both functional and anatomical structure, by reorganising and forming new neural connections between intact neurons. This process of cortical reorganisation mechanism is commonly known as neuroplasticity (also called brain plasticity or neural plasticity). The cortical reorganisation can occur in both in the infarcted and opposite hemispheres around the brain regions immediately adjacent to the infarct or on regions remote from the infarct (Krakauer, 2005). The rate and extent of the neural reorganisation are greatly influenced by the size and location of the lesion as well as the age of the patient (Staines et al., 2009). Non-invasive mapping and neuroimaging studies in the human brain provide evidence for neuroplasticity following brain injury and rehabilitation (Johansson, 2000; Turner et al., 2013).

Owing to the population ageing, the number of people needing upper extremity poststroke therapy is rising rapidly. The early intervention of physiotherapy can accelerate neurological and functional recovery following a stroke. Longitudinal studies have shown that only about 5% to 20% of hemiplegic stroke patients achieve full upper limb functional recovery at six months after stroke. About another 30% to 66% of patients remain with chronic upper limb impairments (Kwakkel et al., 2003; Wade et al., 1983), thereby may find it profoundly difficult to perform activities of daily living independently without getting help from others. Although upper limb motor functional recovery is quite challenging, there is evidence that high-intensity and task-specific exercises consisting of active, functional and highly repetitive movements of the paretic upper limb may lead to long-lasting cortical reorganisation and functional improvements, even in chronic stages of stroke (Bütefisch et al., 1995; Fasoli et al., 2003; Kwakkel, 2006; Lohse et al., 2014; Oujamaa et al., 2009; Veerbeek et al., 2014). In the context of rehabilitation, intensity refers to the duration and frequency (repetitions) of treatment within a given time, usually a day or week. Task-specificity refers to the extent to which the treatment is tailored to the needs and stage of recovery of the patient (Keith, 1997).

The conventional physical therapies used for motor task rehabilitation are usually labour-intensive, time-consuming and often require one-to-one manual interactions with a therapist (Volpe et al., 2002). Therefore, intensive, task-specific therapy sessions can result in excessive fatigue for therapists and may lead to failures in delivery. Thus, the therapy sessions are typically limited to approximately 30 – 60 min sessions per day (Norouzi-Gheidari et al., 2012). The evaluation of the patient's performance and progress during conventional physiotherapy sessions solely rely on the therapist. Moreover, as the cost of hospitalisation is a considerable economic burden to most of the patients, the motivation towards lengthy inpatient rehabilitation is not promising. Therefore, the use of robotic technology to complement conventional therapy is promising since high-intensity, task-specific, interactive exercises can be delivered to the plegic limb with the aid of robotic interventions while reducing the workload of the therapist.

2.3.3 Robot-Mediated Upper Limb Stroke Rehabilitation

Robotics Industry Association (1980) has defined "*a robot is a re-programmable, multi-functional, manipulator designed to move material, parts or specialized devices through variable programmed motions for the performance of a task*" (Pignolo, 2009). Thus, a robot can be programmed to deliver varying degrees of assistance during the exercises depending on the stage of recovery (Fasoli et al., 2004; Lum et al., 2002; Prange et al., 2006). For instance, if the patients are at the early stages of recovery with very low voluntary control,

the robot can be programmed to fully assist the limb movements (passive mode), whereas the patients can perform the the movements with little or no assistance from the robot when they reached the later stages of recovery (active-assisted and active non-assisted modes). The robot can provide a force opposing the movements (progressive-resistive mode) the robot provides a force opposing the movements. Moreover, since robotic motions can be performed in constrained directions (planar, spatial, unilateral or bilateral)(Fasoli et al., 2004) and in controlled velocities, treatments can be tailored to the needs and stage of recovery of the patient. Furthermore, with the use of virtual reality technologies, highly interactive and motivational therapeutic environments can be designed, thereby encouraging active participation and enhancing the motivation towards long-term rehabilitation. (Masiero et al., 2011; Prange et al., 2006). The patient progress and performance can also be estimated in real-time by means of the kinetics (i.e., measures of applied force, torque) and kinematics (i.e., measures of position, velocity, acceleration) of the motion of the robot. Thus, a real-time feedback (visual, auditory or haptic) on the therapy progress can be provided to the patient so that they would be encouraged more to engage in further therapy. Moreover, it allows the patients to continue the rehabilitation therapy independently at home, with lesser expenditure and therapist supervision. The performance measures also allow therapists to customise the treatments to facilitate the individual needs, thus enabling better rehabilitation. Hence, robot-assisted therapies can facilitate longer dedicated and highly motivational training sessions featuring repetitive, intensive, and task-specific exercises to the paretic limb, with no additional work for the therapist.

Many studies have shown that robot-assisted upper limb therapy elicit significant long-lasting improvements in the paretic arm functionality, leading to better rehabilitation (Bertani et al., 2017; Chang and Kim, 2013; Fasoli et al., 2003; Franceschini et al., 2019; Lum et al., 2002; Masiero et al., 2011; Prange et al., 2006), especially when provided in addition to conventional therapy (Masiero et al., 2007; Rosati et al., 2007; Volpe et al., 2000). Lum et al. (2002) showed that when the intensity and duration of conventional rehabilitation are matched with that of robot-assisted movement training, the robot-assisted movement training showed a decrease in impairment, improvement in strength, and increase in reach extent after two months of treatment; however, no significant differences between the two groups were found at the 6-month follow-up. The systematic review by Norouzi-Gheidari et al. (2012) shows that when the intensity/duration of robot-assisted therapy is matched with that of conventional therapy, no statistically significant difference in motor recovery, motor control, strength and activities of daily living were found between intensive conventional therapy and robot-assisted therapy groups. They also found that when compared with standard conventional therapy, additional robot-assisted therapy sessions improve motor recovery of

stroke patients. Volpe et al. (2000) also found improvements in the motor performance of trained shoulder and elbow and functional outcome of stroke patients who received robotic training.

Classification Based on the Mechanical Structure of Rehabilitation Robots

Rehabilitation robots used to provide upper limb post-stroke therapy can be classified into two categories based on the mechanical structure of the robot, namely end-effector-based and exoskeleton- based robots. The end-effector-based robot interacts with the patient through a single distal part (i.e. end effector) which is attached to the forearm or hand. The joints and the rotation axes of the end-effector robot do not align with that of the human upper limb, thereby are simpler in structure, easier to fit with different patient arm lengths and ambidextrous. However, it is challenging to perform isolated movement therapy at a single upper limb joint with an end-effector-based robot, since movements of the end-effector indirectly change the position of the proximal parts of the upper limb due to the existing mechanical chain between the segments of the upper extremity (Maciejasz Paweł and Eschweiler et al., 2014). Exoskeleton-based robots, on the contrary, are wearable robots with a structure that resembles the human arm anatomy. The joints and the rotation axes are aligned with the corresponding upper limb joints and the rotation axes, thereby allow direct control of individual joints to facilitate assistance in retraining a wide variety of movements. In general, these type of robots are specific to a particular side of the arm and require extra adjustments to fit different sizes of paretic limbs due to its design complexity. To date, many end-effector-based and exoskeleton-based robots have been developed to facilitate upper limb stroke rehabilitation, and Table 2.4 summarises the main features of some of them.

2.4 Robotic Interfaces Used in this Thesis

The present research hypothesised that the EEG correlates of fatigue during robot-mediated interactions are specific to the physical or cognitive nature of the task and the differences in the usage of the proximal and distal upper limb. Three robot-mediated interactions, including gross motor, fine motor and visuomotor tracking tasks, were considered to evaluate this hypothesis. HapticMASTER is an end-effector robot that can be customised to provide arm reach/return (gross motor) and visuomotor tracking tasks. Therefore, the HapticMASTER was selected to provide gross motor and visuomotor tracking tasks that mainly involved moving and coordinating the upper limb's proximal joints and muscles (shoulder and arm). In contrast, the SCRIPT passive orthosis is an exoskeleton-based robot designed to perform fine motor skill retraining exercises, including hand open/close. Therefore, SCRIPT passive

Table 2.4: Summary of upper limb robot-mediated stroke rehabilitation

Robotic device	Type	DOF assisted	Supported upper limb segments	Movements	Control type	Sensors	Therapy modalities supported	Features
ARMin III (Nef et al., 2009)	Exoskeleton-based	4 active and 2 passive	Shoulder + elbow	elbow flexion/extension, spatial shoulder movements (flexion/extension, internal/external rotation and abduction/adduction), wrist flexion/extension, forearm pronation/supination	Impedance control paradigm	Position and force	Active, active-assistive and passive	Allows precise joint actuation and complex motions of the distal and proximal arm; can easily be used for left and right arms; facilitates patient-cooperative arm therapy; allows different training modes: passive mobilization, active ADL-training (ADL means activities of daily living) and active game therapy; provides visual and auditory feedback; gravity compensated; backdrivable; commercialised as ARMEO Power.
Assisted Rehabilitation and Measurement Guide (ARM-Guide) (Reinkensmeyer et al., 1999)	End-effector-based	1 active	Shoulder + elbow	Reaching and retrieval movements along a straight line	Not specified	Position and force	Passive, active-assistive and resistive	A simple and relatively inexpensive system; consists of a linear constraint that can be oriented in different directions to facilitate repetitive reaching and retrieval movement via a custom splint that rides along the linear constraint; provides visual or auditory feedback.
BI-MANU-TRACK (Hesse et al., 2003)	End-effector-based	1 active	Forearm + wrist	wrist flexion/extension and forearm pronation/supination	Impedance control paradigm	Position and force	Passive, active-assistive, active-resistive and bilateral	Facilitates mirror image movements; consists of two handles and two arm troughs in which the forearms are placed while keeping elbow bent at 90^0; facilitates individual resistance, speed, and amplitude settings.
GENTLE/S (Loureiro et al., 2003)	End-effector-based	3 + 1 active and 2 passive	Shoulder +forearm + wrist + hand	Reaching and retrieval movements in 3D space, elbow pronation/supination and wrist flexion/extension	Admittance control paradigm	Position and force	Active, active-assistive and passive	Facilitates reaching and retrieval movements in a 3D workspace the of 3-DOF HapticMASTER robot; consists of a passive 3 DOF gimbal mechanism to which the patient's arm is connected via a wrist orthosis; uses an elbow orthosis suspended from the overhead frame to eliminate the effects of gravity and to address the problem of shoulder subluxation; utilises task-oriented virtual reality interfaces providing haptic, visual, auditory and performance feedback to enhance patient's motivation.
Neuro-Rehabilitation-roBot (NeReBot) (Rosati et al., 2007)	End-effector-based	3 active	Shoulder + elbow	spatial movements (flexion/extension, pronation/supination, adduction/abduction, circular) of shoulder and elbow	-	-	Passive and active-assistive	Based on direct-drive wire actuation, reduced complexity, high robot compliance, high reliability and safety in comparison to other devices; facilitates therapy in both sitting and supine (in bed) positions; transportable; provides visual and auditory feedback; arm trajectory can be set by simple teaching-by-showing procedure.
Mirror Image Movement Enhancer (MIME) (Lum et al., 2006)	End-effector-based	3 active	Shoulder + elbow	Reaching movement	-	Position and force	Passive, active-assistive, active-constrained and bilateral	First robotic system designed to provide both unilateral and bilateral therapies; consists of two forearm splints: one splint is attached to a 6 DOF Puma 560 robot manipulator and applies forces/torques to the the paretic limb while the other connects the non-paretic limb to a 6 DOF position digitiser; forearm splint restricts the wrist and hand movement.
MIT-MANUS (Planar module) (Krebs et al., 1998)	End-effector-based	2 active	Shoulder + elbow	2D elbow and forearm motion	Impedance control paradigm	position, velocity, force	Active, active-assistive and passive	Portable; low end-point impedance; consists of a direct-drive five bar-linkage selective compliance assembly robot arm; first robot to introduce game-like exercises to the patient with feedback displayed in a computer; capable of recording motions and mechanical quantities (applied force, position, and velocity), first system to be commercialized as InMotion^2 Shoulder-Elbow Robot.
MIT-MANUS (Wrist module) (Krebs et al., 2007)	End-effector-based	3 active	Wrist	abduction/adduction, flexion/extension, and pronation/supination of the wrist	Impedance control paradigm	position, velocity, force	Active, active-assistive and passive	Can be operated standalone or mounted at the end of the MIT-MANUS (Planar module); allows five active DOF at the shoulder, elbow, and wrist; low end-point impedance; replicates a range of motions that are similar to normal wrist movements; therapy is administered through interactive video games by mapping the 3-DOF movement of the wrist robot to the 2D graphical display.
Supervised Care and Rehabilitation Involving Personal Tele-robotics (SCRIPT) Passive Orthosis (Amirabdollahian et al., 2014)	Exoskeleton-based	-	Forearm + wrist + hand + fingers	wrist flexion/extension and pronation/supination, finger flexion/extension and thumb abduction/adduction allowing hand gestures, and translational movements of the forearm	-	position and flexible bending sensors (measure both the finger movement and the applied force)	-	A passively actuated, wrist, hand and finger orthosis developed to provide self-administrated home-based stroke rehabilitation for hand and wrist; can passively offset the excessive involuntary flexion torques caused by spasticity and abnormal synergies; consists of forearm shell, hand plate and individual finger (digit) caps to physically interface with the forearm, hand and fingers of the paretic arm, respectively; consists of passive leaf springs and elastic tension cords to apply the external extension torques on the fingers, the double parallelogram between forearm shell and hand plate to allow wrist flexion/extension while preventing other wrist movements, integrated measurements units to estimate forearm posture, a microcontroller board to sensor readings and conversions, two user interfaces to be used by the patient and health care professionals, and virtual reality exercise with audio, visual and performance feedback.
Therapy-Wilmington Robotic Exoskeleton (T-WREX) (Sanchez et al., 2004)	Exoskeleton-based	5 passive	Shoulder + elbow	-	-	position and grip (detects hand grip pressure)	-	A passive, body powered arm orthosis with no robotic actuators; facilitates functional task training by means of different virtual reality exercises with audio and visual feedback; provides objective feedback of task performance at the end of each game; gravity and arm weight mitigated.

orthosis was selected to provide fine motor interactions that mainly involved the movement and coordination of the upper limb's distal joints and muscles (wrist, fingers, and hand). The following subsections provide a detailed review of the operational mechanisms of both devices while introducing control strategies based on haptic interfaces.

2.4.1 Haptic Interfaces

Haptic interfaces are devices that enable human-robot interaction by accommodating the sense of touch. The term '*haptics*', derived from the Greek verb '*haptesthai*' meaning '*to touch*', refers to the ability to sense a natural or synthetic mechanical environment through touch (Hayward et al., 2004). Based on the underlying sensory inputs, the human sense of touch mainly comprises of two sub-modalities, namely *cutaneous* and *kinesthetic*. The cutaneous sense receives sensations such as temperature, pain, pressure from receptors embedded in the skin, while the kinesthetic sense receives sensory inputs related to the feeling of motion (such as position, movement, weight) from the receptors within muscles, tendons and joints (Dahiya and Valle, 2012; El Saddik et al., 2011; Otaduy and Lin, 2006). In human-robot interaction, haptic feedback encompasses both tactile (cutaneous) and kinesthetic (force) feedback. Haptic devices initially track the physical manipulation by the human operator on the device (input) and then provide feedback to the operator (output) depending on the interaction in the virtual world. Two control paradigms, namely impedance control paradigm and admittance control paradigm, which differs from each other by the type of input and output, are widely used in haptic interface design.

A. Impedance control paradigm

Hogan first introduced the impedance control paradigm in 1985 (Hogan, 1985). In the impedance control paradigm, the motion exerted by the user is measured, and the reaction force is fed back to the user by the haptic device if a virtual object is met (der Linde et al., 2002; Wen et al., 2008). Hence, from the haptic device point of view, *displacement is the input and force is the output*. Impedance control devices are by nature lightly built and highly backdrivable with low friction and inertia (Abbott et al., 2007; der Linde and Lammertse, 2003). The Touch™, Touch X, Phantom® Premium™ haptic devices from 3D Systems[1] utilizes the impedance control paradigm.

[1] https://www.3dsystems.com/haptics

B. Admittance control paradigm

Admittance control devices generate positional changes according to the force exerted by the operator on the device (der Linde and Lammertse, 2003; Wen et al., 2008). As a result, in the admittance control paradigm, *the force acts as the input providing a displacement as the output*. Therefore, it can be seen as the inverse of the impedance control paradigm. Admittance control allows considerable freedom in the mechanical design of the device since tip inertia and backlash can be eliminated. Therefore, admittance control devices are quite robust and are capable of displaying high force and high stiffness (Abbott et al., 2007; der Linde and Lammertse, 2003). The HapticMASTER (der Linde et al., 2002) is an example for an admittance control device.

2.4.2 HapticMASTER

The HapticMASTER, manufactured by FCS Control Systems (now known as Motekforce Link), is a high-performance haptic device that is specially designed for interacting with the human hand. The HapticMASTER operates under the admittance control paradigm. Thus, the robot controls the displacement (i.e. position, velocity, and acceleration) depending on the force applied by the user and is capable of rendering high stiffness, high forces and high force sensibility. Hence, effective and interactive upper limb therapy sessions with haptic sensation can be designed using the HapticMASTER software architecture.

A. Hardware Arrangement

The HapticMaster hardware mainly consists of the robot arm and the control box (der Linde and Lammertse, 2003; der Linde et al., 2002) (Figure 2.12). The robot arm serves as the actual force display while the control box houses the required electronics such as the haptic server, motor amplifiers, and safety relays. A sensitive strain gauge force sensor attached to the front end of the robot arm (right after the end effector) measures the interaction force applied by the user. The robot arm mechanism facilitates zero backlashes to avoid adverse vibration effects, but this feature results in some increased friction in the robot arm joints. In order to ensure smooth motion at the end effector, this friction is completely eliminated up to the accuracy of the force sensor by the HapticMASTER control loop. The actuators of the HapticMASTER enables three different movements: base rotation, arm up/down, and arm in/out, as illustrated in Figure 2.13. The actuator arrangement allows a 3 degree of freedom at the end effector and creates a volumetric workspace of approximately 80 litres. The workspace uses a right-handed Cartesian coordinate system, as depicted in Figure 2.14. In addition, exchangeable end effectors can be mounted according to different applications.

The haptic server is a dedicated PC with a VxWorks© real-time operating system. Both haptic render and the robot control loop run on the haptic server at a fixed update rate of 2500 Hz, enabling smooth and realistic haptic experience.

B. Control Algorithm

The HapticMaster utilizes an admittance control algorithm as depicted in Figure 2.15 (der Linde et al., 2002). The force exerted by the user is measured and is converted to a position/velocity/acceleration set-point vector by a virtual model, considering the virtual motion that this force would result on an object in space. The virtual model defines the space in which the object lives (e.g. environmental friction, gravity, etc.) as well as the object properties (e.g. mass, stiffness, damping friction, etc.) (der Linde and Lammertse, 2003). The position/velocity/acceleration vector is commanded to the robot realised by a PID servo control servo loop (der Linde and Lammertse, 2003) and the movement of the robot arm is made. The control loop cancels the actual mass and the friction of the device, and a small amount of virtual mass will be presented instead to avoid commanding infinite accelerations.

C. Application Programming Interface

The HapticMASTER is programmed using an application programming interface (API) known as HapticAPI, which is written using the C++ programming language. HapticAPI enables the user to create and manipulate the virtual environment and to control the internal state machine via an Ethernet connection with the HapticMASTER. Haptic effects like spring effects, damper effects, constant force effects, or any combination of them can be added to the virtual haptic world. The virtual world created using haptic objects like spheres, cubes, cones is rendered graphically on the screen by the Open Graphics Library (OpenGL) graphics engine (Ruiter, 2003).

D. GENTLE/S Rehabilitation System

The GENTLE/S rehabilitation system (Amirabdollahian et al., 2007; Coote et al., 2008; Loureiro et al., 2001, 2003) illustrated in Figure 2.16 is designed to provide challenging and motivating upper limb rehabilitation to stroke patients in conjunction with HapticMASTER and virtual reality techniques. A gimbal end effector mounted on the HapticMASTER, as shown in Figure 2.17 enable patients to interact with the haptic environment without grasping the end effector. Three passive rotational degrees of freedom of the gimbal allows flexion and extension of the wrist as well as the pronation and supination of the elbow. Patient's hand is attached to the robot arm by a wrist-orthosis that is connected to the gimbal

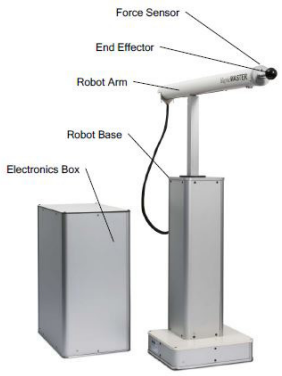

Figure 2.12: HapticMASTER system overview (Ruiter, 2003).

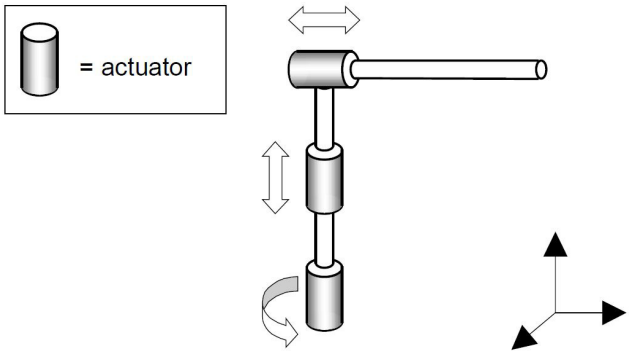

Figure 2.13: The actuator arrangement and the kinematics of the HapticMASTER (der Linde et al., 2002).

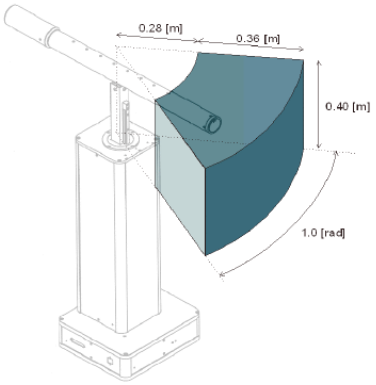

(a) 3D volumetric workspace (der Linde et al., 2002).

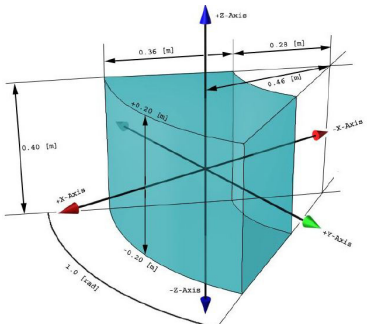

(b) 3D volumetric workspace x, y, z coordinates (Ruiter, 2003).

Figure 2.14: 3D volumetric workspace of the HapticMASTER.

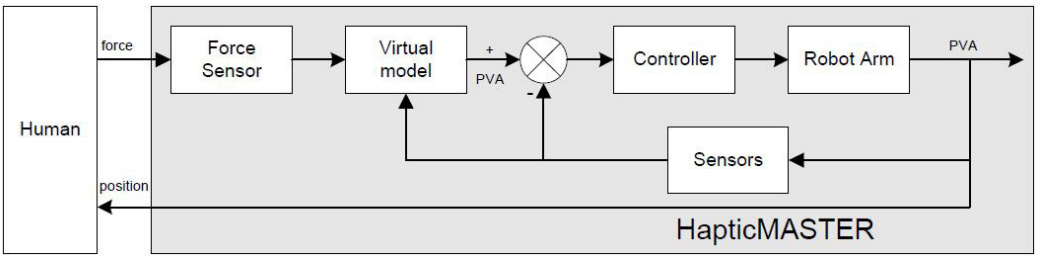

Figure 2.15: The general control scheme used by the HapticMASTER (der Linde et al., 2002).

end effector via a magnetic quick-attach/quick-release mechanism. The elbow-orthosis suspended from the overhead frame (Figure 2.18) is used to support the arm by eliminating the effects of gravity. This ensures user comfortability during the therapy session. Moreover, a harness arrangement is attached to the chair to restrain the user's trunk movement. Three virtual environments (empty room, real room (Figure 2.19) and Joaquim's room) of varying complexity are designed to provide arm reaching-returning exercise. A detailed description of the game interfaces is given in (Loureiro et al., 2003).

The robot arm is controlled in a straight line trajectory (the configuration of the user's wrist in the space) with the minimum jerk (the change of acceleration with respect to time, i.e. the third time derivative of the position) using a model derived from the 7^{th} order polynomial given in equation 2.1,

$$p = a + b\tau + d\tau^3 + f\tau^5 + h\tau^7; \quad where - 1 < \tau < 1 \tag{2.1}$$

and the polynomial coefficients are calculated as,

$$a = \frac{(p|_{\tau=-1} + p|_{\tau=1})}{2} \qquad b = \frac{15}{16}(p|_{\tau=1} - p|_{\tau=-1})$$
$$d = \frac{35}{16}(p|_{\tau=1} - p|_{\tau=-1}) - 3b \qquad f = 3b - \frac{21}{8}(p|_{\tau=1} - p|_{\tau=-1})$$
$$h = \frac{15}{16}(p|_{\tau=1} - p|_{\tau=-1}) - b$$

Here $p|_{\tau=-1}$ and $p|_{\tau=1}$ denote the start and end point position of the movement respectively. A detailed description of the point-to-point generalised minimum jerk approach is given in (Amirabdollahian et al., 2002). The robot end-effector is connected to a virtual spring-damper combination, as shown in Figure 2.20. This virtual configuration constrains the movement of the bead along the pathway defines by the minimum jerk polynomial. The start and end positions of the points, the duration of the movement between two points, spring stiffness, and damping coefficient can be varied depending on the therapeutic needs of the patient.

Three different therapeutic modes are implemented in GENTLE/S system as described below.

- Patient passive therapy:
  In this mode, HapticMASTER moves the patient's arm attached to the gimbal on a predefined trajectory while the patient remains passive. When the patient's arm reaches the target, the movement pauses momentarily and then proceeds to the next segment of the movement. This mode is designed for early-stage stroke patients who cannot move their arm alone.

Figure 2.16: The GENTLE/S rehabilitation system (Amirabdollahian et al., 2007)

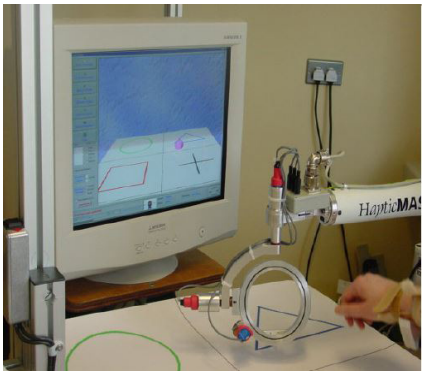

Figure 2.17: Gimbal end effector mounted on the HapticMASTER (Loureiro et al., 2001)

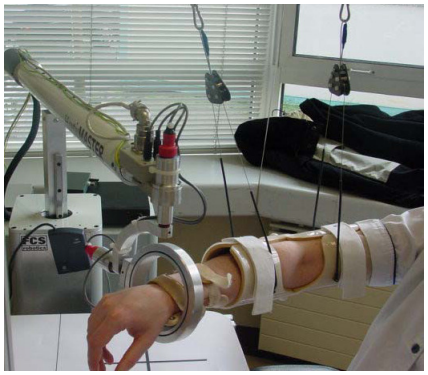

Figure 2.18: Elbow-orthosis used to deweight patient's hand (Loureiro et al., 2001)

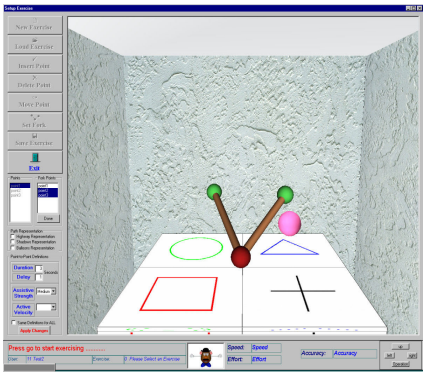

Figure 2.19: GENTLE/S virtual environment (Amirabdollahian et al., 2007)

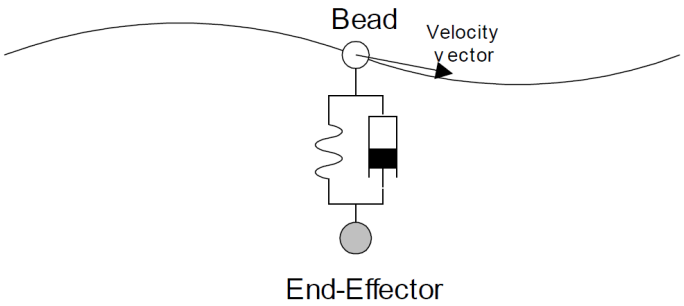

Figure 2.20: Spring-damper combination (Loureiro et al., 2003)

- Patient active-assisted therapy:
  Here the patient has first to initiate the movement, and then the HapticMASTER helps to move along the defined trajectory within a set duration. This mode encourages patients to initiate movement, although they are unable to move without assistance.
- Patient active therapy:
  The patient active mode is implemented for patients who can perform arm movement but lack arm coordination or power. Hence, in this mode, patients have to initiate the movement and reach the target point by themselves. The robot stays passive and only assists the users if they have deviated from the predefined path. No time limitation is provided for the patient to complete the movement between two points, and the spring-damper combination provides the error correction when the patient's hand has deviated from the defined pathway.

E. GENTLE/A Rehabilitation System

The GENTLE/A ('A' for Adaptive) rehabilitation system (Chemuturi et al., 2013*a*) is a successor of the GENTLE/S rehabilitation system. In comparison to the GENTLE/S system, this system can change the assistance/resistance offered by the robot during a therapy based on the contribution of the participant. The GENTLE/A rehabilitation system uses the HapticMASTER similar to the GENTLE/S rehabilitation system to provide robot-mediated therapy, but the gimbal end effector is replaced with the standard end effector that comprises a simple ball grip. This system also inherits the minimum jerk trajectory model (equation 2.1) to create a reference pathway between two points in the workspace. The system is programmed to work in patient active, active-assisted and passive modes with the addition of a lead-lag performance model. Chemuturi et al. (2013*a*) provides a detailed description about the lead-lag performance model. As illustrated in Figure 2.21, the virtual reality interface of GENTLE/A system consists of 12 virtual balls that are placed in the corners of a cube (points on a cube). This interface facilitates different combinations of movements, including reach-return, ground level-against gravity-towards gravity movements.

2.4.3 SCRIPT Passive Orthosis

The SCRIPT (Supervised Care and Rehabilitation Involving Personal Tele-robotics) [2] passive orthosis is a custom-made wrist, hand and finger orthosis, developed to provide home-based stroke rehabilitation. The SCRIPT passive orthosis can passively offset the excessive involuntary flexion torques caused by spasticity and abnormal synergies, so that the individuals can

[2] http://scriptproject.eu/

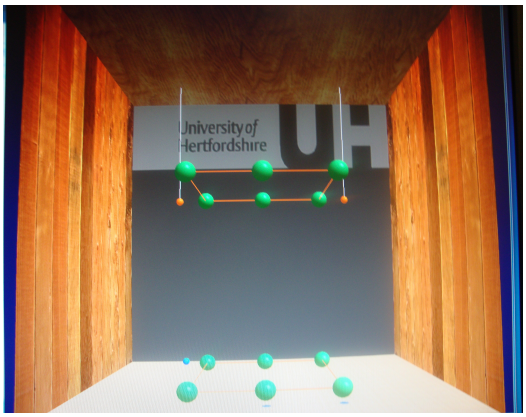

Figure 2.21: The GENTLE/A virtual environment. Green balls represented source and target points (Chemuturi et al., 2013*a*)

actively engage with the therapeutic environment using their impaired arm (Amirabdollahian et al., 2014). The components of the SCRIPT passive orthosis is illustrated in Figure 2.22. The forearm shell, the hand plate and individual finger (digit) caps of the orthosis are used to physically interface with the forearm, hand and fingers of the users respectively. The hand plate prevents overextension of the metacarpophalangeal (MCP) joint and the finger caps blocks most of the distal interphalangeal (DIP) rotations (Ates et al., 2013). The double parallelogram mechanism between forearm shell and the hand plate (Figure 2.23a) allows wrist flexion/extension while preventing other wrist movements. The rotary potentiometer attached to the wrist double parallelogram is used to measure the wrist flexion/extension. The pronation/supination at the wrist and the translational movement of the forearm are measured by an inertial measurement unit (Ates et al., 2014). Furthermore, external torque to assist the extension of each finger is applied via a leaf spring that is connected to the corresponding finger cap through an elastic tension cord (Leon et al., 2014) (Figure 2.23b). The external extension forces on the fingers and the wrist can be adjusted by tensioning the elastic cord more or less using the tension-cord stops on the top of the hand plate. Also, the freedom of movement of the finger relative to the leaf spring is controlled by the tension cord. Finger abduction/adduction and thumb opposition are also possible due to the use of elastic tension cords, but these movements are not supported nor sensed by the SCRIPT passive orthosis (Leon et al., 2014).

The resistive flex sensors[3] attached to each leaf spring measure the flexion of the corresponding finger with approximately 1-degree resolution. The rotation of MCP, PIP (Proximal Interphalangeal), and DIP joints are estimated using equations 2.2 and 2.3 with the assump-

[3]Spectra Symbol, SEN-10264, 55 [mm]

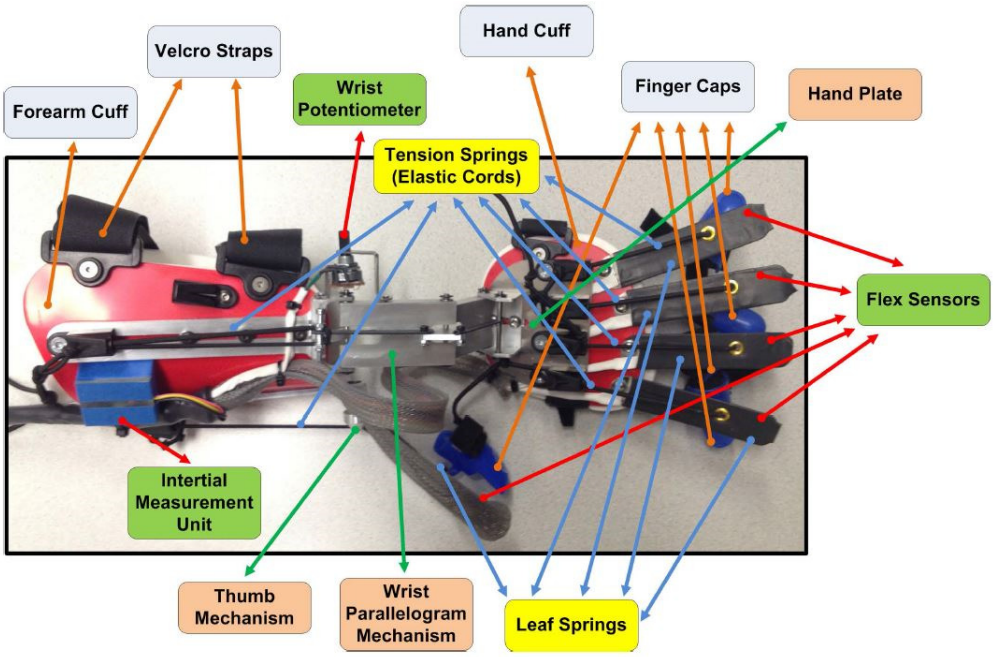

Figure 2.22: SCRIPT Passive Orthosis (Ates et al., 2013)

(a) Wrist mechanism

(b) Finger mechanism

Figure 2.23: SCRIPT passive orthosis wrist and finger mechanisms (Ates et al., 2013)

tions that there is no dead signal zone[4] with the flex sensors and rotation of each phalanx is linear and covers the full range of motion except the distal phalanx.

$$\theta_{joint}(k = \theta_{joint\,max}.|BSensor_{norm}(k) - 1| \tag{2.2}$$

$$BSensor_{norm}(k = \frac{BSensor(k) - BSensor_{min}}{BSensor_{max} - BSensormin} \tag{2.3}$$

In equation 2.2 $\theta_{joint}(k)$ and $\theta_{joint\,max}$ refer to estimated rotation of joints and maximum rotation of joints in degree respectively. The index *joint* refers to a set of variables, {MCP, PIP, DIP}. The flex sensor reading at sample k is denoted by $BSensor(k)$ and the indices *max*, *min*, and *norm* refers to maximum, minimum and normalized values of *BSensor*. The $BSensor_{min}$ and $BSensor_{max}$ are measured while all fingers are stretched on a flat surface and while the user performs a full grasp without any object respectively. Arduino Nano microprocessor board is used to sample the flex sensor readings and the potentiometer output of the wrist mechanisms, and also to send the sampled data to the main PC where the SCRIPT games reside. The 3D position of the hand in space is measured by optically tracking a green colour spherical marker placed on the hand plate of the orthosis (Nijenhuis et al., 2016).

The SCRIPT system enables self-administrated home-based therapy for hand and wrist. Since the SCRIPT passive orthosis can assist and sense different finger, hand, wrist and arm motion (finger flexion/extension, thumb flexion/extension and adduction/abduction, wrist flexion/extension and pronation/supination, and translational movement of the forearm), interactive therapeutic sessions are designed to retrain different hand and wrist gestures. The virtual environment of the game, 'Sea Shell', that is used to retrain hand and wrist movements is shown in Figure 2.24. In this game, the user is put in control of opening and closing a seashell underwater to catch as many fishes. Firstly, the user is required to open hand to open the seashell and keep it ready to catch a fish. The user should open and close the hand when a fish reaches the seashell in order to open and close the seashell, thereby to catch the fish. Also, if the wrist is flexed for a certain threshold duration (50% of the range of motion (Qin, Rahman and Amirabdollahian, 2014)), the seashell goes to sleep mode. Hence, the user needs to bend the wrist up to activate the shell. This feature encourages the patients to perform wrist extension before flexion of the fingers as the stroke patients hands are excessively flexed due to spasticity and abnormal synergies. Each patient exhibits a different range of motion, depending on his/her recovery progress. Therefore, a calibration procedure is included at the beginning of each game, so that the game is adapted to the subject's range

[4] zero offset change of the sensor

of motion. Also, a mobile arm support (SaeboMAS) is used to unweight the proximal arm so that the gravity compensation and fatigue are minimised. The SCRIPT system has two different interfaces available for both patients and the healthcare professionals. The patient user interface allows the user not only to quickly access the games and performance history to monitor progress (game scores and training duration) but also to communicate with the healthcare professionals by sending a message. The user interface available to healthcare professionals enables them to remotely and indirectly monitor the progress of the patient and to provide feedback and assign therapy accordingly (Amirabdollahian et al., 2014). The remote supervision facility could reduce the burden on the patient to visit therapists and has many indirect benefits.

The SCRIPT system has been clinically tested in terms of user acceptance, the actual amount of use, usability and patient motivation and the arm and hand function. The system was successfully used at home by chronic stroke patients with impaired arm/hand function. Although some usability issues are present in the SCRIPT system, the findings in (Nijenhuis et al., 2016) shows that the system is feasible since the patients accepted the training and were motivated to continue therapy at home. In addition, participants also showed improvements in arm and hand function and dexterity after training.

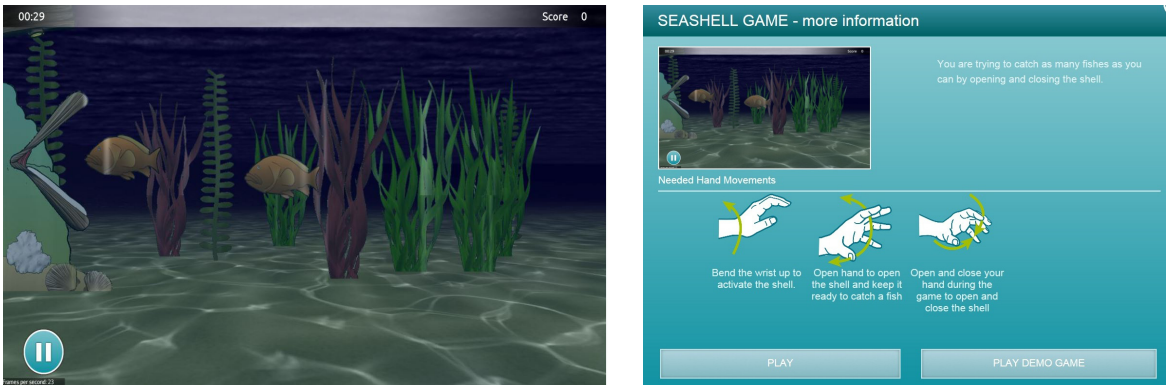

(a) ‘Sea Shell’ game interface

(b) Hand movement instructions

Figure 2.24: ‘Sea Shell’ game interface and hand movement guidelines to operate the sea shell and catch fish.

Chapter 3

EEG Data Processing Pipeline

The present research work was focused on assessing fatigue in robot-mediated interactions using EEG. In this chapter, EEG data processing pipeline followed for each participant and each recording in the two studies conducted is discussed in detail. As shown in Figure 3.1, EEG data processing pipeline adopted for this research mainly consisted of three steps: EEG data preprocessing, EEG feature extraction and statistical analysis.

3.1 EEG Data Preprocessing

EEG data are preprocessed to obtain relatively clean EEG data by removing or reducing the artifactual components. When limited data are available, rejecting EEG segments with artifacts may result in a considerable loss of information. Therefore, DC correction, high-pass and low-pass filtering, bad channel removal, and blind source separation (BSS) by independent component analysis (ICA) were considered in the present work to remove or attenuate the artifacts and improve the signal-to-noise ratio. The following sections will discuss each step taken in detail.

3.1.1 DC Correction

EEG signals can be contaminated with DC offset due to the analogue circuits involved in the data acquisition. The DC offset makes the signals mean amplitude not equal to zero. Hence, the channel-wise mean was deducted from each data point to perform DC correction.

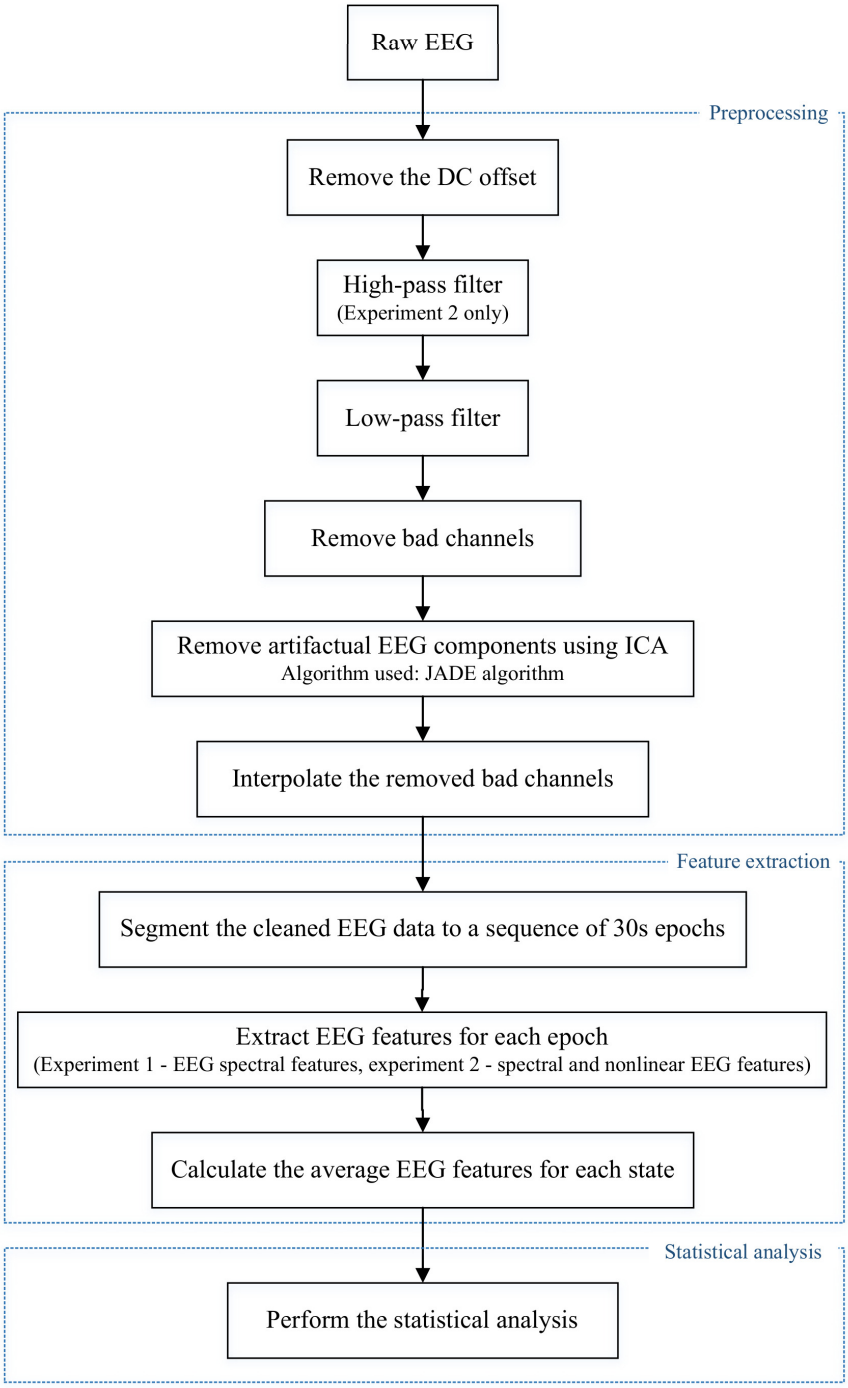

Figure 3.1: EEG data processing pipeline used in this thesis. The dotted box represents the three main steps involved in the pipeline: data preprocessing, feature extraction, and statistical analysis.

3.1.2 Filtering

Filtering can be used to remove or attenuate high-frequency noise components, low-frequency drifts, and electrical line noise mixed in the EEG recording while preserving the signal of interest. Since filtering cause changes to the temporal signal, filter parameters (filter type, cutoff frequencies, order, attenuation, ripple, roll-off) should be selected cautiously considering the effects of filtering on the signal of interest and the application; thereby the signal-to-noise ratio can be improved (Widmann et al., 2015). The characteristics of a filter are described by filter responses (Figure 3.2). The impulse response gives the transfer function of a filter in the time domain. The impulse response shows the filter output when filtering a single very sharp pulse (i.e., an impulse). The filter's characteristics in the frequency domain are described by the Fourier transform of the impulse response (i.e., the frequency response). The frequency response consists of two parts, namely the magnitude and the phase response.

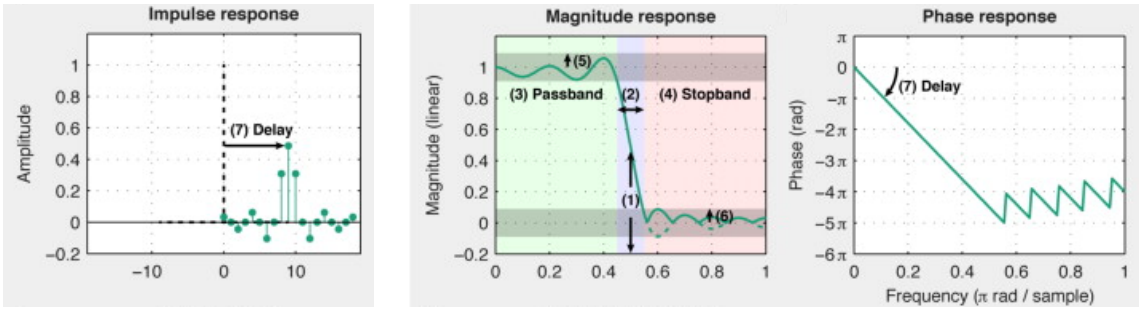

(a) Time domain

(b) Frequency domain

Figure 3.2: Time domain and frequency domain responses of an example filter of order 18 linear-phase finite impulse response (FIR) low-pass filter. Black dashed lines represent the impulse signal. (1) cutoff frequency, (2) transition band, (3) passband, (4) stopband, (5) passband ripple, and (6) stopband attenuation. (Widmann et al., 2015)

The cutoff frequency characterises a boundary between the passband and stopband of the filter. Depending on the type of the filter, the -3dB (half-energy) cutoff or -6dB (half amplitude) cutoff are used when designing a filter. The transition region between passband and stopband is defined as the transition band. The cutoff frequency always lies in the transition band. The roll-off is the slope of the magnitude response in the transition band. Filters with a shallow roll-off have a wide transition band whereas filters with a steep roll-off have a narrow transition band. Frequency bands in the passband ideally have magnitude values of one, whereas the frequency bands in the stopband ideally have zero magnitude values. Hence, the spectral components in the passband pass without changing the amplitude, whereas the spectral components in the stopband are completely removed. However, digital filter

characteristics usually deviate from the ideal filter characteristics (zero/one) depending on the design criteria. The deviation in the passband and stopband are known as passband ripple and stopband attenuation. For example, with a passband ripple of 0.002, the filter output in the passband does not amplify or attenuate the signal by more than 0.2%. With a stopband attenuation of -60 dB (or 0.001), the signal in the stopband is attenuated by a factor of 1000. Passband ripple of 0.002-0.001 (0.2-0.1%) and stopband attenuation of -54 to -60 dB can be chosen for EEG signal processing (Widmann et al., 2015). Filtering also introduces a delay in the output signal relative to the filter input. However, a zero-phase delay can be achieved using the '*filtfilt*' function in MATLAB.

High-pass, low-pass, band-pass and band-stop filters are commonly used in EEG signal processing. In high-pass filtering, signals with frequencies below the defined cutoff frequency are attenuated. Therefore, a high-pass filter with a cutoff frequency of 0.1 or 0.5 Hz is useful and recommended to minimise slow drifts. Furthermore, since the edge artifact of a 0.5 Hz high-pass filter may last up to 6s, high-pass filters should be applied on the continuous data before segmented into epochs (Cohen, 2014). The frequencies above the defined cutoff frequency are attenuated with the use of low-pass filters, thereby smoothing the filter output. In band-pass filtering, signals with frequencies within the given frequency band are passed while the signals outside the range are attenuated, and the opposite is true in band-stop filters. A separate successive application of a steep high-pass filter and a shallow low-pass filter is preferred in electrophysiology instead of a band-pass filter (Widmann et al., 2015). In addition, a notch filter is widely used to suppress line noise (50/60 Hz). A notch filter is a bandstop filter which attenuates signals over a narrow range of frequencies.

There are two types of digital filter implementations, namely, *infinite impulse response (IIR)* and *finite impulse response (FIR)* filters. The cutoff frequency of IIR filters is usually defined as -3 dB cutoff, whereas the cutoff frequency of FIR filters is usually defined as -6 dB cutoff. Butterworth IIR filters have no passband and stopband ripples and have a shallow roll-off in comparison to Chebyshev and elliptic IIR filters. Elliptic filters have a steep roll-off near the cutoff frequency and also have ripple in both the passband and the stopband. Chebyshev filters have a steeper roll-off. Chebyshev Type I filters only allow ripple in the passband, whereas the Chebyshev Type II filters have ripple only in the stopband.

In this research work, both high-pass and low-pass filtering was considered when preprocessing EEG data in experiment 2, whereas only low-pass filtering was considered in experiment 1. The characteristics of the filters used in the two experiments are given in Chapter 4 and 5, respectively.

3.1.3 EEG Bad Channel Removal and Interpolation

An EEG electrode is considered as a bad channel when the EEG data recorded from that electrode has a low signal-to-noise ratio or very low or no signal throughout a considerable time span (Pedroni et al., 2019). Changes in the electrode-skin interface impedance or displacement of an electrode due to head or body movement during the recording session may cause bad channels. Since bad channels are localised to specific electrodes, it is more sensible to exclude the bad channel from the original EEG data and interpolate the EEG signal of that channel by combining the signals.

In this research work, bad channels were identified and removed after filtering the DC corrected EEG data. Following the removal of remaining artifacts using ICA, the missing channels were interpolated using the spherical spline interpolation procedure ('*eeg_interp*' function) which is implemented in EEGLAB toolbox (Debnath et al., 2020).

3.1.4 Blind Source Separation by Independent Component Analysis

A. Blind Source Separation (BSS)

Blind source separation (BSS) is a signal processing methodology used to recover the underlying source signals from a set of sensor observations, where the mixing matrix is unknown. In general, each sensor records a different mixture of source signals when the sensors are spatially separated (i.e., placed in different locations). The term 'blind' means that neither the source signals are observed, nor the information about how the signals were mixed is available (Cardoso, 1998). Therefore, estimating the original source signals exactly is not possible. However, the source signals can be estimated up to certain indeterminacies, i.e., the estimated source signals preserve the waveforms of the original source signals, but there exist permutations, arbitrary scaling and change in signs. As the most relevant information about the source signals are contained in the time-frequency patterns or the temporal waveforms of the source signals, the change in the signal amplitudes or the order in which they are arranged in the output of the system has a negligible effect in most applications of BSS (Naik and Kumar, 2011).

BSS is best explained by the 'cocktail-party problem', where one can selectively listen to, and follow one speaker in the presence of many people talking simultaneously with background noise and loud noise. This psychoacoustic phenomenon was first proposed by Colin Cherry (Cherry, 1957). For instance, assume that two people are speaking simultaneously in a room and two microphones are placed in two different locations. The time-series data recorded by the two microphones (observations) are a weighted sum of the speech signals emitted by

the two speakers (sources) and it is of interest to separate each voice into a separate speaker channel for better understanding. This is the goal of BSS (Hyvärinen and Oja, 2000). If the amplitudes of the recorded signals at time point t are denoted by $x_1(t)$ and $x_2(t)$, then the linear mixing equation could be expressed as:

$$\begin{aligned} x_1(t) &= a_{11}s_1(t) + a_{12}s_2(t) \\ x_2(t) &= a_{21}s_1(t) + a_{22}s_2(t), \end{aligned} \tag{3.1}$$

where $s_1(t)$ and $s_2(t)$ represents the signals emitted by the two speakers (sources) and a_{11}, a_{12}, a_{21}, and a_{22} represents the mixing weights (coefficients) that depend on the distances between the speakers and the microphones. Here both the source signals and the mixing coefficients are unknown. Thus, BSS is used to find the original acoustic signals generated by each speaker, $s_i(t)$ from the recorded mixtures $x_i(t)$. The lack of prior information about the mixture is compensated by the assumption of statistical independence of the source signals (Cardoso, 1998). An illustration of the above-mentioned signal decomposition process is shown in Figure 3.3.

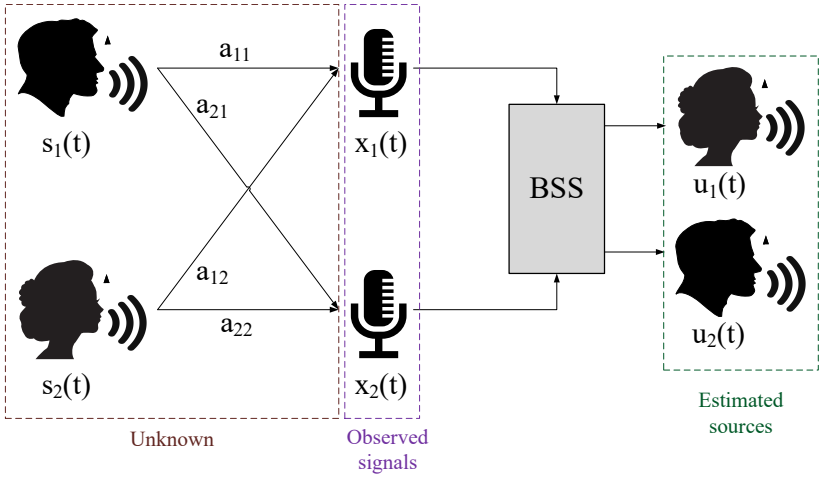

Figure 3.3: Illustration of source separation in the 'cocktail-party problem'.

The simplest BSS model can be represented by the mixing equations:

$$\mathbf{x}(t) = \mathbf{A}\mathbf{s}(t), \tag{3.2}$$

where $\mathbf{x}(t) = [x_1(t), x_2(t), x_3(t), \ldots, x_n(t)]^T$ is an $n \times 1$ column vector representing the observed signals, and $\mathbf{s}(t) = [s_1(t), s_2(t), s_3(t), \ldots, s_n(t)]^T$ is also an $n \times 1$ column vector representing a finite number of independent source signals. Here $[\ldots]^T$ means transpose of a row vector. In addition, $\mathbf{A}$ is the square $n \times n$ 'mixing matrix' that contains the mixing weights or

the mixture coefficients as:

$$\mathbf{A} = \begin{pmatrix} a_{11} & a_{12} & a_{13} & \cdots & a_{1n} \\ a_{21} & a_{22} & a_{23} & \cdots & a_{2n} \\ \vdots & \vdots & \ddots & \ddots & \vdots \\ a_{n1} & a_{n2} & a_{n3} & \cdots & a_{nn} \end{pmatrix}. \tag{3.3}$$

The aim of BSS is to compute a $n \times n$ separation matrix, $\mathbf{W}$, with the coefficients w_{ij}, such that an estimate of the source signal vector, $\mathbf{u}(t)$, can be separated using only the observed signal vector, $\mathbf{x}(t)$ by considering the statistical independence of the source signals. Using vector-matrix notation, this signal decomposition can be expressed as:

$$\mathbf{u}(t) = \mathbf{W}\mathbf{x}(t). \tag{3.4}$$

Here the recovered source signals are identical to the original source signals up to permutations and changes of scales and signs (Cardoso, 1998). The block diagram in Figure 3.4 illustrates both mixing and separation processes involved in BSS.

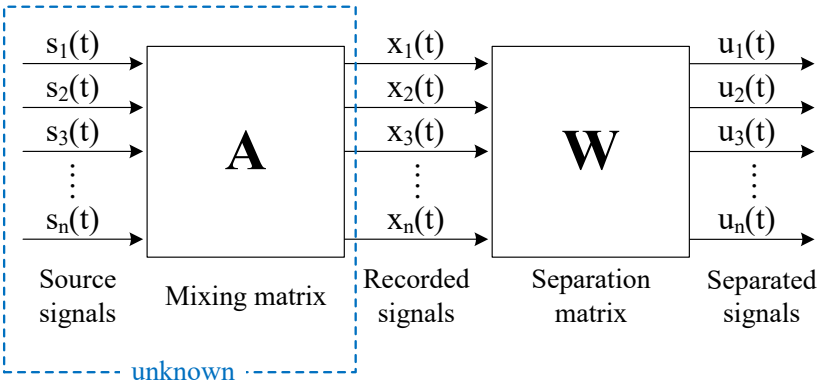

Figure 3.4: Block diagram illustrating the blind source separation. The $\mathbf{s}(t)$ are the source signals, $\mathbf{x}(t)$ are the recorded signals, $\mathbf{u}(t)$ are the separated source signals, $\mathbf{A}$ is the mixing matrix and $\mathbf{W}$ is the separation matrix.

BSS techniques are successfully used in many applications including processing biomedical signals such as EEG (Congedo et al., 2008; Jung et al., 2000; Peterson et al., 2005; Vázquez et al., 2012; Vorobyov and Cichocki, 2002), ECG (Castells et al., 2005; Zarzoso et al., 1997) and magnetoencephalograms (Escudero et al., 2007, 2008), speech recognition and enhancement in noisy environments (Kokkinakis and Loizou, 2008; Rahbar and Reilly, 2005), analysis of mechanical signals such as vibration and engine noise for fault detection and diagnosis (Li et al., 2001; Roan et al., 2002). In this thesis, BSS is used to remove

artifacts in recorded EEG data. Among the several techniques developed to perform BSS, independent component analysis (ICA) is one of the most widely used BSS technique to separate artifactual EEG components from data recorded from the scalp (Jung et al., 1998, 2000; Makeig et al., 1996). Hence, the following section gives an overview of the ICA model and how it can be applied to EEG artifact correction.

B. Independent Component Analysis (ICA)

Independent component analysis (often abbreviated as ICA) is a most promising approach to solve the BSS problem (Hyvärinen and Oja, 2000). ICA is essentially a method used to recover a set of n independent source signals from $m \geq n$ observed instantaneous mixtures of these source signals. If we denote the n independent source signals at time t by a $n \times 1$ vector $\mathbf{s}(t)$ and the observed signals (sensor outputs) by a $m \times 1$ vector $\mathbf{x}(t)$, the mixing model can be written as,

$$\mathbf{x}(t) = \mathbf{A}\mathbf{s}(t), \tag{3.5}$$

where the $m \times n$ matrix $\mathbf{A}$ represents the 'mixing matrix':

$$\mathbf{A} = \begin{pmatrix} a_{11} & a_{12} & a_{13} & \cdots & a_{1n} \\ a_{21} & a_{22} & a_{13} & \cdots & a_{2n} \\ \vdots & \vdots & \vdots & \ddots & \vdots \\ a_{m1} & a_{m2} & a_{13} & \cdots & a_{mn} \end{pmatrix}. \tag{3.6}$$

The elements in each row of $\mathbf{A}$ corresponds to the contributions from each source signal to each observation (i.e., $x_i(t) = \sum_{j=1}^{n} a_{ij} s_j(t)$ for all $i = 1$ to m).

The ICA model is a generative model as it describes how the observed data are generated by the process of mixing independent source signal components (Hyvärinen and Oja, 2000). The independent source signal components are latent source signals, meaning that they cannot be directly observed. Moreover, the mixing coefficients, a_{ij}, are also unknown. Therefore, both the mixing matrix coefficients and the original source signals need to be estimated. The objective of ICA is to find a separating matrix, i.e., a $n \times m$ matrix $\mathbf{W}$ such that:

$$\mathbf{u}(t) = \mathbf{W}\mathbf{x}(t) \tag{3.7}$$

is an estimate of the original source signals. The elements in the $n \times 1$ vector $\mathbf{u}(t)$ are known as independent components (ICs). The independent components obtained by this model are

identical to the original source signals up to permutations and changes of scales and signs (Cardoso, 1998).

ICA assumptions

When performing ICA, the following assumptions are made (Naik and Kumar, 2011; Ullsperger and Debener, 2010).

- The source signals are statistically independent.
  Random variables $s_1, s_2, \ldots, s_n$ are said to be independent if information on the value of s_i does not give any information on the value of s_j for $i \neq j$. Mathematically, statistical independence can be defined by the probability densities. If the joint probability density function of the s_i is denoted by $p(s_1, s_2, \ldots, , s_n)$ and the marginal probability density functions of s_i are denoted by $p_i(s_i)$ for all $i = 1 : n$, then the random variables s_i are said to be independent if and only if $p(s_1, s_2, \ldots, , s_n) = p_1(s_1)p_2(s_2)\ldots p_n(s_n)$, i.e, the joint density $p(s_1, s_2, \ldots, , s_n)$ of s_i must factorize into the product of their marginal densities $p_1(s_1)p_2(s_2)\ldots p_n(s_n)$.
- The source signals (at least some) must have nongaussian distributions.
  The central limit theorem states that although the distribution of independent source signals are not Gaussian, the distribution of a sum of independent random variables tends toward a Gaussian distribution, under certain conditions.
- There must be at least as many observed signals than the source signals. i.e, if m observations are made from n sources, then $m \geq n$.
- The location of the sources does not change relative to the location of sensors used to record the observed signals.
- The observed signals are considered as an instantaneous linear mixture of a number of source signals.

Ambiguities of ICA

The following ambiguities or indeterminacies are often visible in the ICA model.

- The variances (energies) of the independent components cannot be determined.
  Since both $\mathbf{s}(t)$ and $\mathbf{A}$ are unknown, any scalar multiplier in one of the sources s_i could always be cancelled by dividing the corresponding column a_i of $\mathbf{A}$ by the same scalar. Therefore, it is assumed that each has unit variance: $E\{s_i^2\} = 1$, but this will leave the ambiguity of the sign.
- The order of the independent components cannot be determined.

Preprocessing Methods Used Before ICA

Generally, before doing ICA, the following preprocessing steps are taken in the given order.

1. Centering the observed data vector $\mathbf{x}$ by subtracting its mean vector $m = E\{\mathbf{x}\}$. (Mean will be added after extracting the components).
2. Whitening the observed data vector $\mathbf{x}$ by linearly transforming the centred observed data such that its components are uncorrelated and have unit variance (Naik and Kumar, 2011).

ICA Algorithms

There are many ICA algorithms available in the literature. All these ICA algorithms have the same aim, i.e., separating latent source signals given only sensor observations that are unknown linear mixtures of source signals. Also, generally all algorithms produce near-identical results when applied to idealised source mixtures. However, the criteria used to determine the statistical independence and the method used to maximise it are different (Delorme, Sejnowski and Makeig, 2007). The Infomax algorithm (Bell and Sejnowski, 1995) is based on maximising the output entropy, or information flow, of a neural network with nonlinear outputs whereas FastICA algorithm (Hyvarinen, 1999) maximises the nongaussianity measured by the approximation of negentropy using a fixed-point algorithm. Both JADE algorithm (joint approximate diagonalisation of eigenmatrices) (Cardoso, 1999; Cardoso and Souloumiac, 1993) and SOBI (second-order blind identification) (Belouchrani et al., 1997) are based on joint diagonalisation. The SOBI assumes that the sample data is gathered from a set of temporally correlated sources and tries to separate sources by joint diagonalisation of several correlation matrices. JADE algorithm, on the other hand, is based on the diagonalisation of fourth-order cumulant matrices. Comparisons of the accuracy, convergence speed, computational load, and other relevant properties of different ICA algorithms have been published in (Delorme, Plamer, Oostenveld, Onton and Makeig, 2007; Delorme, Sejnowski and Makeig, 2007; Giannakopoulos et al., 1999; Kachenoura et al., 2007; Sahonero-Alvarez and Calderón, 2017).

In the present research work, JADE ICA algorithm implemented by Cardoso and Souloumiac (1993) was used to identify and remove the artifactual EEG components mixed in the multi-channel EEG data. The JADE ICA was performed offline using the MATLAB code found on website `http://www2.iap.fr/users/cardoso/code/Jade/jadeR.m`.

Applying ICA to EEG Artifacts Removal

The EEG research community widely accepts ICA as a promising method for isolating artifactual components in multi-channel EEG data, including eye blinks and movements, cardiac activity, line noise, muscle activity, electrode movements. For example, EEG data taken at different electrode locations consists of measures of electrical potentials generated not only by the neural brain activity but also by artifactual signals that overlap with the cerebral activity. In order to eliminate false results and interpretation of EEG data, the original components of brain activity need to be separated from the observed signals. This is closely related to the cocktail party problem explained before. ICA, by its nature, can separate these observed EEG data into maximally independent waveforms generated either within the brain or outside of it. These separated signals may have, for instance, specific activity patterns, power spectrum and component maps, which will enable the identification of artifactual and brain activity by visual observation. By removing the artifactual signals, the EEG data can be cleaned up to some extent. Makeig et al. (1996) reported the first results of applying ICA to EEG and event-related potential (ERP) data recorded during a sustained auditory detection task. There onwards, ICA has been widely used in the EEG research community, most often to remove EEG artifacts.

To build intuition about how ICA is used for artifact detection, consider that the EEG signals recorded from different electrodes at time t are represented by the rows of the input matrix $\mathbf{x}(t)$ and the underlying maximally independent EEG source signal components are represented by $\mathbf{s}(t)$ in the ICA model defined equation 3.5. The column vectors of the mixing matrix $\mathbf{A}$ in equation 3.5 give the projection strengths of the respective source signal components onto each of the scalp sensors, which is unknown (Jung et al., 2000). Thus, the objective is to find a linear separation matrix $\mathbf{W}$ that can decompose the observed EEG data $\mathbf{x}(t)$ into a mutually independent output $\mathbf{u}(t)$ as expressed in equation 3.7, where $\mathbf{u}(t)$ is the best possible estimate of the sources, $\mathbf{s}(t)$. The rows of the output matrix, $\mathbf{u}(t)$ represents the time courses of activations of the independent components, and these independent components represent the underlying cerebral and non-cerebral source activities (Li et al., 2006). The columns of the inverse separation matrix $\mathbf{W}^{-1}$, which is an estimate of the mixing matrix $\mathbf{A}$ in equation 3.5, gives the relative projection strengths of each independent component onto the scalp electrodes (Jung et al., 1998). Therefore, information about the location of the sources can be obtained from the scalp topographies of independent components drawn from the corresponding column vectors of $\mathbf{W}^{-1}$ (e.g. eye activity should project mainly to frontal sites, the cardiac activity will look almost like a linear gradient scalp topography).

The projection of the independent components onto the original data channels is given by,

$$\mathbf{x}_{\text{projections}}(t) = \mathbf{W}^{-1}\mathbf{u}(t) \approx \mathbf{A}\mathbf{u}(t). \tag{3.8}$$

Hence, the 'corrected' EEG signal can be derived as,

$$\hat{\mathbf{x}}(t) = W^{-1}\hat{\mathbf{u}}(t), \tag{3.9}$$

where $\hat{\mathbf{u}}(t)$ is derived from the matrix of activation waveforms $\mathbf{u}(t)$, by setting the rows representing the artifactual components to zero (Jung et al., 2000). Therefore, the rank of the corrected EEG data is less than the rank of the original data.

Figure 3.5 extracted from Jung et al. (1998) demonstrates the EEG artifact removal by ICA. The artifactual components can be identified by visually inspecting the time courses, scalp topographies and power spectrum of activations of the independent components. For example, the time series of the independent components that captures eye blinks and movement of the eyes show clear quick or sustained 'square' DC-shifts, respectively. The power spectrum of ocular artifacts, in general, is concentrated on frequencies below 5 Hz. Also, the scalp topographies show that the source origin of eye blink and movement artifacts are in or near the eyes since the activities are located in the frontal channels. The independent components that show near linear gradient scalp topographies and clear QRS complexes in the time series plots at about 1 Hz represent ECG artifacts (Pion-Tonachini et al., 2019). The independent components containing muscle artifacts are easy to identify since the power spectrum is concentrated mostly in higher frequencies (20 Hz and above) and the activities are localised in the peripheral channels (around the neck, ears, and eyes) (Hames, 2014). Figure 3.6 extracted from Hames (2014) shows the time series, scalp topographies and power spectra of the eye blink, horizontal eye movement, muscle artifact and cardiac artifact independent components.

When applying ICA to the observed EEG, the following assumptions are made (Jung et al., 2000; Makeig et al., 1996):

1. The summation of currents at the scalp electrodes is linear, and the propagation delays of the 'mixing medium' are negligible.
2. Source activations are temporally independent of one another across the input data.
3. The number of independent EEG signal sources is the same as the number of sensors, meaning that if EEG data is recorded from n EEG electrodes, the ICA algorithm can separate n sources.
4. Spatial projections of components are fixed across time and conditions.

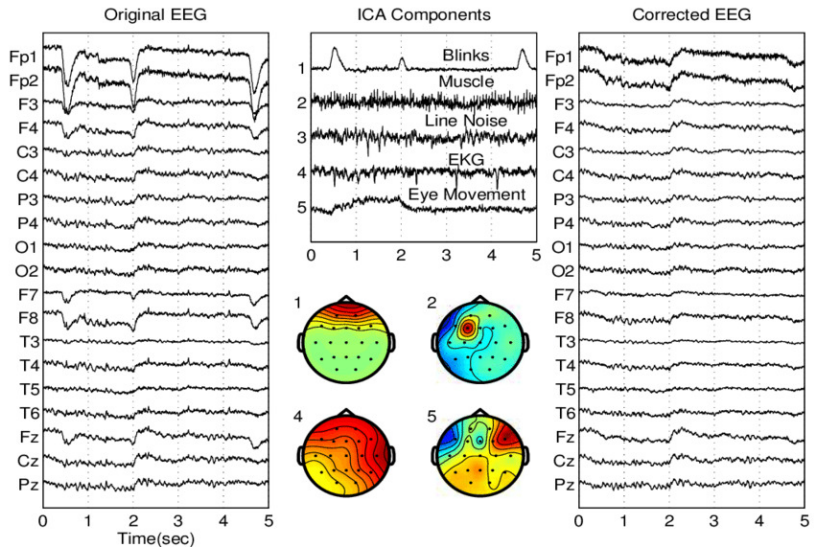

Figure 3.5: Illustration of EEG artifact removal by independent component analysis (ICA). The left image shows a 5-sec portion of an EEG time series. The top center image shows the time series of the independent components corresponding to eye blinks, muscle, line noise, cardiac artifacts, and eye movements. The bottom center image shows the scalp topographies of eye blinks, muscle, cardiac artifacts, and eye movements. The right image shows the 'corrected' EEG signals after removing the selected artifactual components (Jung et al., 1998).

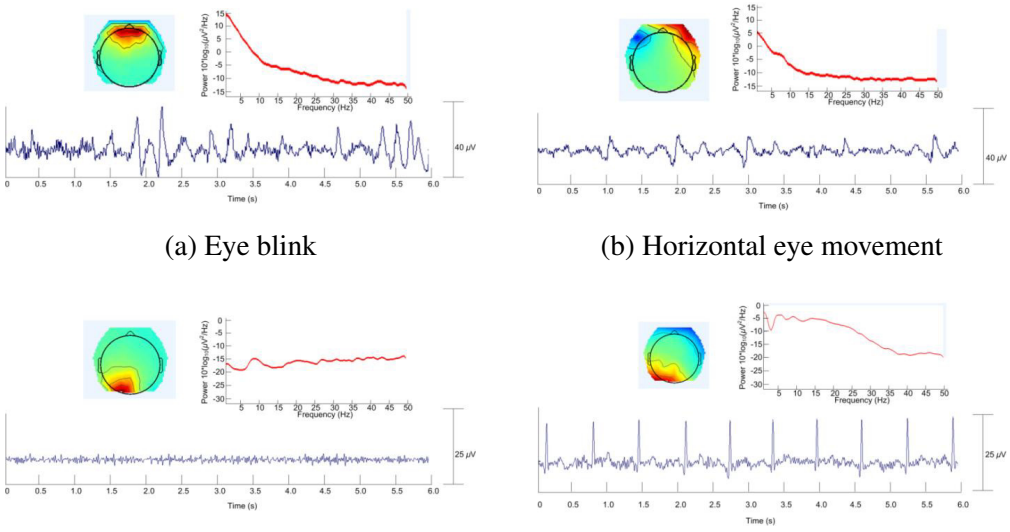

(a) Eye blink

(b) Horizontal eye movement

(c) Muscle artifact

(d) ECG artifact

Figure 3.6: Independent components that indicates (a) eye blink, (b) horizontal eye movement, (c) muscle, and (d) ECG artifacts. The top left image is the scalp topography, top right is the power spectrum and bottom center is the time series of each independent component (Hames, 2014).

5. Statistical distributions of the component activation values are not Gaussian.

Assumption (1) is usually considered to be fulfilled for EEG data (Ullsperger and Debener, 2010) and assumption (2) is reasonable since the sources of the eye, muscle and cardiac activity, and line noise are not generally time-locked to the sources of EEG activity. Since the effective number of statistically independent signals contributing to scalp EEG recordings is unknown, assumption (3) is questionable (Jung et al., 1998).

When using ICA to decompose EEG signals, the number of time points of n-channel data used in the decomposition must be sufficient to learn the n^2 weights of the separation matrix. Therefore, as a general rule, to find n stable components from n-channel EEG data, $k * n^2$, where $k = 20$ or a larger number of data points at each channel is required; i.e., if there are 32 channels, ICA decomposition will require $20 * 32^2 = 20480$ or more data points (Onton et al., 2006).

3.2 EEG Feature Extraction

Quantitative electroencephalography (QEEG) analysis techniques are widely used for assessing the functional states of the brain. QEEG is the processing and analysis of digitally recorded EEG data in order to transform the EEG data into a format or domain that elucidates relevant information, highlight specific waveform components typically derived by Fourier transform, or associate numerical results with the EEG data for subsequent review or comparison (Kane et al., 2017; Nuwer, 1997). QEEG techniques include, but not limited to, time-domain analysis, frequency-domain analysis, spatial-domain analysis, and multiway processing (Sanei and Chambers, 2013). QEEG measures are widely used to detect abnormal brain states such as epileptic seizures, to classify sleep stages, fatigue levels, and emotional states, to measure the depth of anaesthesia, to detect and monitor brain injuries and the recovery process. In this section, the QEEG analysis methods used in this thesis to estimate the changes in brain activity with the progression of fatigue is summarised. They are:

1. Spectral features: Relative delta (δ), theta (θ), alpha (α) and beta (β) band powers and (θ+α)/β, α/β, (θ+α)/(α+β), θ/β and δ/α ratio band powers.
2. Largest Lyapunov exponent
3. Approximate entropy

3.2.1 EEG Spectral Features

A. Fourier Transform

Frequency domain analysis or spectrum analysis is a process of decomposing a signal into a representation of its constituent frequency components, so that information about the signal that cannot be easily seen in the time domain is revealed for exploration (Tong and Thakor, 2009). The Fourier transform is a mathematical technique that has long been used to transform data from the time domain into the frequency domain. It decomposes or separates a waveform (a function or a signal) into a sum of sinusoids of different frequencies, which added together gives the original waveform. The Fourier transform of a continuous aperiodic function $x(t)$ is defined as follows:

$$X(f) = \int_{-\infty}^{\infty} x(t) \mathrm{e}^{-i2\pi ft} \, \mathrm{d}t, \tag{3.10}$$

where x(f) is the Fourier transform of X(t), and $i = \sqrt{-1}$. The uppercase $X(f)$ represents the frequency domain function, and the lowercase $x(t)$ represents the time domain function. The inverse Fourier transform is the operator that transforms data from the frequency domain into the time domain. It represents the synthesis of the continuous aperiodic function $x(t)$ as a weighted combination of the complex exponential basis functions, and is defined as:

$$x(t) = \int_{-\infty}^{\infty} X(f) \mathrm{e}^{i2\pi ft} \, \mathrm{d}f, \tag{3.11}$$

where $i = \sqrt{-1}$.

The discrete-time signals are created by sampling a continuous waveform. For instance, the EEG data are discretely sampled with a frequency of $f_s = \frac{1}{T_s}$, where T_s is the sampling time interval and have finite intervals. The sampling process generates the sequence $x(n)$ where n denotes the discrete sample time. Therefore, the discrete approximation of the continuous Fourier transform that applies to the sampled waveforms is defined by:

$$X(k) = \frac{1}{N} \sum_{n=0}^{N-1} x(n) \mathrm{e}^{-i2\pi kn/N}, \tag{3.12}$$

where $X(k)$ is the k^{th} coefficient of the discrete Fourier transform, $x(n)$ is the n^{th} sample of the time series which consists of N samples, $k = 0, 1, \ldots, N$, and $i = \sqrt{-1}$. The discrete

inverse Fourier transform is given by:

$$x(n) = \frac{1}{N} \sum_{k=0}^{N-1} X(k) \mathrm{e}^{2\pi jkn/N}, \tag{3.13}$$

Each Fourier coefficient corresponds to one frequency, and each Fourier coefficient contains information about the amplitude and the phase of each sine wave. The pictorial representation of the Fourier transform is a diagram which displays the amplitude and frequency of each of the determined sinusoids (Brigham, 1973). The square of the magnitude of the set of complex Fourier coefficients (i.e., the periodogram) is used to estimate the power spectrum of the original signal. The square of the magnitudes at each frequency, usually given by the units μ^2 (or in dB if the values are transformed into log-scale) shows the amount of energy at each that the original EEG signal carry at each frequency (Nuwer, 1997).

B. Welch's Averaged Periodogram

The fast Fourier transform (FFT) is a method used to compute the discrete Fourier transform of time series efficiently, and the spectrum estimation of discrete-time series data is usually based on procedures employing FFT. In this thesis, the power spectrum was estimated using Welch's averaged modified periodogram method that is based on time averaging over short, modified periodograms. The Welch's power spectral density estimation method, firstly, divides the discrete-time series into possibly overlapping segments; then, takes the modified periodograms of these segments by using FFT and averages these modified periodograms to obtain an estimation of the power spectra. The advantages of this method are a reduction in the number of computations, thus requiring less computing time, and a reduction in the required core storage since the method involves the transformation of sequences which are shorter than the whole record. The steps involved in Welch's method for estimating the power spectral density is as follows (Welch, 1967).

Algorithm: Welch's Averaged Periodogram

1) Let $x[n]$, $n = 0, 1, \ldots, N-1$, where N is the total number of samples, be a sample from a stationary, second-order stochastic sequence. Assume for simplicity the mean of the sequence is zero (i.e., $E(x[n]) = 0$).
2) Divide the data sequence $x[n]$ into K segments $\left(\text{i.e., } K = \frac{N-L}{D} + 1\right)$ with L data points in each segment, possibly overlapping and with the starting points of these segments D

units apart from the previous segment, i.e.:

$$\begin{aligned} &\text{Segment 1: } x_1 = x[0], x[1], \ldots, x[L-1] \\ &\text{Segment 2: } x_2 = x[D], x[D+1], \ldots, x[D+L-1] \\ &\qquad\vdots \\ &\text{Segment N: } x_K = x[N-L], x[N-L+1], \ldots, x[N-1]. \end{aligned} \tag{3.14}$$

This segmenting is illustrated in Figure 3.7. The number of points in common to two adjacent segments is $L-D$; when $L=D$, the segments do not overlap and when $D=0.5L$, there exists a 50% overlapping between the segments.

3) Select a data window $w[j]$, where $j=0,1,\ldots,L-1$, and form the sequences $x_1[j]w[j]$, $x_2[j]w[j],\ldots,x_K[j]w[j]$. Welch (1967) suggests that Welch window (similar to the Hanning or cosine arch spectral window) or the Parzen window are two reasonable choices for the data window $w[j]$.
4) Compute the discrete Fourier transforms, $X_k(n)$ for each sequence $x_k[j]w[j]$. Here,

$$X_k(n) = \frac{1}{L}\sum_{j=0}^{L-1} x_k(j)w(j)\mathrm{e}^{-i2\pi jn/L}, \tag{3.15}$$

where $k=1,\ldots,K$ and $i=\sqrt{-1}$.
5) Obtain the modified periodogram, $I_k(f_n)$ for each segment:

$$I_k(f_n) = \frac{L}{U}\left|X_k(n)\right|^2; \quad \text{for } k=1,2,\ldots,K, \tag{3.16}$$

where

$$f_n = \frac{n}{L}; \quad \text{for } n=0,\ldots,L/2, \tag{3.17}$$

and

$$U = \frac{1}{L}\sum_{j=0}^{L-1} w^2[j]. \tag{3.18}$$

6) Average the periodogram values to obtain Welch's estimate of the power spectra, i.e.,

$$\hat{P}(f_n) = \frac{1}{K}\sum_{k=1}^{K} I_k(f_n). \tag{3.19}$$

In this thesis, Welch's averaged modified periodogram method was applied to EEG epochs of 30 s length, i.e., N=7680. The power spectral density at each frequency (units: $\mu V^2/Hz$)

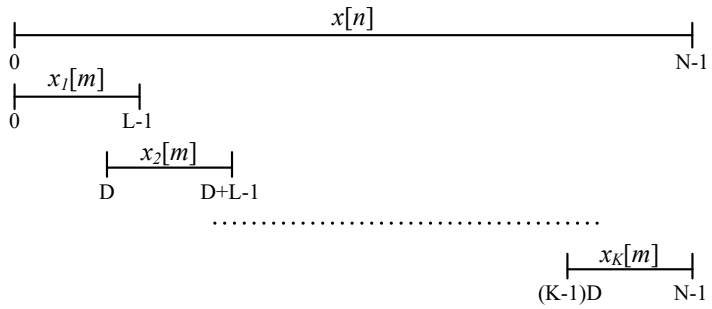

Figure 3.7: Illustration of the data segmentation in Welch's averaged modified periodogram method. Here N is the total number of samples in the sequence, $x[n]$, L is the number of points in each segment, D is the number of points to shift between segments, K is the total number of segments, $n = 0, 1, \ldots, N-1$ and $m = (k-1)D, (k-1)D+1, \ldots, (k-1)D+L-1$.

was calculated using the *pwelch()* command in MATLAB. A 3s segment length (i.e., L=768 samples), 50% overlap and a Parzen window were chosen as parameters for this analysis.

C. Extracting Spectral Features from Welch's Power Spectral Density

EEG recording contains a broad frequency spectrum and is often divided into five frequency bands, namely delta (δ), theta (θ), alpha (α), beta (β), and gamma (γ). Therefore, the interpretation of the association between EEG power and fatigue is often based on examining the power associated with traditional frequency bands (Kubitz and Mott, 1996). EEG power is often expressed in terms of absolute and relative band power (basic indices) and a ratio between different absolute band powers (ratio indices). In this thesis, only the delta, theta, alpha and beta frequency bands were considered since the modulations in these four band powers were often studied in fatigue literature (Table 2.1). EEG spectral features were extracted from the power spectral density, as explained below.

Absolute Band Power

The absolute band power for each frequency band was calculated by taking the average power at each frequency band (Miyakoshi, n.d.). That means, if the power spectral density estimated using the Welch's averaged modified periodogram method is given by $\hat{P}(f)$, then the absolute band power is calculated as:

$$\text{Absolute band power} = \frac{\sum_{f=f_1}^{f_2}(\hat{P}(f))}{N_{[f_1,f_2]}}, \tag{3.20}$$

where f_1 and f_2 are the lower and upper frequency limit of each frequency band $[f_1, f_2]$, and $N_{[f_1,f_2]}$ is the number of data points in the frequency band $[f_1, f_2]$.

Relative Band Power

The amplitudes of EEG signals varies from participant to participant due to the variations in neurophysiological, anatomical, and physical properties of the brain and surrounding tissues. The effects of inter-subject differences can be reduced by calculating the relative band power (Kropotov, 2010). Therefore, the relative band powers were often considered. The relative band power indices for each frequency band was calculated as the ratio between the absolute band power at each frequency and the total power of all the frequency bands considered. The total power is usually expressed as the sum of the absolute band powers of interest. Therefore, the relative power of each frequency band was calculated as follows.

$$\begin{aligned}
\delta_{\text{relative}} &= \frac{\delta_{\text{absolute}}}{\delta_{\text{absolute}} + \theta_{\text{absolute}} + \alpha_{\text{absolute}} + \beta_{\text{absolute}}} \\
\theta_{\text{relative}} &= \frac{\theta_{\text{absolute}}}{\delta_{\text{absolute}} + \theta_{\text{absolute}} + \alpha_{\text{absolute}} + \beta_{\text{absolute}}} \\
\alpha_{\text{relative}} &= \frac{\alpha_{\text{absolute}}}{\delta_{\text{absolute}} + \theta_{\text{absolute}} + \alpha_{\text{absolute}} + \beta_{\text{absolute}}} \\
\beta_{\text{relative}} &= \frac{\beta_{\text{absolute}}}{\delta_{\text{absolute}} + \theta_{\text{absolute}} + \alpha_{\text{absolute}} + \beta_{\text{absolute}}}
\end{aligned} \tag{3.21}$$

Here, the δ_{absolute}, θ_{absolute}, α_{absolute}, and β_{absolute} are the absolute delta, theta, alpha and beta band powers. The δ_{relative}, θ_{relative}, α_{relative}, and β_{relative} are the corresponding relative band powers.

Power Ratios

Power ratio indices are also used in fatigue studies since the basic band powers can be insufficient to observe the shift of brain activity from fast waves to slow waves (De Waard and Brookhuis, 1991; Eoh et al., 2005; Fan et al., 2015; Jap et al., 2009). The most commonly used power ratio indices to assess fatigue are: $(\theta+\alpha)/\beta$, α/β, $(\theta+\alpha)/(\alpha+\beta)$, and θ/β. All four ratio indices reflect the ratio between slow and fast wave activities over time (Jap et al., 2009). Eoh et al. (2005) stated that the index $(\theta+\alpha)/\beta$ was a more reliable fatigue indicator during a simulated driving task due to the mutual addition effect of theta and alpha activity

during the repetitive phase transition between wakefulness and microsleep. Jap et al. (2009) also reported a greater increase in the index $(\theta+\alpha)/\beta$, in comparison to the other power ratios, when a person experienced a fatigued state at the end of a monotonous simulated driving task.

The following power ratio indices were considered in the present research work.

$$\begin{aligned}
\frac{(\theta+\alpha)}{\beta} &= \frac{(\theta_{absolute}+\alpha_{absolute})}{\beta_{absolute}} \\
\frac{\alpha}{\beta} &= \frac{\alpha_{absolute}}{\beta_{absolute}} \\
\frac{(\theta+\alpha)}{(\alpha+\beta)} &= \frac{(\theta_{absolute}+\alpha_{absolute})}{(\alpha_{absolute}+\beta_{absolute})} \\
\frac{\theta}{\beta} &= \frac{\theta_{absolute}}{\beta_{absolute}} \\
\frac{\delta}{\alpha} &= \frac{\delta_{absolute}}{\alpha_{absolute}}
\end{aligned} \tag{3.22}$$

3.2.2 EEG Largest Lyapunov Exponent

Over the past years, there has been an increasing interest in detecting the presence of chaos in EEG signals by estimating the largest Lyapunov exponent, to better understand the behaviour of the brain. There is no universal definition for chaos. Strogatz (Strogatz, 2018) provided a working definition for chaos, which is *"chaos is aperiodic long-term behaviour in a deterministic system that exhibits sensitive dependence on initial conditions"*. In this definition, *"aperiodic long-term behaviour"* means that the trajectories do not settle down to fixed points, periodic or quasiperiodic orbits as $t \to \infty$, thereby shows irregular behaviour without periodicity. *"Deterministic"* means that the systems has no random and noisy parameters or inputs. Therefore, the irregular behaviour of the system derives from the system's nonlinearity. *"Sensitive dependence on initial conditions"* means that trajectories starting very close to each other will separate exponentially fast.

Lyapunov exponents can detect and quantify the presence of chaos in a dynamical system. Lyapunov exponents quantify the average exponential rates at which nearby orbits in phase space diverges or converges as the system evolves in time (Wolf et al., 1985). For example, consider $x(t)$ is a point on a trajectory at time t, and the nearby point is $x(t)+\delta(t)$, where δ is

the separation vector between two trajectories (Figure 3.8). If the initial length of separation is $|\delta_0|$, $|\delta(t)|$ can be approximated by $|\delta_0|\, e^{\lambda t}$, where λ is the Lyapunov exponent and e is the mathematical constant ($e \approx 2.72$). There is neither divergence nor convergence of the trajectories if $\lambda = 0$. If λ is positive, then $|\delta(t)|$ will have an exponential growth whereas if λ is negative, then $|\delta(t)|$ will have an exponential decay. Therefore the two trajectories will show exponential divergence when λ is positive and an exponential convergence when λ is negative (Stergiou, 2018). A system with one or more positive λ is defined to be chaotic (Strogatz, 2018).

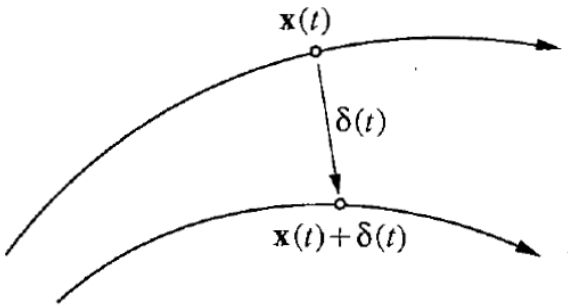

Figure 3.8: Divergence of two nearby trajectories (Strogatz, 2018)

There are many algorithms proposed to calculate the largest Lyapunov exponent. The first algorithm to compute the largest Lyapunov exponent from experimental time series was introduced by Wolf et al. (1985) in 1985. The algorithm introduced by Rosenstein et al. (1993) was used in the present research work to calculate the largest Lyapunov exponent in EEG data.

A. Rosenstein *et al.*'s algorithm

The algorithm introduced by Rosenstein et al. (1993) to estimate the largest Lyapunov exponent expects that two randomly chosen initial conditions will diverge exponentially at a rate given by the largest Lyapunov exponent. Therefore, the largest Lyapunov exponent λ can be defined as

$$d(t) = Ce^{\lambda t}, \tag{3.23}$$

where $d(t)$ is the average divergence at time t and C is a constant that normalizes the initial separation. Rosenstein et al. (1993)'s algorithm is fast and works well with small data sets. Also, it is easy to implement and robust to the changes in embedding dimension, reconstruction delay, size of the data set, and noise level. The following steps are involved in the calculation of largest Lyapunov exponent from a time series.

The first step in calculating the largest Lyapunov exponent involved reconstructing the attractor dynamics from the time series using the method of delays. Let $x(1)$, $x(2)$, ... $x(N)$ be the time series with N points. The reconstructed trajectory $\mathbf{X}$ can be expressed as a matrix where each row is a phase-space vector. That is,

$$\mathbf{X} = (\mathbf{X}_1 \quad \mathbf{X}_2 \quad \dots \quad \mathbf{X}_M)^T, \tag{3.24}$$

where $\mathbf{X}_i$ is the state of the system at discrete time i. Each $\mathbf{X}_i$ is given by,

$$\mathbf{X}_i = (x(i) \quad x(i+\tau) \quad \dots \quad x(i+(m-1)\tau)), \tag{3.25}$$

where τ is the reconstruction delay or lag and m is the embedding dimension. Therefore, $\mathbf{X}$ is an $M \times m$ where $M = N-(m-1)\tau$. The reconstruction delay or lag τ and embedding dimension m was estimated using average mutual information method and false nearest neighbour method, respectively.

Average Mutual Information (AMI) Method

Each state space contains information of the system at a specific time (Stergiou, 2018). Therefore, an appropriate reconstruction delay, τ should be determined so that new information about the system, which could not be obtained from the previous state-space can be given. If τ is small, successive elements of the delay vectors are strongly correlated, thereby no new information is given from that state-space. If τ is taken too large, successive elements of the delay vectors are highly independent, and information may be lost (Kantz and Schreiber, 2004; Stergiou, 2018). The τ was estimated using the average mutual information (AMI) method (Fraser and Swinney, 1986). AMI is a measure of the amount of information one measurement gives about a second measurement of the same variable and is calculated as,

$$I_{x(i),x(i+T)} = \sum_{i=1}^{N} P(x(i),x(i+T)) log_2 \left[\frac{P(x(i),x(i+T))}{P(x(i))P(x(i+T))} \right], \tag{3.26}$$

where N is the length of the time series and T is the lag. AMI was calculated for various time delays and the first local minimum of the I vs T plot is selected as the best value of the reconstruction delay τ. For example, Figure 3.9 shows the AMI vs lag plot for the Lorenz attractor, a well-known sets of equations developed by Edward Lorenz (1917-2008) to describe a chaotic system (Lorenz, 1963). The best value for τ is 11 since the first local minimum average mutual information is at a time lag of 11.

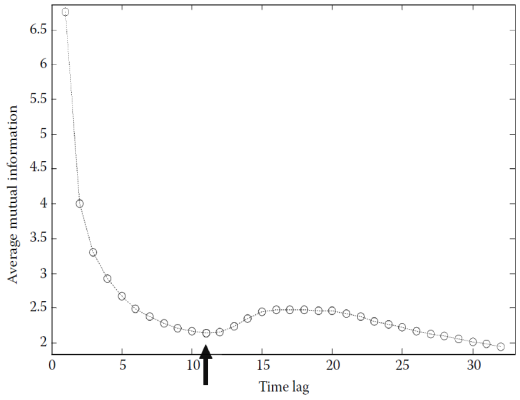

Figure 3.9: Estimation of the reconstruction delay (τ) for the Lorenz attractor using average mutual information (Stergiou, 2018).

False Nearest Neighbour (FNN) Method

The embedding dimension is the dimension of the space that contains the true structure of the system. The false nearest neighbour (FNN) method can be used to estimate the embedding dimension of a time series, thereby determining the number of time-delay coordinates needed to reconstruct the state-space from a given time series (Abarbanel, 1996; Rhodes and Morari, 1997; Stergiou, 2018). Suppose a state space reconstruction in dimension m with data vectors

$$\mathbf{X}_i = (x(i) \quad x(i+\tau) \quad \dots \quad x(i+(m-1)\tau)), \tag{3.27}$$

is made using a reconstruction delay τ. Consider that the nearest neighbour in phase space for $\mathbf{X}_i$ is $\mathbf{X}_i^{NN}$, where

$$\mathbf{X}_i^{NN} = (x(i)^{NN} \quad x(i+\tau)^{NN} \quad \dots \quad x(i+(m-1)\tau)^{NN}), \tag{3.28}$$

The Euclidean distance between these vectors at m-dimension is given by, $||\mathbf{X}_i - \mathbf{X}_i^{NN}||$. In going from dimension m to $m+1$ by time-delay embedding, $x(i+m\tau)$ component is added to $\mathbf{X}_i$ and $x(i+m\tau)^{NN}$ component is added to $\mathbf{X}_i^{NN}$; thereby the distance between the two vectors at $m+1$ is give by $||\hat{\mathbf{X}}_i - \hat{\mathbf{X}}_i^{NN}||$. By comparing $||\mathbf{X}_i - \mathbf{X}_i^{NN}||$ with $||\hat{\mathbf{X}}_i - \hat{\mathbf{X}}_i^{NN}||$, true and false neighbours can be identified. The square of the Euclidean distance between the nearest neighbour points in dimension m is given by,

$$R_m(i)^2 = \sum_{d=1}^{m} [x(i+(d-1)\tau) - x^{NN}(i+(d-1)\tau)]^2. \tag{3.29}$$

The square of the Euclidean distance between the nearest neighbour points in dimension $m+1$ is given by,

$$\begin{aligned} R_{m+1}(i)^2 &= \sum_{d=1}^{m+1} [x(i+(d-1)\tau) - x^{NN}(i+(d-1)\tau)]^2 \\ &= R_m(i)^2 + ||x(i+m\tau) - x(i+m\tau)^{NN}||^2 \end{aligned} \tag{3.30}$$

Therefore, the distance between points in dimension $m+1$ relative to the distance in dimension m is given by,

$$\sqrt{\frac{R_{m+1}(i)^2 - R_m(i)^2}{R_m(i)^2}} = \frac{||x(i+m\tau) - x(i+m\tau)^{NN}||}{R_m(i)} \tag{3.31}$$

If this ratio is larger than a certain threshold value, R_{tol}, the vector is a false neighbour. Abarbanel (1996) suggested a R_{tol} value of 15 to define a false neighbour. The number of false nearest neighbours are computed by examining every point on the trajectory. Then the percentage of false nearest neighbours to true nearest neighbours is calculated at different dimensional spaces and the percentage of false nearest neighbours versus embedding dimension is plotted. At higher dimensional space, the percentage of false nearest neighbours should fall since the dynamics of attractor are being unfolded. The value of the dimension where the percentage of false nearest neighbours drops to zero or is closest to zero is considered as the dimension that is large enough to describe the dynamics of the system. This dimension is selected as the embedding dimension m. Figure 3.10 shows the plot of the percentage of false nearest neighbours versus embedding dimension for the Lorenz attractor. It shows that the embedding dimension of the Lorenz attractor is 3 since the percentage of false nearest neighbours becomes zero when the dimension is three (Stergiou, 2018).

After reconstructing the phase-space using τ and m obtained from the above mentioned methods, the nearest neighbour of each point on the trajectory is found. The nearest neighbour $\mathbf{X}_j^{NN}$ is found by searching for the point that minimizes the distance to the reference point $\mathbf{X}_j$, which is expressed as,

$$d_j(0) = min_{x_j^{NN}} ||\mathbf{X}_j - \mathbf{X}_j^{NN}||, \tag{3.32}$$

where $d_i(0)$ is the initial distance from the j^{th} point to its nearest neighbour. An additional constraint that is the nearest neighbours have a temporal separation greater than the mean period of the time series (i.e., $|j - j^{NN}| >$ mean period) is also considered as it allow to consider each pair of neighbours as nearby initial conditions for different trajectories. The reciprocal of the the mean frequency of the power spectrum is considered as the mean period.

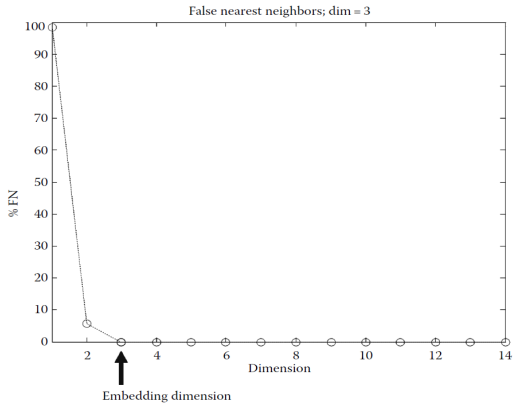

Figure 3.10: The percentage of false nearest neighbours for the Lorenz attractor. The embedding dimension of 3 is considered since the percentage of false nearest neighbours becomes zero when the dimension is three (Stergiou, 2018).

Then, the largest Lyapunov exponent is estimated as the mean rate of separation of the nearest neighbours.

From equation 3.23, it was assumed that the j^{th} pair of nearest neighbours diverge approximately at a rate given by the largest Lyapunov exponent:

$$d_j(i) \approx C_j \, e^{\lambda(i\Delta t)}, \tag{3.33}$$

where C_j is the initial separation. Equation 3.34 is obtained by taking the logarithm of both sides of equation 3.33.

$$ln(d_j(i)) \approx ln(C_j) + \lambda(i\Delta t), \tag{3.34}$$

For $j = 1, 2, \ldots, M$, equation 3.34 represents a set of approximately parallel lines, each with a slope roughly proportional to λ. The largest Lyapunov exponent is calculated using a least-squared fit to the average line defined by

$$y(i) = \frac{1}{\Delta t}\langle ln(d_j(i))\rangle, \tag{3.35}$$

where $\langle\,\rangle$ denotes the average over all values of j (Figure 3.11). The unit for largest Lyapunov exponent is divergence/second, when time is converted to seconds.

Phase space reconstruction of recorded EEG data and the calculation of the largest Lyapunov exponent were performed using the MATLAB functions *phaseSpaceReconstruction()* and *lyapunovExponent()* available in the *predictive maintenance toolbox*.

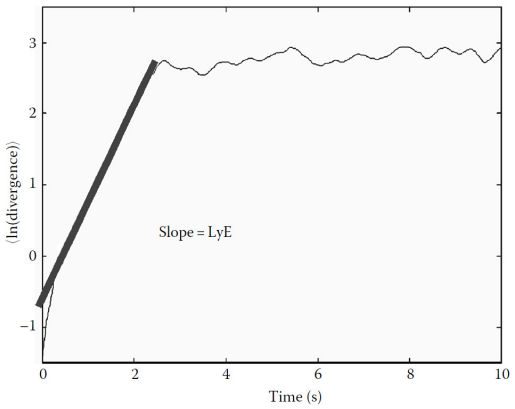

Figure 3.11: Estimation of the largest Lyapunov exponent. The largest Lyapunov exponent (LyE) is the slope of the initial region of rapid exponential expansion (Stergiou, 2018).

3.2.3 EEG Approximate Entropy

Approximate entropy, introduced by Pincus (Pincus, 1995), quantify the regularity and complexity in time series data. Approximate entropy is calculated as follows.

- Given a time series of N data points $x(1), x(2), \ldots, x(N)$, form a sequence of vectors $u(1)$ through $u(N-m+1)$ defined by $u(i) = [x(i), \ldots, x(i+m-1)]$, where m is the length of compared runs and r is effectively a filter, also known as the similarity criterion or the radius of similarity.
- Define the distance between vectors $u(i)$ and $u(j)$, $d[u(i), u(j)]$ as the maximum difference in their respective scalar components. That is,

$$d[u(i), u(j)] = max_{k=1,2,\ldots,m}(\mid x(i+k-1) - x(j+k-1) \mid) \tag{3.36}$$

- Then, construct for each i, $1 \leq i \leq N-m+1$,

$$C_i^m(r) = \frac{\text{number of } j \leq N-m+1 \text{ such that } d[u(i), u(j)] \leq r}{N-m+1}. \tag{3.37}$$

- From $C_i^m(r)$, define

$$\Phi^m(r) = \frac{1}{N-m+1} \sum_{i=1}^{N-m+1} ln(C_i^m(r)), \tag{3.38}$$

where ln is the natural logarithm.

- Approximate entropy (AppEn) is then defined as,

$$\text{AppEn}(m,r,N) = \Phi^m(r) - \Phi^{m+1}(r). \tag{3.39}$$

Approximate entropy measures the likelihood that runs of patterns that are close for m observations remain close on next incremental comparison (Pincus, 1991). A higher approximate entropy value corresponds to a higher complexity whereas a smaller approximate entropy value correspond to the greater likelihood of remaining close thereby showing greater regularity. Approximate entropy is robust to outliers and is applicable to noisy, medium sized data sets (between 100 and 5000 data points). Pincus (1995) have suggested that $m = 1$ and 2 and $r = 0.1$ to $0.25\times$ standard deviations (std) of the $x(i)$ produce good statistical validity of *AppEn{m, r, N}*. In the present work, $m = 2$ and $r = 0.2 \times std$ are selected as the parameters respectively from literature on EEG-based fatigue estimation. Approximate entropy of the recorded EEG signals were calculated using the MATLAB function *approximateEntropy()* available in the *predictive maintenance toolbox*.

3.3 Statistical Analysis

Inferential statistics are used to describe and make generalisations about a population based on samples of data taken from the population. This section summarises the inferential statistical methods used in the present research work to compare and contrast the EEG feature modulations with fatigue in robot-mediated interactions. The statistical analysis was conducted using the *IBM SPSS Statistics, Version 25* software.

3.3.1 Statistical Terminology and General Interpretations Used

Hypothesis (a prediction from a theory) testing requires measuring variables that can vary between subjects or time or location. A variable thought to be the cause of some effect is expressed as the independent variable (or predictor variable). In contrast, a variable thought to be affected by changes in an independent variable is expressed as the dependent variable (or outcome variable). In experimental research, the independent variable is the variable that is manipulated by the experimenter (Field, 2018). In the design of studies to test a hypothesis, a between-subjects design is a study where participants are assigned into different groups with each group experiencing differential experimental conditions (Bethel and Murphy, 2010). In other words, the independent variable(s) of the study is manipulated using different participants. Conversely, in within-subject or repeated-measures study designs, each participant is exposed to all levels of the experimental conditions or

provide data at multiple time points; i.e., the independent variable(s) is manipulated using the same participants (Field, 2018). Besides, the mixed-model factorial design includes both between-subjects and within-subject design components (Bethel and Murphy, 2010).

In inferential statistics, the term "null hypothesis" states that treatment did not have an effect, while the term "alternative hypothesis" states that the treatment had an effect (Yockey, 2016). In the present work, the level of significance (α level), i.e., the probability of rejecting a null hypothesis by the test when it is true, was set at 0.05. It is related to the 95% confidence interval (CI). A *p*-value indicates the exact probability of obtaining the specific results if the null hypothesis is true (Yockey, 2016). If the *p*-value obtained was *less than or equal to the* α *value (i.e., 0.05)*, the null hypothesis was rejected and was concluded that the treatment had a significant effect. Conversely, if the *p*-value was *greater than* α, then it was accepted that the null hypothesis was plausibly true. In hypothesis testing, a type I error occurs when the null hypothesis is falsely rejected (i.e., one concludes there is a real effect when it does not). In contrast, a type II error occurs when the null hypothesis is accepted even when it is false. Statistical power is the probability of correctly rejecting the null hypothesis when it is false. Statistical power ranges from 0 to 1 and is inversely related to the probability of making a Type II error. Therefore, as the statistical power increases, the probability of making a Type II error or in other words concluding that there is no effect when, in fact, there is an effect, decreases.

The *p*-value can only say whether an effect exists; it will not reflect the size of the effect (Sullivan and Feinn, 2012). Therefore, in addition to the *p*-value, the effect size is also reported in this thesis. The effect size is the magnitude of the difference between groups (Sullivan and Feinn, 2012) and is estimated with different indices depending on the type of comparison under study. The Pearsons' correlation coefficient *r* and partial eta-squared (η_P^2) were used in this thesis to calculate the effect size. The Pearsons' correlation coefficient, *r*, which is a measure of the strength of relationship between two variables, is also a versatile measure of the strength of an experimental effect (Field, 2018). The *r*-value can be calculated using the following equation.

$$r = \sqrt{\frac{t^2}{(t^2 + df^2)}}, \tag{3.40}$$

where t is the t-statistic and df is the degree of freedom. Cohen has also interpreted the effect is large or small depending on the value of r = 0.1 (small), 0.3 (medium) and 0.5 (large). Partial eta-squared (η_P^2) is calculated using the variance associated with an effect and

the associated error variance. The formula for η_P^2 is

$$\eta_P^2 = \frac{SS_{\text{Effect}}}{SS_{\text{Effect}} + SS_{\text{Error}}} \tag{3.41}$$

where SS is short for "sums of squares". A small, medium, and large effects would be reflected in η_P^2 values of 0.0099, 0.0588, and 0.1379, respectively (Cohen, 2013; Richardson, 2011).

The standard deviation (std) is a measure used to quantify the variability or the dispersion within the data of interest. Throughout this thesis, the estimates of interest (i.e., mean) is accompanied by the standard deviation and is written as *mean* $\pm$ *std*. Also, the error bars represent the standard deviation of the data sets.

The assumption of normality was tested using the Kolmogorov–Smirnov test. The Kolmogorov–Smirnov test compares the observations in the sample to a normally distributed set of scores with the same mean and standard deviation (Field, 2018). If the test is non-significant (i.e., $p > 0.05$), it can be identified that the distribution of the sample is not significantly different from the normal distribution. In other words, the samples are approximately normally distributed. In contrast, if the test is significant (i.e., $p < 0.05$), then the sample distribution is non-normal. The Kolmogorov-Smirnov test was applied either to the sampling distribution of the observations at each level or to the difference between paired observations depending on the type of experiment conducted. Statistical tests for the analysis of EEG features were selected based on the outcomes of the normality test. For experiment 1, the difference between paired observations (baseline and recovery as stated in Chapter 4) of all participants were normally distributed; therefore, paired-samples *t*-tests were considered. For experiment 2, the sampling distribution of the EEG features at each level (baseline, level 1, level 2, level 3, level 4, level 5, and recovery as stated in Chapter 5) were approximately normally distributed; therefore, two-way repeated-measures analysis of variance (ANOVA) was used to find the significant variations in EEG features. Robust statistical methods such as trimmed mean, M-estimators, Winsorized variance, bootstrapping (Wilcox, 2012) or non-parametric tests (Field, 2018) can be used when the assumption of normality is not met.

3.3.2 Statistical Tests Used to Compare and Contrast EEG Feature Modulations

In this thesis, the paired-samples *t*-test and two-way repeated-measures analysis of variance (ANOVA) were used to find the significant variations in EEG features with the development of fatigue.

The paired-samples *t*-test (also known as the dependent-means *t*-test or matched-pairs *t*-test) is performed to compare the means of two samples, where the two samples are related in some way (i.e., the same individuals or entities are exposed to both experimental conditions). This is applicable if the differences between the paired observations are normally distributed. The null hypothesis assumes that the means from two random samples are very similar; thus the difference between the two values is equal to zero. If the *p*-value corresponding to the test statistic t is less than 0.05, the null hypothesis is rejected and is assumed that the means are significantly different from each other. Conversely, if $p > 0.05$, the null hypothesis is accepted. The effect size for the paired-samples *t* test is estimated using Pearsons' correlation coefficient, r calculated as in equation 3.40. For paired-samples *t*-test, the degree of freedom, df is given by sample size minus 1.

A two-way repeated-measures analysis of variance (ANOVA) (also known as a two-factor repeated measures ANOVA) compares several means when there are two within-subjects factors (also known as independent variables), and the same participants have been used in all experimental conditions (Field, 2018). The sphericity refers to the equality of variances of the differences between treatment levels and when the variances are roughly equal, the sphericity is met. The assumption of sphericity is tested using Mauchly's test and if Mauchly's test statistic is non-significant (i.e., $p > 0.05$), it can be concluded that the assumption of sphericity is met. However, if the Mauchly's test statistic is significant (i.e., $p < 0.05$), the assumption of sphericity is violated, thereby it can be concluded that there are significant differences between the variances of differences. The *p*-value corrected using the Greenhouse–Geisser was used if the assumption of sphericity is violated (Field, 2018). In this thesis, the uncorrected degree of freedom, the corrected *p*-value and the degree of sphericity (i.e., epsilon (ε) value) are reported for each two-way repeated measures ANOVA. The degree of freedom values of the within-subject factors, interaction, and the error degree of freedom were reported along with the corresponding F-values (i.e., $F(df_{factor/interaction}, df_{error})$. Effect sizes are expressed as partial eta-squared (η_P^2) (Equation 3.41). Moreover, Tukey least significant difference (LSD) for comparison of means is used to perform the pairwise comparisons if significant main effects or interaction effects were found.

Chapter 4

Experiment 1: EEG Spectral Feature Modulations Associated with Fatigue in Robot-Mediated Upper Limb Gross Motor and Fine Motor Interactions

This chapter presents the experiment design and findings of the preliminary EEG-based fatigue estimation experiment conducted to address the research question 1: *'Are the EEG spectral feature modulations associated with fatigue localised to different brain regions depending on the type of robotic interaction and the underlying physical and mental workload?'*.

4.1 Methods and Materials

4.1.1 Ethical Approval

The experiment was approved by the Ethics Committees with Delegated Authority for Science and Technology of the University of Hertfordshire (Protocol numbers: COM/PG/UH/00100 and aCOM/PG/UH/00100).

4.1.2 Participants

Twenty healthy right-handed volunteers (6 females and 14 males), who were at least 20 years of age (average age of the sample was 32 $\pm$ 10 years; mean $\pm$ SD) and with no

history of severe injury to the head, brain, or right hand participated in this experiment. Right-handedness was considered since both robotic interfaces were constrained to be used only by the right upper limb due to their hardware configurations and setup. The SCRIPT passive orthosis used in this experiment could only be worn using the right hand. Similarly, the HapticMASTER was installed to work with right hand and changing the orientation of the HapticMASTER was hazardous. Participants were informed about potential hazards and risk mitigations as well as inconveniences associated with the experiment. All participants signed informed consent forms before participation. A summary of the participant demographic is given in Table 4.1. All participants had normal vision or corrected to normal vision. The self-reports showed that most participants had around 7 to 9 hours of sleep the night before the experiment and can assume that they had sufficient hours of sleep as recommend by (Hirshkowitz et al., 2015). Therefore, it can be assumed that fatigue build-up was solely due to the robotic interaction.

Table 4.1: Participants demography of experiment 1.

Subject ID	Robotic interface interacted with	Age	Gender	Wearing glasses/ contacts	Hours slept prior to the experiment
A01	HapticMASTER	42	Male	No	4
A02	HapticMASTER	27	Female	No	7
A03	HapticMASTER	33	Male	No	8
A04	HapticMASTER	28	Male	Yes	6
A05	HapticMASTER	21	Male	No	8
A06	HapticMASTER	35	Male	No	7
A07	HapticMASTER	31	Female	Yes	7
A08	HapticMASTER	24	Male	No	8
A09	HapticMASTER	48	Male	No	7
A10	HapticMASTER	27	Female	No	7
B01	SCRIPT passive orthosis	56	Male	Yes	6
B02	SCRIPT passive orthosis	23	Male	No	9
B03	SCRIPT passive orthosis	32	Male	No	6
B04	SCRIPT passive orthosis	44	Male	No	7
B05	SCRIPT passive orthosis	21	Male	Yes	8
B06	SCRIPT passive orthosis	32	Female	Yes	8
B07	SCRIPT passive orthosis	37	Female	Yes	8
B08	SCRIPT passive orthosis	30	Male	No	5
B09	SCRIPT passive orthosis	25	Female	Yes	7
B10	SCRIPT passive orthosis	21	Male	No	6

4.1.3 Fatigue Inducing Robot-Mediated Interactions

Given the consent to take part in the experiment, participants were randomly assigned to two groups: A and B, so that each group consists of 10 participants (age of the group A participants was 32 $\pm$ 8 years and group B participants was 31 $\pm$ 11 years). The random assignment of participants also reduces the potential for confounding from individual differences. Participants in group A performed visually guided arm reach/return movements (gross motor task) with HapticMASTER (Figure 4.1a) whereas participants in group B performed hand open/close movements (fine motor task) with SCRIPT passive orthosis (Figure 4.2a). Both robot-mediated interactions were performed for 20-minutes or until volitional fatigue. The virtual reality environment of the GENTLE/A rehabilitation system (Chemuturi et al., 2013*a*) was used for the gross motor task. Target point locations were modified so that the trajectory covered by the movement of HapticMASTER robot arm was mapped into a straight line connecting only two virtual target points, as shown in Figure 4.1b. The HapticMASTER was set to the active mode so that the participants should initiate the movement and reach the target points by themselves. The virtual reality game 'sea shell' (Figure 4.2b), developed for the SCRIPT system was used as the fine motor task (Amirabdollahian et al., 2014). Participants wore the SCRIPT passive orthosis and performed the hand open/close gestures to open/close a seashell underwater. Participants were asked to perform these hand open/close gestures when a fish is near to the seashell, thereby catching it. Both robot-mediated interactions were performed using only the right hand, and the participants were asked to keep their left hand in a relaxed position throughout the task. The distance between the computer monitor and the participant's eye was set to around 120 cm for both groups.

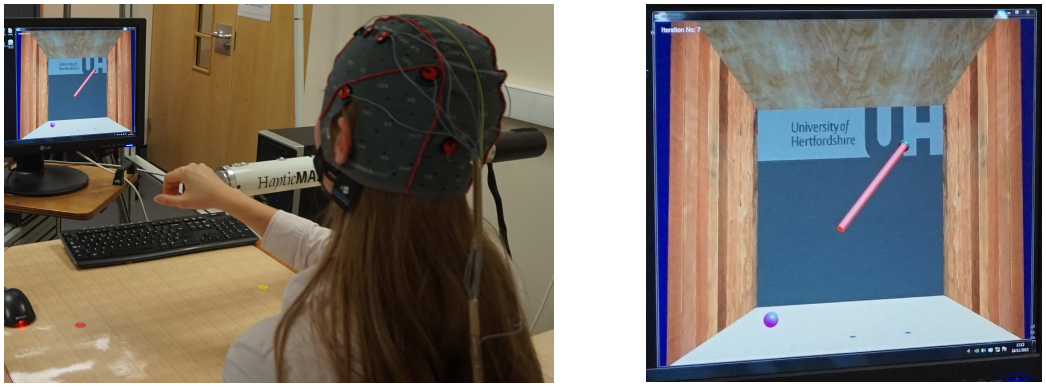

(a) Robot-mediated gross motor interaction (b) Virtual reality interface

Figure 4.1: Robot-mediated gross motor interaction (arm reach/return task) using HapticMASTER.

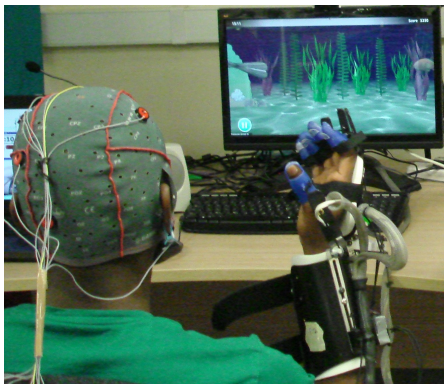

(a) Robot-mediated fine motor interaction

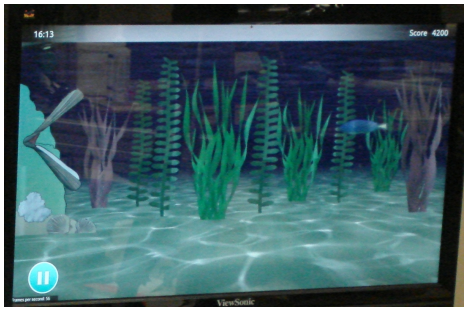

(b) Virtual reality interface

Figure 4.2: Robot-mediated fine motor interaction (hand open/close task) using SCRIPT passive orthosis.

4.1.4 EEG Data Acquisition

A. Selection of EEG Electrodes

For this experiment, only right-handed participants were recruited and the robot-mediated movements were performed using their dominant hand. The studies on handedness and brain activation suggest that movements of the dominant hand are predominantly controlled by the hemisphere contralateral to that hand. Therefore, more significant contralateral brain activations are visible (Grabowska et al., 2012; Gut et al., 2007). From the literature review, it was found that the modulations in the EEG spectral features exhibited a widespread topographical distribution in the majority of the fatigue studies. However, the EEG data acquisition system used for the experiment had only eight channels. Therefore, according to the International 10-10 system of electrode placement (Epstein, 2006), FP1, F3, FC3, C3, C4, P3, O1 and T7 electrode locations were selected so that majority of the electrodes are placed in the left hemisphere. All electrodes were referenced to the right earlobe (A2), and FPz was used as a ground. The electrode placement is shown in Figure 4.3.

B. Hardware Configuration

Continuous EEG signals were recorded using an eight-channel EEG data acquisition system, g.MOBIlab+ (g.tec medical engineering GmbH, Austria), before, during and after the robotic interactions. The flow diagram of the hardware configuration of the EEG data acquisition system is shown in Figure 4.4. The eight Ag/AgCl active electrodes (g.LADYbird) and one Ag/AgCl passive ground electrode (g.LADYbird) were attached to the FP1, F3, FC3, C3, C4, P3, O1, T7 and FPz electrode location markers of the EEG electrode cap (g.GAMMACap2).

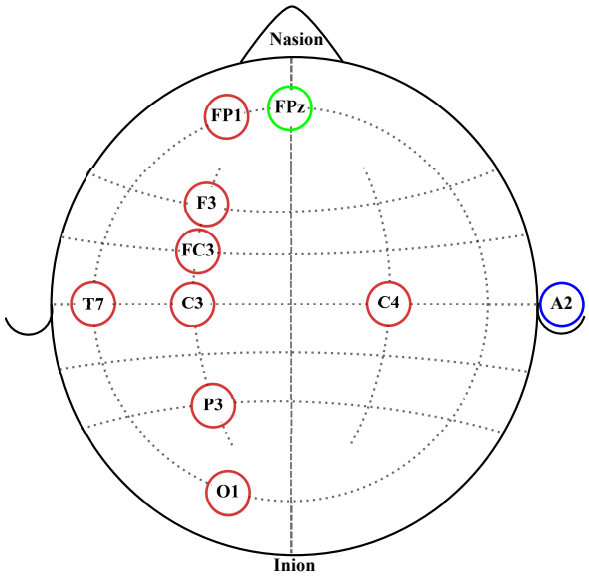

Figure 4.3: EEG electrode placement according to the International 10-10 system of electrode placement. Red circles represent the eight active electrodes selected for the data acquisition. The blue circle represents the reference electrode location. The green circle represents the ground electrode location.

The eight active electrodes, the passive ground electrode, and the Ag/AgCl active ear clip reference electrode (g.GAMMAearclip) were then connected to the active electrode driver box (g.GAMMAbox). The active electrode system reduces or avoids artifacts caused by high impedance between the electrode(s) and the skin (e.g. 50/60 Hz coupling, electrode or cable movement artifacts, background noise) (g.tec medical engineering GmbH, 2014*b*). The g.GAMMAbox provided the interface between the electrodes and the amplifier, g.MOBIlab+ (8 channel monopolar EEG version). The amplifier consists of an integrated 16-bit analogue to digital converter. The sampling rate, the lower and upper cut-off frequencies of the bandpass filter of the amplifier are fixed at 256 Hz, 0.5 Hz, and 100 Hz, respectively by the manufacturer. Therefore, the signals acquired from this device were sampled at 256 Hz and had a fixed EEG bandwidth of 0.5 to 100 Hz. The amplified, filtered and digitised EEG signal was transmitted via a Bluetooth connection for display and storage for further analysis.

C. Skin Preparation and Placement of the EEG Electrode Cap

Since a passive electrode was used as the ground electrode, skin near FPz (forehead) was cleaned using abrasive gel before placing the EEG cap on the participant's head to reduce the skin-electrode interface impedance. It was not necessary to abrade the skin around other electrode locations since the signals acquired by the active electrodes are pre-amplified directly at the electrode (Pinegger et al., 2016). The EEG cap was positioned correctly

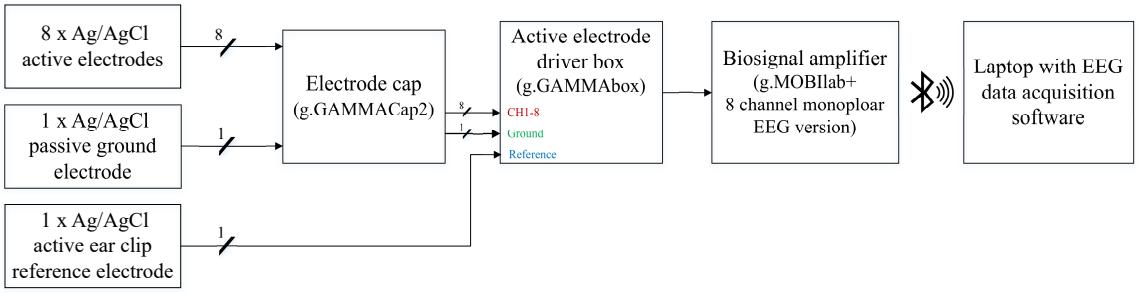

Figure 4.4: Block diagram of the hardware configuration of the EEG data acquisition system.

based on the distances between the anatomical landmarks: nasion and inion, and left and right preauricular points of the participant so that the deviation between the 'true' 10-10 positions and the positions indicated on the cap was minimised. The EEG cap was fixed firmly to the head using the adjustable chin strap to reduce the movement of the cap during the robotic interactions (g.tec medical engineering GmbH, 2014*a*). A highly-conductive, high-viscosity, non-abrasive, non-greasy and non-irritant electrode gel (g.GAMMAgel) was used to bridge the gap between the electrode(s) and the skin surface. All electrodes were filled with electrode gel using a syringe (without needle), and the ear clip reference electrode was also connected to the right earlobe after applying gel on the electrode. The electrode gel was wiped out from the hair at the end of the session.

4.1.5 Experimental Procedure

On arrival at the laboratory, participants were informed about the experiment protocol, given time to familiarise with the assigned robotic interaction and were prepared for the EEG data collection according to the guidelines given in g.tec medical engineering GmbH (2014*a*). The flow diagram of the proposed fatigue estimation experiment is given in Figure 4.5. Following the standardised EEG recording protocol, EEG data were recorded before, during and after the robot-mediated interactions. Participants were instructed to close and open their eyes for 180 s each when EEG data were recorded before and after the tasks. In order to avoid or reduce artifacts in the eyes open/closed EEG recordings, participants were instructed to sit still while minimising eye blinks, eye movements, swallowing, jaw clenching or any other severe body movements. In this preliminary experiment, EEG data recorded before and after the gross motor and fine motor tasks with eyes opened and closed were further analysed. Participants also completed two questionnaires before and after the robot-mediated interactions and provided feedback on the level of fatigue, task-associated workload and comfortability. Video recordings were also made during the session and were mainly used to cross-check the artifactual EEG components at the data preprocessing.

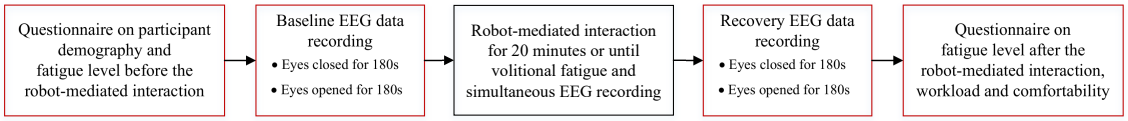

Figure 4.5: Flow diagram of the experimental procedure.

4.1.6 EEG Data Analysis

The EEG data recorded before the robotic interactions will be referred to as 'baseline' (e.g.: 'baseline-eyes-opened' and 'baseline-eyes-closed') and the EEG data recorded after the robotic interactions will be referred to as 'recovery' (e.g.: 'recovery-eyes-opened' and 'recovery-eyes-closed') throughout this chapter. These states can be considered to reflect the restfulness of the participant before and after the robotic interactions; thereby, any changes in these states could be a reflection of the fatigue. Previous studies have also compared EEG data recorded before and after a task to identify EEG feature modulations associated with fatigue induced by physical and mental tasks (Chen et al., 2013; Cheng and Hsu, 2011; Ng and Raveendran, 2007; Tanaka et al., 2012). The EEG data processing pipeline followed for each participant during each state is illustrated in Figure 4.6. It mainly consisted of three steps: preprocessing, feature extraction and statistical analysis. EEG preprocessing and feature extraction were performed offline using custom MATLAB scripts.

A. Preprocessing

EEG data recorded before and after the robotic interactions included artifacts such as blinking, eye movement, cardiac activity, swallowing, jaw clenching and power line noise to some extent, although the participants were instructed to relax their muscles, and look straight without excessively blinking and moving eyes and other body parts. Since limited data were available and eye blinks and movements frequently occurred in some participants (mainly in the data recorded with eyes opened), rejecting EEG segments with artifacts may result in a considerable loss of information. Therefore, the following preprocessing steps were performed on the data to obtain relatively clean EEG data.

Firstly, the DC offset of each recording was removed by subtracting the channel-wise mean from each data point. Then, a Type II Chebyshev low-pass filter with a stopband frequency of 45 Hz and an order of 20 was applied to eliminate the power line noise (50 Hz) distortions. The stopband frequency was determined so that the filtering would not attenuate the signal of interest that lies within the frequency range of 1 Hz to 30 Hz. As the recording device has a bandpass analogue filter with a lower and higher cut-off frequency of 0.5 Hz and 100 Hz respectively, digital high-pass filtering was not considered in this experiment, as it

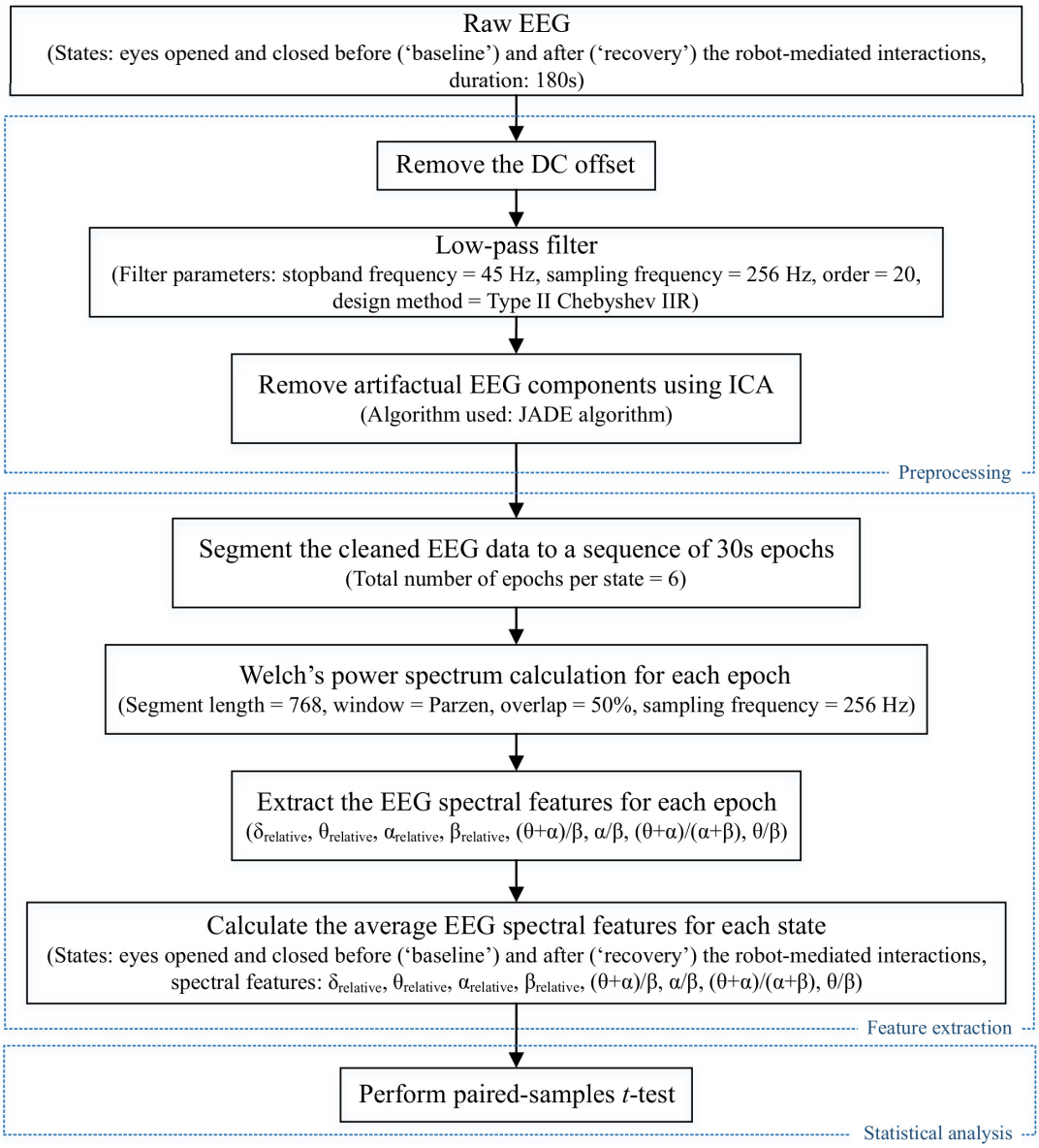

Figure 4.6: EEG data processing pipeline followed to preprocess the raw EEG data and to extract EEG spectral features of each state for each participant in order to perform the statistical analysis. Dotted boxes represent the three main steps involved in the pipeline: data preprocessing, feature extraction, and statistical analysis. δ_{relative}, $\theta_{relative}$, α_{relative}, and $\beta_{relative}$ indicate the relative δ, θ, α and β band powers respectively, and $(\theta+\alpha)/\beta$, α/β, $(\theta+\alpha)/(\alpha+\beta)$, and θ/β indicate the power ratios.

may distort the lower frequencies of interest in this analysis. Then, ICA based on the joint approximate diagonalisation of eigenmatrices (JADE) algorithm (Cardoso and Souloumiac, 1993) was performed to separate and remove in-band (or remaining) artifacts including eye blinks, eye movement, swallowing, jaw clenching, and cardiac activity from the independent components. A detailed description of the ICA model and how to identify artifactual EEG components is given in Section 3.1.4. When applying ICA to separate EEG artifacts from brain activity patterns, it was assumed that the signals emitted by the unobserved sources are independent and the number of independent sources is same as the number of electrodes used in the experiment (i.e., = 8). Figure 4.7 illustrates the artifact removal process using ICA for a single subject. The low-pass filtered EEG data $\mathbf{x}(t)$ were multiplied by the separating matrix **W** estimated via JADE ICA algorithm to obtain the time courses of activations of the independent components $\mathbf{u}(t)$; i.e., **u**(t) = **W**x(t) as expressed in equation 3.7. The time courses of the ICA components represent the separated artifactual and neurally generated EEG sources which are maximally independent of one another (Li et al., 2006). The relative projection strengths of each independent component onto the scalp electrodes were given by the columns of the inverse separation matrix $\mathbf{W}^{-1}$, which is an estimate of the mixing matrix **A** in equation 3.5. The 'corrected' EEG signal was then derived as, $\hat{\mathbf{x}}(t) = W^{-1}\hat{\mathbf{u}}(t)$, where $\hat{\mathbf{u}}(t)$ was derived from the matrix of activation waveforms $\mathbf{u}(t)$, by setting the rows representing the artifactual components identified by visual inspection to zero (Jung et al., 2000).

B. Feature Extraction

The corrected EEG signals at the four states: 'baseline-eyes-opened', 'baseline-eyes-closed', 'recovery-eyes-opened' and 'recovery-eyes-closed' for each participant were segmented into epochs of 30 s length (i.e., 7680 samples per epoch, and six epochs in total per state). Previous studies have reported that reliable changes in EEG during fatigue and brain functional states were visible in data spanning between 15s to 1 minute (Lal and Craig, 2002). The power spectral density for all epochs was estimated using the Welch's averaged modified periodogram method (Welch, 1967) with a 3s segment length (i.e., 768 samples), 50% overlap, and a Parzen window. The Welch's averaged modified periodogram method is explained in section 3.2.1. Subsequently, the relative band power of delta (1-<4 Hz), theta (4-<8 Hz), alpha (8-13 Hz), and beta (<13-30 Hz) for each epoch were calculated as a ratio between the average band power of each frequency band and the total band power (i.e., the summation of the average delta, theta, alpha and beta band powers). The four ratio band power measures for each epoch $(\theta+\alpha)/\beta$, α/β, $(\theta+\alpha)/(\alpha+\beta)$, and θ/β were also calculated. Finally, the average of each EEG spectral feature within the 180 s duration

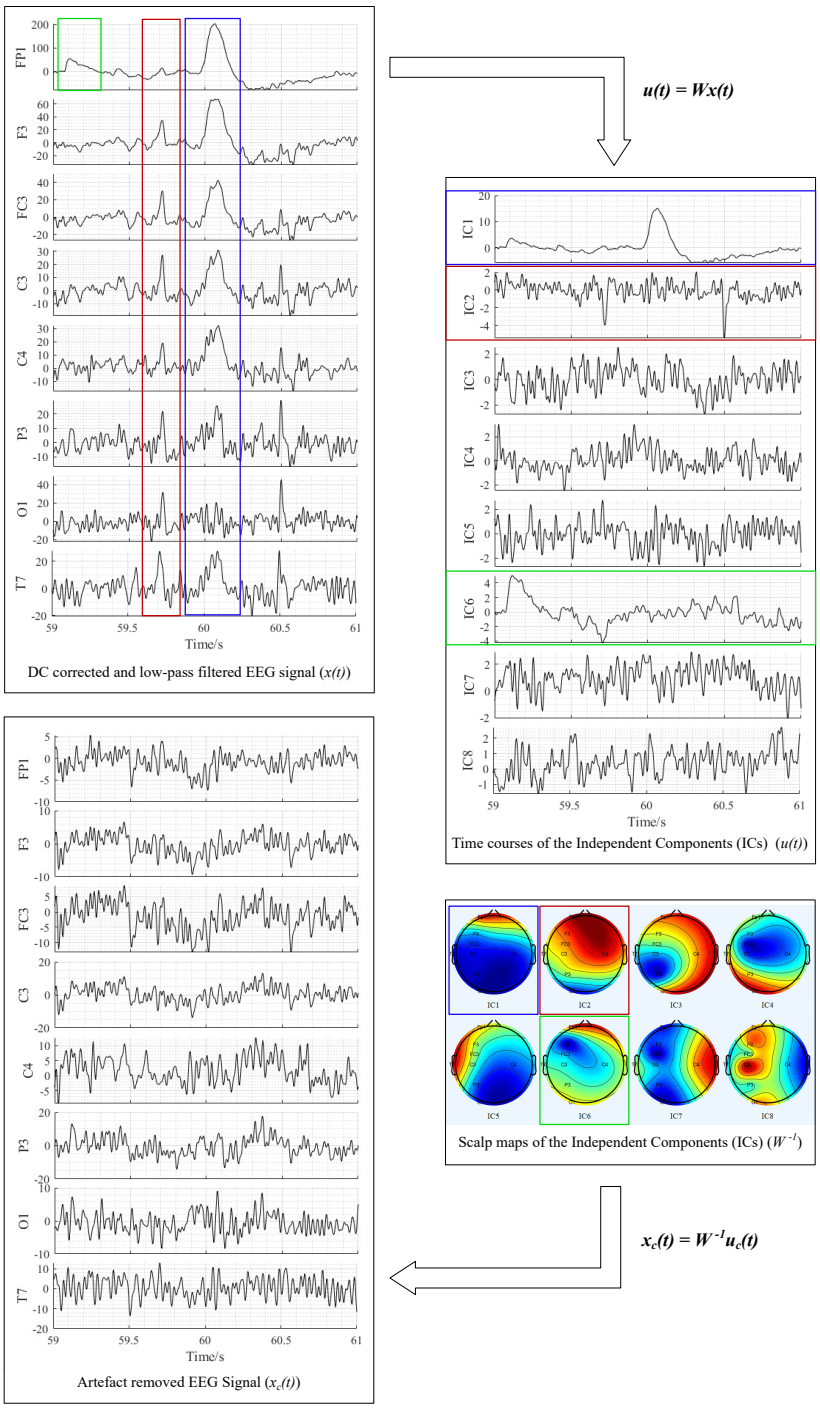

Figure 4.7: Illustration of EEG artifactual components identification using ICA for a single subject (SubID: A01). The red, blue and green rectangles marked in the time courses of activations of the independent components represent the independent components corresponding to cardiac activity, eye blink and eye movement artifacts respectively. The red, blue and green rectangles marked in the DC corrected and filtered EEG signal show how cardiac activity, eye blink and eye movement artifacts distort the EEG recordings taken from the eight electrode locations, respectively. All these data were referenced to the right earlobe (A1).

(i.e., six epochs) of each state was calculated to represent the corresponding spectral feature index of the 'baseline-eyes-opened', 'baseline-eyes-closed', 'recovery-eyes-opened' and 'recovery-eyes-closed' states. The average of EEG spectral features across the number of epochs or trials were considered in many past studies (Abásolo et al., 2006; Cao et al., 2014; Chen et al., 2013; Jap et al., 2009; Lal and Craig, 2002).

4.1.7 Subjective Measures of Level of Fatigue, Workload, and Comfortability

The questionnaires used in this experiment are given in Appendix C.1. The questionnaire given before the robotic interactions gathered information about the participant's demographics and a subjective measure of their physical and mental fatigue level before performing the assigned robot-mediated interaction. The questionnaire given after the interaction was used to obtain a subjective measure of the physical and mental fatigue levels following the robotic interaction. Furthermore, it also obtained the subjective evaluation of physical and mental workload across the robotic interaction and the comfortability of the session.

The statements used to measure the fatigue levels, workload and comfortability were as follows,

- Fatigue levels:
  - How would you rate your current physical fatigue level?
  - How would you rate your current mental fatigue level?
- Workload:
  - How physically demanding was the task?
  - How mentally demanding was the task?
- Comfortability:
  - How would you rate your current eye strain level?
  - How comfortable were you with wearing the EEG headset?
  - How would you think that wearing the EEG headset affected your fatigue state?
  - How would you think that using the robotic interface affected your fatigue state?

The two questions used to identify the workload during the robot-mediated interactions was adopted from the National Aeronautics and Space Administration–Task Load Index (NASA-TLX) (Hart, 1986).

Each statement had a 5-point Likert rating scale to obtain the corresponding subjective measures, with 1 representing 'Not at all', 2 representing 'somewhat/slightly', 3 representing 'moderately', 4 representing 'very/largely' and '5' representing 'Extremely'. For the two

statements that reflect the subjective measure of fatigue level, the responses starting from the extreme left were assigned the scores 0, 1, 2, 3, and 4, so that a score of '0' indicates that the participant was not fatigued at all while a score of '5' indicates that the participant was extremely fatigued. Scores assigned to the fatigue level ratings before and after the robotic interaction were used to compare and contrast the changes in individual physical and mental fatigue level following the assigned robot-mediated interaction. It was of interest compare and contrast the effects of underlying physical and mental workload on the development of fatigue in the assigned tasks. Therefore, the difference between the change in physical and mental fatigue scores before and after each robotic interaction (i.e., fatigue score after the task - fatigue score before the task) were calculated and were compared with difference in the ratings given to the physical and mental demand. The findings obtained by analysing the subjective measures of level of fatigue, underlying workload and comfortability of the experiment are discussed in section 4.2.3.

4.1.8 Statistical Analysis

The statistical analysis was conducted using *IBM SPSS Statistics 25* software. A p-value<0.05 was considered statistically significant denoting a 95% confidence interval. The normality was assessed using the Kolmogorov–Smirnov test.

As explained in section 4.1.6, eight EEG spectral features were extracted from each EEG data recorded before and after the robot-mediated interactions from each participant with the eyes opened and closed. It was of interest to investigate whether the significant differences in the EEG spectral features caused by fatigue are localised to different electrodes due to the differences in the task definition (fine vs gross motor movements). Therefore, the statistical analysis was separately performed on the eight electrode locations and the two robot-mediated upper limb interactions for eyes opened and eyes closed states (i.e., in total $8 \times 2 \times 2 = 32$ paired-samples t-tests). The differences between the EEG spectral features extracted from 'baseline-eyes-opened' and 'recovery-eyes-opened' of all participants were normally distributed. Similarly, the differences between the EEG spectral features extracted from 'baseline-eyes-closed' and 'recovery-eyes-closed' of all participants were normally distributed. Therefore, upon confirmation of normal distribution of the difference between 'baseline' and 'recovery' EEG features, two-tailed paired-samples t-tests were performed on each EEG feature gathered from all participants. The effect sizes were expressed by the Pearsons' correlation coefficient, r calculated using the equation 3.40. Multiple paired-samples t-tests were also used in previous fatigue studies to evaluate the changes in EEG

features at different brain regions (Chen et al., 2013; Fan et al., 2015; Tanaka et al., 2012; Zhao et al., 2012).

4.2 Results

4.2.1 Modulations in EEG Spectral Features Following the Robot-Mediated Gross Motor Interaction with HapticMASTER

Table 4.2 summarises the paired-samples *t*-test results of the statistically significant EEG spectral feature modulations and the corresponding electrode locations for eyes opened state following the gross motor interaction with HapticMASTER. The paired-samples *t*-test results of all electrodes are summarised in Appendix A.

Table 4.2: Significant EEG spectral feature modulations and the corresponding electrode locations for eyes opened state following the gross motor interaction with HapticMASTER.

Spectral Feature	Electrode Location	Sample mean ± std		Paired samples *t*-test				Direction of change
		Baseline	Recovery	*t*	*df*	*p*-value	*r*	
δ_{relative}	C3	0.542 ± 0.109	0.476 ± 0.067	2.593	9	0.029	0.654	↓
α_{relative}	FC3	0.180 ± 0.068	0.225 ± 0.069	-2.378	9	0.041	0.621	↑
	C3	0.198 ± 0.070	0.259 ± 0.095	-3.148	9	0.012	0.724	↑
	P3	0.271 ± 0.094	0.330 ± 0.154	-2.646	9	0.027	0.661	↑
$\frac{(\theta+\alpha)}{\beta}$	C3	8.151 ± 4.349	8.923 ± 4.167	-2.787	9	0.021	0.681	↑
$\frac{\alpha}{\beta}$	C3	4.213 ± 2.612	4.997 ± 2.812	-2.403	9	0.040	0.625	↑

Notes. ↑ = significant increase. ↓ = significant decrease.

The sample mean and standard deviation of EEG spectral features during the 'baseline' and the 'recovery' states with eyes opened following the robot-mediated gross motor interaction are shown in Figure 4.8. Comparison of the sub-figures in Figure 4.8 shows that α_{relative} changed the most as a result of fatigue induced by the interaction with HapticMASTER. In Figure 4.8c, there is a clear increase of α_{relative} across all electrodes, with statistically significant differences visible on the three electrodes placed over the contralateral motor cortex: FC3 ($t(9)$ = -2.378, p = 0.041, r = 0.621), C3 ($t(9)$ = -3.148, p = 0.012, r = 0.724) and P3 ($t(9)$ = -2.646, p = 0.027, r = 0.661). As well as being statistically significant, the effect of the variation in α_{relative} on FC3, C3, and P3 electrodes were large. These electrodes correspond to motor activities using the right hand; thereby, the significant increase in α_{relative} reflects a decreased cortical activation, which is an indication of fatigue. Similarly, Figures 4.8e and 4.8f show that fatigue induced by the gross motor task significantly increased both

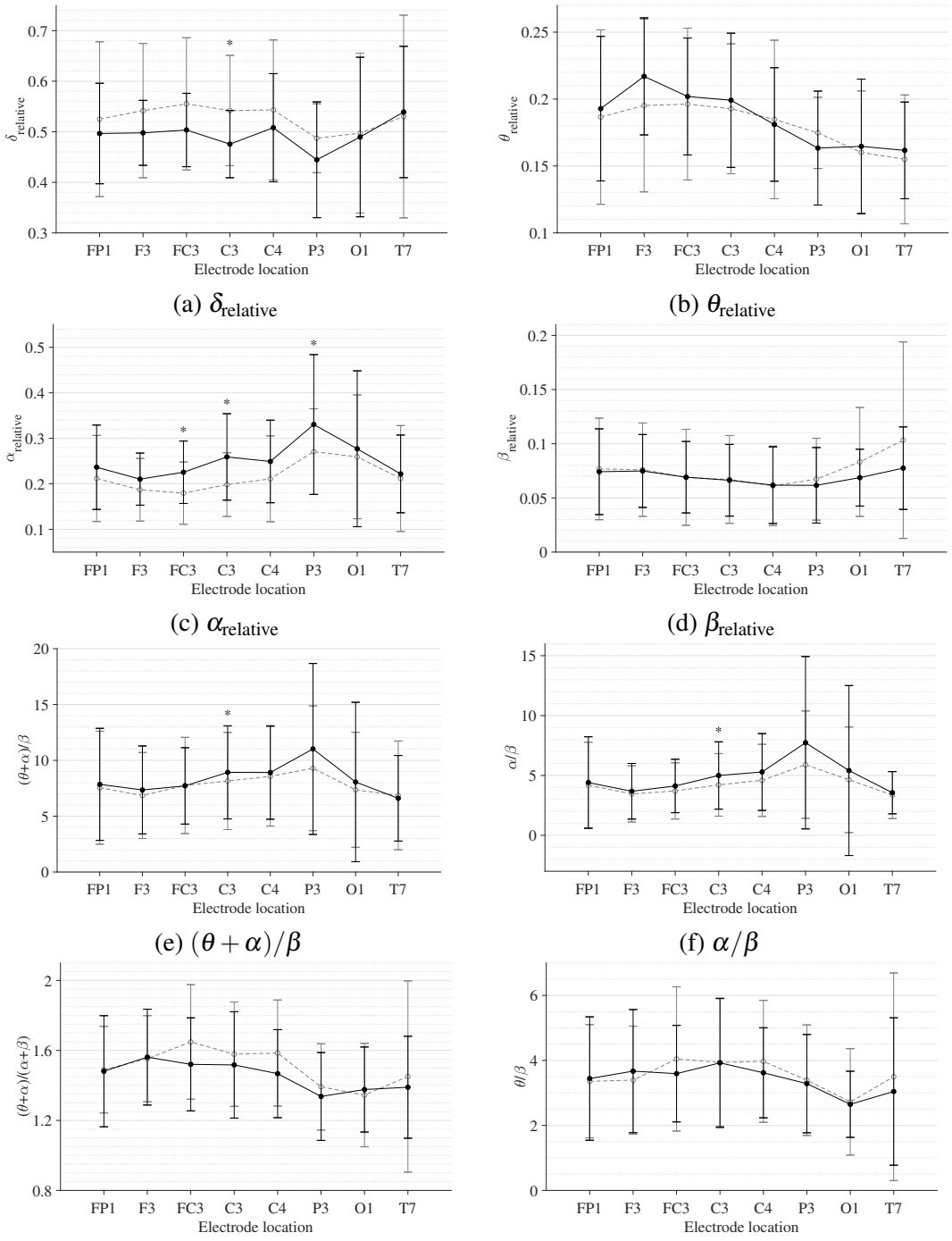

(a) δ_{relative} (b) θ_{relative}

(c) α_{relative} (d) β_{relative}

(e) $(\theta+\alpha)/\beta$ (f) α/β

(g) $(\theta+\alpha)/(\alpha+\beta)$ (h) θ/β

Figure 4.8: Comparison of the sample mean and standard deviation of EEG spectral features of all participants between 'baseline' and 'recovery' states with eyes opened for the gross motor interaction with HapticMASTER.. The '- - -○- - -' represents the 'baseline-eyes-opened' and '—●—' represents the 'recovery-eyes-opened'. The statistical significance is represented by an asterisk: i.e., * = $p < 0.05$. *Connecting lines in subfigures do not imply a linear relationship between electrode locations but merely for the ease of identifying the numerical changes between baseline and recovery states.*

$(\theta+\alpha)/\beta$ ($t(9)$ = -2.787, p = 0.021, r = 0.681) and α/β ($t(9)$ = -2.403, p = 0.040, r = 0.625) on C3 electrode, while no significant differences are visible on other electrode locations. A larger effect size was also visible on C3 electrode for both $(\theta+\alpha)/\beta$ and α/β. These findings show that fatigue induced by gross movements increased the low-frequency power on C3 and decreased the fast wave activities; thereby resulting in a significant difference when combined. In contrast, Figure 4.8d shows that β_{relative} has not significantly affected in the 'recovery' state. However, the decrease of variation across the sample implies that at the 'recovery' state, all participants show similar high-frequency brain activities, which could be a result of the prolonged robot-mediated interaction. Figure 4.8a indicates that there has been a drop in δ_{relative} following gross movements (except on T7). Also, a significant variation with larger effect was found on C3 ($t(9)$ = 2.593, p = 0.029, r = 0.654) electrode. This result is somewhat counter-intuitive because previous studies have either shown a significant increase or no change in delta activity as fatigue progressed; however, it is reasonable to assume that this inconsistency may be related to the differences of experimental protocols. There are no significant differences visible in θ_{relative}, $(\theta+\alpha)/(\alpha+\beta)$, and θ/β due to fatigue induced by the gross motor task. Overall, these results show a reduced activation around the sensorimotor cortex due to fatigue induced by robot-mediated gross movements. Figure 4.9 shows the brain topographies of the difference between 'recovery' and 'baseline' states (i.e., difference = 'recovery' - 'baseline') of the substantive EEG features for one participant who reported a higher increase in the physical fatigue level than the mental fatigue level following the gross motor task. The topographical distributions also confirm that the modulations in

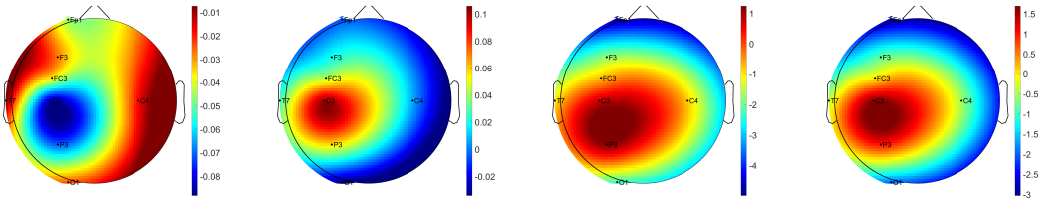

(a) δ_{relative} (b) α_{relative} (c) $(\theta+\alpha)/\beta$ (d) α/β

Figure 4.9: Brain topographies of substantive EEG spectral features for the difference between 'recovery' and 'baseline' states (i.e., difference = 'recovery' - 'baseline') with eyes opened for one participant following the gross motor interaction with HapticMASTER. In each brain map, the nose is represented by the triangle on the top, and the right hemisphere is on the right. For α_{relative}, $(\theta+\alpha)/\beta$, and α/β, the red-shaded areas indicate a larger increase whereas the blue-shaded areas indicate a decrease. For δ_{relative}, the blue-shaded areas indicate a larger decrease whereas the red-shaded areas indicate a smaller decrease.

δ_{relative}, α_{relative}, $(\theta+\alpha)/\beta$, and α/β due to fatigue are localised around the left central and left parietal regions.

The sample mean and standard deviation of EEG spectral features during the 'baseline' and the 'recovery' states with eyes closed following robot-mediated gross motor interaction is shown in Figure 4.10. There were no significant differences in the EEG spectral features between the 'baseline' and 'recovery' states when estimated with eyes closed. However, similar trends were found on the EEG spectral features that showed significant differences when estimated from the eyes opened EEG data. For instance, an increase in the α_{relative}, $(\theta+\alpha)/\beta$, and α/β and a decrease in δ_{relative} are visible following the gross motor task. The findings of the paired-samples t-test performed on eyes-closed EEG spectral features are summarised in Appendix A.

4.2.2 Modulations in EEG Spectral Features Following the Robot-Mediated Fine Motor Interaction with SCRIPT Passive Orthosis

Table 4.3 summarises the paired-samples t-test results of the statistically significant EEG spectral feature modulations and the corresponding electrode locations for eyes opened state following the fine motor interaction with SCRIPT passive orthosis. The paired-samples t-test result of all electrodes are summarised in Appendix A.

Table 4.3: Significant EEG spectral feature modulations and the corresponding electrode locations for eyes opened state following the fine motor interaction with SCRIPT passive orthosis.

Spectral Feature	Electrode Location	Sample mean ± std		Paired samples t-test				Direction of change
		Baseline	Recovery	t	df	p-value	r	
δ_{relative}	FP1	0.550 ± 0.096	0.504 ± 0.106	3.066	9	0.013	0.715	↓
$\theta_{relative}$	C4	0.193 ± 0.033	0.226 ± 0.039	-3.507	9	0.007	0.760	↑
α_{relative}	FP1	0.179 ± 0.075	0.211 ± 0.104	-2.871	9	0.018	0.691	↑
	C3	0.202 ± 0.127	0.227 ± 0.117	-2.555	9	0.031	0.648	↑

Notes. ↑ = significant increase. ↓ = significant decrease.

The sample mean and standard deviation of EEG spectral features during the 'baseline' and the 'recovery' states with eyes opened following robot-mediated fine motor interaction are shown in Figure 4.11. An increase of θ_{relative} and α_{relative} is visible in both Figure 4.11b and Figure 4.11c on all electrodes. Further, a significant increase in α_{relative} is visible on FP1 (t = -2.871, p = 0.018, r = 0.691) and C3 (t = -2.555, p = 0.031, r = 0.648), whereas

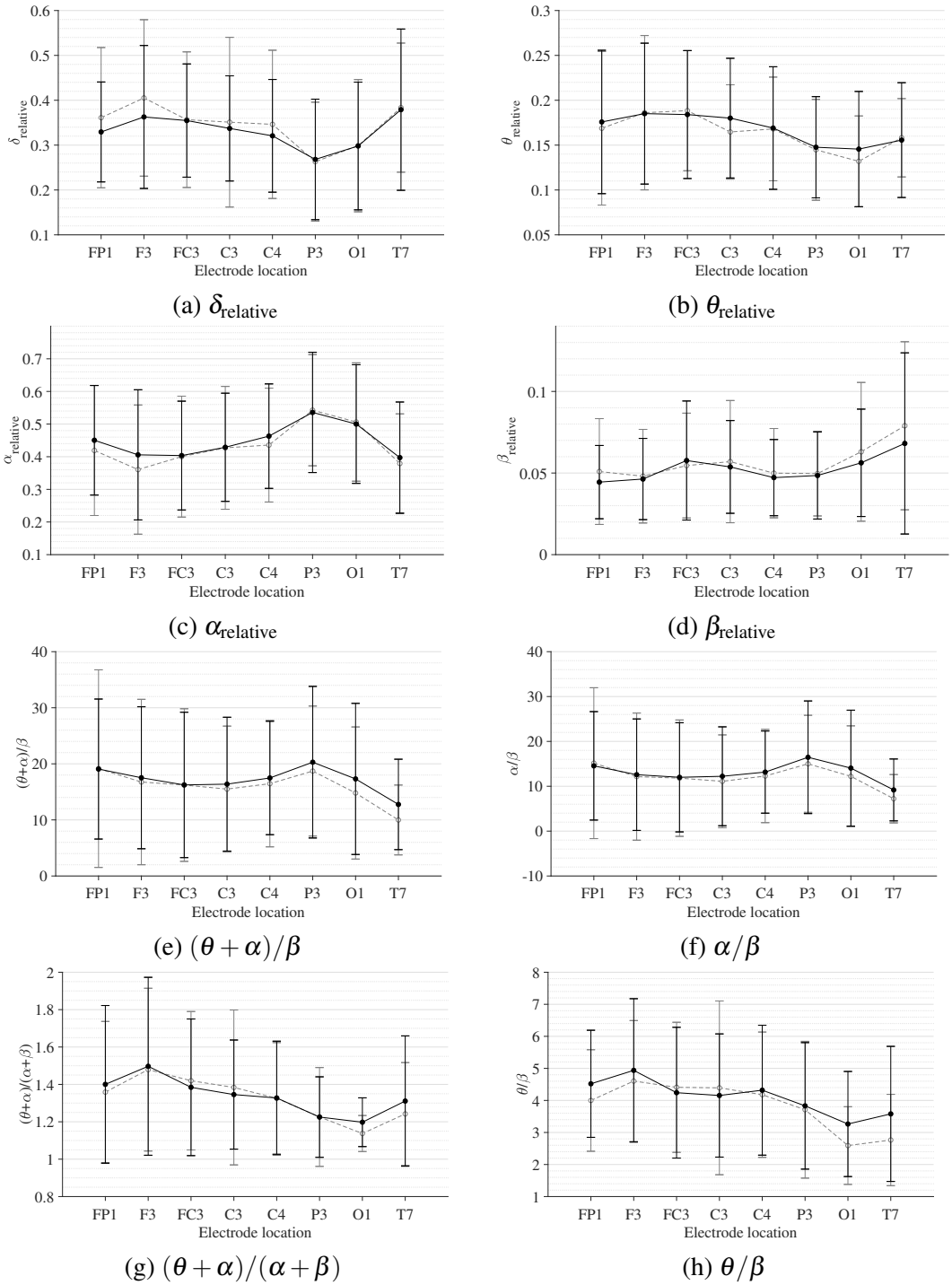

(a) δ_{relative} (b) θ_{relative}

(c) α_{relative} (d) β_{relative}

(e) $(\theta+\alpha)/\beta$ (f) α/β

(g) $(\theta+\alpha)/(\alpha+\beta)$ (h) θ/β

Figure 4.10: Comparison of the sample mean and standard deviation of EEG spectral features of all participants between 'baseline' and 'recovery' states with eyes closed for the gross motor interaction with HapticMASTER. The '- - ○ - - ' represents the 'baseline-eyes-closed' and '—●—' represents the 'recovery-eyes-closed'. *Connecting lines in subfigures do not imply a linear relationship between electrode locations but merely for the ease of identifying the numerical changes between baseline and recovery states.*

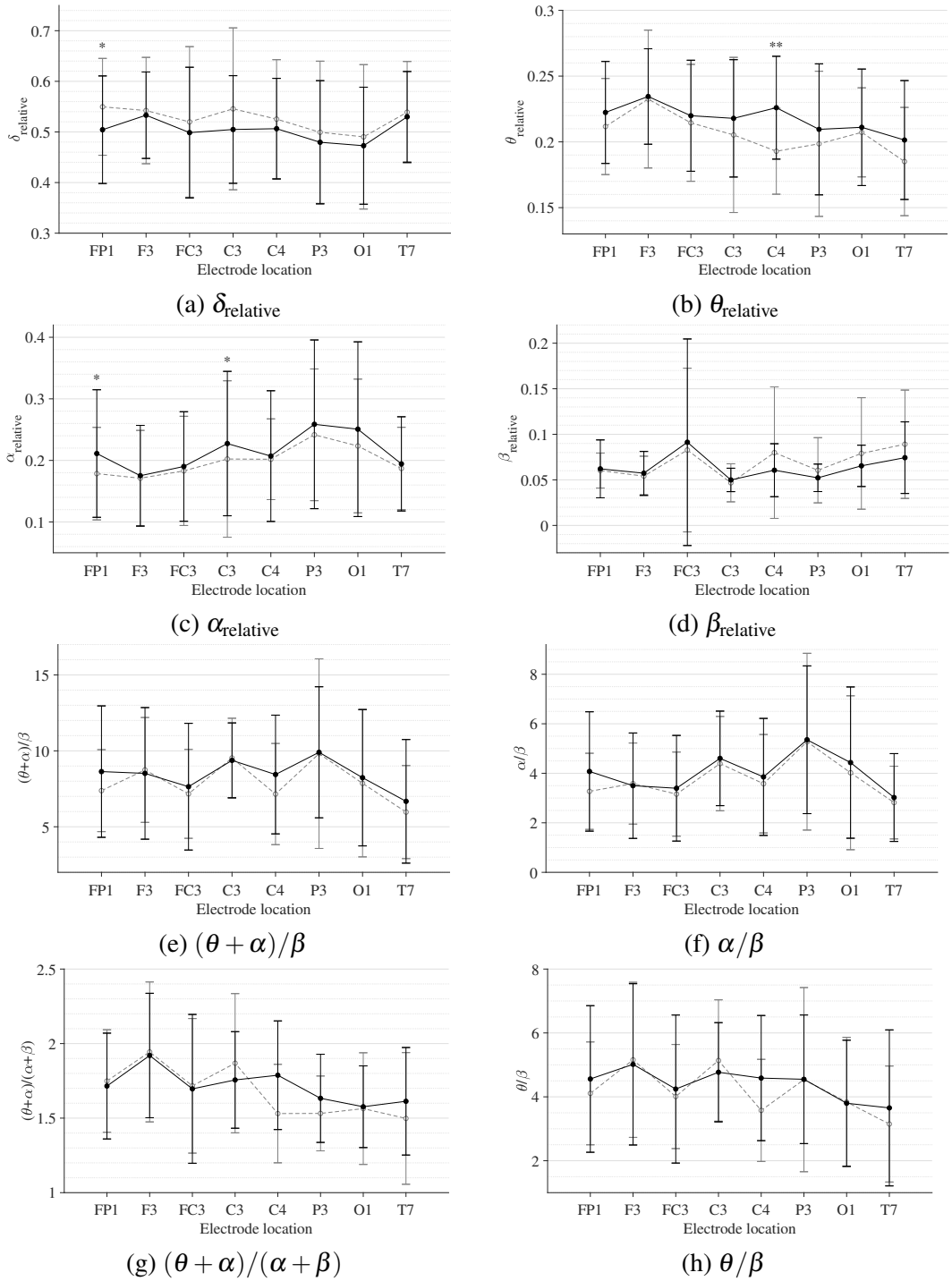

(a) δ_{relative} (b) θ_{relative}

(c) α_{relative} (d) β_{relative}

(e) $(\theta+\alpha)/\beta$ (f) α/β

(g) $(\theta+\alpha)/(\alpha+\beta)$ (h) θ/β

Figure 4.11: Comparison of the sample mean and standard deviation of EEG spectral features of all participants between 'baseline' and 'recovery' states with eyes opened for the fine motor interaction with SCRIPT passive orthosis. The '- - -○- - -' represents the 'baseline-eyes-opened' and '—●—' represents the 'recovery-eyes-opened' The statistical significance is represented by asterisks: i.e., * = $p < 0.05$ and ** = $p < 0.01$. *Connecting lines in subfigures do not imply a linear relationship between electrode locations but merely for the ease of identifying the numerical changes between baseline and recovery states.*

the significant difference in θ_{relative} is on C4 (t = -3.507, p = 0.007, r = 0.760). The effect of these variations in α_{relative} and θ_{relative} are also of larger magnitude, thereby suggesting that these variations are substantive findings. Similar to the aforementioned findings using gross motor task, Figure 4.11d shows that β activity has not significantly changed, and a decrease of variation across the sample is visible. Also, a general decrease in δ_{relative} on all electrodes and a significant decrease on FP1 with a larger effect size (t = 3.066, p = 0.013, r = 0.715) can be found in Figure 4.11a. No significant differences are visible in ratio band power measures (Figure 4.11d to Figure 4.11f). In general, these results show that the fatigue induced by fine motor interactions alters not only the activities around sensorimotor cortex but also the frontopolar cortex. Figure 4.12 shows the brain topographies of the difference between 'recovery' and 'baseline' states (i.e., difference = 'recovery' - 'baseline') of the substantive EEG features for one participant who reported a higher increase in the mental fatigue level than the physical fatigue level following the fine motor task. The topographical distributions also show that the modulations in the substantive EEG features following the fatiguing robot-mediated fine motor interaction are localised around frontopolar and central brain regions.

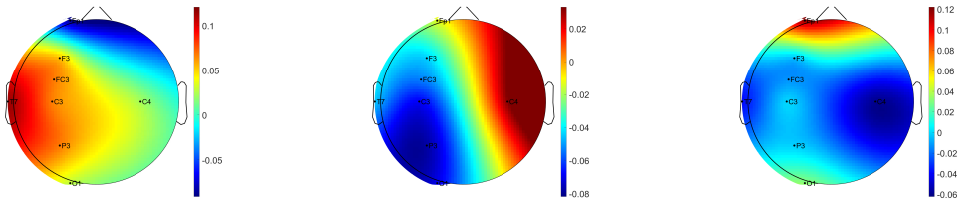

(a) δ_{relative} (b) θ_{relative} (c) α_{relative}

Figure 4.12: Brain topographies of substantive EEG spectral features for the difference between 'recovery' and 'baseline' states (i.e., difference = 'recovery' - 'baseline') with eyes opened for one participant following the fine motor interaction with SCRIPT passive orthosis. In each brain map, the nose is represented by the triangle on the top, and the right hemisphere is on the right. The red-shaded areas indicate a larger increase whereas the blue-shaded areas indicate a larger decrease.

The sample mean and standard deviation of EEG spectral features during the 'baseline' and the 'recovery' states with eyes closed following robot-mediated fine motor interaction is shown in Figure 4.13. Similar to the modulations in EEG spectral features estimated with eyes closed during the gross motor task, no significant variations are found in the eyes closed EEG spectral features following the fine motor task. However, similar trends are visible

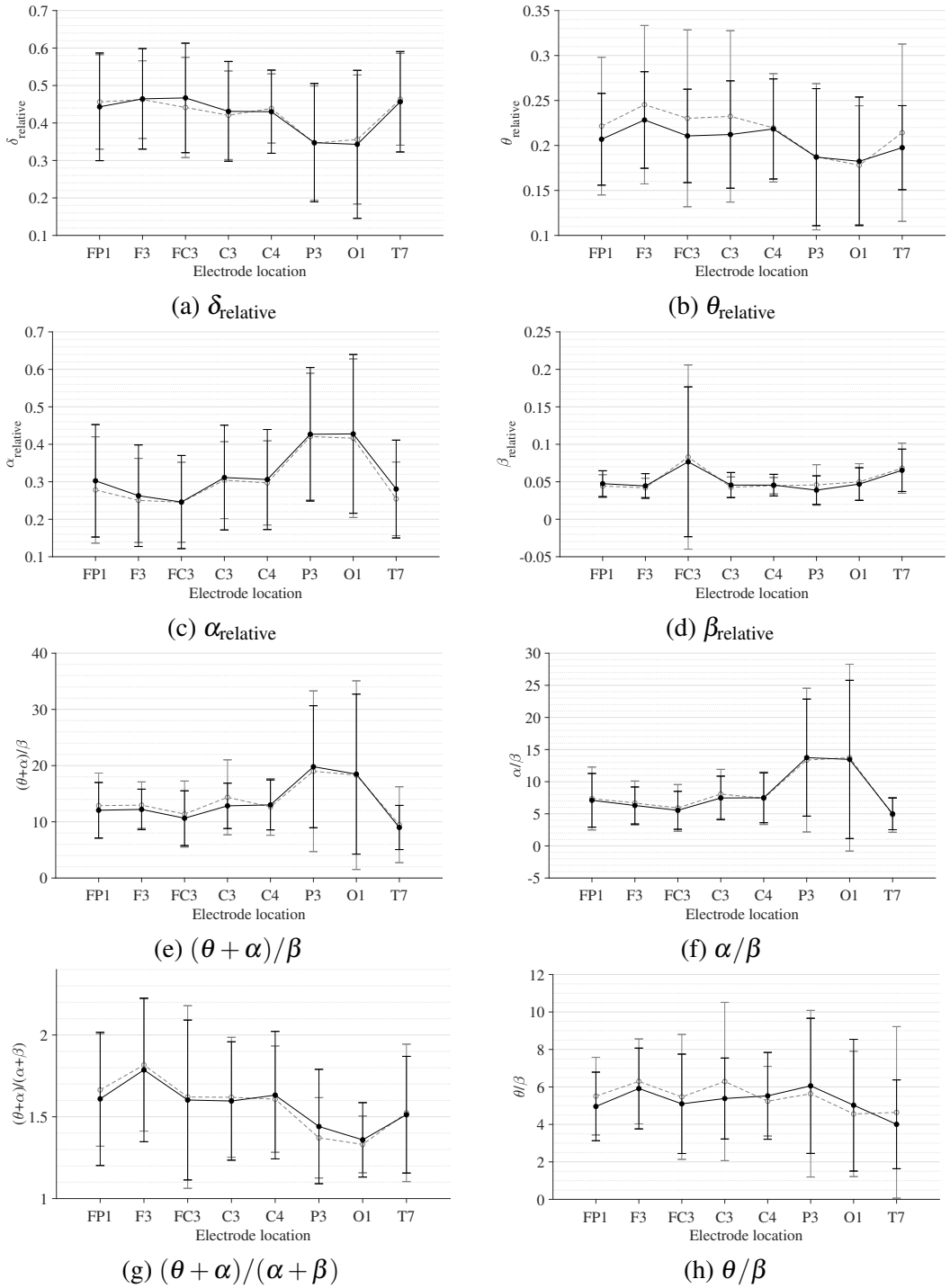

(a) δ_{relative} (b) θ_{relative}

(c) α_{relative} (d) β_{relative}

(e) $(\theta+\alpha)/\beta$ (f) α/β

(g) $(\theta+\alpha)/(\alpha+\beta)$ (h) θ/β

Figure 4.13: Comparison of the sample mean and standard deviation of EEG spectral features of all participants between 'baseline' and 'recovery' states with eyes closed for the fine motor interaction with SCRIPT passive orthosis. The '- - -○- - -' represents the 'baseline-eyes-closed' and '—●—' represents the 'recovery-eyes-closed'. *Connecting lines in subfigures do not imply a linear relationship between electrode locations but merely for the ease of identifying the numerical changes between baseline and recovery states.*

on the electrode locations that reported larger effect sizes during the eyes opened states following the fine motor task. The α_{relative} on FP1 and C3, $\theta_{relative}$ on C4 show an increasing trend, whereas δ_{relative} on FP1, shows a decreasing trend during the eyes-closed state. The findings of the paired-samples *t*-test performed on eyes-closed EEG spectral features are summarised in Appendix A.

4.2.3 Subjective Measures of Level of Fatigue, Workload, and Comfortability

A summary of the subjective responses on the level of fatigue, underlying workload and the comfortability of the experiment is given in Table 4.4.

Table 4.4: Summary of the subjective measures of level of fatigue, workload, and comfortability following the robot-mediated gross motor and fine motor interactions.

Subject ID	Robotic interface interacted with	Physical fatigue score		Mental fatigue score		Workload		Comfortability			
		Before	After	Before	After	Physical demand	Mental demand	Eye strain level	Comfortability in wearing the EEG cap	Effects of wearing the EEG cap on fatigue level	Effects of robotic interaction on fatigue level
A01	HM	2	3	2	3	Moderately	Moderately	Very	Somewhat	Moderately	Moderately
A02	HM	0	1	1	0	Somewhat	Not at all	Not at all	Moderately	Not at all	Moderately
A03	HM	0	1	1	1	Somewhat	Not at all	Not at all	Moderately	Not at all	Slightly
A04	HM	0	2	1	1	Moderately	Not at all	Not at all	Very	Not at all	Extremely
A05	HM	0	1	0	1	Somewhat	Moderately	Moderately	Very	Not at all	Slightly
A06	HM	1	2	1	1	Moderately	Somewhat	Somewhat	Moderately	Not at all	Moderately
A07	HM	1	2	2	1	Somewhat	Not at all	Moderately	Extremely	Not at all	Slightly
A08	HM	0	1	0	0	Moderately	Not at all	Somewhat	Extremely	Not at all	Slightly
A09	HM	0	0	0	0	Not at all	Not at all	Not at all	Very	Not at all	Not at all
A10	HM	3	2	3	2	Moderately	Somewhat	Somewhat	Moderately	Moderately	Not at all
B01	SPO	0	1	0	1	Somewhat	Somewhat	Not at all	Very	Not at all	Not at all
B02	SPO	1	3	1	4	Very	Extremely	Very	Very	Not at all	Slightly
B03	SPO	2	2	2	2	Somewhat	Somewhat	Moderately	Very	Not at all	Moderately
B04	SPO	0	0	0	1	Not at all	Somewhat	Not at all	Very	Not at all	Slightly
B05	SPO	1	0	0	3	Moderately	Very	Moderately	Moderately	Slightly	Slightly
B06	SPO	1	1	1	1	Somewhat	Not at all	Somewhat	Very	Slightly	Moderately
B07	SPO	0	0	1	1	Not at all	Not at all	Somewhat	Very	Not at all	Slightly
B08	SPO	1	2	1	2	Somewhat	Not at all	Moderately	Very	Slightly	Slightly
B09	SPO	2	1	3	1	Not at all	Not at all	Very	Moderately	Not at all	Slightly
B10	SPO	2	2	2	3	Somewhat	Moderately	Somewhat	Very	Slightly	Moderately

Notes. HM and SPO represents HapticMASTER and SCRIPT passive orthosis

A. Level of Fatigue and Workload

Figures 4.14 and 4.15 show the variations in physical and mental fatigue scores before and after the robot-mediated gross motor and fine motor tasks for each participant, respectively. As can be seen in Table 4.4 and Figure 4.14a, the majority of participants who performed the robot-mediated gross motor interaction with HapticMASTER reported an increase in their physical fatigue level following the task (8/10 participants). An increase in mental fatigue level was reported by two participants, only (Figure 4.14b). Among the participants who reported an increase in physical fatigue level, six participants showed a higher change in

physical fatigue scores than the change in mental fatigue scores following the gross motor task whereas two participants showed an equal rise in both physical and mental fatigue scores. Only one participant reported that he/she was physically and mentally very tired after the interaction, whereas the majority reported that they were somewhat to moderately physically fatigued after performing the gross motor task. Therefore, the subjective ratings suggest that the gross motor interaction may have induced physical fatigue. In contrast, as can be seen in Figure 4.15b, the majority of participants who performed the fine motor task revealed that their mental fatigue levels were increased following the robotic interaction (6/10 participants). An increase in physical fatigue level was only reported by three participants (Figure 4.15a). Among the participants who reported an increase in mental fatigue level

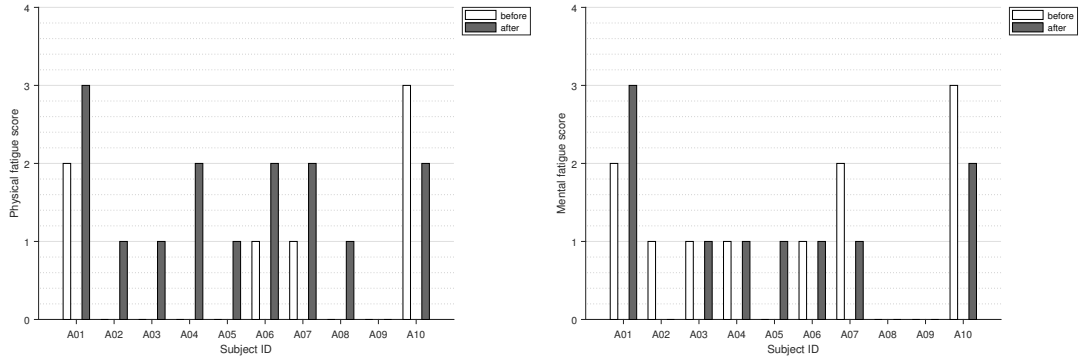

(a) Physical fatigue score (b) Mental fatigue score

Figure 4.14: Variations in subjective measures of (a) physical and (b) mental fatigue following gross motor interaction with HapticMATER for all participants.

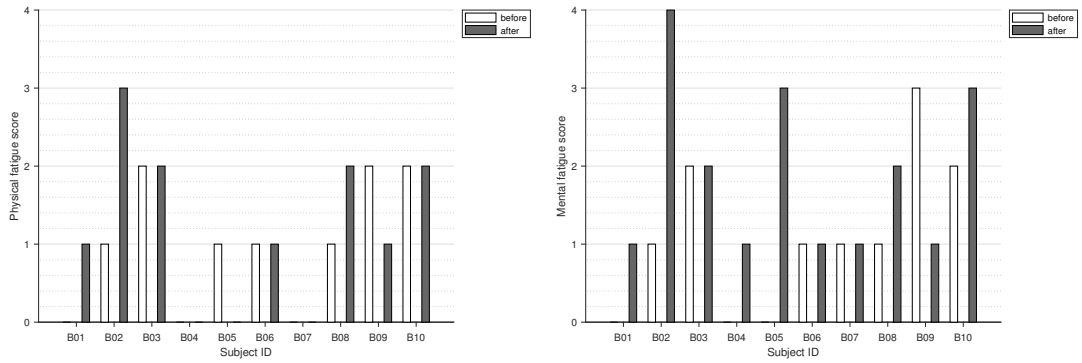

(a) Physical fatigue score (b) Mental fatigue score

Figure 4.15: Variations in subjective measures of (a) physical and (b) mental fatigue following fine motor interaction with SCRIPT passive orthosis for all participants.

following the fine motor task, four participants showed a higher change in mental fatigue scores than the change in physical fatigue scores whereas two participants showed an equal rise in both physical and mental fatigue scores. Three participants were very to extremely mentally fatigued after the fine motor task whereas the others were somewhat to moderately mentally fatigued. Therefore, the subjective ratings suggest that the fine motor interaction, on the other hand, may have induced mental fatigue.

The majority of participants (7/10 participants) also rated that the underlying physical workload of the gross motor task was greater than the mental workload. Most participants reported that the gross motor task was somewhat to moderately physically demanding whereas there was no mental demand. Figure 4.16a shows that all participants who experienced a greater increase in their physical fatigue levels in comparison to the change in mental fatigue levels also rated that the underlying physical workload of the gross motor task was greater than the mental workload. Participants feedback on the underlying workload of the fine motor task was highly subjective. Four participants reported that the fine motor task required higher mental demand than physical demand whereas two participants reported that the task required higher physical demand. Two participants also reported that the task was somewhat physically and mentally demanding whereas two participants reported that the task was not at all physically or mentally demanding. Figure 4.16b also illustrates that all participants who experienced a greater increase in their mental fatigue levels than the change in physical

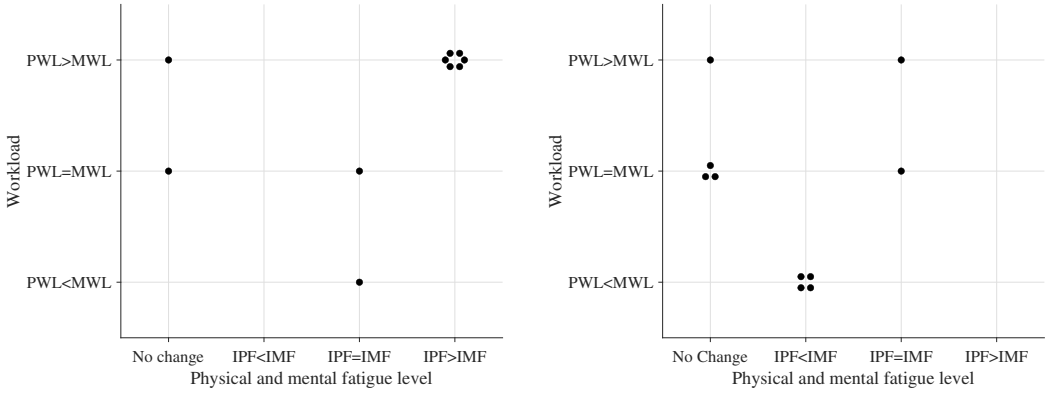

(a) Gross motor interaction with HapticMASTER

(b) Fine motor interaction with SCRIPT passive orthosis

Figure 4.16: Association of the variations in fatigue levels and the rated workload following the robot-mediated (a) gross motor and (b) fine motor interactions. The 'IPF' and 'IMF' refers to the increase in physical and mental fatigue scores following the robot-mediated interactions, respectively. No change refers to no increase or decrease in both fatigue levels. The 'PWL' and 'MWL' refers to the rated physical and mental workload, respectively.

fatigue level rated that the fine motor task required a greater mental demand than the physical demand. The gross motor task involves the movement and coordination of proximal joints and muscles of the upper limb (shoulder and arm) to control the robot arm between target points. The fine motor task requires considerable attention and decision-making skills combined with hand and finger movements to catch the fish when it reach the seashell. Therefore, the subjective responses imply that the gross motor task performed with HapticMASTER may have greatly contributed to the development of physical fatigue due to the increased physical demand. In contrast, the fine motor task performed with SCRIPT passive orthosis may have mainly induced mental fatigue due to the increased mental demand required during the task.

B. Comfortability

Figure 4.17 compares the subjective measures of task comfortability between robot-mediated gross motor and fine motor interactions. As can be seen in Table 4.4, the majority of participants who performed the gross motor task reported that the task was somewhat or not at all straining the eyes (7/10 participants). However, the eyes strain level caused by the fine motor task was highly dependent on the participant since 5/10 participants have rated the task to be somewhat or not at all straining the eyes, while 5/10 participants have reported the task very or moderately strained the eyes. Figure 4.17a also shows that the eye strain caused by the fine motor task is moderately higher than the gross motor task. In general, the majority of participants were very to extremely comfortable in wearing the EEG cap (13/20 participants) and reported that wearing the EEG cap does not affect the fatigue build-up (14/20 participants). Figure 4.17b shows that the participants who interacted with SCRIPT passive orthosis were very comfortable in wearing the EEG cap in comparison to the participants who interacted with HapticMASTER. Also, Figure 4.17c shows that wearing the EEG cap during the session is less likely to affect the fatigue level of an individual. The majority of participants have reported that the interaction with robot has either slight (10/20 participants) or moderate (6/20 participants) effect on their fatigue levels, while one participant reported that the use of the HapticMASTER has extremely affected the level of fatigue (Figure 4.17d).

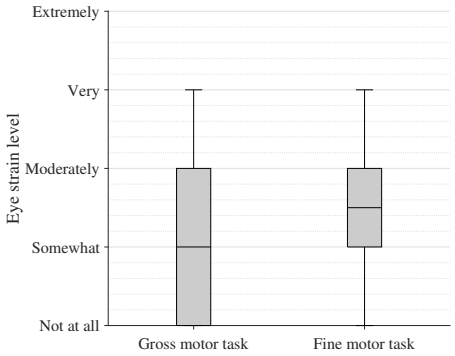

(a) Eye strain level

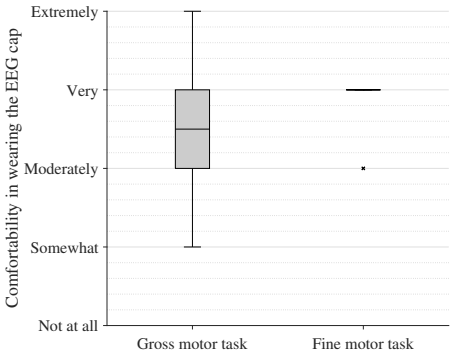

(b) Comfortability in wearing the EEG cap

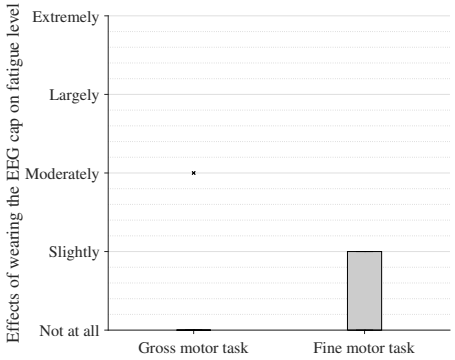

(c) Effects of wearing the EEG cap on fatigue level

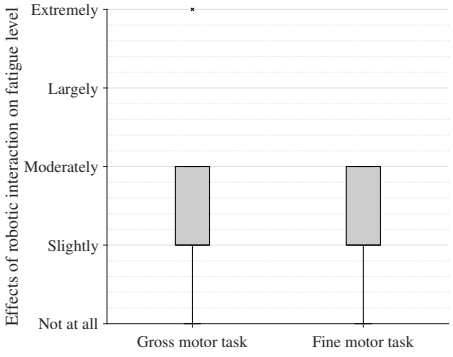

(d) Effects of robotic interaction on fatigue level

Figure 4.17: Comparison of the subjective measures of task comfortability between robot-mediated gross motor and fine motor interactions.

4.2.4 Association of the Changes in the Level of Fatigue with Substantive EEG Feature Modulations

The association of the substantive EEG feature modulations and the variations in the rated physical and mental fatigue levels following the robot-mediated gross motor task are shown in Table 4.5 and Figure 4.18. As can be seen in Figure 4.18, most participants who reported an increase in their physical fatigue level following the robot-mediated gross motor interaction also showed a greater increase in α_{relative} on FC3, C3, and P3 electrodes, $(\theta+\alpha)/\beta$ on C3 electrode and α/β on C3 electrode in comparison to the increase in the corresponding EEG features found in the participants who reported no change or reduction in the physical fatigue level. Similarly, a greater decrease in δ_{relative} on C3 electrode was also found in most participants who experienced a rise in their physical fatigue level. Therefore, the above findings show that the significant changes in δ_{relative}, α_{relative}, $(\theta+\alpha)/\beta$ and α/β around

the motor cortex are likely related to the rise in physical fatigue level following the gross motor task.

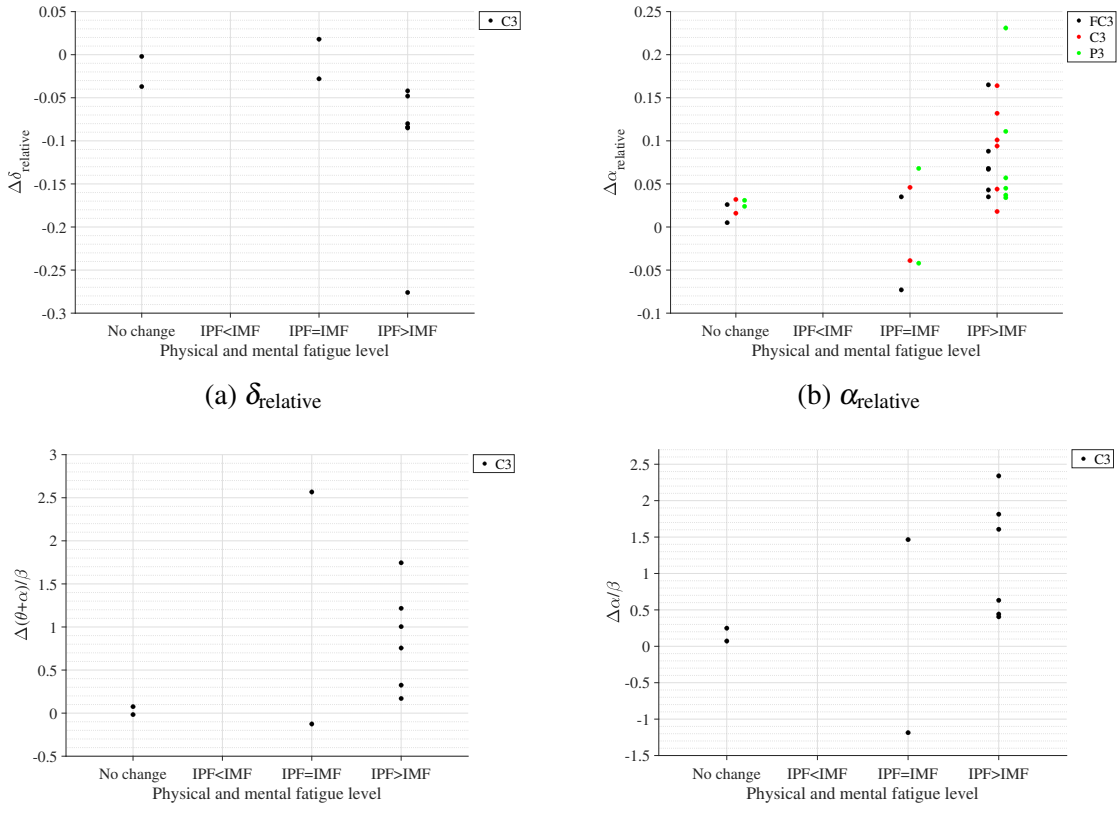

(a) δ_{relative} (b) α_{relative}

(c) $(\theta+\alpha)/\beta$ (d) α/β

Figure 4.18: Association of the substantive EEG feature modulations with variations in fatigue levels following the robot-mediated gross motor interaction. The Δ represents the difference in each EEG feature following the gross motor task (i.e., 'recovery' - 'baseline'). The 'IPF' and 'IMF' refers to the amount of increase in physical and mental fatigue scores following the robot-mediated interactions, respectively. No change refers to no increase or decrease in both fatigue levels.

Table 4.6 and Figure 4.19 show the association of the substantive EEG feature modulations following the robot-mediated fine motor task with variations in the rated physical and mental fatigue levels. Figure 4.19 shows that all six participants who reported an increase in mental fatigue level following the robot-mediated fine motor interaction showed a decrease in δ_{relative} on FP1 electrode. Among them five participants also showed an increase in α_{relative} on FP1 and C3 electrodes, and four participants showed an increase in $\theta_{relative}$ on C4. Therefore, the modulations in EEG spectral features around the prefrontal cortex presumably reflects an increase in the mental fatigue level.

Table 4.5: Association of the substantive EEG feature modulations with variations in fatigue levels following the robot-mediated gross motor interaction.

Subject ID	$\Delta\delta_{relative}$	$\Delta\alpha_{relative}$			$\Delta((\theta+\alpha)/\beta)$	$\Delta(\alpha/\beta)$	Comparison of the fatigue levels
	C3	FC3	C3	P3	C3	C3	
A01	-0.028	0.035	0.046	0.068	2.567	1.465	IPF=IMF
A02	-0.085	0.035	0.044	0.034	0.170	0.405	IPF>IMF
A03	-0.042	0.088	0.018	0.045	1.004	0.442	IPF>IMF
A04	-0.048	0.067	0.132	0.037	1.745	2.340	IPF>IMF
A05	0.018	-0.073	-0.039	-0.042	-0.126	-1.186	IPF=IMF
A06	-0.276	0.165	0.164	0.111	1.217	0.632	IPF>IMF
A07	-0.084	0.043	0.101	0.057	0.756	1.607	IPF>IMF
A08	-0.080	0.068	0.094	0.231	0.325	1.814	IPF>IMF
A09	-0.002	0.026	0.032	0.031	-0.017	0.249	No change
A10	-0.037	0.005	0.016	0.024	0.075	0.072	No change

Notes. The Δ represents the difference in each EEG feature following the gross motor task (i.e., 'recovery' - 'baseline'). The 'IPF' and 'IMF' refers to the amount of increase in physical and mental fatigue scores following the robot-mediated interactions, respectively. No change refers to no increase or decrease in both fatigue levels.

Table 4.6: Association of the substantive EEG feature modulations with variations in fatigue levels following the robot-mediated fine motor interaction.

Subject ID	$\Delta\delta_{relative}$	$\Delta\theta_{relative}$	$\Delta\alpha_{relative}$		Comparison of the fatigue levels
	FP1	C4	FP1	C3	
B01	-0.121	0.065	0.024	0.098	IPF=IMF
B02	-0.025	0.025	-0.003	0.020	IPF<IMF
B03	-0.061	0.053	0.021	-0.006	No change
B04	-0.007	-0.012	0.025	0.005	IPF<IMF
B05	-0.040	0.055	0.033	0.029	IPF<IMF
B06	-0.030	0.038	0.013	0.051	No change
B07	0.009	0.067	-0.001	0.014	No change
B08	-0.103	-0.020	0.072	0.033	IPF=IMF
B09	0.012	0.028	0.028	0.007	No change
B10	-0.086	0.031	0.116	-0.001	IPF<IMF

Notes. The Δ represents the difference in each EEG feature following the fine motor task (i.e., 'recovery' - 'baseline'). The 'IPF' and 'IMF' refers to the amount of increase in physical and mental fatigue scores following the robot-mediated interactions, respectively. No change refers to no increase or decrease in both fatigue levels.

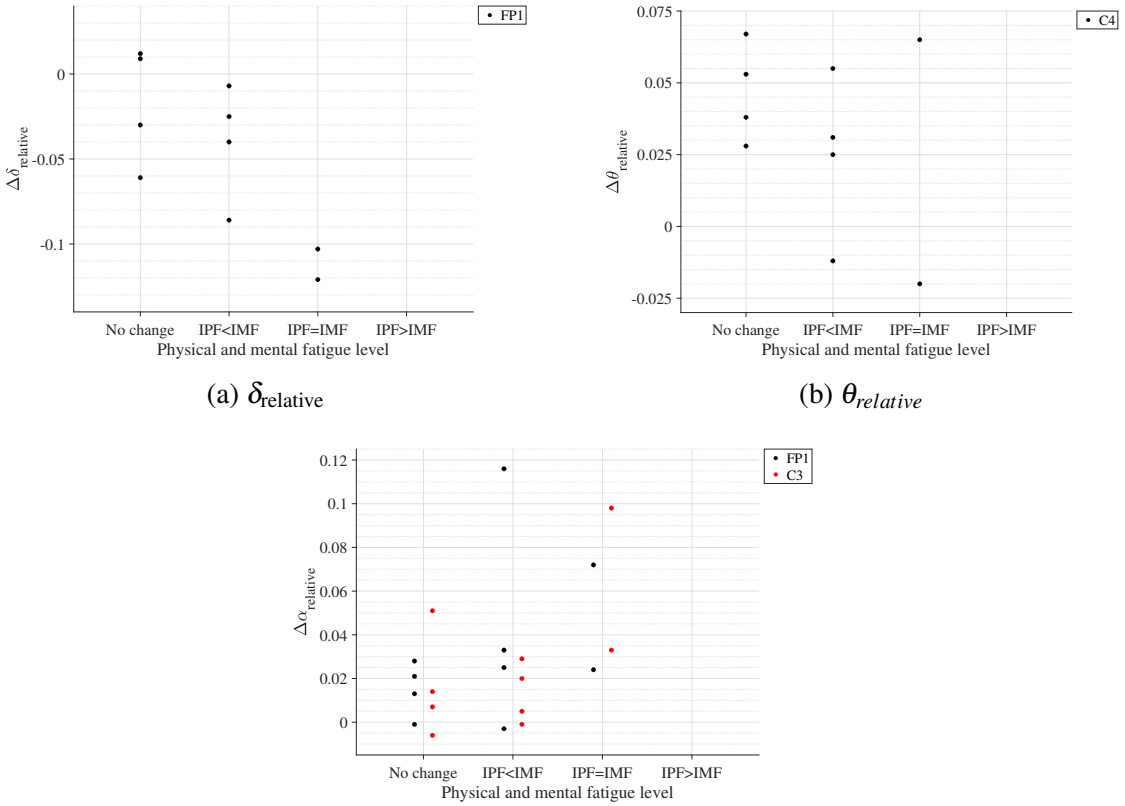

(a) δ_{relative}

(b) $\theta_{relative}$

(c) α_{relative}

Figure 4.19: Association of the substantive EEG feature modulations with variations in fatigue levels following the robot-mediated fine motor interaction. The Δ represents the difference in each EEG feature following the fine motor task (i.e., 'recovery' - 'baseline'). The 'IPF' and 'IMF' refers to the amount of increase in physical and mental fatigue scores following the robot-mediated interactions, respectively. No change refers to no increase or decrease in both fatigue levels.

4.3 Discussion

This preliminary experiment investigated the changes in cortical activities associated with fatigue induced by upper limb robot-mediated gross motor and fine motor interactions. The findings of this experiment indicate that it is possible to monitor fatigue introduced by these interactions using EEG spectral features, which can have further utility for robot-mediated rehabilitation.

The most prominent finding of this experiment was a significant increase of α_{relative} following both the robot-mediated gross motor and fine motor interactions. It is known that α activity is most commonly visible during relaxed conditions and decreased attention levels. Also,

in drowsy but wakeful states when increased efforts are taken to maintain the level of attention and alertness, increased α activity is visible (Klimesch, 1999). On the other hand, when an individual is in an alert state, suppression of α activity is visible. The task-related desynchronisation, which leads to a decrease in α activity, can be interpreted as an electrophysiological correlate of increased activation of the cortical areas (excited neural structures) that produce motor behaviour or process sensory or cognitive information (Pfurtscheller, 1997; Pfurtscheller et al., 1996). Therefore, the increased α_{relative} following the robot-mediated interactions may reflect decreased cortical activity and a reduced capacity for information processing in the underlying cortical regions as a result of fatigue. This finding is in agreement with the findings of previous fatigue studies (Barwick et al., 2012; Eoh et al., 2005; Fan et al., 2015; Zhao et al., 2012; Zou et al., 2015).

The topographical differences found in the prominent EEG spectral features indicate that the brain regions most affected by fatigue may depend on the physical and mental workload associated with the task as well as on the differences in the usage of the proximal and distal upper arm. In the gross motor interaction, participants were instructed to move the HapticMASTER robot arm in a linear trajectory so that the two target points visible in the virtual reality environment can be reached. In a visually guided reaching task, the spatial information about the target is extracted by the sensory system, and a movement plan is created and executed by the motor cortex (Gevins and Smith, 2007; Sabes, 2000). The premotor cortex, primary somatosensory cortex, and posterior parietal cortex integrate motor and sensory information for planning and coordinating complex movements. Also, the HapticMASTER is an end-effector based robot, and the proximal upper limbs (arm and shoulder) are predominantly used when moving the robot arm between the target points during the gross motor task. Therefore, the significant rise in α_{relative} found over FC3, C3, and P3 electrode locations presumably reflect the inhibition of premotor cortex, primary somatosensory cortex, and posterior parietal cortex activation due to the physical fatigue accumulated during the arm reach/return task. Conversely, in the fine motor task participants were expected to perform hand open/close gesture only when a fish was near the seashell in the virtual environment. Therefore, the fine motor task required more sustained attention and decision-making, in comparison to the gross motor task. Laureiro-Martinez et al. (2014) also found that a stronger activation in the frontopolar cortex is associated with higher decision-making efficiency. In addition, active movements consisting of repetitive opening and closing of the hand are shown to activate the contralateral primary sensorimotor cortex (Guzzetta et al., 2007). Therefore, the increased α_{relative} over FP1 and C3 electrodes following the repetitive fine movements appear to reflect an altered decision-making efficiency of an individual, in addition to the deactivation in motor cortex associated with fatigue. The

topographical variations in α_{relative} were also supported by the participants' feedback on their fatigue level after each interaction. The greater changes in α_{relative} following the gross motor task were also associated with more increase in the physical fatigue level than the mental fatigue level. In contrast, the greater changes in α_{relative} following the fine motor task were associated with more increase in the mental fatigue level than the physical fatigue level or an equal increase in both physical and mental fatigue levels.

It has been established in the literature that EEG activity shifts from high frequencies towards slower waves with the progression of fatigue, thus, the ratio between low-frequency and high-frequency power can also be considered as a reliable measure of fatigue (Eoh et al., 2005; Jap et al., 2009). In this experiment, significant differences were found only in $(\theta+\alpha)/\beta$ and α/β on C3 electrode following the physically fatiguing gross motor task. These findings were also supported by the participants' feedback on their fatigue level. There were no significant differences in the power ratios due to the fine motor task. Although the significant changes on C3 were only visible for α_{relative}, a slight increase in $\theta_{relative}$ and a decrease in $\beta_{relative}$ were also found after the gross motor task. Therefore, the findings suggest that gross motor interaction increased the low-frequency activities while suppressing the high-frequency activities on C3 electrode, which may have caused the significant increase of $(\theta+\alpha)/\beta$ and α/β. Jap et al. (2009), Eoh et al. (2005), Fan et al. (2015), Chen et al. (2013) also reported a significant rise in both $(\theta+\alpha)/\beta$ and α/β with fatigue.

The suppression in δ_{relative} following the robot-mediated interactions is contrary to some previous studies which have suggested a significant increase or no significant difference in δ activities due to fatigue (Craig et al., 2012; Lal and Craig, 2002; Zhao et al., 2012). Although not significant, Zhao et al. (2012) also showed a reduction in δ_{relative} around all brain regions after a simulated driving task. In this experiment, significant decrease in δ_{relative} was found on C3 electrode following the gross motor task and on FP1 electrode following the fine motor task. Most participants who reported an increase in their physical fatigue level after the robot-mediated gross motor task also have experienced a decrease in δ_{relative} on C3 electrode. Similarly, all participants who reported an increase in their mental fatigue level following the robot-mediated fine motor task also showed a decrease in δ_{relative}. Therefore, the suppression in δ_{relative} due to fatigue build-up and the topographical variations found in the two tasks are supported by the subjective measures of fatigue level. The methodological differences of the previous studies could be an explanation for these discrepancies as these studies were based on vehicle driving tasks, whereas our study was focused on gross and fine motor tasks in a human-robot interaction scenario. Harmony et al. (1996) proposed that increased attention to internal processing (i.e., 'internal concentration') during mental tasks might cause an increase in the delta activity. In order to accurately perform the two tasks in this

experiment, higher concentration and attention levels are essential. Therefore, the reduction in δ_{relative} associated with the robotic interactions may suggest a deficient inhibitory control and information-processing mechanisms. This finding, while preliminary, suggests that the fatigue may have negatively affected an individual's attention and internal concentration levels.

The ipsilateral primary somatosensory cortex is also shown to increase its level of activation during prolonged sustained and intermittent sub-maximal muscle contractions to compensate for fatigue (Liu et al., 2003). In this experiment, the significant change in C4 electrode was visible only for θ_{relative} following fine motor task. Theta oscillations in EEG have shown to be prominent during cognitive processing that requires higher mental effort and is positively related to the task difficulty (Gevins et al., 1997). Barwick et al. (2012), Cheng and Hsu (2011) and Zhao et al. (2012) also reported an increase in θ_{relative} due to fatigue build-up. Therefore, the rise in θ_{relative} on C4 may reflect the fatigue-related changes in the ipsilateral brain activation caused by the fine motor task.

4.3.1 Limitations in the Experiment Design

Although the present experiment found that fatigue in robot-mediated interactions can be estimated using EEG spectral features, there were some limitations in this experiment design. The spatial precision of the recordings was limited since the EEG data acquisition system could only support eight electrode locations. In this experiment the majority of the electrodes were placed on the left hemisphere and only one electrode was placed on the right hemisphere. Also, only one electrode location was considered in each brain region, except in the central region where two electrodes locations were investigated. The findings showed that regional EEG spectral feature differences exist between the two tasks; and the differences were associated with the variations in type of fatigue mostly experienced by the individuals. Therefore, further exploration is needed with a higher number of electrodes to confirm whether the brain regions mostly affected by fatigue in robot-mediated interactions depend on the physical and cognitive nature of the task and the differences in the usage of upper limbs. Moreover, in this study EEG data recorded before and after the robotic interactions were further analysed since previous studies have found significant alterations in resting-state EEG spectral features following fatigue-inducing physical and mental tasks (Chen et al., 2013; Cheng and Hsu, 2011; Ng and Raveendran, 2007; Tanaka et al., 2012). Further exploration is needed to identify the EEG feature modulations caused by fatigue build-up during the robot-mediated interaction as well. These limitations were addressed in the second experiment conducted in this thesis.

4.4 Conclusions

The modulations in EEG spectral features due to fatigue induced by robot-mediated fine motor and gross motor interactions were presented in this chapter. The modulations in α_{relative} presumably reflect the changes in an individual's fatigue level following upper limb robot-mediated interactions. The above inference was also supported by the participants' feedback on the changes in their physical and mental fatigue levels following the given task; thereby suggesting that α_{relative} is a reliable EEG-based fatigue index that can be used to monitor the progression in fatigue during human-robot interactions. Although the suppression in δ_{relative} is contrary to the findings of previous studies, it was supported by the participants' feedback. Therefore, δ_{relative} could also be used as an EEG-based measure of fatigue in robot-mediated interactions. It can also be concluded that $(\theta+\alpha)/\beta$ and α/β can describe the underlying changes in brain caused by the rise in physical fatigue level following a robot-mediated interaction.

Investigation of regional differences in EEG spectral feature modulations revealed that the fatigue induced by gross motor and fine motor tasks suppresses the activation of different brain regions. The participant's feedback also revealed that the gross motor task increased the physical fatigue level of most participants whereas the fine motor task increased the mental fatigue level of most participants. Also, the gross motor task was found to be more physically demanding than mentally demanding. In contrast, most participants revealed that the fine motor task required either a greater mental demand or an equal physical and mental demand. In conclusion, regional differences in significant EEG spectral features associated with fatigue are most likely due to the differences in task definition that may have differently altered the physical and mental fatigue level of an individual. Therefore, EEG correlates of fatigue during robot-mediated interactions are specific to the physical or cognitive nature of the task performed using the proximal or distal upper limb. Developing on the findings of this chapter, the following chapters further explore EEG features and brain regions that can be used to estimated fatigue induced by a robot-mediated visuomotor tracking task.

Chapter 5

Experiment 2 - Part I: Modulations in Spectral and Nonlinear EEG Features Associated with Fatigue in a Visuomotor Tracking Task Performed Using the GENTLE/EEG Robot-Mediated System

The preliminary experiment presented in Chapter 4 showed that the EEG correlates of fatigue during robot-mediated interactions are specific to the physical or cognitive nature of the task performed using the proximal or distal upper limb. However, since the experiment was conducted using a limited number of EEG electrodes, an in-depth analysis of the regional variations in EEG patterns due to fatigue could not be explored. Developing further on the outcomes of the preliminary experiment, the GENTLE/EEG robot-mediated system explained in this chapter was implemented to evaluate the modulations in both spectral and nonlinear EEG features during a fatiguing robot-mediated visuomotor tracking task. The association of the substantive EEG-based fatigue indices with the movement variability measures and subjective measures of fatigue is further discussed in Chapter 6. Therefore, findings discussed in Chapter 5 and Chapter 6 taken together address the research question 2: *'Which spectral and nonlinear EEG features and which EEG electrode locations are most capable and reliable in estimating the progression of fatigue during a robot-mediated visuomotor tracking task?'*.

5.1 Methods and Materials

5.1.1 Ethical Approval

The experiment was approved by the Ethics Committees with Delegated Authority for Science and Technology of University of Hertfordshire (Protocol number: COM/PGR/UH/02973).

5.1.2 Participants

Twenty-five healthy individuals (13 females and 12 males) that were at least 18 years of age (average age of the sample was 32 ± 12 years; mean $\pm$ SD) were recruited for the experiment. Eligibility criteria required individuals to be right-handed with no previous injuries to the right hand that caused arm functional difficulties and no previous severe injuries to the head or the brain, and not suffering from epilepsy. Moreover, the participants were instructed to wash their hair the night before or on the day of the test with shampoo without using any conditioners and not to use any hair care products such as hair creams, sprays or styling gel as these products may affect the quality of the recording. They were asked to abstain from taking caffeine, nicotine, or alcohol, eating a heavy meal or chewing gum, and engaging in any strenuous exercise at least 2 hours before the experiment as these could create adverse effects on the progression of fatigue and on the EEG data recordings which are of major interest in the experiment (Docter et al., 1966; Gilbert, 1987; Hall et al., 2007; Masumoto et al., 1999; Siepmann and Kirch, 2002). All participants signed the informed consent forms before participation. A summary of the participant demography is given in table 5.1. All participants had normal vision or had corrected to normal vision. The participant's self-reports showed that most participants had around 7 to 9 hours of sleep the night before the experiment, that is recommended for adults (Hirshkowitz et al., 2015); thus, it can be assumed that fatigue build-up was solely due to the robotic interaction. While this experiment aimed at the observation of EEG feature modulations with increasing level of fatigue, participants were free to stop the experiment at any point in time. All participants completed 5 levels of the visuomotor tracking task.

5.1.3 GENTLE/EEG Robot-Mediated System

The GENTLE/EEG robot-mediated system was implemented by the author, as explained below, to investigate the variations in brain activation patterns caused by the fatigue in robot-mediated visuomotor tracking task. The complete experiment, including obtaining the participants consent and questionnaire responses, preparation for EEG data acquisition, EEG data acquisition before, during, and after the robot-mediated visuomotor tracking

Table 5.1: Participants demography of experiment 2.

Subject ID	Age	Gender	Wearing glasses/ contacts	Hours slept prior to the experiment
C01	64	M	N	7
C02	21	F	Y	6
C03	23	M	N	7
C04	19	M	N	6
C05	22	F	N	5
C06	44	F	Y	7
C07	22	M	N	6
C08	22	F	Y	4
C09	22	F	N	7
C10	20	F	N	>9
C11	39	F	Y	7
C12	36	F	N	6
C13	36	F	Y	7
C14	38	M	N	8
C15	29	F	Y	7
C16	59	F	N	8
C17	33	M	Y	6
C18	25	M	N	8
C19	24	F	N	8
C20	24	F	Y	7
C21	32	M	N	>9
C22	19	M	N	>9
C23	29	M	N	5
C24	35	M	N	5
C25	69	M	Y	7
Summary	32 ± 12	M=12, F=13	Y=9	$\geq 7 = 16$

task, and cleaning the electrode gel after the EEG data recording session lasted for about 1 hour. The duration of the robotic interaction was limited to 25-minutes due to difficulties in obtaining ethical clearance for more extended duration studies and recruiting participants in an academic environment. Therefore, to obtain measurable fatigue-induced EEG signal pattern changes in a duration of 25-minutes, the difficulty level during the robotic interaction was gradually increased.

The GENTLE/EEG robot-mediated system mainly comprised of three components: the HapticMASTER, 32-channel non-invasive EEG data acquisition system, and a virtual reality environment that facilitates a visuomotor tracking task (Figure 5.1). The user controls the movement of the robot arm using their right arm and performs the visuomotor tracking task as explained in Section 5.1.3. The changes in the brain activities, before, during and after the robotic interaction were measured using the EEG data acquisition system explained in Section 5.1.3. Figure 5.2 shows the experimental environment of the GENTLE/EEG robot-mediated system.

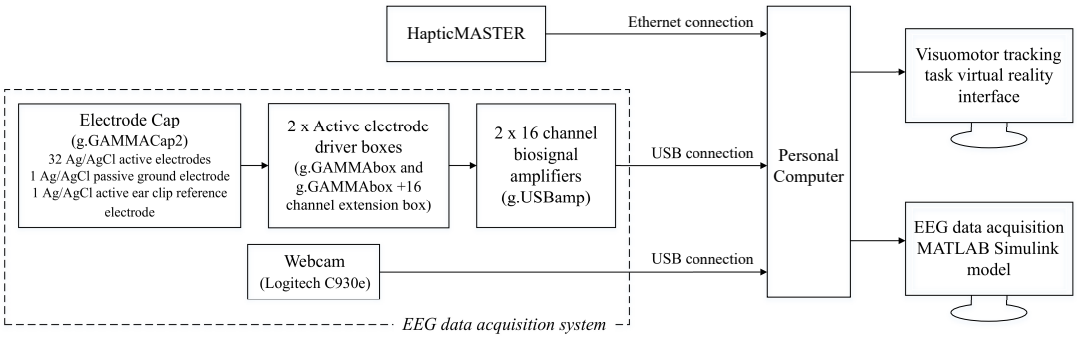

Figure 5.1: Components of the GENTLE/EEG robot-mediated system.

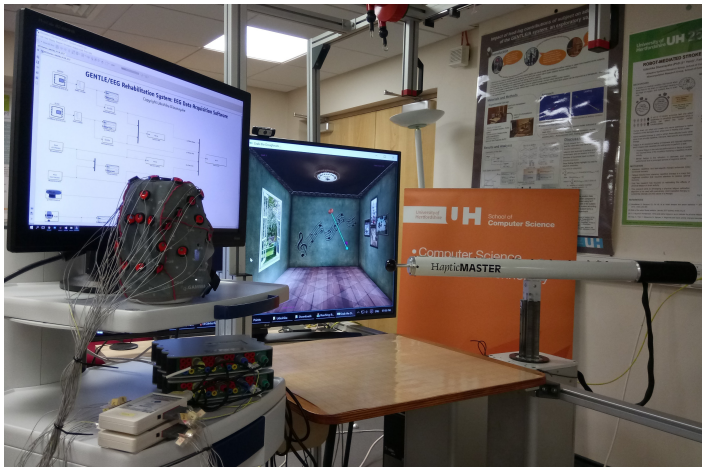

Figure 5.2: The experimental environment of the GENTLE/EEG robot-mediated system.

A. Visuomotor Tracking Task

Exercises that involve moving the arm away from the body (reaching) and returning towards the body (returning) are extensively used in robot-mediated stroke therapies since arm reach/return is the primary motion involved in many activities of daily living. Therefore,

a similar arm reach/return task named 'Grab the Doughnuts' which involves an additional point tracking component was implemented as explained below to build a fatiguing state for the user gradually. In the context of this thesis, this robotic interaction will be called as a *'robot-mediated visuomotor tracking task'* since it involves tracking a guide point while reaching and returning from one target point to the other.

Mode of Operation

The HapticMaster works under the admittance control paradigm in which positional changes are generated according to the force exerted by the operator on the device. The HapticMASTER API provides the facility to change the spring or damper haptic effects or any combination of them in real-time to introduce different therapeutic modes. In patient passive, active and active-assisted modes, the robot assists the arm movement entirely or to some extent. The assistance provided by the robot could negatively affect the fatigue build-up of healthy participants within a limited duration of interaction. Therefore, in this experiment, the damping or 'accommodation' mode that is purely viscous and has no stiffness (Carignan and Akin, 2003) was introduced to let the participants move the robot arm between the target points voluntarily with no assistance from the robot. In this mode of operation, the difficulty level of the interaction was increased by gradually increasing the damping coefficient parameter in real-time while keeping the spring stiffness equal to zero. Damping force of the robot can then be increased if the movement of the robot arm is constraint to a constant velocity since $F_d = C_d \times V$, where F_d, C_d and V are Damping force, damping coefficient and velocity respectively. Movement of the robot arm at a constant velocity was achieved by instructing the participants to follow the trajectory covered by the guide point visible in the virtual reality environment while maintaining the movement of the robot arm at a speed similar to the speed of the guide point. The force exerted by the user will rise in response to the increment in the damping force, thereby contributing towards an increase in the work done by the subject. Therefore, the participants will experience a gradual increase in their fatigue level during the robot-mediated interaction.

Damping Coefficient Parameter and Duration Settings of the Interaction

The robot-mediated interaction had five levels, with each lasting for 5-minutes. Therefore, the participants would interact with the robot for 25-minutes in total, without having a break in between each level. The damping coefficient parameter was set to be 80 at level 1, 100 at level 2, 120 at level 3, 140 at level 4, and 160 at level 5.

Virtual Reality Environment

The HapticMASTER end effector has a 3D volumetric workspace as explained in Section 2.4.2. Hence, a virtual reality environment resembling a real empty 3D room with three walls, a marble floor, and a ceiling was created so that a better depth perception could be achieved when displayed in a 2D monitor (Figure 5.3). Inside the virtual room, the target points to be reached were represented by the Sienna colour solid tori to resemble the shape and texture of doughnuts. In addition, the solid tori were set to rotate so that they were easily distinguishable as target points. Thirteen (13) target points as shown in Figure 5.4 (the (x,y,z) coordinates of set target points are given in Table B.1) were carefully chosen so that the non-planar robot arm movements throughout the given duration would traverse the HapticMASTER workspace while positively contributing towards the progression of fatigue. Moreover, with the use of a substantial number of target locations, random point placement was achieved, thus prevented the ability of the user to predict the next segment. The movement between two adjacent target points (or doughnuts) was termed as a '*segment*'. All target points were reached in twenty-four (24) segments, with 12 segments consisting of movement from points 1 to 13 (forward loop) and the next 12 segments consisting of movement from points 13 to 1 (reverse loop). The movement order was repeated until the maximum interaction duration of the level was reached, and the same movement order was repeated at each level. Also, the distance between two adjacent targets (i.e., the '*segment length*') was equal in each segment. The position of the purple colour ball in the virtual room represented the projection of the current position of the end effector, thereby giving feedback to the user on the direction of the next move in real space. In the context of the thesis, this point will be referred to as the control point. Furthermore, the constrained motion of the robot arm was introduced by forcing the subject to follow the path covered by the guide point while maintaining the speed of the control point (i.e. the speed of the robot arm motion) similar to the speed indicated by the motion of the guide point. The guide point, represented by a deep sky blue icosahedron, moved towards the target to be reached at a constant set speed. A straight line trajectory that connects the previously reached target point and the target to be reached next was considered as the trajectory of the guide point.

Message boxes were used to inform the start of a new level, and the end of the session. The participants were instructed to press the *return key* of the keyboard to continue after each message prompt. The key-press event was used here so that the EEG data recordings can be synchronised with the interaction level for data post-processing. The robot arm moved to the starting location (point 1 in Figure 5.4) while following a straight line trajectory with the minimum jerk settings after the key-press event at the start of each interaction level. Then, a

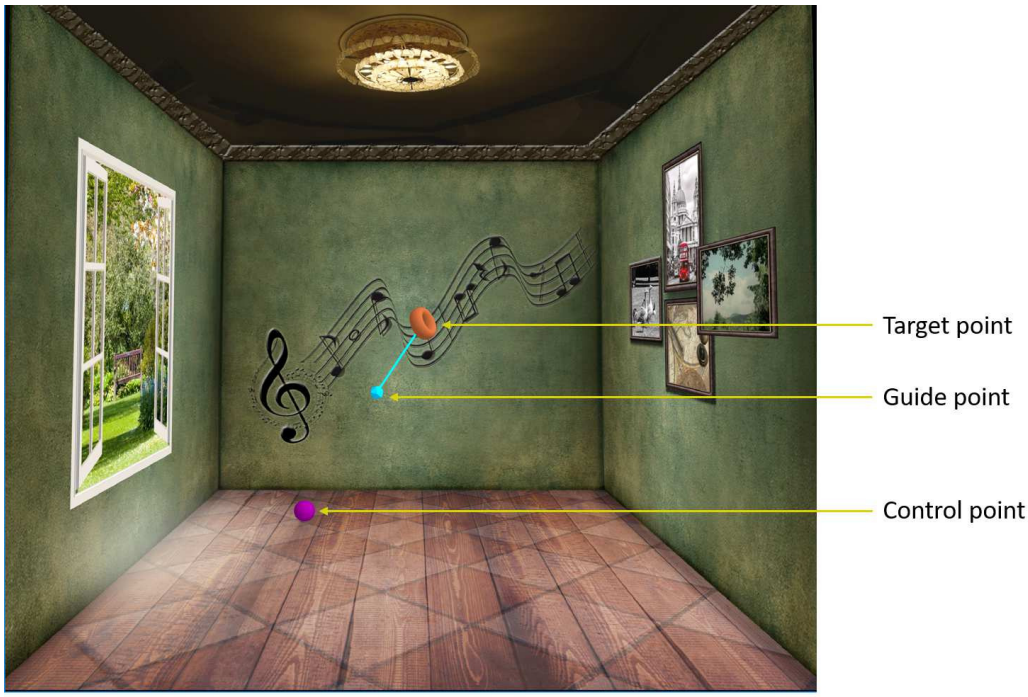

Figure 5.3: The GENTLE/EEG virtual environment. The target point is represented as a doughnut. The purple ball indicated the position of the end effector. The deep sky blue icosahedron moved according to the assigned speed.

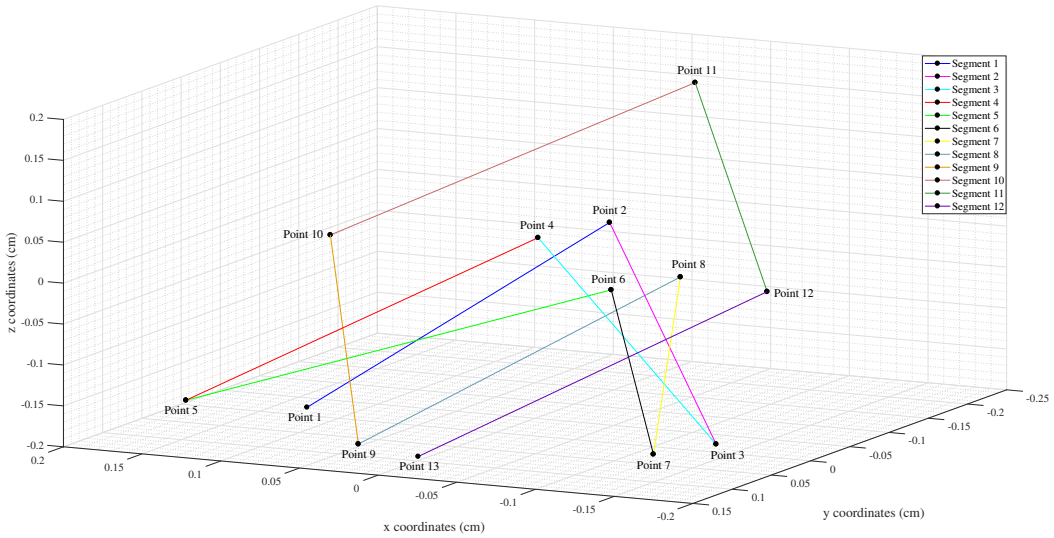

Figure 5.4: Target point locations in the virtual reality environment. The forward loop of the motion is from Point 1 to 13. The reverse loop of motion is from Point 13 to 1.

short sound prompt was played, and the new target point appeared in order to inform the user to begin the next move.

Updating the System Parameters and Data Logging

Visual C++ programming language enables the use of timers and multi-threading features to run two or more programs concurrently. Therefore, a 50-millisecond timer was used to update the damping coefficient and the spring constant values according to the interaction level settings and to read and update the 3-dimensional values of the force, position and velocity of the end effector. Simultaneously, a thread function was used to record the kinetic and kinematic data (applied force, position, velocity) of the HapticMASTER. The thread was activated at the beginning of the interaction and was called at each 50-millisecond instance, until the end of the interaction. Thus, the kinetics and kinematics data were logged at a sampling rate of 20 Hz (with a 50 ms period) using Comma-Separated-Values (CSV) files.

B. EEG Data Acquisition System

Selection of the EEG electrodes

In this experiment, it was of interest to find the EEG electrode locations that best describe the modulations associated with fatigue in robot-mediated interactions. According to the International 10-10 system of electrode placement (Epstein, 2006), FP1, FP2, F3, Fz, F4, FC3, FCz, FC4, C5, C3, C1, Cz, C2, C4, C6, CP3, CPz, CP4, P3, P1, Pz, P2, P4, PO3, PO4, O1, Oz, O2, T7, T8, P7, and P8 electrode locations were selected so that a wider brain region can be explored. The electrode distribution among the brain regions was as follows (Liu et al., 2014):

- Frontal region: FP1, FP2, F3, Fz and F4
- Central region: FC3, FCz, FC4, C5, C3, C1, Cz, C2, C4, and C6
- Parietal region: CP3, CPz, CP4, P3, P1, Pz, P2, and P4
- Occipital region: PO3, PO4, O1, Oz, and O2
- Temporal region: T7, T8, P7, and P8

All electrodes were referenced to the right earlobe (A2), and FPz was used as a ground. The electrode placement is shown in Figure 5.5.

Hardware Configuration

Continuous EEG signals were recorded before, during and after the robot-mediated visuomotor tracking task using a 32-channel EEG data acquisition system commercialised by g.tec

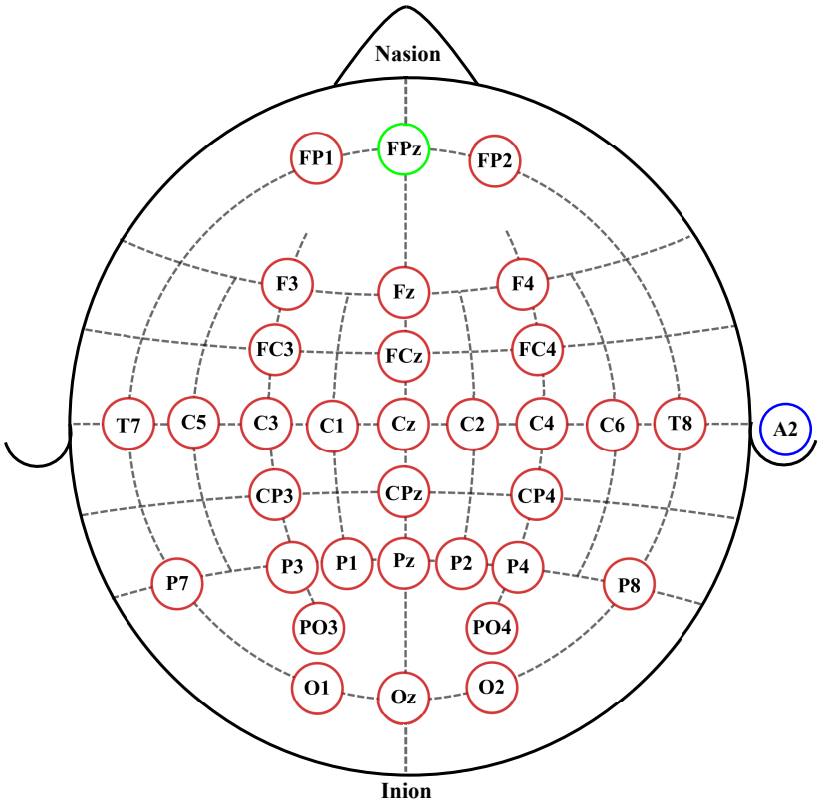

Figure 5.5: EEG electrode placement according to the International 10-10 system of electrode placement. Red circles represent the eight active electrodes selected for the data acquisition. The blue circle represents the reference electrode location. The green circle represents the ground electrode location.

medical engineering GmbH, Austria. The flow diagram of the hardware configuration of the EEG data acquisition system is shown in Figure 5.6. The 32 Ag/AgCl active electrodes (*g.LADYbird*) and the Ag/AgCl passive ground electrode (*g.LADYbird*) were mounted on the electrode cap (*g.GAMMACap2*). The 32 active electrodes, the passive ground electrode, and the Ag/AgCl active ear clip reference electrode (*g.GAMMAearclip*) were then connected to the active electrode driver boxes. The ground, reference and 16 active electrodes were connected to the standard *g.GAMMAbox* and the additional 16 active electrodes were connected to the *g.GAMMAbox* +16 channel extension box, which is similar to the standard *g.GAMMAbox* but without a reference or a ground channel. The outputs of the electrode driver boxes were connected to the input sockets of two *g.USBamp*s (master and slave) via two *LEMO* connectors (a push-pull connector named *g.USBamp*GAMMAconnector). The *g.USBamp* is a 16 channel biosignal (EEG, EOG, EMG and ECG) amplifier with an integrated 24-bit analogue-to-digital converter and a software adjustable sampling frequency range of 64 Hz to 38.4 kHz per channel. The digital signal processor of the amplifier per-

forms over-sampling, bandpass filtering, notch filtering, and calculates bipolar derivations to improve the signal-to-noise ratio (Ortner et al., 2013). The signals acquired from this device were sampled at 256 Hz, bandpass filtered with a cut-off frequency between 0.1 - 100 Hz and notch filtered with a cut-off frequency 50 Hz. The two *g.USBamp*s were connected via a synchronous cable. Also, the ground and reference terminals of the two devices were connected with jumper wires to provide a common reference and a common ground for both devices. The amplified, filtered and digitised EEG signal was then transmitted to the PC via USB 2.0 for display and storage for further analysis. Moreover, all participants wore an anti-static wrist strap in their left wrist so that the artifactual signals resulting from electrostatic charges in a laboratory environment can be avoided or reduced.

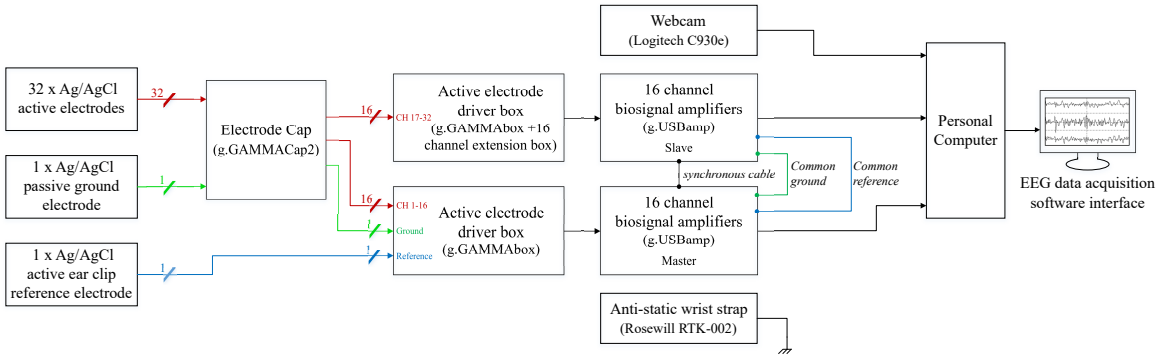

Figure 5.6: Block diagram of the hardware configuration of the EEG data acquisition system of GENTLE/EEG robot-mediated system.

EEG Data Acquisition MATLAB Simulink Model

The real-time EEG data acquisition Simulink model used in this experiment was solely developed by the author using the HighSpeed On-Line Processing (*g.HIsys*) API (g.tec medical engineering GmbH, Austria) (g.tec medical engineering GmbH, 2016). The HighSpeed On-Line Processing API is based on MATLAB Simulink and contains Simulink blocksets that can be used to customise amplifier settings (sampling frequency, filter characteristics, digital input/output lines). It is also compatible with all standard Simulink blocksets and allows to write new blocksets in MATLAB or C code. The data acquisition model implemented in this experiment was capable of:

- real-time EEG data acquisition, visualisation and storage,
- real-time user activity video recording, visualisation and storage to identify behavioural changes during the exercise,
- synchronisation of the EEG data acquisition with the robot-mediated visuomotor tracking task since both software was run in two different platforms.

Figure 5.7 illustrates the components and the data flow of the EEG data acquisition MATLAB Simulink model and the functionality of each block is explained below.

- **The *g.USBamp* Simulink block**
  The *g.USBamp* Simulink block provides a graphical interface to the *g.USBamp* hardware and allows recording the EEG data. The amplifier settings, including the 'master/slave' configuration, sampling frequency, bandpass and notch filter, and electrode montage, were customised using this block. One *g.USBamp* amplifier was configured as the 'master' and the other as the 'slave'. The sampling frequency of both amplifiers was set to 256 Hz. In addition, a bandpass filter with a higher cut-off frequency of 100 Hz and a lower cut-off frequency of 0.1 Hz was introduced so that the recorded data were pre-filtered by the hardware to the most frequently studied EEG frequency range. The notch filter with a 50 Hz cut-off frequency was included to eliminate or attenuate the 50 Hz line noise. The bipolar setting was set to 0 as the referential montage was of interest. The output of the *g.USBamp* block is scaled in microvolts (μV).

- **The *unbuffer* Simulink block**
  The *g.USBamp* outputs were fed to the two *unbuffer* blocks so that the input frames were unbuffered into a sequence of scalar outputs before storing or displaying.

- **The *g.CAMERAcapture* and *audio* Simulink blocks**
  Video and audio recordings were also performed simultaneously using the *g.CAMERAcapture* and *audio* Simulink blocks. The *g.CAMERAcapture* block was used to record the behavioural changes of the subject simultaneously with the EEG recording using the *Logitech C930e webcam*. The video recordings were mainly used in this context to cross-check whether the artifacts such as eye blink, swallowing that distort the data are identified correctly in the data preprocessing stages. Besides, these recordings give an overall view of the participants' behaviour throughout the experiment, which could be used for future data validation processes (this was not performed in the current context).

- **The *marker* Simulink block**
  The EEG data acquisition software and the virtual reality environment that facilitates the visuomotor tracking task were developed in two different software packages and was executed independently. As explained in Section 5.1.3, message boxes were displayed at the beginning of each level and at the end of the robotic interaction to synchronise the EEG recordings with the robot-mediated interaction. The participants were instructed to press the *return key* of the keyboard provided to continue with the interaction. These key-press events were captured by the *marker* Simulink block so that the EEG data corresponding to

each level of the robotic interaction could be easily identified during the off-line EEG data preprocessing.

- ***g.SCOPE* Simulink block**
  The *g.SCOPE* was used to display the recorded EEG and return key-press events.
- ***Data Type Conversion* and *g.TOfile* Simulink block**
  The EEG data and key-press events were stored in *.mat* format and were used for post-processing. As the output of the *g.USBamp* was in single (float32) a *Data Type Conversion* block was used to convert the data in to double before storing. The *g.TOfile* blocks were used to save the data under the given file name.

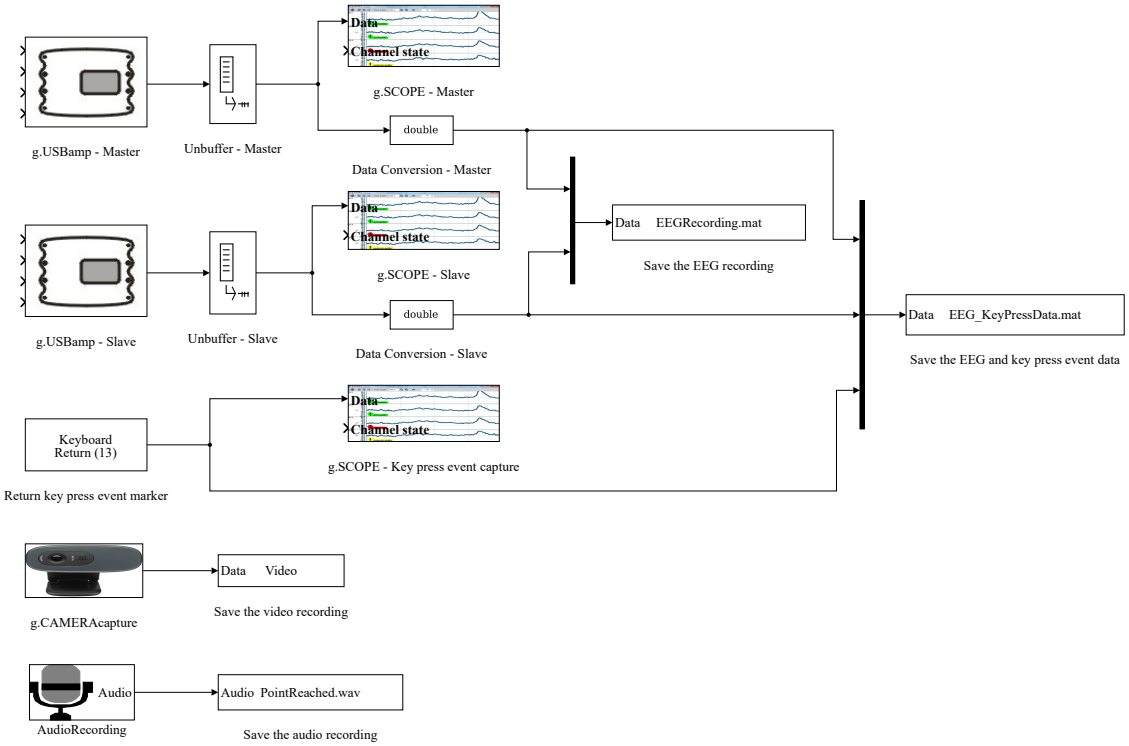

Figure 5.7: EEG data acquisition MATLAB SIMULINK model.

C. Comparison of GENTLE/EEG system with GENTLE/A system

The GENTLE/EEG robot-mediated system shares some software components of GENTLE/S (Amirabdollahian et al., 2007; Loureiro et al., 2001, 2003) and GENTLE/A (Chemuturi et al., 2013*a*,*b*) rehabilitation systems, but with major modifications to the control algorithm implemented solely by the author to cater the needs of the fatigue-inducing experimental protocol and the hardware upgrades. Table 5.2 gives a comparison of the major modifications

made to the GENTLE/A system while developing the GENTLE/EEG system. GENTLE/EEG system software mainly consists of two parts: software that enables the robotic interaction with the virtual reality environment and the software used to acquire EEG data in real-time. The operating system of the HapticMASTER was upgraded to *Microsoft Windows 10 Education 64-bit* so that both HapticMASTER and the EEG data acquisition system could be run in the same desktop computer (Intel(R) Core(TM) i7-6700 CPU with NVIDIA GeForce GTX 980 graphics). The control algorithm of the HapticMASTER and the virtual reality environment was re-programmed in *Microsoft Visual C++ 2015* programming language using *Microsoft Visual Studio Community 2015* platform, solely by the author so that the robot will be controlled in the damping or 'accommodation' mode (Carignan and Akin, 2003). The *Open Graphics Library (OpenGL)* was used to render the 3D virtual reality environment. The EEG data acquisition software was implemented in *MATLAB Simulink 2017a*.

Table 5.2: Comparison of GENTLE/A and GENTLE/EEG system specifications.

Specification	**GENTLE/A system**	**GENTLE/EEG system**
Operating system	Microsoft Windows 7 (64-bit)	Microsoft Windows 10 (64-bit)
Visual Studio platform	Visual Studio 9.0	Visual Studio Community 2015
Programming language	Microsoft Visual C++	Microsoft Visual C++ 2015
Graphics rendering library	OpenGL	OpenGL
Mode of operation	Passive, active-assisted, active	Damping or 'accommodation'
Data logging	CSV (Comma-separated values) file	CSV file updated via multithreading in C++
EEG data acquisition	Not included	Included

5.1.4 Experimental Procedure

On arrival at the laboratory, participants were informed about the experiment protocol and safety measures, given time to familiarise with the robot-mediated visuomotor tracking task, and were prepared for the EEG data collection as explained in Section 4.1.4. Participants were instructed to perform, eye blinks, eye movement, jaw clenching, swallowing, and head movement to identify the individual signal alterations caused by the physiological artifacts during the robotic interaction. These recordings were used to validate the EEG artifacts during EEG preprocessing. Figure 5.8 given below illustrates the flow diagram of the proposed fatigue estimation experiment. Following the standardised EEG recording protocol, EEG data were recorded with eyes opened for 4-minutes. Afterwards, a continuous EEG recording was taken while participants performed the robot-mediated visuomotor tracking task with the HapticMASTER using their right hand, as explained in Section 5.1.3. Simultaneously, the

kinetics and kinematic data of the robot (force applied, the position and velocity of the end effector) was also recorded to evaluate the movement variability associated with fatigue in robot-mediated interactions. Participants were instructed to perform the task for 25-minutes, without taking any break in between or until volitional fatigue. In this experiment, all participants interacted with the HapticMASTER until the end of five levels (i.e., 25-minutes). Finally, another EEG recording was taken with the eyes opened for 4-minutes following the robotic interaction. When EEG data were recorded before and after the task, participants were instructed to sit still and minimise eye blinks, eye movements, swallowing, jaw clenching or any other severe body movement. Video recordings were also made during the session and were mainly used to cross-check the artifactual EEG components at the data preprocessing. As all participants were exposed to the same experimental manipulations, this experiment incorporates a repeated-measures design. Figure 5.9 shows a participant interacting with the GENTLE/EEG robot-mediated system and performing the visuomotor tracking task.

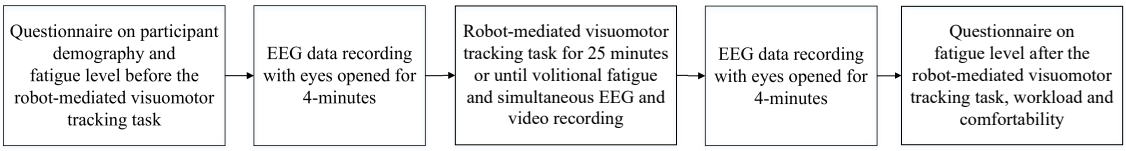

Figure 5.8: Flow diagram of the experimental procedure.

Figure 5.9: Interaction with the GENTLE/EEG system.

5.1.5 EEG Data Analysis

The continuous EEG data recorded during the robotic interaction were segmented into the corresponding interaction levels using the *'key-press'* event data recorded via the MATLAB Simulink model. Then, the first and the last 15s of EEG data (i.e., 3840×2 samples) were eliminated as these EEG data were related to the participant responding to message boxes and the movement of the robot arm to the starting position following the *'key-press'* event. The remaining EEG data belonging to each level (i.e., 69,120 samples per level) are referred to as level 1, level 2, level 3, level 4, and level 5, respectively, in the following chapters of this thesis. Similarly, the first and the last 30s of the EEG data (i.e., 7680×2 samples) recorded before and after the robot-mediated visuomotor tracking task were also removed from preprocessing. The remaining EEG data belonging to eyes opened before and after the robotic interaction (i.e., 46,080 samples per state) are referred to as 'baseline' and 'recovery', respectively. Therefore, baseline, level 1, level 2, level 3, level 4, level 5, and recovery are the EEG data measurement time periods that were further analysed in this experiment. A pictorial representation of the EEG data segmentation at each measurement time is given in Figure 5.10.

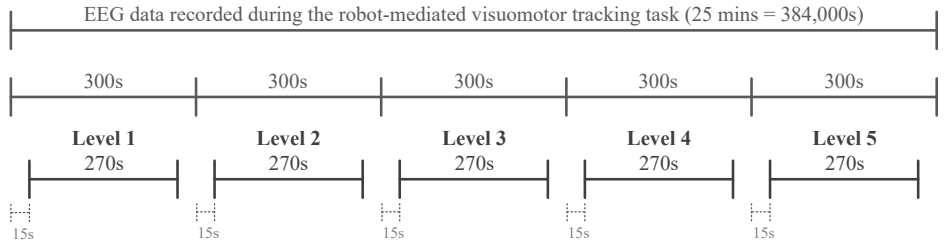

(a) During the robot-mediated interaction.

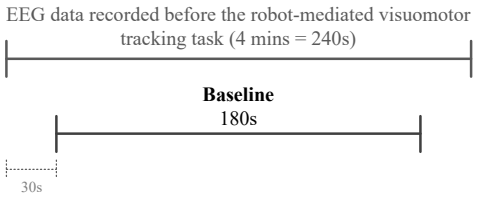

(b) Before the robot-mediated interaction.

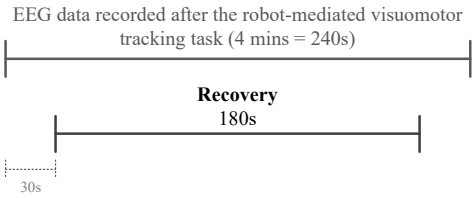

(c) After the robot-mediated interaction.

Figure 5.10: EEG data segmentation before, during, and after the robot-mediated visuomotor tracking task.

The EEG data processing pipeline followed for each participant during each measurement time is illustrated in Figure 5.11. It mainly consisted of three steps: data preprocessing, feature extraction and statistical analysis. EEG preprocessing and feature extraction was

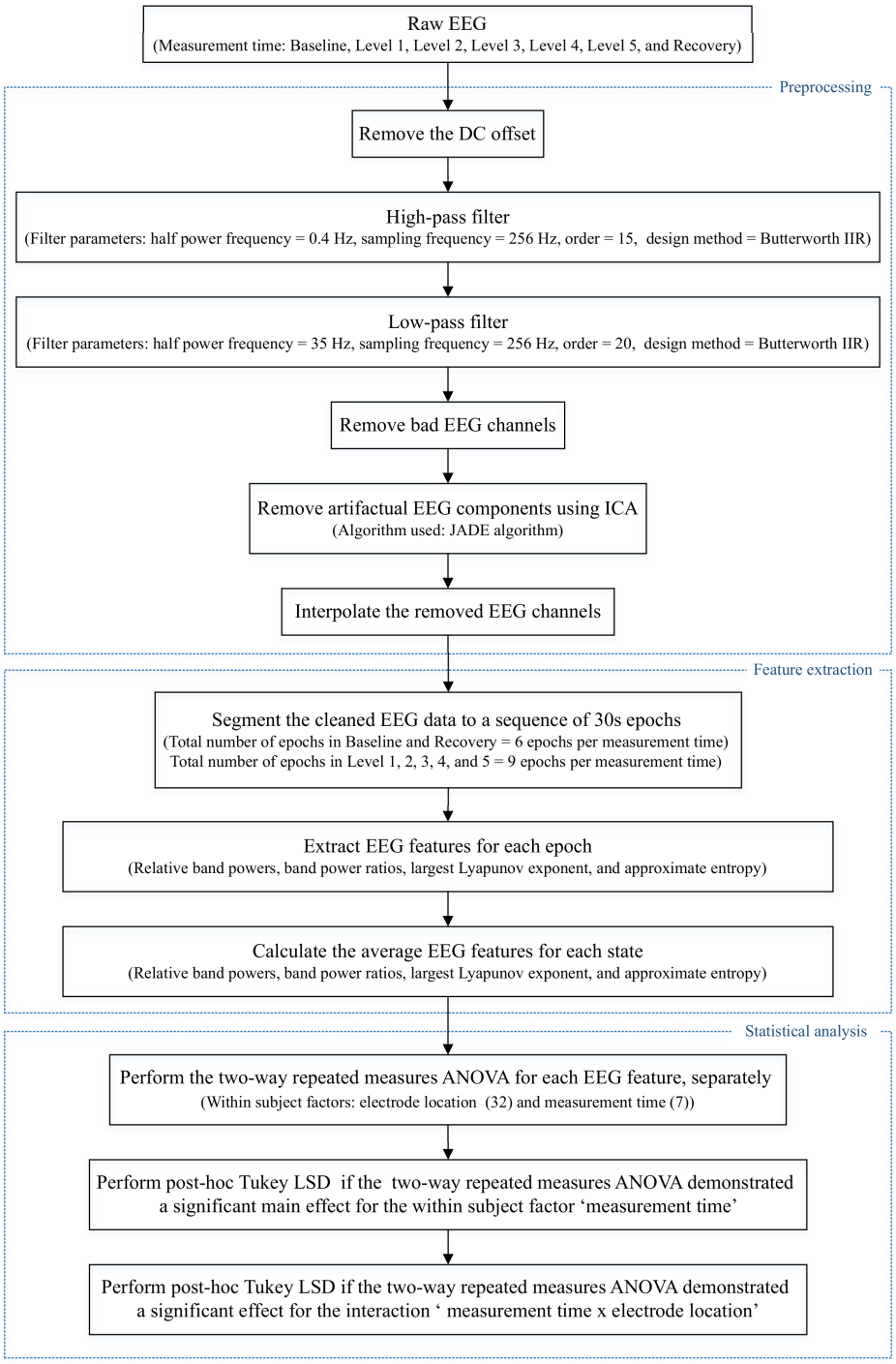

Figure 5.11: EEG data processing pipeline followed to preprocess the raw EEG data and to extract EEG features in each measurement time for each participant in order to perform the statistical analysis. The dotted box represents the three main steps involved in the pipeline: data preprocessing, feature extraction, and statistical analysis.

performed offline using custom MATLAB scripts, and the statistical analysis was performed using custom-written SPSS command syntaxes.

A. Preprocessing

The following preprocessing steps were performed separately on the channel-wise EEG data corresponding to baseline, level 1, level 2, level 3, level 4, level 5, and recovery states to remove or reduce the EEG artifacts. Since limited data was available, rejecting EEG segments with artifacts was not considered in this experiment as well, as it may result in a considerable loss of information.

Firstly, the DC offset was removed by subtracting the channel-wise mean from each data point. Then, a Butterworth high-pass filter with a half-power frequency of 0.4 Hz and an order of 15 and a Butterworth low-pass filter with a half-power frequency of 35 Hz and an order of 20 were applied since the EEG data of interest was in between 0.5 - 30 Hz frequency range (i.e., δ, θ, α, and β frequency bands). Then, ICA based on the joint approximate diagonalisation of eigenmatrices (JADE) algorithm (Cardoso and Souloumiac, 1993) was performed to separate and remove in-band (or remaining) artifacts including eye blinks, eye movement, swallowing, jaw clenching, and cardiac activity from the independent components as explained in Section 3.1.4. When applying ICA to separate EEG artifacts from brain activity patterns, it was assumed that the signals emitted by the unobserved sources are independent and the number of independent sources was the same as the number of electrodes used in the experiment (i.e., = 32). EEG data recorded from two participants, C12 and C19, contained a bad channel (i.e., P3 electrode in all measurement times for C12 and FP1 electrode in level 1 and level 2 for C19). Therefore, these bad channels were removed from the corresponding original EEG data before performing ICA. Following the ICA, these removed bad channels were interpolated with the spherical interpolation method available in EEGLAB toolbox.

B. Feature Extraction

The corrected EEG signals at the seven measurement time periods: baseline, level 1, level 2, level 3, level 4, level 5, and recovery for each participant were segmented into epochs of 30 s length (i.e., 7680 samples per epoch, and 2×6 epochs in total for the baseline and recovery measurement times, and 5×9 epochs in total for the levels 1-5). EEG spectral features (relative band powers and band power ratios), largest Lyapunov exponent, and approximate entropy were calculated for all epochs as explained below.

EEG Spectral Features

The power spectral density for all epochs was estimated using Welch's averaged modified periodogram method (Welch, 1967) with a 3s segment length (i.e., 768 samples), 50% overlap, and a Parzen window. The Welch's averaged modified periodogram method is explained in section 3.2.1. Subsequently, the relative band power of δ (0.5-<4 Hz), θ (4-<8 Hz), α (8-13 Hz), and β (<13-30 Hz) (δ_{relative}, θ_{relative}, α_{relative}, and β_{relative}, respectively) for each epoch was calculated as a ratio between the average band power of each frequency band and the total band power (i.e, the summation of average δ, θ, α and β band powers). The four ratio band power measures for each epoch $(\theta+\alpha)/\beta$, α/β, $(\theta+\alpha)/(\alpha+\beta)$, and θ/β were also calculated. Since findings in experiment 1 showed a significant decrease in δ_{relative} and a significant increase in α_{relative}, the ratio between δ_{relative} and α_{relative} (i.e., δ/α) was also calculated and further analysed in this study. Finally, the average of each EEG spectral feature within each measurement time (i.e., six epochs each for baseline and recovery, nine epochs each for levels 1 to 5) was calculated to represent the corresponding spectral feature index of baseline, level 1, level 2, level 3, level 4, level 5, and recovery. The average of EEG spectral features across the number of epochs or trials were considered in many past studies (Abásolo et al., 2006; Cao et al., 2014; Chen et al., 2013; Jap et al., 2009; Lal and Craig, 2002).

Largest Lyapunov Exponent

The largest Lyapunov exponent values for all epochs in the seven measurement time periods for each participant was calculated using the function '*lyapunovExponent()*' available in the '*predictive maintenance toolbox'* of MATLAB. The embedding dimension, $m = 5$ and the reconstruction delay or lag, $\tau = 11$ was estimated using the function '*phaseSpaceReconstruction()*' also available in *'predictive maintenance toolbox'* of MATLAB. In this function, *m* was estimated using the false nearest neighbour methods and τ was estimated using the average mutual information method as explained in Section 3.2.2. The average of largest Lyapunov exponent values within each measurement time (i.e., six epochs each for baseline and recovery, nine epochs each for levels 1 to 5) was calculated to represent the corresponding largest Lyapunov exponent value of the baseline, level 1, level 2, level 3, level 4, level 5, and recovery.

Approximate Entropy

The approximate entropy for all epochs in the seven measurement time periods for each participant was calculated using the function '*approximateEntropy()*' available in the *'predic-*

tive maintenance toolbox' of MATLAB. An embedding dimension (m) of 2 and a similarity criterion (r) of $0.2 \times std$ where std denotes the standard deviation of the time series were often used in the fatigue literature (Hu and Min, 2018; Min et al., 2017; Mu et al., 2017; Zhang et al., 2013). Therefore, $m = 2$ and $r = 0.2 \times std$ were selected as the parameters in this experiment. The average approximate entropy value within each measurement time (i.e., six epochs each for baseline and recovery, nine epochs each for levels 1 to 5) was calculated and used with the statistical analysis. These average values represent the corresponding approximate entropy value of the baseline, level 1, level 2, level 3, level 4, level 5, and recovery.

5.1.6 Statistical Analysis

The statistical analysis was conducted using *IBM SPSS Statistics 25* software. A p-value<0.05 was considered statistically significant denoting a 95% confidence interval. The normality was assessed using Kolmogorov–Smirnov test.

As explained in section 5.1.5, eleven EEG features were extracted from the EEG data recorded before, during and after the robot-mediated visuomotor tracking task from each participant. A series of two-way repeated measures ANOVAs with within-subject factors: measurement time and electrode location, were performed on these EEG features extracted from all 25 participants to determine whether spectral and nonlinear EEG features significantly varies before, during and after the robot-mediated interactions (i.e., in total eleven two-way repeated measures ANOVAs). The measurement time factor consisted of seven levels: baseline, level 1, level 2, level 3, level 4, level 5, and recovery. The electrode location factor consisted of the 32 electrodes: FP1, FP2, F3, Fz, F4, FC3, FCz, FC4, C5, C3, C1, Cz, C2, C4, C6, CP3, CPz, CP4, P3, P1, Pz, P2, P4, PO3, PO4, O1, Oz, O2, T7, T8, P7, and P8, used in this experiment. The Greenhouse–Geisser correction was applied to the F statistic of each two-way repeated measures ANOVA since Mauchly's tests were significant and the assumption of sphericity was violated (Field, 2018). The uncorrected degree of freedom, the corrected p-value and the degree of sphericity (i.e., epsilon (ε) value) were reported for each two-way repeated measures ANOVA. In this experiment, it was of main interest to find whether any changes in EEG features were due to the interaction between the measurement time and electrode location (i.e., measurement time $\times$ electrode location). Therefore, significant interaction between measurement time and electrode location were further analysed using Tukey least significant difference (LSD) for comparison of means to determine specifically where differences existed. Furthermore, significant main effect of measurement time was also further analysed using Tukey LSD for comparison of means. Significant main effect of

electrode locations were not further analysed in this thesis. The effect sizes were expressed by the partial eta-squared (η_P^2) (Equation 3.41) and a small, medium, and large effects would be reflected in η_P^2 values of 0.0099, 0.0588, and 0.1379, respectively (Cohen, 2013; Richardson, 2011).

5.2 Results

In the present work nine spectral EEG features (δ_{relative}, θ_{relative}, α_{relative}, β_{relative}, $(\theta+\alpha)/\beta$, α/β, $(\theta+\alpha)/(\alpha+\beta)$, θ/β, and δ/α) and two nonlinear EEG features (largest Lyapunov exponent and approximate entropy) were extracted from each participant. The aim of this experiment was to examine how EEG features changed before, during and after the robot-mediated visuomotor tracking task and to find the associations between EEG feature modulations and fatigue induced by interacting with the GENTLE/EEG robot-mediated system. In this section, the main findings related to the effects of fatigue induced by the visuomotor tracking task are further discussed. The complete analysis of all EEG features is given in Appendix B.2.

5.2.1 Modulations in EEG Spectral Features

Figure 5.12 shows the variations in sample mean of δ_{relative}, α_{relative}, $(\theta+\alpha)/(\alpha+\beta)$, and δ/α, respectively, on all 32 electrodes across the measurement times: baseline, level 1, level 2, level 3, level 4, level 5, and recovery. In general, a decreasing trend in δ_{relative}, $(\theta+\alpha)/(\alpha+\beta)$, and δ/α was visible when progressing from level 1 to level 5 of the robot-mediated visuomotor tracking task. The δ_{relative}, $(\theta+\alpha)/(\alpha+\beta)$, and δ/α during recovery was also lower than the corresponding values during baseline. The above observations suggest that the transition to fatigue may have caused a decrease in δ_{relative}, $(\theta+\alpha)/(\alpha+\beta)$, and δ/α. In contrast, α_{relative} increased from level 1 to level 5. The α_{relative} at recovery was also greater than the α_{relative} at baseline. Therefore, the rise in α_{relative} may also reflect the effects of fatigue. Moreover, greater differences were visible from baseline to level 1 and from level 5 to recovery, thereby reflecting a change in EEG activity caused by the task on-set from the resting state and then when moving back to the resting state following the task. For example, α_{relative} during both baseline and recovery were greater than that during the robotic interaction whereas δ_{relative}, $(\theta+\alpha)/(\alpha+\beta)$, and δ/α during baseline and recovery were lower than that during the robotic interaction. The above observation showed that α_{relative} decreased during the onset of the robot-mediated interaction whereas and δ_{relative}, $(\theta+\alpha)/(\alpha+\beta)$, and δ/α increased in comparison to the resting state EEG activity.

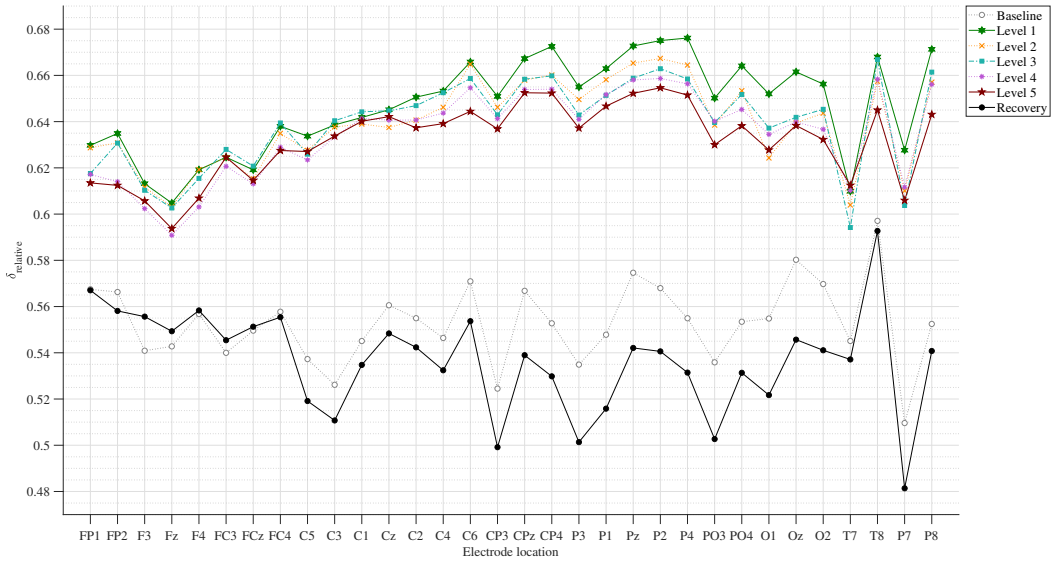

(a) δ_{relative}

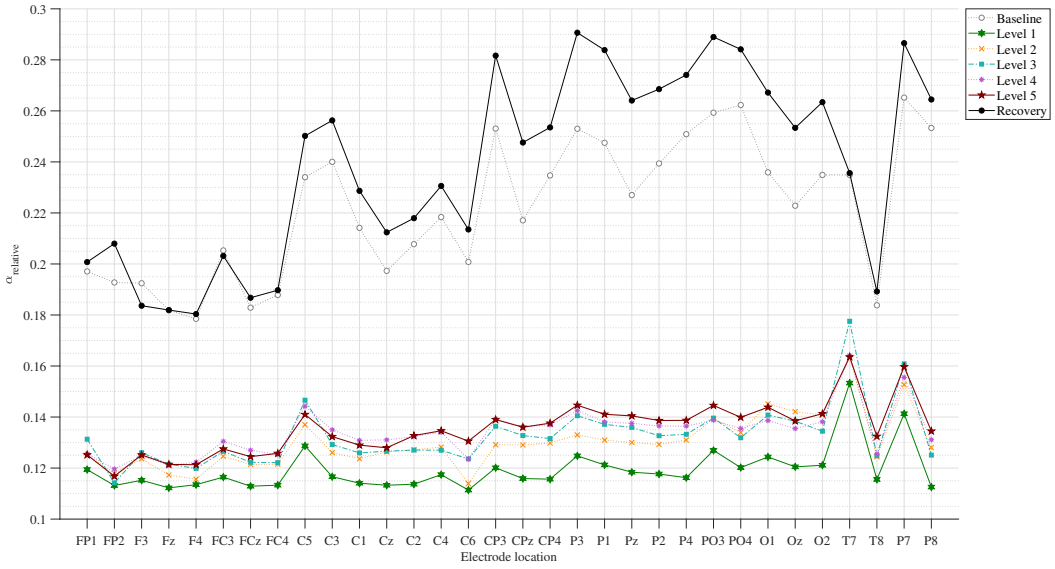

(b) α_{relative}

Figure 5.12: Comparison of the sample mean of (a) δ_{relative}, (b) α_{relative}, (c) $(\theta+\alpha)/(\alpha+\beta)$, and (d) δ/α on all 32 electrodes between measurement times (baseline, level 1, level 2, level 3, level 4, level 5 and recovery) of the robot-mediated visuomotor tracking task. The amount of change in each EEG feature from level 1 to level 5 (i.e., level 2 - level 1, level 3 - level 1, level 4 - level 1, and level 5 - level 1) may reflect the effects of fatigue build-up on the corresponding EEG feature. The amount of change in each EEG feature from baseline to recovery (i.e., recovery - baseline) may also reflect the effects of fatigue on the corresponding EEG feature. *Connecting lines in subfigures do not imply a linear relationship between electrode locations but merely for the ease of identifying the numerical changes between baseline, level 1, level 2, level 3, level 4, level 5 and recovery states.* (continued on next page)

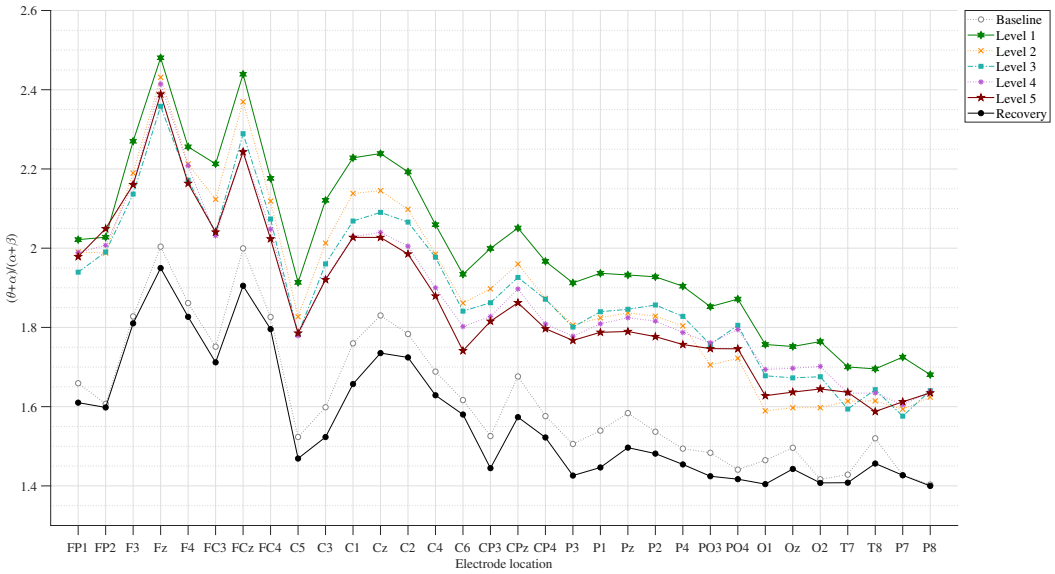

(c) $(\theta+\alpha)/(\alpha+\beta)$

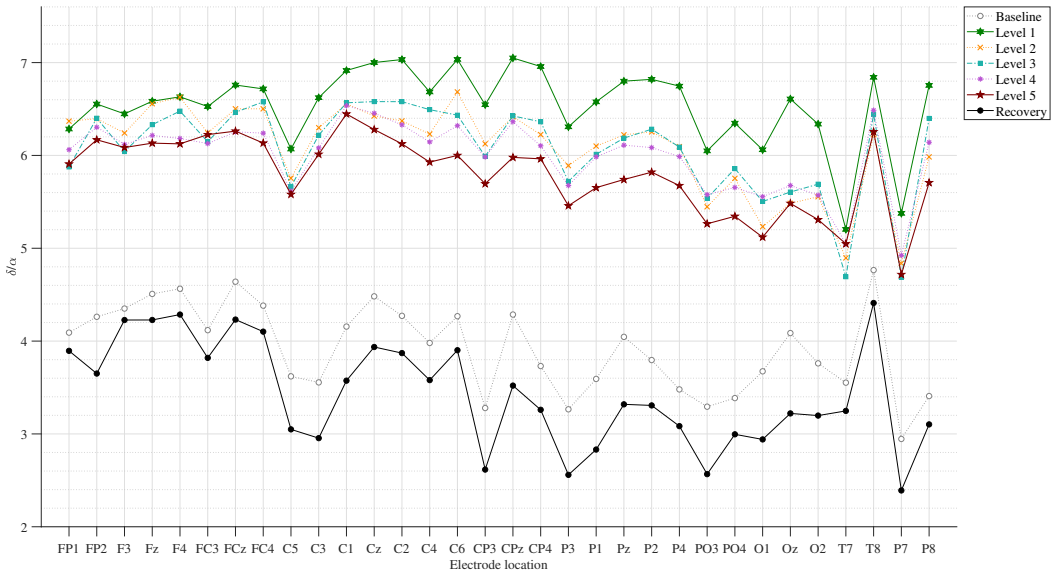

(d) δ/α

Figure 5.12: Comparison of the sample mean of (a) δ_{relative}, (b) α_{relative}, (c) $(\theta+\alpha)/(\alpha+\beta)$, and (d) δ/α on all 32 electrodes between measurement times (baseline, level 1, level 2, level 3, level 4, level 5 and recovery) of the robot-mediated visuomotor tracking task. The amount of change in each EEG feature from level 1 to level 5 (i.e., level 2 - level 1, level 3 - level 1, level 4 - level 1, and level 5 - level 1) may reflect the effects of fatigue build-up on the corresponding EEG feature. The amount of change in each EEG feature from baseline to recovery (i.e., recovery - baseline) may also reflect the effects of fatigue on the corresponding EEG feature. *Connecting lines in subfigures do not imply a linear relationship between electrode locations but merely for the ease of identifying the numerical changes between baseline, level 1, level 2, level 3, level 4, level 5 and recovery states.*

Two-way repeated measures ANOVAs performed on δ_{relative}, α_{relative}, $(\theta+\alpha)/(\alpha+\beta)$, and δ/α revealed statistically significant interaction between measurement time and electrode locations (δ_{relative}: F(186,4464) = 4.90, p = 0.000, ε = 0.046, η_P^2 = 0.170, power = 0.999; α_{relative}: F(186, 4464) = 6.182, p = 0.000, ε = 0.026, η_P^2 = 0.205, power = 0.995; $(\theta+\alpha)/(\alpha+\beta)$: F(186, 4464) = 2.310, p = 0.017, ε = 0.048, η_P^2 = 0.088, power = 0.900; and δ/α: F(186, 4464) = 2.248, p = 0.010, ε = 0.064, η_P^2 = 0.086, power = 0.950). The interaction effect of δ_{relative} and α_{relative} showed a larger effect size whereas $(\theta+\alpha)/(\alpha+\beta)$ and δ/α showed a medium to large effect size. All features had sufficient power (i.e, over 80%) to find statistical differences in the interaction between measurement time and electrode locations. Tables B.4, B.6, B.10, B.12 in Appendix B.2.14 summarise the p-values obtained from the pairwise comparison of the interaction between measurement time and electrode locations of δ_{relative}, α_{relative}, $(\theta+\alpha)/(\alpha+\beta)$, and δ/α, respectively.

Pairwise comparisons of the interaction between measurement time and electrode location revealed significant variations in δ_{relative}, α_{relative}, $(\theta+\alpha)/(\alpha+\beta)$, and δ/α mostly localised around central, parietal, and occipital brain regions when progressing from level 1 to level 2, 3, 4, and 5 of the visuomotor tracking task. Figure 5.13 shows the topographical distribution of these significant differences between level 1-2, level 1-3, level 1-4, and level 1-5. All electrodes in the central, parietal and occipital brain regions except O2 showed a significant decrease in $(\theta+\alpha)/(\alpha+\beta)$ from level 1 to level 5 of the task. Similarly, all electrodes in the central, parietal and occipital brain regions except C5, C3, and C1 showed a significant decrease in δ/α during the interaction. The δ_{relative} showed significant decrease in all electrodes in parietal and occipital brain regions except CP3 and CPz from level 1 to level 5. In contrast, all electrodes in the central, parietal and occipital brain regions except C5 showed a significant increase in α_{relative} from level 1 to level 5. The above observations suggest that fatigue may have developed during the robot-mediated visuomotor tracking task, thereby altering the brain activation patterns with time on task. Significant differences in α_{relative} were also visible on the majority of electrodes localised around central, parietal and occipital regions during the transition from level 1 to level 4. Also, $(\theta+\alpha)/(\alpha+\beta)$ on the majority of electrodes in central and parietal regions were significantly decreased from level 1 to level 4 whereas the significant decrease in δ/α from level 1 to level 4 were mostly around the parietal brain region.

Figure 5.14 shows the comparison of the brain topographies of the difference in δ_{relative}, α_{relative}, $(\theta+\alpha)/(\alpha+\beta)$, and δ/α between level 1 and level 5 (i.e., level 5 - level 1) of the robotic interaction for four participants who showed higher and lower differences in the subjective measures of fatigue with the difference in the sample mean. The selected participants showed an increase in their fatigue levels as follows: physical fatigue level

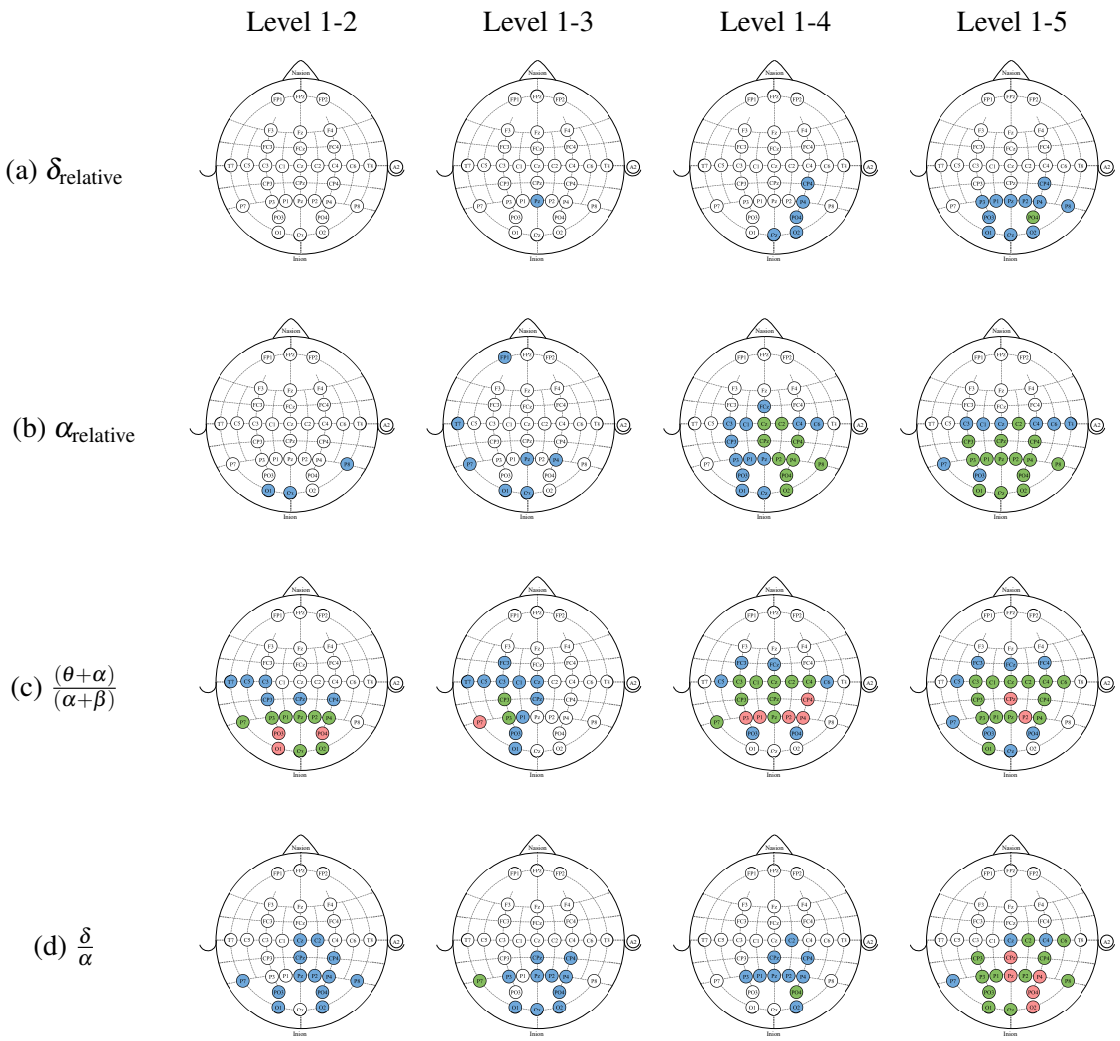

Figure 5.13: The topographical distribution of the significant differences in (a) δ_{relative}, (b) α_{relative}, (c) $(\theta+\alpha)/(\alpha+\beta)$, and (d) δ/α between robot-mediated visuomotor tracking task interaction levels. Circle colours blue, green and red represents p-values < 0.05, < 0.01, and < 0.001, respectively.

percentages of C04 = 40.00%, C17 = 16.67%, C18 = 66.67%, C21 = 90.00%; mental fatigue level percentages of C04 = 45.83%, C17 = 0.00%, C18 = 62.50%, C21 = 54.17%; and global fatigue level percentages of C04 = 42.59%, C17 = 9.26%, C18 = 64.81%, C21 = 74.07%; respectively. The analysis of the subjective measures of fatigue level is discussed in Chapter 6. A greater reduction in δ_{relative} was visible in the parietal and occipital regions for the sample mean as well as for these selected participants. Participants C18 and C21 showed larger decrease in δ_{relative} on the majority of electrodes in posterior region. An increase in α_{relative} were visible in the sample mean of all participants and the largest variations were

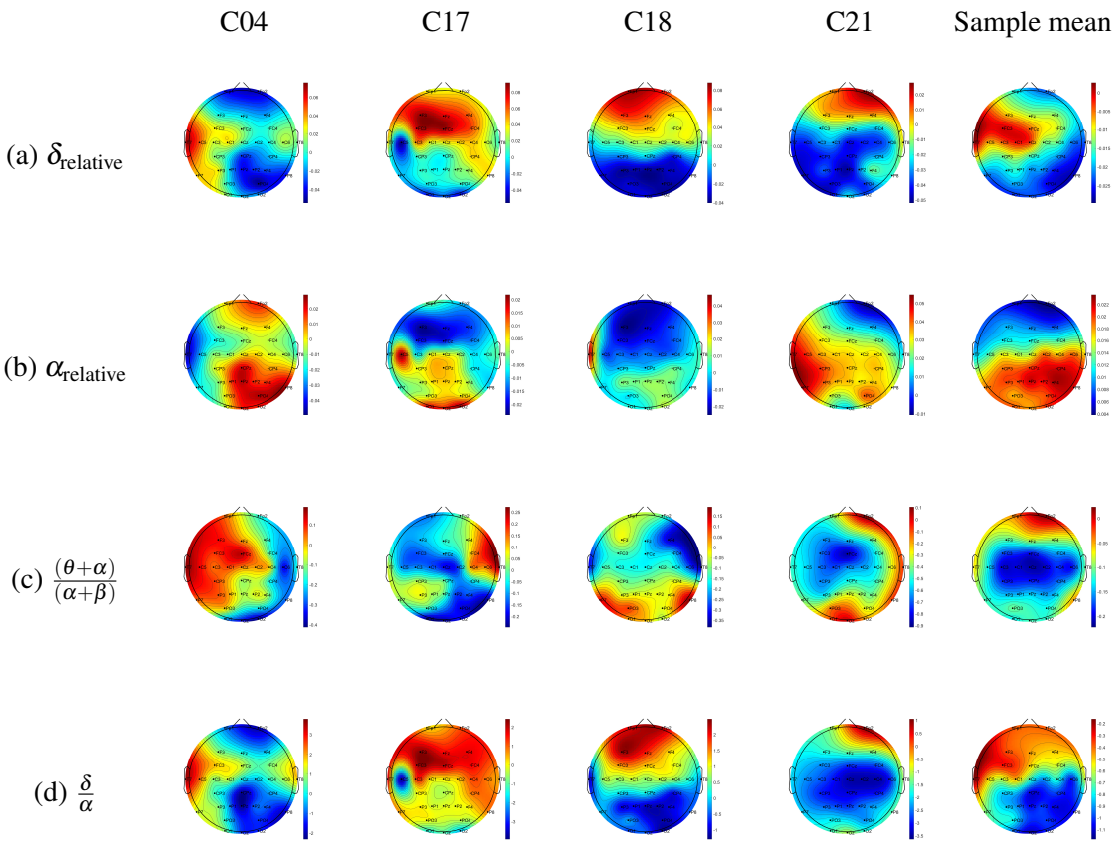

Figure 5.14: Comparison of the brain topographies of the difference in (a) δ_{relative}, (b) α_{relative}, (c) $(\theta+\alpha)/(\alpha+\beta)$, and (d) δ/α between level 5 and level 1 (i.e., level 5 - level 1) for C04, C17, C18, C21, and sample mean of all participants. In each brain map, the nose is represented by the triangle on the top, and the right hemisphere is on the right. For δ_{relative}, $(\theta+\alpha)/(\alpha+\beta)$, and δ/α, the blue-shaded areas indicate a larger decrease whereas the red-shaded areas indicate an increase. For α_{relative}, the red-shaded areas indicate a larger increase whereas the blue-shaded areas indicate a decrease.

observed around the central, parietal, and occipital brain regions. A greater increase in α_{relative} for C04 was visible on right parietal region; for C17 on occipital region; and for C21 on central, parietal, occipital and temporal regions. A larger reduction in sample mean of $(\theta+\alpha)/(\alpha+\beta)$ were visible around the central and parietal regions, whereas the a larger reduction in sample mean of δ/α were visible around the parietal and occipital regions. The participants C17, C18 and C21 also shows a reduction in $(\theta+\alpha)/(\alpha+\beta)$ around the central and parietal regions. The participants C04, C18 and C21 shows a reduction in δ/α around the parietal and occipital regions. Therefore, it was found that the individual variations in the

brain topographies of the participants C04, C17, C18, and C21 were mostly similar to the variations in the brain topographies of the sample mean of all participants.

Figure 5.15 shows the topographical distribution of significant differences in δ_{relative}, α_{relative}, $(\theta+\alpha)/(\alpha+\beta)$, and δ/α from baseline to recovery of the robot-mediated visuomotor tracking task. It can be seen that δ/α on left and midline central, parietal, and occipital brain regions were mostly changed following the robot-mediated interaction. Also, all electrodes in left and midline central and parietal regions except FC3 showed a significant decrease in $(\theta+\alpha)/(\alpha+\beta)$ from baseline to recovery. The reduction in δ_{relative} from baseline to recovery was visible on P3, PO3, and Oz electrodes whereas the increase in α_{relative} was visible on P3 electrode only. Moreover, the direction of change in each EEG feature from baseline to recovery were similar to the direction of change during the robot-mediated interaction (i.e., from level 1 to level 5). Previous studies have also compared EEG data recorded before and after a task to identify EEG feature modulations associated with fatigue induced by physical and mental tasks (Chen et al., 2013; Cheng and Hsu, 2011; Ng and Raveendran, 2007; Tanaka et al., 2012). Therefore, the significant variations observed from baseline to recovery may have caused by fatigue accumulated during the robot-mediated visuomotor tracking task.

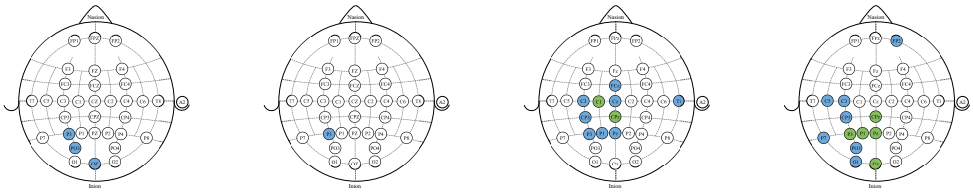

(a) δ_{relative} (b) α_{relative} (c) $(\theta+\alpha)/(\alpha+\beta)$ (d) δ/α

Figure 5.15: The topographical distribution of the significant differences in (a) δ_{relative}, (b) α_{relative}, (c) $(\theta+\alpha)/(\alpha+\beta)$, and (d) δ/α from baseline to recovery of the robot-mediated visuomotor tracking task. Circle colours blue and green represents p-values < 0.05 and < 0.01, respectively.

Pairwise comparisons also revealed that δ_{relative}, $(\theta+\alpha)/(\alpha+\beta)$, and δ/α on all electrodes were significantly increased from baseline to level 1 and then significantly decreased from level 5 to recovery (except on T8 for $(\theta+\alpha)/(\alpha+\beta)$). In contrast α_{relative} on all electrodes were significantly decreased from baseline to level 1 and then significantly increased from level 5 to recovery. The widespread significant differences in the EEG features from baseline to level 1 and from level 5 to recovery may explain the changes in the brain activation patterns from resting phase to an active movement phase and vice versa.

5.2.2 Modulations in EEG Nonlinear Features

Figure 5.16 shows the variations in sample mean of largest Lyapunov exponent and approximate entropy, respectively, on all 32 electrodes across the measurement times: baseline, level 1, level 2, level 3, level 4, level 5, and recovery. In general, a decreasing trend was visible in largest Lyapunov exponent on all electrodes except T7 when progressing from level 1 to level 5 of the robot-mediated visuomotor tracking task. Also, largest Lyapunov exponent values around central, parietal and occipital brain regions during recovery were lower than the corresponding values during baseline. In contrast, a higher decrease in approximate entropy from level 1 to level 5 were mostly visible around central and left parietal brain regions and from baseline to recovery were mostly visible around left parietal brain region. The above observations suggest that the transition to fatigue may have caused a decrease in largest Lyapunov exponent and approximate entropy values of the recorded EEG data.

Two-way repeated measures ANOVAs performed on largest Lyapunov exponent and approximate entropy revealed statistically significant interaction between measurement time and electrode locations (largest Lyapunov exponent: F(186, 4464) = 2.660, $p = 0.005$, $\varepsilon = 0.053$, $\eta_P^2 = 0.100$, power = 0.958; and approximate entropy: F(186, 4464) = 6.620, $p = 0.000$, $\varepsilon = 0.041$, $\eta_P^2 = 0.216$, power = 1.000). The interaction effect of the largest Lyapunov exponent had a medium to large effect size and the interaction effect of the approximate entropy had a larger effect sizes. Both nonlinear features had sufficient power (i.e, over 80%) to find statistical differences in the interaction between measurement time and electrode locations. Tables B.13 and B.14 in Appendix B.2.14 summarise the p-values obtained from the pairwise comparison of the interaction between measurement time and electrode locations of largest Lyapunov exponent and approximate entropy respectively.

Figure 5.17a shows the topographical distribution of the significant differences in largest Lyapunov exponent between level 1-2, level 1-3, level 1-4, and level 1-5 of the visuomotor tracking task. Pairwise comparisons of the interaction between measurement time and electrode location showed a significant decrease in largest Lyapunov exponent localised around parietal and occipital brain regions when progressing from level 1 to level 5. In contrast, as can be seen in Figure 5.17b, left central brain regions showed a significant decrease in approximate entropy when progressing from level 1 to level 5. The above observations also suggest that fatigue may have developed during the robot-mediated visuomotor tracking task. However, only the variations in largest Lyapunov exponent showed a widespread topographical distribution similar to the EEG spectral feature modulations. Figure 5.18 which compares the brain topographies of the difference in largest Lyapunov exponent and approximate entropy between level 1 and level 5 (i.e., level 5 - level 1) for four participants

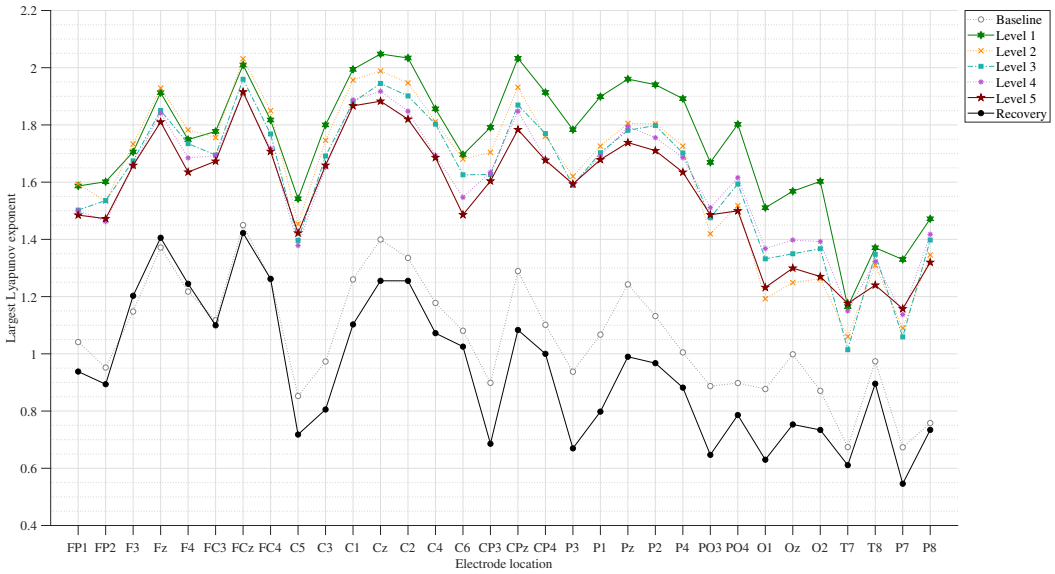

(a) Largest Lyapunov exponent.

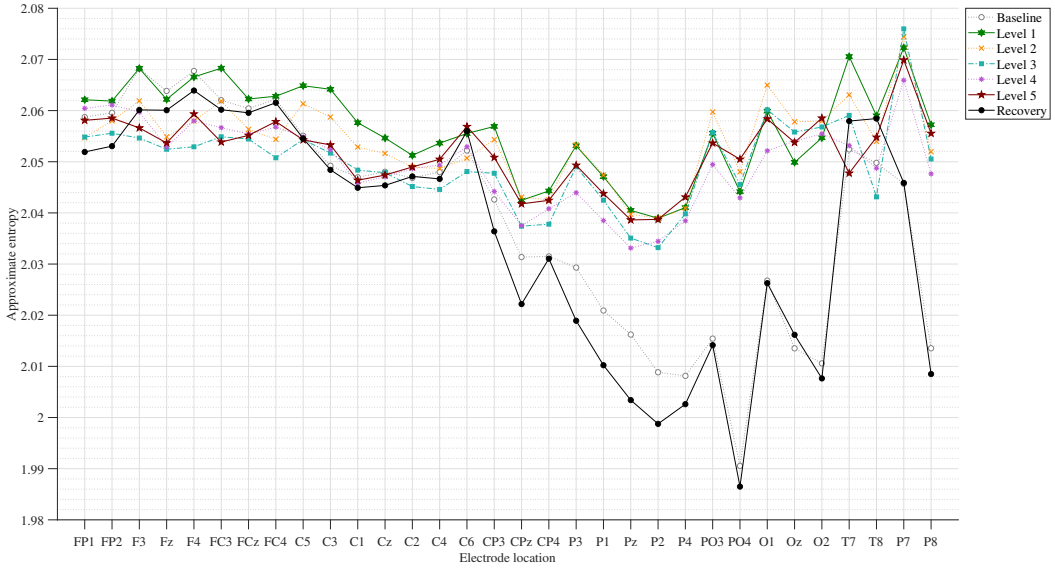

(b) Approximate entropy.

Figure 5.16: Comparison of the sample mean of (a) largest Lyapunov exponent and (b) approximate entropy on all 32 electrodes between measurement times (baseline, level 1, level 2, level 3, level 4, level 5 and recovery) of the robot-mediated visuomotor tracking task. The amount of change in each EEG feature from level 1 to level 5 (i.e., level 2 - level 1, level 3 - level 1, level 4 - level 1, and level 5 - level 1) may reflect the effects of fatigue build-up on the corresponding EEG feature. The amount of change in each EEG feature from baseline to recovery (i.e., recovery - baseline) may also reflect the effects of fatigue on the corresponding EEG feature. *Connecting lines in subfigures do not imply a linear relationship between electrode locations but merely for the ease of identifying the numerical changes between baseline, level 1, level 2, level 3, level 4, level 5 and recovery states.*

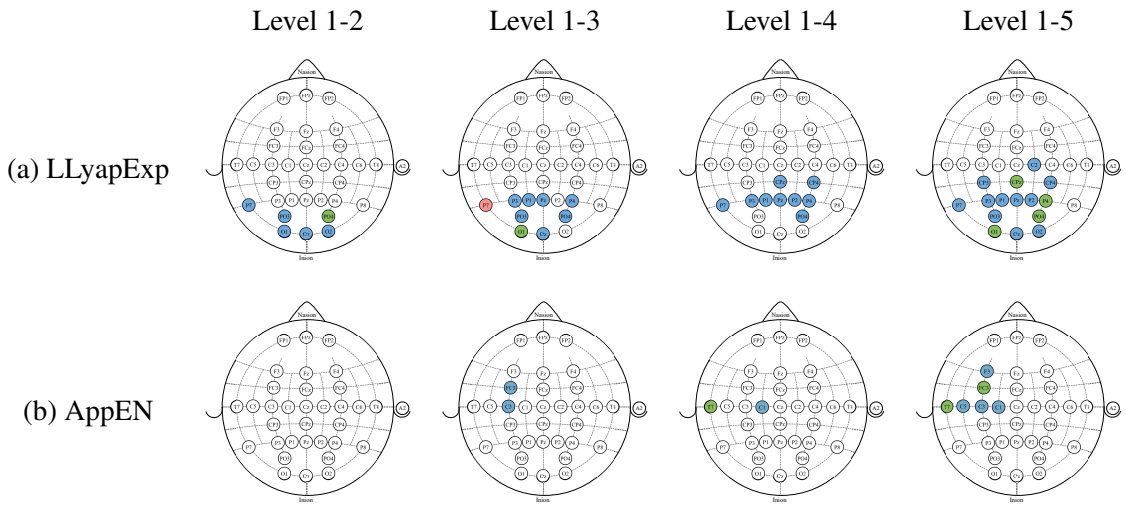

Figure 5.17: The topographical distribution of the significant differences in (a) largest Lyapunov exponent (LLyapExp) and (b) approximate entropy (AppEN) between visuomotor tracking task interaction levels. Circle colours blue, green and red represents p-values < 0.05, < 0.01, and < 0.001, respectively.

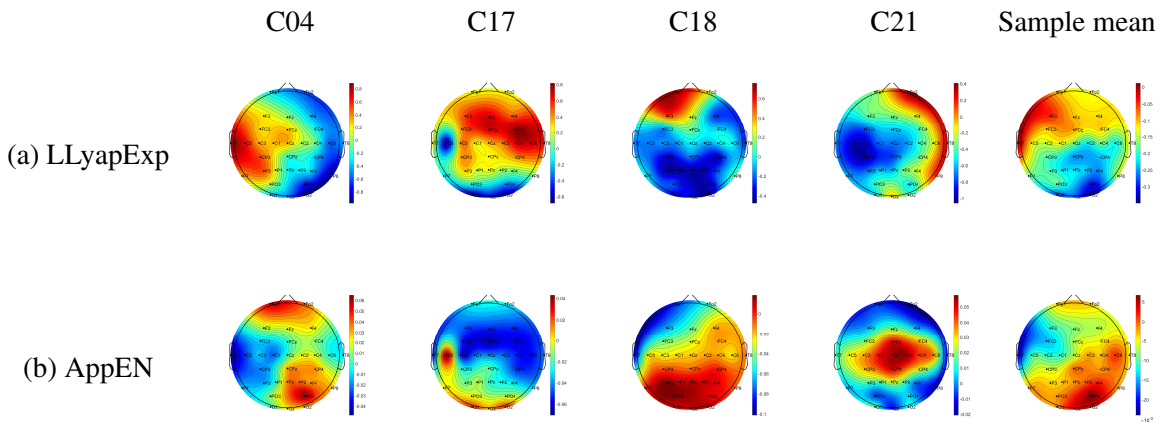

Figure 5.18: Comparison of the brain topographies of the difference in (a) largest Lyapunov exponent (LLyapExp) and (b) approximate entropy (AppEN) between level 5 and level 1 (i.e., level 5 - level 1) for C04, C17, C18, C21, and sample mean of all participants. In each brain map, the nose is represented by the triangle on the top, and the right hemisphere is on the right. The blue-shaded areas indicate a larger decrease whereas the red-shaded areas indicate an increase.

and the sample mean also supported the above finding. As can be seen in Figure 5.18a, the higher reduction in sample mean of largest Lyapunov exponent were mostly localised around the posterior brain regions. Similarly, C18 and C21 participants showed larger reduction in largest Lyapunov exponent around parietal and occipital regions and C17 showed larger reduction around occipital region. However, the reduction in approximate entropy values were mostly visible around the central region for the participants C04, C17, C18, and for the sample mean of all participants (Figure 5.18b). Moreover, significant reduction from baseline to recovery were only observed in the largest Lyapunov exponent (Figure 5.19). The significant variations were localised mostly around the left central, left and midline parietal and occipital brain regions. Therefore, the findings reveal that largest Lyapunov exponent may be a better fatigue index than the approximate entropy to quantify the changes in the complexity of brain with fatigue in robot-mediated visuomotor tracking task.

(a) Largest Lyapunov exponent (b) Approximate entropy

Figure 5.19: The topographical distribution of the significant differences in (a) largest Lyapunov exponent and (b) approximate entropy from baseline to recovery of the robot-mediated visuomotor tracking task.

Pairwise comparisons also revealed that largest Lyapunov exponent on all electrodes were significantly increased from baseline to level 1 and then significantly decreased from level 5 to recovery. These differences may also reflect the changes in the complexity of the brain from resting phase to an active movement phase and vice versa since a larger number of neurons are recruited to perform the task in hand during the active movement phase in comparison to a resting phase.

5.2.3 Summary of EEG Spectral and Nonlinear Feature Variations With Fatigue Induced by Robot-Mediated Visuomotor Tracking Task

Pairwise comparisons of interaction between measurement time and electrode locations on spectral and nonlinear EEG features found that the significant increase in α_{relative} and

the significant decrease in δ_{relative}, $(\theta+\alpha)/(\alpha+\beta)$, δ/α and largest Lyapunov exponent from level 1 to level 5 were mostly localised around central, parietal and occipital brain regions. The EEG electrodes in the central, parietal and occipital brain regions that showed significant variations are summarised in Table 5.3. These findings suggest that fatigue may have accumulated during the visuomotor tracking task. Therefore, it can be inferred that the significant modulations in spectral and nonlinear EEG features observed during level 5 when compared with level 1 may reflect the effects of fatigue on brain activity during a robot-mediated interaction. The association of the change in these substantive EEG features with the changes in subjective measures of fatigue and movement variability measures are discussed in Chapter 6.

Table 5.3: Summary of spectral and nonlinear EEG features that showed significant variations between level 1 and level 5 of the robot-mediated visuomotor interaction.

EEG Features	Electrode locations	Direction of change
δ_{relative}	CP4, P3, P1, Pz, P2, P4, PO3, PO4, O1, Oz, O2	↓
α_{relative}	C3, C1, Cz, C2, C4, C6, CP3, CPz, CP4, P3, P1, Pz, P2, P4, PO3, PO4, O1, Oz, O2	↑
$(\theta+\alpha)/(\alpha+\beta)$	FC3, FCz, FC4, C5, C3, C1, Cz, C2, C4, C6, CP3, CPz, CP4, P3, P1, Pz, P2, P4, PO3, PO4, O1, Oz	↓
δ/α	Cz, C2, C4, C6, CP3, CPz, CP4, P3, P1, Pz, P2, P4, PO3, PO4, O1, Oz, O2	↓
Largest Lyapunov exponent	C2, CP3, CPz, CP4, P3, P1, Pz, P2, P4, PO3, PO4, O1, Oz, O2	↓

Notes. ↑ and ↓ represents the significant increase and decrease in the corresponding EEG features.

5.2.4 Modulations in the Largest Lyapunov Exponent and Relative Alpha Band Power When Combined Together

Table 5.3 shows that only α_{relative} significantly increased with fatigue induced by robot-mediated visuomotor tracking task, whereas the other EEG features significantly decreased. Furthermore, findings of α_{relative} and largest Lyapunov exponent were in-line with findings in the literature. Therefore, the effect of fatigue when both α_{relative} and largest Lyapunov exponent features are combined together was also evaluated in this study. A new feature was derived by dividing the largest Lyapunov exponent values (LLyapExp) from the corresponding α_{relative} values (i.e., LLyapExp$/\alpha_{\text{relative}}$).

Figure 5.20 shows the variations in sample mean of LLyapExp$/\alpha_{\text{relative}}$ on all 32 electrodes across the measurement times: baseline, level 1, level 2, level 3, level 4, level 5, and recovery. A decreasing trend was visible on all electrodes except T7 when progressing from level 1 to level 5 of the robot-mediated visuomotor tracking task as well as from baseline to recovery. Two-way repeated measures ANOVA found a statistically significant interaction between

measurement time and electrode locations (F(186, 4464) = 2.336, $p = 0.010$, $\varepsilon = 0.057$, η_p^2 = 0.089, power = 0.941). The interaction had a medium effect size and the power to find differences was also high. The pairwise comparison of interaction between measurement time and electrode locations is summarised in Table B.15 in Appendix B.2.14 . The topographical distribution of the significant differences in LLyapExp/α_{relative} from level 1-2, level 1-3, level 1-4, level 1-5, and baseline-recovery are shown in Figure 5.21. A significant decrease in LLyapExp/α_{relative} localised mostly around the parietal and occipital brain regions were visible on level 2, 3, 4, and 5 when compared with level 1 of the visuomotor tracking task. Some EEG electrodes around central brain region (Cz, C2, C6) also showed significant differences in LLyapExp/α_{relative} from level 1 to level 5. A significant reduction was also visible from baseline to recovery around left and midline central, parietal and occipital brain regions. As can be seen in Figure 5.22, the larger decrease in the sample mean of LLyapExp/α_{relative} were mostly localised to the central, parietal and occipital regions. Similar observations were also made for the participants C18 and C21. The above findings

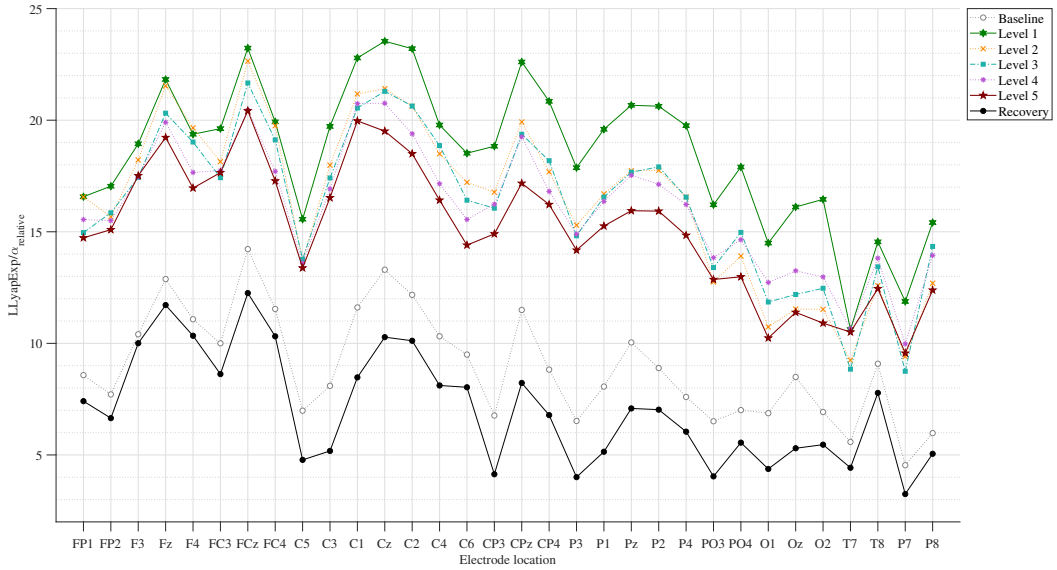

Figure 5.20: Comparison of the sample mean of LLyapExp/α_{relative} on all 32 electrodes between measurement times (baseline, level 1, level 2, level 3, level 4, level 5 and recovery) of the robot-mediated interaction. The amount of change in LLyapExp/α_{relative} from level 1 to level 5 (i.e., level 2 - level 1, level 3 - level 1, level 4 - level 1, and level 5 - level 1) may reflect the effects of fatigue build-up on LLyapExp/α_{relative}. The amount of change in LLyapExp/α_{relative} from baseline to recovery (i.e., recovery - baseline) may also reflect the effects of fatigue on LLyapExp/α_{relative}. *Connecting lines in the figure do not imply a linear relationship between electrode locations but merely for the ease of identifying the numerical changes between baseline, level 1, level 2, level 3, level 4, level 5 and recovery states.*

suggest that fatigue in a robot-mediated visuomotor tracking task could be evaluated by the amount of decrease in LLyapExp/α_{relative}.

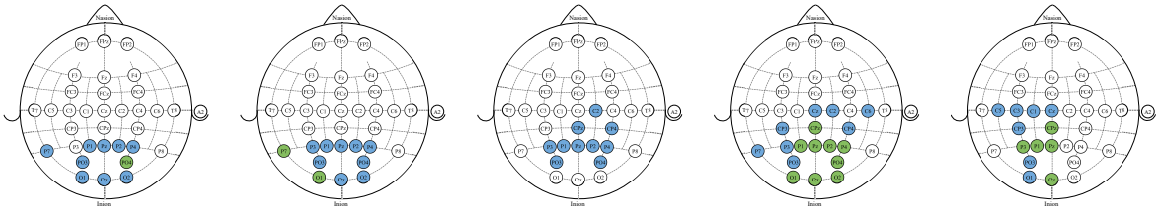

Level 1-2 | Level 1-3 | Level 1-4 | Level 1-5 | Baseline-Recovery

Figure 5.21: The topographical distribution of the significant differences in LLyapExp/α_{relative} between visuomotor tracking task interaction levels and from baseline to recovery of the robot-mediated visuomotor tracking task.

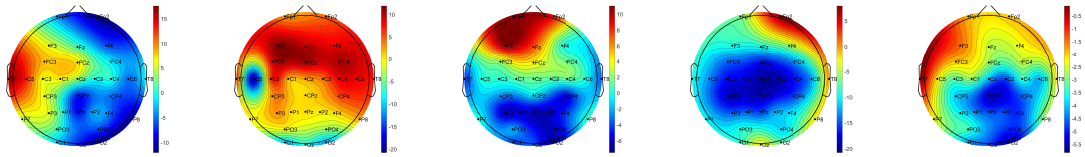

C04 | C17 | C18 | C21 | Sample mean

Figure 5.22: Comparison of the brain topographies of the difference in LLyapExp/α_{relative} for C04, C17, C18, C21, and sample mean of all participants. In each brain map, the nose is represented by the triangle on the top, and the right hemisphere is on the right. The blue-shaded areas indicate a larger decrease whereas the red-shaded areas indicate an increase.

5.3 Discussion

This chapter investigated the modulations in spectral and nonlinear EEG features with fatigue induced by a robot-mediated visuomotor tracking task. The main findings of this experiment were a significant increase in α_{relative} and a significant decrease in δ_{relative}, $(\theta+\alpha)/(\alpha+\beta)$, δ/α, largest Lyapunov exponent, and LLyapExp/α_{relative} from level 1 to level 5 which is localised mostly around central, parietal and occipital regions. These observations suggest that fatigue may have accumulated during the robotic interaction. Neurophysiological evidence has shown that the premotor, motor, parietal and occipital regions are collectively engaged in visually guided arm reaching tasks (Berndt et al., 2002; Grafton et al., 1996;

Naranjo et al., 2007). When reaching movements towards a visual target are performed, the information about the target is selected by integrating both visual and somatosensory information and the appropriate motor plan is formulated (Naranjo et al., 2007; Sabes, 2000). The posterior parietal region is predominantly involved in visuospatial attention and spatial orienting, transforming the location of the visual target into motor coordinates and forming and updating the internal representations of limb and target positions (Berndt et al., 2002; Lacquaniti et al., 1998; Yamaguchi et al., 1994). The premotor region is involved in receiving visual input from parietal cortex and projecting to the primary motor area (Berndt et al., 2002). Therefore, the topographical distribution of the significant observations may suggest the deactivation of central, parietal and occipital brain regions due to fatigue progressed during robot-mediated visuomotor tracking task.

A significant increase in α_{relative} was observed over the central, parietal, and occipital brain regions from level 1 to level 5 of the robot-mediated visuomotor tracking task. An increase in alpha activity with fatigue was also reported in the literature as summarised in Table 2.1. Furthermore, the preliminary experiment performed as part of this thesis also found an increase in α_{relative} due to fatigue in robot-mediated gross motor and fine motor interactions. The localised synchronisation of EEG alpha activity may represent electrophysiological correlate of deactivated cortical areas, thereby suggesting that the brain regions are not adequately processing sensory information or motor output and can be considered to be in an idling state (Pfurtscheller et al., 1996). Therefore, the increase in α_{relative} during the robot-mediated visuomotor tracking task may reflect a reduced capacity for information processing in the central, parietal, and occipital cortical regions as a result of fatigue. The significant decrease in the largest Lyapunov exponent and approximate entropy was also consistent with previous observations (Liu et al., 2010; Xiong et al., 2016; Yao et al., 2009). Both largest Lyapunov exponent and approximate entropy measures of EEG are used to characterize the complexity and flexibility of information processing by the brain (Fell et al., 1993; Kim et al., 2000; Liu et al., 2010; Stam et al., 1994). Here, the term 'flexibility' means the facility of the central nervous system to reach different states of information processing from similar initial states (Fell et al., 1993). Lyapunov exponents estimate the average exponential rates of divergence or convergence of nearby trajectories in phase space. A system with at least one positive Lyapunov exponent is defined to be chaotic (Wolf et al., 1985), reflecting the sensitive dependence on initial conditions (Röschke et al., 1993). The largest Lyapunov exponents observed were positive, thereby suggesting a chaotic behaviour of the EEG during robot-mediated interaction. Yao et al. (2009) stated that the increase in the largest Lyapunov exponents with increasing force levels during intermittent handgrip maximal voluntary contractions may relate to increased neuronal firing and the recruitment

of corticomotor cells associated with increased voluntary isometric effort (Thickbroom et al., 1998). Therefore, the increased largest Lyapunov exponent may reflect increased complexity in the signal and the increased flexibility of information processing. Furthermore, past studies on sleep EEG analysis reported a fall in largest Lyapunov exponent as the person moves from sleep stage I to sleep stage IV, thereby suggesting lesser neurons are available for information processing due to cortical inactivation (Acharya et al., 2005; Fell et al., 1996; Röschke et al., 1995*a*). The observed decrease in the largest Lyapunov exponent following the robot-mediated visuomotor tracking task mostly over the parietal and occipital regions, may thereby reflect a decrease in information processing flexibility around the motor cortex. A larger value of approximate entropy correspond to greater randomness and unpredictability, whereas a lower value of approximate entropy reflects a higher degree of regularity and predictability in a time series (Pincus and Viscarello, 1992; Richman and Moorman, 2000). Bruhn et al. (2000) found a decrease in approximate entropy with increasing desflurane concentrations during anaesthesia, thereby suggesting an increased amount of regularity under high desflurane concentrations. Abásolo et al. (2005) found lower approximate entropy in Alzheimer's disease patients than in control subjects, thereby suggesting a more regular and less complex electorphysiological behaviour of the brain. Therefore, the reduction in approximate entropy values observed around the central brain regions following the robot-mediated interaction may suggest the deficient information processing of the cortex due to the progression of fatigue.

The observed suppression in δ_{relative} over parietal and occipital cortical regions following the robot-mediated visuomotor tracking task is contrary to some previous studies which have suggested a significant increase or no significant difference in δ activities due to fatigue (Craig et al., 2012; Lal and Craig, 2002; Zhao et al., 2012). However, a similar observation was made in the preliminary experiment; therefore, it can be confirmed that fatigue induced by robot-mediated interactions may suppress δ_{relative}. Since visuomotor tracking task required more concentration and attention levels, this finding can also be related to deficient inhibitory control and information-processing mechanisms. In general, an increase in θ band power was observed in the fatigue literature (Barwick et al., 2012; Cheng and Hsu, 2011; Craig et al., 2012; Zhao et al., 2012). Therefore, the reduction in θ_{relative} on FC3, C3, C1, Cz, and CP3 electrodes is also contrary to some previous studies (Section B.2.2). However, Baumeister et al. (2012) has reported a significant reduction in θ band power over frontal and fronto-central brain regions due to the effects of fatigue induced by a cycling exercise on knee joint reproduction task. Thus, the above finding, while preliminary, may suggest that fatigue induced by robot-mediated visuomotor tracking tasks suppress the θ_{relative} over central brain regions.

Both $(\theta+\alpha)/(\alpha+\beta)$ and δ/α power ratios also significantly decreased following the robot-mediated interaction. A widespread increase in $(\theta+\alpha)/(\alpha+\beta)$ was visible with mental fatigue in visual search task (Fan et al., 2015). Driver fatigue also increased $(\theta+\alpha)/(\alpha+\beta)$ on temporal brain regions (Jap et al., 2009). Therefore, the decrease in $(\theta+\alpha)/(\alpha+\beta)$ over central, parietal and occipital brain regions observed in this experiment do not support the previous research. Since there was an increase in α_{relative} (Figures 5.12b) and β_{relative} (Figure B.4) and decrease in θ_{relative} (Figure B.2) over the central, parietal and occipital regions, the suppression in $(\theta+\alpha)/(\alpha+\beta)$ may be caused by the mutual addition of band powers. The suppression of δ/α also showed a widespread topographical distribution. Since the variation in δ_{relative} and α_{relative} were consistent with findings of the preliminary experiment, δ/α can be considered collectively as a measure of fatigue in robot-mediated interactions. Although not significant, an increase in $(\theta+\alpha)/\beta$ over the parietal region and an increase in α/β on all EEG electrodes were observed from level 1 to level 5 of the robotic interaction (Sections B.2.5 and B.2.6). These observations were in line with those of previous studies, thereby suggesting that the fatigue induced by the visuomotor task may have increased the low-frequency activities while suppressing the high-frequency activities. The modulations in $(\theta+\alpha)/\beta$ and α/β were not further explored in this study since significant variations were not found between level 1 and 5.

In addition to the EEG-based fatigue measures used in literature, a new feature was derived in this study by combing the modulations in α_{relative} and largest Lyapunov exponent. A decreasing trend was visible in this new feature, $\text{LLyapExp}/\alpha_{\text{relative}}$ for all EEG electrodes. The significant decrease was localised mostly around central, parietal and occipital brain regions from level 1 to level 5. Also, the left and midline central, parietal and occipital brain regions showed significant differences from baseline to recovery. Therefore, this new feature can be used instead of the two EEG features, α_{relative} and largest Lyapunov exponent, thereby reducing the complexity of the EEG-based fatigue estimation system.

A widespread significant differences were also observed from baseline to level 1 and from level 5 to recovery on the majority of EEG features. These differences explain the changes in the brain activation patterns from resting phase to an active movement phase and vice versa. For instance, a suppression in alpha activity over sensorimotor cortex relative to the resting conditions were observed by active or passive movements of the hand/arm, planning of voluntary movement, attention to or preparation for activity (Arroyo et al., 1993; Chatrian et al., 1959; Pellouchoud et al., 1999; Pfurtscheller et al., 1996). Also, the complexity and the information processing flexibility of the brain greatly increase when a larger number of cortical neurons are recruited to perform the task in hand (Thickbroom et al., 1998). A significant increase in the largest Lyapunov exponent on all EEG electrode locations

from baseline to level 1 of the robotic interaction and a significant decrease from level 5 to recovery were observed in this experiment. The above observations may reflect the increased neuronal firing and the recruitment of corticomotor cells during the robot-mediated visuomotor tracking task in comparison to resting state of the brain.

5.4 Conclusions

Modulations in spectral and nonlinear EEG features due to fatigue induced by robot-mediated visuomotor tracking task were presented in this chapter. The observed significant differences in δ_{relative}, α_{relative}, $(\theta+\alpha)/(\alpha+\beta)$, δ/α, and largest Lyapunov exponent may reflect the changes in participant's level of fatigue during the robot-mediated visuomotor tracking task. Also, a new feature which evaluated the combined effect of modulations in largest Lyapunov exponent and α_{relative} was proposed in this chapter. The new feature, LLyapExp$/\alpha_{\text{relative}}$ also showed a significant decrease following the robot-mediated interaction, thereby may be considered as a EEG-based fatigue measure in future studies. Furthermore, the significant differences in the substantive EEG features were mostly localised to central, parietal and occipital brain regions. Therefore, it can be concluded that the fatigue accumulated during robot-mediated visuomotor tracking tasks mostly reduce the information processing capacity and the complexity of the central, parietal and occipital brain regions. Chapter 6 will further explore the association of these EEG-based fatigue measures with the subjective measures of level of fatigue and movement-variability measures of the upper limb.

Chapter 6

Experiment 2 - Part II: Association of the Modulations in EEG Features with Subjective Measures of the Level of Fatigue and Movement Variability Measures

Chapter 5 discussed the design of experiment 2 in detail and the modulations in spectral and nonlinear EEG features with fatigue accumulated during the robot-mediated visuomotor tracking task. A significant increase in α_{relative} and a significant decrease in δ_{relative}, $(\theta+\alpha)/(\alpha+\beta)$, δ/α, largest Lyapunov exponent (LLyapExp), and LLyapExp$/\alpha_{\text{relative}}$ were found mostly localised around central, parietal, and occipital brain regions when progressing from Level 1 of the visuomotor tracking task to Level 5. Therefore, it was of interest to see how these EEG feature variations during the task are related to the change in subjective measures of the level of fatigue following the task and the movement variability measures estimated during the task. In this chapter, firstly, the participant's feedback obtained using questionnaires given before and after the robotic interaction are further analysed to evaluate the variations in the level of fatigue following the visuomotor tracking task and the comfortability of the task. Then, the variations in the mean absolute distance (MAD) and root mean square distance (RMSD) between control and guide points from Level 1 to Level 5 of the robotic interaction are investigated. These two movement variability measures reflect the accuracy of tracking the guide point during the task. Finally, the association between the

EEG feature modulations, change in the subjective measures of the level of fatigue and the movement variability measures are investigated.

6.1 Methods and Materials

In the following sections the methods used to analyse the subjective measures of fatigue and the movement variability measures are discussed.

6.1.1 Subjective Measures of the Level of Fatigue and Comfortability

The questionnaires used in this experiment are given in Appendix C.2. The questionnaire given before the task was used to gather information about the participant's demographics, and subjective measures of their physical and mental fatigue level before performing the robot-mediated visuomotor tracking task. The questionnaire given after the task, on the other hand, was used to obtain a subjective measure of the physical and mental fatigue levels following the robot-mediated visuomotor tracking task, and a feedback on the underlying comfortability of the experiment. The following sections describe the questionnaires used to estimate the level of fatigue and comfortability in this experiment in detail.

A. Subjective Measures of the Level of Fatigue

Many self-administered questionnaires have been developed to obtain a subjective measure of fatigue (Jackson, 2014; Neuberger, 2003; Shahid et al., 2010). Most of these questionnaires were explicitly made to assess the effects of fatigue due to medical conditions. In this experiment, a 9-item questionnaire was used to obtain a self-report of the fatigue state of each individual before and after the robot-mediated interaction. The nine statements are as follows,

1. Physically, do you feel exhausted?
2. Do you feel sleepy or drowsy?
3. Mentally, do you feel exhausted?
4. Do you feel less strength in your muscles?
5. Do you have difficulties in concentrating?
6. Do you need to rest?
7. Are you motivated?
8. Do you feel tired?
9. How alert do you feel?

Statements 1 and 3 were adapted from the Fatigue Assessment Scale (FAS) (Michielsen et al., 2003) and the statements 2, 4, 5, and 6 from the Chalder Fatigue Scale (CFQ 11) (Chalder et al., 1993). Statements 1, 2, 4, 6, and 8 are related to the symptoms of physical fatigue. Statements 3, 5, 7, and 9 are related to the symptoms of mental fatigue. Each statement contains a 7-point scale, with '1' representing 'Not at all' and '7' representing 'Extremely'. The scoring of each statement was done by using a Likert score with weights assigned to each response choice. For statements 1, 2, 3, 4, 5, 6, and 8, the Likert scale responses starting from the extreme left were assigned the scores 0, 1, 2, 3, 4, 5, and 6. For statements 7 and 9, the responses starting from the extreme left were assigned the scores 6, 5, 4, 3, 2, 1, and 0, as a higher rating for motivation or alert reflects a fatigue-free state. The sum of all individual response scores contributed to the global fatigue level scores. Therefore, the global fatigue score for this study ranged from 0 to 54, and a higher score indicated a greater fatigue level. In addition, separate scores for both physical and mental fatigue levels were calculated by summing the individual response scores corresponding to the statements related to physical and mental symptoms of fatigue. The physical fatigue scores ranged from 0 to 30, and the mental fatigue score ranged from 0 to 24. The percentage value of physical, mental and global fatigue scores from the maximum value of each fatigue type was calculated to compare the differences between fatigue levels obtained before and after the interaction. The percentage fatigue levels were also used to identify physical and mental fatigue contributions towards the global fatigue level.

B. Feedback on the Comfortability of the Robot-Mediated Visuomotor Tracking Task

A subjective assessment was also performed to obtain feedback on the comfortability of the robot-mediated interaction. The following five statements which also contain a 7-point rating scale, with '1' representing 'Not at all' and '7' representing 'Extremely' was used to obtain the participant's feedback on the experiment protocol.

1. Performing the task was physically exhausting
2. Performing the task was mentally exhausting
3. It was difficult to move the robot arm in early stages of the interaction
4. It was difficult to move the robot arm in later stages of the interaction
5. Eye strain was experienced during the task

6.1.2 Measures of Movement Variability

In robot-mediated interactions the movement variability is often reported as the mean absolute values of the distance (MAD) of each point of the path from the theoretic path or as the root

mean square distance (RMSD) between the target trajectory followed by the user and the actual trajectory needs to be followed (Colombo et al., 2005; Huang et al., 2020; Song et al., 2008). In this experiment, participants were instructed to track the trajectory followed by the guide point at a speed similar to the speed of the guide point. Therefore, both mean absolute distance and root mean square distance between control and guide points provide a measure of movement variability during the task. These two measures were calculated and compared to evaluate the association of fatigue and movement variability measures. Findings can be used to infer whether fatigue was developed as a consequence of maintaining increased tracking accuracies or whether participants followed adaptation strategies to reduce the fatigue build-up. EEG data analysis of this experiment (Chapter 5) found significant differences in EEG features between level 1 and level 5 of the visuomotor tracking task localised mostly around central, parietal and occipital brain regions. Therefore, the movement variability measures for each participant were only calculated for the kinematic data gathered during level 1 and level 5. A pictorial representation of the kinematic data segmentation at level 1 and 5 is given in Figure 6.1. Kinematic data recorded when participants respond to message boxes and the robot arm moves to the starting position following the *'key-press'* event (Section 5.1.3) were eliminated from further analysis.

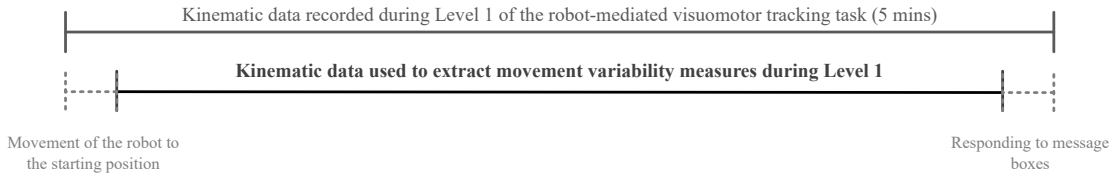

(a) Level 1

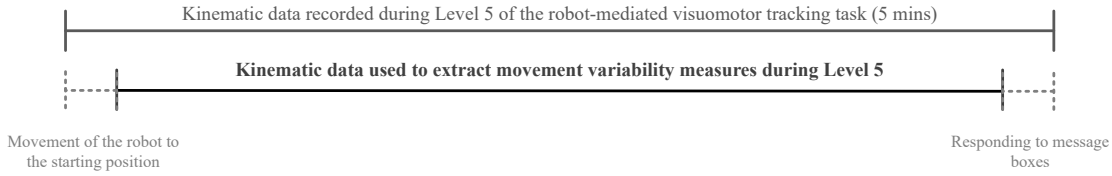

(b) Level 5

Figure 6.1: Kinematic data segmentation at level 1 and level 5 of the robot-mediated visuomotor tracking task.

The mean absolute distance and the root mean square distance between control and guide points at level 1 and level 5 were calculated separately as explained below. Firstly, the absolute distance between the control point position, $p_{c_i} = [x_{c_i}, y_{c_i}, z_{c_i}]$ (a 3 dimensional space position vector) and the guide point position $p_{g_i} = [x_{g_i}, y_{g_i}, z_{g_i}]$ at each sampling point,

i was calculated as the Euclidean distance between the two points, d_i,

$$d_i = \sqrt{(x_{c_i} - x_{g_i})^2 + (y_{c_i} - y_{g_i})^2 + (z_{c_i} - z_{g_i})^2} \tag{6.1}$$

where $i = 1, \ldots, N$ and N is the total number of positional data samples within each level. Then, the mean absolute distance between control and guide points at each level (MAD) was calculated using equation 6.2,

$$\text{MAD} = \frac{\sum_{i=1}^{N} d_i}{N}. \tag{6.2}$$

The root mean absolute distance between control and guide points at each level was calculated using equation 6.3,

$$\text{RMSD} = \sqrt{\sum_{i=1}^{N} \frac{d_i^2}{N}}. \tag{6.3}$$

For a perfectly traced path, these measures will approximate zero (Colombo et al., 2005; MacKenzie et al., 2001). An increment in both measures with time may imply a rise in movement variability during the tracking task.

6.1.3 Statistical Analysis

The statistical analysis was conducted using *IBM SPSS Statistics 25* software. A p-value$<$0.05 was considered statistically significant denoting a 95% confidence interval. The normality was assessed using Kolmogorov–Smirnov test.

A. Statistical Analysis of Subjective Measures of the Level of Fatigue

Differences in the percentage values of physical, mental and global fatigue levels of all participants calculated before and after the robot-mediated visuomotor tracking task were normally distributed. Therefore, paired-samples t-tests were performed separately on each subjective measure of fatigue level to identify the significant differences in fatigue level following the robot-mediated visuomotor tracking task. The effect sizes were expressed by the Pearsons' correlation coefficient calculated using the equation 3.40. Cohen's benchmarks were used to interpret the effect sizes (i.e., r value of 0.1, 0.3, 0.5 represents small, medium and large effect respectively).

B. Statistical Analysis of Movement Variability Measures

The difference in mean absolute distance between level 1 and level 5 of the robot-mediated visuomotor tracking task of all participants was normally distributed. Similarly, the difference

in root mean square distance between level 1 and level 5 of the task of all participants was normally distributed. Therefore, paired-samples t-tests were performed separately on each movement variability measure to find whether these measures significantly changed during the task. The effect sizes were expressed by the Pearsons' correlation coefficient calculated using the equation 3.40. Cohen's benchmarks were used to interpret the effect sizes (i.e., r value of 0.1, 0.3, 0.5 represents small, medium and large effect respectively).

C. Correlation Analysis of EEG Features, Subjective Measures of the Level of Fatigue and Movement Variability Measures

The association of the change in prominent EEG features (δ_{relative}, α_{relative}, $(\theta+\alpha)/(\alpha+\beta)$, δ/α, largest Lyapunov exponent (LLyapExp), LLyapExp$/\alpha_{\text{relative}}$) around central, parietal and occipital brain regions with the change in subjective measures of fatigue level and the change in movement variability measures of all participants were analysed using the Pearson's correlation coefficient. Also, the relationship between the subjective measures of fatigue level and the movement variability measures were analysed using the Pearson's correlation coefficient. The change in each EEG feature was calculated by deducting the EEG feature value during level 1 of the task from the EEG feature value during level 5 of the task (i.e., value of EEG feature at level 5 - value of EEG feature at level 1) around central, parietal and occipital regions. Similarly, the change in each subjective measure of fatigue level was calculated by deducting the subjective measure obtained before the robotic interaction from the subjective measure obtained after the robotic interaction (i.e., subjective fatigue level percentage after the task - subjective fatigue level percentage before the task). The change in movement variability measures (MAD and RMSD) were calculated by deducting the movement variability value during level 1 of the task from the movement variability value during level 5 of the task (i.e., value of MAD or RMSD at level 5 - value of MAD or RMSD at level 1).

6.2 Results

6.2.1 Subjective Measures of the Level of Fatigue and Comfortability

A. Subjective Measures of the Level of Fatigue

Tables 6.1 and 6.2 summarise the total number and percentage of responses received for each Likert scale category of individual statements before and after interacting with the robot-mediated visuomotor tracking task. The two tables clearly show an increase in the

Table 6.1: Total number (percentage) of fatigue state questionnaire responses in each Likert scale category before the robot-mediated visuomotor tracking task.

	Statement	Total number (percentage) of participants in each response						
		1	2	3	4	5	6	7
1	Physically, do you feel exhausted?	17 (68%)	7 (28%)	1 (4%)	0 (0%)	0 (0%)	0 (0%)	0 (0%)
2	Do you feel sleepy or drowsy?	15 (60%)	8 (32%)	1 (4%)	1 (4%)	0 (0%)	0 (0%)	0 (0%)
3	Mentally, do you feel exhausted?	18 (72%)	4 (16%)	2 (8%)	1 (4%)	0 (0%)	0 (0%)	0 (0%)
4	Do you feel less strength in your muscles?	21 (84%)	3 (12%)	1 (4%)	0 (0%)	0 (0%)	0 (0%)	0 (0%)
5	Do you have difficulties in concentrating?	19 (76%)	6 (24%)	0 (0%)	0 (0%)	0 (0%)	0 (0%)	0 (0%)
6	Do you need to rest?	20 (80%)	5 (20%)	0 (0%)	0 (0%)	0 (0%)	0 (0%)	0 (0%)
7	Are you motivated?	0 (0%)	0 (0%)	0 (0%)	0 (0%)	1 (4%)	7 (28%)	17 (68%)
8	Do you feel tired?	16 (64%)	8 (32%)	1 (4%)	0 (0%)	0 (0%)	0 (0%)	0 (0%)
9	How alert do you feel?	0 (0%)	0 (0%)	0 (0%)	1 (4%)	2 (8%)	8 (32%)	14 (56%)

Table 6.2: Total number (percentage) of fatigue state questionnaire responses in each Likert scale category after the robot-mediated visuomotor tracking task.

	Statement	Total number (percentage) of participants in each response						
		1	2	3	4	5	6	7
1	Physically, do you feel exhausted?	3 (12%)	4 (16%)	3 (12%)	4 (16%)	6 (24%)	4 (16%)	1 (4%)
2	Do you feel sleepy or drowsy?	3 (12%)	2 (8%)	4 (16%)	8 (32%)	2 (8%)	6 (24%)	0 (0%)
3	Mentally, do you feel exhausted?	7 (28%)	6 (24%)	2 (8%)	5 (20%)	3 (12%)	2 (8%)	0 (0%)
4	Do you feel less strength in your muscles?	1 (4%)	1 (4%)	5 (20%)	7 (28%)	5 (20%)	4 (16%)	2 (8%)
5	Do you have difficulties in concentrating?	4 (16%)	4 (16%)	3 (12%)	4 (16%)	4 (16%)	5 (20%)	1 (4%)
6	Do you need to rest?	1 (4%)	3 (12%)	2 (8%)	8 (32%)	3 (12%)	4 (16%)	4 (16%)
7	Are you motivated?	2 (8%)	1 (4%)	5 (20%)	3 (12%)	4 (16%)	5 (20%)	5 (20%)
8	Do you feel tired?	1 (4%)	1 (4%)	5 (20%)	2 (8%)	8 (32%)	6 (24%)	2 (8%)
9	How alert do you feel?	0 (0%)	2 (8%)	6 (24%)	6 (24%)	3 (12%)	5 (20%)	3 (12%)

ratings given for statements 1, 2, 3, 4, 5, 6, and 8 after the task whereas a decrease in the ratings given for statements 7 and 9. These observations suggest that the participants fatigue levels were changed following the robotic interaction.

A summary of the calculated individual physical, mental and global fatigue level percentages is given in Table 6.3. Figure 6.2 shows the variations in physical, mental and global fatigue level percentages obtained before and after the visuomotor tracking task for each participant. It was found that the majority of participants experienced an increase in their physical (23/25 participants) and mental (20/25 participants) fatigue levels following the visuomotor tracking task, thereby leading towards an increase in their global fatigue levels (23/25 participants). The participant's feedback also revealed that most participants experienced a comparatively larger increase in the physical fatigue levels than the increase in the mental fatigue levels. Therefore, the subjective responses may imply that the visuomotor tracking task performed using HapticMASTER caused more physical fatigue than mental fatigue. Also, the greater

Table 6.3: Summary of the subjective measures of the level of fatigue following the robot-mediated visuomotor tracking task.

Subject ID	Physical fatigue level (%)			Mental fatigue level (%)			Global fatigue level (%)		
	Before	After	After-Before	Before	After	After-Before	Before	After	After-Before
C01	0.00	26.67	26.67	0.00	20.83	20.83	0.00	24.07	24.07
C02	13.33	86.67	73.33	16.67	75.00	58.33	14.81	81.48	66.67
C03	0.00	40.00	40.00	8.33	8.33	0.00	3.70	25.93	22.22
C04	0.00	40.00	40.00	0.00	45.83	45.83	0.00	42.59	42.59
C05	0.00	66.67	66.67	0.00	62.50	62.50	0.00	64.81	64.81
C06	0.00	30.00	30.00	0.00	29.17	29.17	0.00	29.63	29.63
C07	0.00	60.00	60.00	0.00	58.33	58.33	0.00	59.26	59.26
C08	13.33	86.67	73.33	16.67	54.17	37.50	14.81	72.22	57.41
C09	10.00	73.33	63.33	0.00	58.33	58.33	5.56	66.67	61.11
C10	0.00	70.00	70.00	8.33	62.50	54.17	3.70	66.67	62.96
C11	6.67	70.00	63.33	12.50	50.00	37.50	9.26	61.11	51.85
C12	23.33	23.33	0.00	20.83	16.67	-4.17	22.22	20.37	-1.85
C13	13.33	60.00	46.67	16.67	54.17	37.50	14.81	57.41	42.59
C14	3.33	33.33	30.00	0.00	0.00	0.00	1.85	18.52	16.67
C15	20.00	46.67	26.67	25.00	29.17	4.17	22.22	38.89	16.67
C16	0.00	53.33	53.33	0.00	12.50	12.50	0.00	35.19	35.19
C17	0.00	16.67	16.67	4.17	4.17	0.00	1.85	11.11	9.26
C18	0.00	66.67	66.67	0.00	62.50	62.50	0.00	64.81	64.81
C19	0.00	60.00	60.00	0.00	54.17	54.17	0.00	57.41	57.41
C20	0.00	60.00	60.00	4.17	25.00	20.83	1.85	44.44	42.59
C21	0.00	90.00	90.00	0.00	54.17	54.17	0.00	74.07	74.07
C22	0.00	33.33	33.33	16.67	20.83	4.17	7.41	27.78	20.37
C23	6.67	53.33	46.67	0.00	41.67	41.67	3.70	48.15	44.44
C24	10.00	90.00	80.00	0.00	75.00	75.00	5.56	83.33	77.78
C25	20.00	16.67	-3.33	20.83	16.67	-4.17	20.37	16.67	-3.70

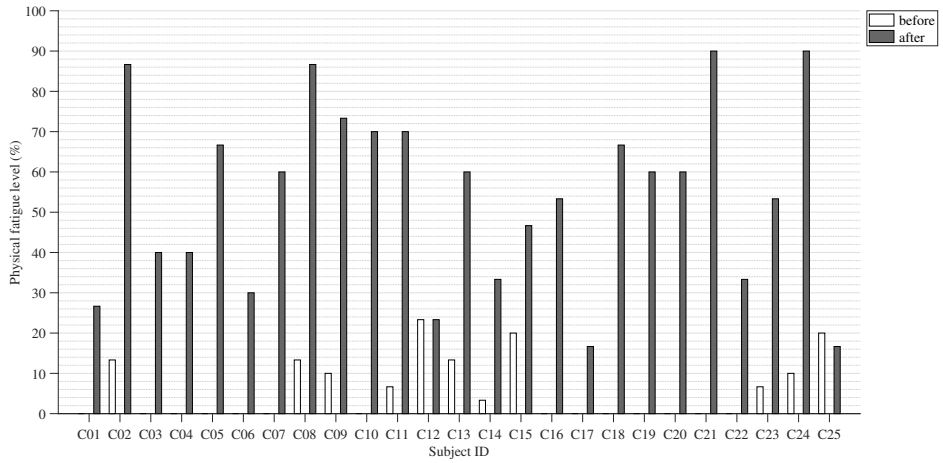

(a) Physical fatigue level percentage.

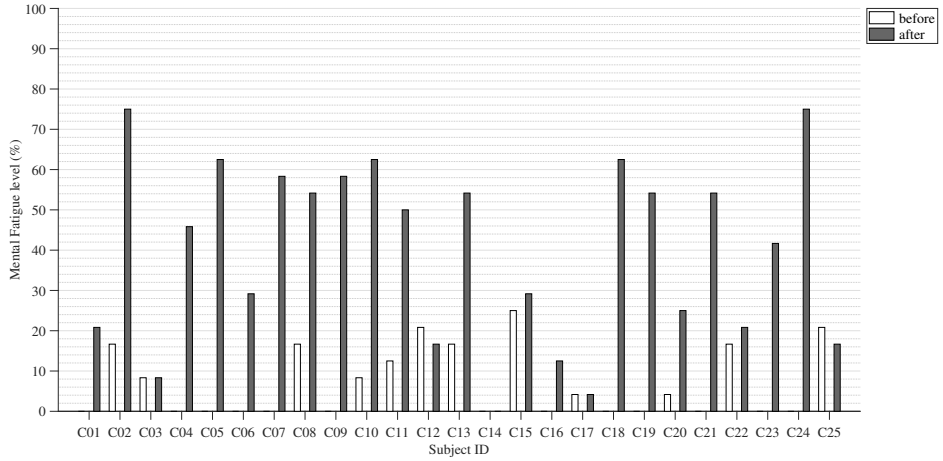

(b) Mental fatigue level percentage.

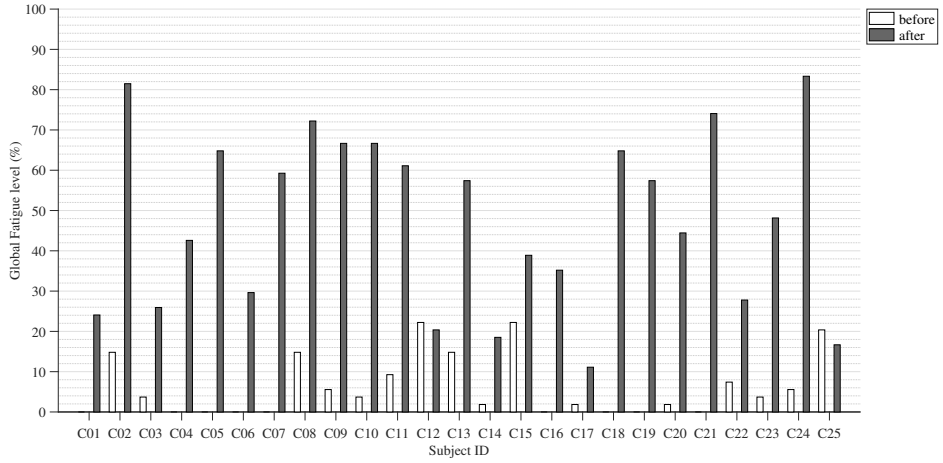

(c) Global fatigue level percentage.

Figure 6.2: Subjective measures of (a) physical, (b) mental, and (c) global fatigue level percentages before and after the robot-mediated visuomotor tracking task for all participants.

increase in physical fatigue level may have mostly contributed to the increase in global fatigue level following the robot-mediated visuomotor tracking task.

Table 6.4 summarises the paired-samples *t*-test results of subjective measures of the level of fatigue. Also, the sample mean and standard deviation of the subjective measures obtained before and after the robot-mediated visuomotor tracking task is shown in Figure 6.3. The paired-samples *t*-test revealed that the physical (t = -10.047, p = 0.000, r = 0.899), mental (t = -6.461, p = 0.000, r = 0.797) and global (t = -8.800, p = 0.000, r = 0.874) fatigue levels increased significantly following the robotic interaction. Moreover, these significant differences had a larger effect size.

Table 6.4: Paired-samples *t*-test results of the subjective measures of level of fatigue following the robot-mediated visuomotor tracking task.

Type of fatigue	**Sample mean ± std (%)**		**Paired samples *t*-test**				**Direction of change**
	Before	**After**	***t***	***df***	***p*-value**	***r***	
Physical fatigue level	5.60±7.62	54.14±22.76	-10.047	24	0.000	0.899	↑
Mental fatigue level	6.83±8.58	39.67±22.82	-6.461	24	0.000	0.797	↑
Global fatigue level	6.15±7.55	47.707±21.83	-8.800	24	0.000	0.874	↑

Notes. ↑ = significant increase.

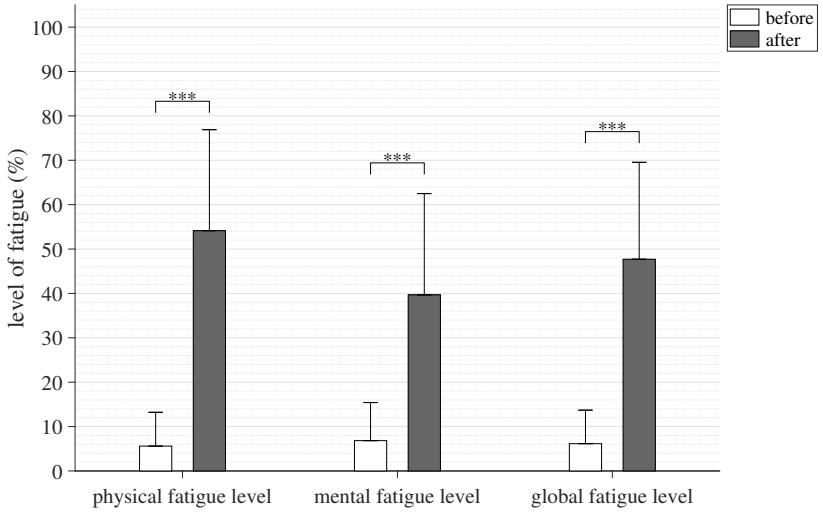

Figure 6.3: Comparison of sample mean and standard deviation of physical, mental and global fatigue level percentages before and after the robot-mediated visuomotor tracking task. The statistical significance, $p < 0.00$ is represented by asterisks (***).

B. Feedback on the Comfortability of the Robot-Mediated Visuomotor Tracking Task

Table 6.5 summarises the total number and percentage of responses received for each Likert scale category of the individual statements related to comfortability of the robot-mediated visuomotor tracking task. The responses showed that the majority of the participants felt that performing the task was physically exhausting than mentally exhausting. Also, it was found that the task caused an eye strain on most participants, thereby suggesting that tracking the guide point may have caused the increase in eye strain. Furthermore, most participants reported that it was difficult to move the robot arm in latter stages of the interaction than the early stages of the interaction. These responses showed that although participants were not aware of the increase in the damping coefficient values with time, they felt the increase in difficulty level with time.

6.2.2 Measures of Movement Variability

Figures 6.4a and 6.4b illustrate the first forward loop motion (i.e., from Segment 1 to 12) of the control point and the guide point for two participants, C05 and C11, respectively. Paths of the control point reflect that both participants were unable to perfectly trace the trajectories covered by the guide point during the first forward loop of each level. Both participants also showed an increase in mean absolute distance (MAD) between control and guide points when progressing from level 1 to level 5 (i.e., MAD at level 1 for C05 = 4.21, C11 = 2.59 and MAD at level 5 for C05 = 6.12, C11 = 3.38). Similarly, an increase in root mean square distance (RMSD) between control and guide points were also visible from level 1 to level 5 (i.e., RMSD at level 1 for C05 = 4.92, C11 = 3.22 and RMSD at level 5 for C05 = 7.40, C11 = 4.53). Since both participants reported an increase in their physical and mental fatigue levels following the task (i.e., physical fatigue level before the task for C05 = 0.00%, C11 = 6.67% and after the task for C05 = 66.67%, C11 = 70.00%; mental fatigue level before the task for C05 = 0.00%, C11 = 12.50% and after the task for C05 = 62.50%, C11 = 50.00%), the increased irregularity in the control point trajectory from level 1 to level 5 of the task may be due to the fatigue accumulated during the interaction.

Table 6.6 summarises the paired-samples *t*-test results of mean absolute distance and root mean square distance between control and guide points. Although the sample mean of both measures showed an increase when progressing from level 1 to level 5 of the visuomotor tracking task, the differences were not significant. Figure 6.5 shows the variations in both movement variability measures from level 1 to level 5 of the visuomotor tracking task for each participant. As can be seen in Figure 6.5a, most participants (15/25 participants) showed an

Table 6.5: Total number (percentage) of task comfortability questionnaire responses in each Likert scale category following the robot-mediated visuomotor tracking task.

	Statement	Total number (percentage) of participants in each response						
		1	2	3	4	5	6	7
1	Performing the task was physically exhausting	1 (4%)	4 (16%)	3 (12%)	6 (24%)	4 (16%)	7 (28%)	0 (0%)
2	Performing the task was mentally exhausting	3 (12%)	6 (24%)	2 (8%)	8 (32%)	5 (16%)	1 (4%)	1 (4%)
3	It was difficult to move the robot arm in early stages of the interaction	10 (40%)	7 (28%)	3 (8%)	3 (12%)	2 (8%)	2 (4%)	0 (0%)
4	It was difficult to move the robot arm in latter stages of the interaction	5 (20%)	3 (12%)	4 (8%)	1 (4%)	5 (20%)	6 (24%)	3 (12%)
5	Eye strain was experienced during the task	5 (20%)	2 (8%)	1 (4%)	3 (12%)	6 (24%)	7 (24%)	2 (8%)

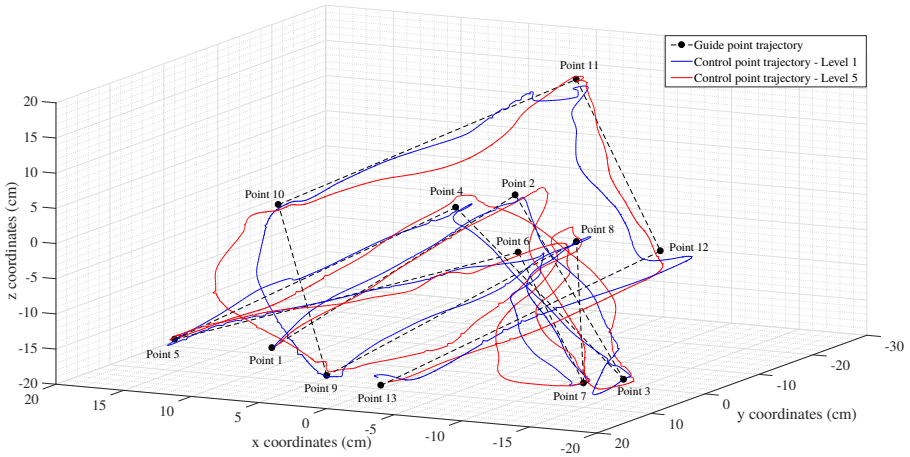

(a) Participant ID: C05, change in MAD = 1.92, RMSD = 0.79, physical fatigue = 66.67% and mental fatigue level = 62.50%

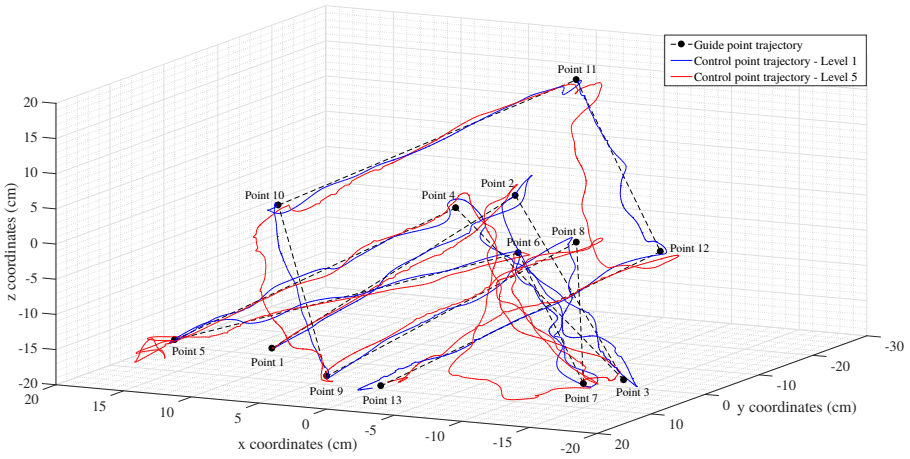

(b) Participant ID: C11, change in MAD = 2.48, RMSD = 1.31, physical fatigue = 63.33% and mental fatigue level = 37.50%

Figure 6.4: The first forward loop motion (i.e., segments 1 to 12) of the guide point and control point during the robot-mediated visuomotor tracking task for the participants (a) C05 and (b) C11. MAD and RMSD refers to mean absolute distance and root mean square distance between control and guide points.

Table 6.6: Paired-samples *t*-test results of movement variability measures between level 1 and level 5 of the robot-mediated visuomotor interaction.

Movement variability measure	Sample mean ± std (cm)		Paired samples *t*-test			
	Level 1	Level 5	*t*	*df*	*p*-value	*r*
Mean absolute distance	3.48±1.55	3.70±2.06	-1.160	24	0.258	0.230
Root mean square distance	4.23±1.83	4.53±2.46	-1.229	24	0.000	0.243

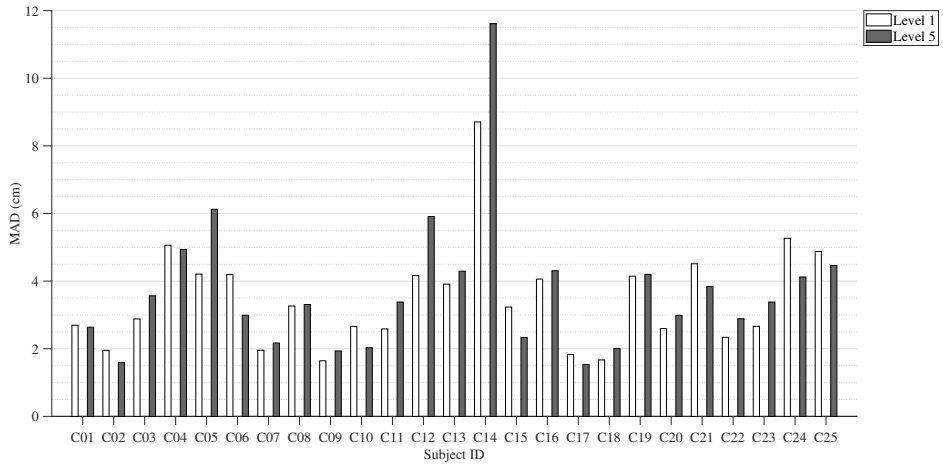

(a) Mean absolute distance (MAD).

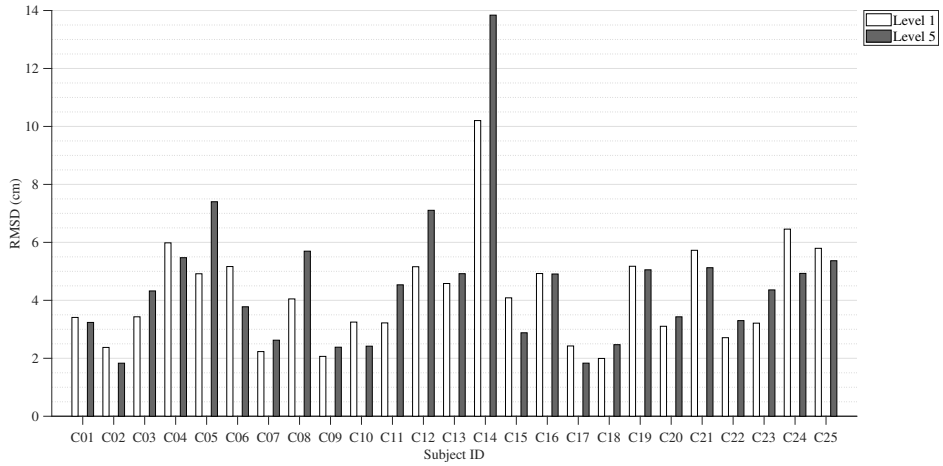

(b) Root mean square distance (RMSD).

Figure 6.5: Variations in movement variability measures during level 1 and level 5 of the robot-mediated visuomotor tracking task for all participants. (a) Mean absolute distance (MAD) between control and guide points and (b) root mean square distance (RMSD) between control and guide points.

increase in mean absolute distance between guide and control points. Also, most participants (13/25 participants) showed an increase in root mean square distance between guide and control points. Therefore, findings may suggest that although not significant, an increase in both movement variability measures from level 1 to level 5 of the task were found for most participants.

6.2.3 Association of the Subjective Measures of the Level of Fatigue with the Significant EEG Feature Variations

Chapter 5 found a significant increase in α_{relative} and significant decrease in δ_{relative}, $(\theta+\alpha)/(\alpha+\beta)$, δ/α, largest Lyapunov exponent, and LLyapExp/α_{relative} EEG features from level 1 to level 5 of the robot-mediated visuomotor tracking task. The variations in the substantive EEG features were mainly localised around the central, parietal and occipital brain regions. Participant's feedback showed a significant increase in both physical and mental fatigue levels following the robotic interaction. Also, most participants experienced a comparatively larger increase in the physical fatigue levels than the increase in the mental fatigue levels. Therefore, the correlation analysis was performed to identify the association between the change in substantive EEG features (value of each EEG feature at level 5 - value of each EEG feature at level 1) and the change in subjective measures of physical and mental fatigue level (fatigue level percentage after the task - fatigue level percentage before the task).

Table 6.7 summarises the findings of Pearson's correlation coefficient (r and p-value) performed on the change in subjective measures of physical fatigue level and the change in δ_{relative}, α_{relative}, $(\theta+\alpha)/(\alpha+\beta)$, δ/α, largest Lyapunov exponent, LLyapExp/α_{relative}, respectively. The change in α_{relative} on all EEG electrodes around central, parietal and occipital brain regions were positively correlated with the change in physical fatigue level. Negative correlations were found between the change in physical fatigue level and the change in $(\theta+\alpha)/(\alpha+\beta)$, δ/α, largest Lyapunov exponent, LLyapExp/α_{relative}, respectively on all EEG electrodes around central, parietal and occipital brain regions. Significant negative correlations were visible on FC3, C5, C3, C1, Cz, CP3, CPz, P3, P1, and Pz electrodes for $(\theta+\alpha)/(\alpha+\beta)$; on FC3, CP3, and P3 electrodes for largest Lyapunov exponent, and on FC3, C3, C1, Cz, and CP3 electrodes for LLyapExp/α_{relative}. Figure 6.6 shows the correlation between the change in physical fatigue level and the change in $(\theta+\alpha)/(\alpha+\beta)$, largest Lyapunov exponent, and LLyapExp/α_{relative} on CP3 electrode. It was visible that most participants who reported a greater increase in their physical fatigue level also showed a greater reduction in $(\theta+\alpha)/(\alpha+\beta)$, largest Lyapunov exponent, and LLyapExp/α_{relative} on CP3 electrode. Table 6.8, on the other hand, summarises the findings of Pearson's correlation

Table 6.7: Correlation between the change in substantive EEG features from level 1 to level 5 and the change in subjective measures of physical fatigue level.

EEG feature	Pearson's correlation coefficient	FC3	FCz	FC4	C5	C3	C1	Cz	C2	C4	C6	CP3	CPz	CP4	P3	P1	Pz	P2	P4	PO3	PO4	O1	Oz	O2
δ_{relative}	r	0.020	0.061	0.042	0.082	-0.075	-0.088	-0.202	0.011	0.024	0.137	-0.053	-0.123	-0.113	-0.111	-0.133	-0.192	-0.174	-0.091	-0.098	-0.241	0.001	0.003	-0.101
	p-value	0.926	0.772	0.843	0.695	0.722	0.677	0.334	0.959	0.911	0.513	0.801	0.560	0.590	0.599	0.526	0.357	0.405	0.665	0.640	0.246	0.998	0.987	0.629
α_{relative}	r	0.138	0.188	0.120	0.130	0.266	0.238	0.332	0.126	0.078	0.023	0.273	0.283	0.190	0.220	0.231	0.269	0.240	0.161	0.154	0.233	0.074	0.068	0.162
	p-value	0.511	0.369	0.569	0.536	0.199	0.251	0.105	0.549	0.711	0.913	0.187	0.170	0.362	0.290	0.266	0.193	0.248	0.443	0.461	0.262	0.724	0.748	0.439
$(\theta+\alpha)/(\alpha+\beta)$	r	-0.411	-0.388	-0.350	-0.415	-0.447	-0.462	-0.441	-0.382	-0.271	-0.287	-0.436	-0.449	-0.347	-0.436	-0.421	-0.405	-0.348	-0.316	-0.296	-0.395	-0.165	-0.072	-0.239
	p-value	0.041	0.055	0.086	0.039	0.025	0.020	0.027	0.060	0.190	0.164	0.029	0.024	0.089	0.029	0.036	0.045	0.088	0.124	0.150	0.051	0.430	0.732	0.249
δ/α	r	-0.248	-0.192	-0.252	-0.011	-0.344	-0.352	-0.380	-0.270	-0.223	-0.144	-0.282	-0.306	-0.345	-0.278	-0.292	-0.334	-0.307	-0.238	-0.151	-0.251	-0.045	-0.045	-0.050
	p-value	0.232	0.357	0.224	0.959	0.092	0.084	0.061	0.192	0.283	0.491	0.172	0.136	0.091	0.178	0.157	0.102	0.136	0.252	0.471	0.226	0.832	0.833	0.811
Largest Lyapunov exponent	r	-0.398	-0.238	-0.179	-0.259	-0.376	-0.375	-0.388	-0.249	-0.115	-0.159	-0.430	-0.319	-0.250	-0.407	-0.352	-0.348	-0.296	-0.216	-0.256	-0.353	-0.119	-0.051	-0.142
	p-value	0.049	0.251	0.393	0.212	0.064	0.065	0.055	0.229	0.584	0.447	0.032	0.120	0.227	0.044	0.085	0.088	0.151	0.301	0.216	0.084	0.570	0.810	0.499
LLyapExp/α_{relative}	r	-0.419	-0.300	-0.249	-0.122	-0.408	-0.426	-0.415	-0.299	-0.190	-0.188	-0.408	-0.344	-0.343	-0.389	-0.368	-0.378	-0.324	-0.268	-0.233	-0.322	-0.133	-0.073	-0.124
	p-value	0.037	0.145	0.230	0.562	0.043	0.034	0.039	0.146	0.363	0.368	0.043	0.092	0.093	0.055	0.070	0.063	0.114	0.196	0.263	0.116	0.527	0.728	0.555

Notes. The highlighted cells represent the electrodes that showed a significant correlation between the change in substantive EEG feature and subjective measure of physical fatigue level

Table 6.8: Correlation between the change in substantive EEG features from level 1 to level 5 and the change in subjective measures of mental fatigue level.

EEG feature	Pearson's correlation coefficient	FC3	FCz	FC4	C5	C3	C1	Cz	C2	C4	C6	CP3	CPz	CP4	P3	P1	Pz	P2	P4	PO3	PO4	O1	Oz	O2
δ_{relative}	r	0.017	0.052	0.033	0.097	-0.045	-0.001	-0.105	-0.004	0.017	0.040	0.005	-0.045	-0.091	0.007	-0.037	-0.071	-0.108	-0.059	0.123	-0.133	0.240	0.146	0.003
	p-value	0.935	0.806	0.874	0.645	0.832	0.998	0.616	0.984	0.935	0.849	0.979	0.832	0.666	0.972	0.861	0.735	0.608	0.778	0.557	0.525	0.247	0.486	0.988
α_{relative}	r	0.070	0.171	0.120	0.043	0.187	0.178	0.283	0.163	0.061	0.055	0.172	0.233	0.164	0.133	0.202	0.224	0.228	0.166	0.033	0.246	0.024	0.138	0.227
	p-value	0.739	0.413	0.566	0.838	0.372	0.396	0.170	0.438	0.773	0.795	0.410	0.262	0.435	0.526	0.334	0.283	0.272	0.429	0.875	0.235	0.909	0.511	0.276
$(\theta+\alpha)/(\alpha+\beta)$	r	-0.324	-0.287	-0.292	-0.321	-0.339	-0.357	-0.335	-0.297	-0.185	-0.294	-0.332	-0.365	-0.240	-0.330	-0.364	-0.367	-0.308	-0.238	-0.182	-0.335	-0.112	-0.120	-0.224
	p-value	0.114	0.165	0.157	0.118	0.097	0.079	0.102	0.150	0.375	0.153	0.105	0.072	0.248	0.107	0.074	0.071	0.134	0.252	0.384	0.101	0.593	0.567	0.282
δ/α	r	-0.119	-0.050	-0.165	0.147	-0.164	-0.157	-0.188	-0.162	-0.113	-0.079	-0.081	-0.166	-0.206	-0.067	-0.121	-0.197	-0.203	-0.157	0.135	-0.170	0.195	0.089	-0.064
	p-value	0.572	0.812	0.430	0.484	0.432	0.454	0.367	0.438	0.590	0.707	0.702	0.427	0.323	0.750	0.565	0.344	0.331	0.455	0.521	0.416	0.350	0.671	0.761
Largest Lyapunov exponent	r	-0.309	-0.146	-0.151	-0.095	-0.262	-0.249	-0.246	-0.180	-0.080	-0.221	-0.266	-0.184	-0.164	-0.198	-0.166	-0.178	-0.191	-0.090	0.031	-0.182	0.133	0.076	-0.052
	p-value	0.132	0.486	0.470	0.653	0.206	0.230	0.236	0.390	0.703	0.289	0.198	0.378	0.434	0.343	0.427	0.394	0.361	0.667	0.883	0.383	0.525	0.718	0.804
LLyapExp/α_{relative}	r	-0.259	-0.130	-0.160	0.067	-0.225	-0.222	-0.200	-0.157	-0.061	-0.153	-0.197	-0.171	-0.175	-0.154	-0.156	-0.194	-0.173	-0.113	0.075	-0.172	0.123	0.066	-0.070
	p-value	0.210	0.534	0.444	0.749	0.279	0.286	0.337	0.454	0.771	0.467	0.346	0.415	0.404	0.462	0.458	0.353	0.408	0.590	0.722	0.410	0.559	0.754	0.741

coefficient (r and p-value) performed on the change in subjective measure of mental fatigue level and the change in δ_{relative}, α_{relative}, $(\theta+\alpha)/(\alpha+\beta)$, δ/α, largest Lyapunov exponent, LLyapExp$/\alpha_{\text{relative}}$, respectively. Positive correlations were found between the change in mental fatigue level and the change in α_{relative} on all EEG electrodes around central, parietal and occipital brain regions. In contrast, negative correlations were found between the change in mental fatigue level and the change in $(\theta+\alpha)/(\alpha+\beta)$ on all EEG electrodes around central, parietal and occipital brain regions. Significant correlations were not visible between the change in mental fatigue level and the change in EEG features. Therefore, the above findings may suggest that the increase in α_{relative}, and the decrease in $(\theta+\alpha)/(\alpha+\beta)$, δ/α, largest Lyapunov exponent, LLyapExp$/\alpha_{\text{relative}}$ were most likely caused by the increase in physical fatigue level during the robot-mediated visuomotor tracking task.

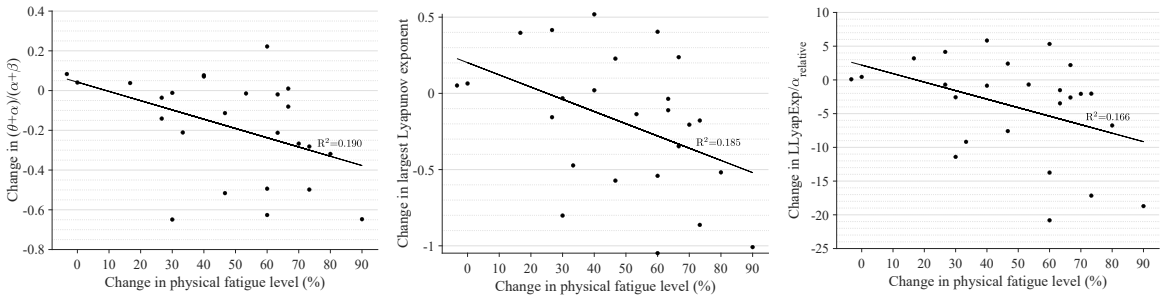

(a) $(\theta+\alpha)/(\alpha+\beta)$ (b) largest Lyapunov exponent (c) LLyapExp$/\alpha_{\text{relative}}$

Figure 6.6: Correlation between the change in physical fatigue level and the change in (a) $(\theta+\alpha)/(\alpha+\beta)$, (b) largest Lyapunov exponent, and (c) LLyapExp$/\alpha_{\text{relative}}$ from level 1 to level 5 of the robot-mediated visuomotor tracking task on CP3 electrode.

6.2.4 Association of the Movement Variability Measures with the Significant EEG Feature Variations

The correlation analysis was also performed to identify the association between the change in substantive EEG features (value of EEG feature at level 5 - value of EEG feature at level 1) around central, parietal and occipital brain regions and the change in movement variability measures (value of MAD or RMSD at level 5 - value of MAD or RMSD at level 1) during the robot-mediated visuomotor tracking task. Table 6.9 summarises the findings of Pearson's correlation coefficient (r and p-value) performed on the change in mean absolute distance and the change in δ_{relative}, α_{relative}, $(\theta+\alpha)/(\alpha+\beta)$, δ/α, largest Lyapunov exponent, LLyapExp$/\alpha_{\text{relative}}$, respectively. The change in α_{relative} on all EEG electrodes around central, parietal and occipital brain regions were negatively correlated

Table 6.9: Correlation between the change in substantive EEG features from level 1 to level 5 and the change in mean absolute distance between control and guide points from level 1 to level 5.

EEG feature	Pearson's correlation coefficient	FC3	FCz	FC4	C5	C3	C1	Cz	C2	C4	C6	CP3	CPz	CP4	P3	P1	Pz	P2	P4	PO3	PO4	O1	Oz	O2
δ_{relative}	r	0.248	0.121	0.180	0.322	0.346	0.355	0.255	0.216	0.244	0.109	0.326	0.254	0.199	0.286	0.330	0.243	0.211	0.223	0.237	0.256	0.216	0.190	0.195
	p-value	0.233	0.566	0.389	0.116	0.090	0.082	0.218	0.300	0.240	0.605	0.112	0.220	0.340	0.166	0.107	0.242	0.312	0.284	0.253	0.217	0.299	0.363	0.349
α_{relative}	r	-0.356	-0.442	-0.360	-0.354	-0.430	-0.473	-0.457	-0.415	-0.334	-0.167	-0.411	-0.432	-0.328	-0.391	-0.458	-0.423	-0.399	-0.400	-0.367	-0.437	-0.370	-0.420	-0.429
	p-value	0.081	0.027	0.077	0.083	0.032	0.017	0.022	0.039	0.103	0.424	0.041	0.031	0.109	0.053	0.021	0.035	0.048	0.047	0.071	0.029	0.068	0.036	0.032
$(\theta+\alpha)/(\alpha+\beta)$	r	0.480	0.492	0.344	0.248	0.407	0.498	0.477	0.335	0.170	0.088	0.361	0.438	0.332	0.424	0.483	0.498	0.461	0.421	0.399	0.413	0.273	0.184	0.214
	p-value	0.015	0.013	0.092	0.232	0.044	0.011	0.016	0.101	0.416	0.677	0.076	0.029	0.105	0.035	0.015	0.011	0.021	0.036	0.048	0.040	0.187	0.379	0.304
δ/α	r	0.266	0.280	0.227	0.247	0.366	0.420	0.360	0.224	0.202	0.049	0.293	0.301	0.233	0.193	0.297	0.244	0.190	0.240	0.132	0.234	0.132	0.086	0.184
	p-value	0.199	0.175	0.276	0.235	0.072	0.037	0.077	0.283	0.334	0.814	0.155	0.144	0.263	0.354	0.150	0.240	0.364	0.248	0.531	0.261	0.530	0.683	0.380
Largest Lyapunov exponent	r	0.345	0.238	0.112	0.217	0.285	0.367	0.270	0.093	0.031	0.035	0.232	0.193	0.072	0.256	0.240	0.225	0.137	0.122	0.229	0.249	0.203	0.138	0.143
	p-value	0.091	0.252	0.593	0.298	0.167	0.071	0.192	0.657	0.884	0.867	0.264	0.356	0.733	0.217	0.247	0.279	0.515	0.560	0.271	0.230	0.331	0.511	0.496
$\text{LLyapExp}/\alpha_{\text{relative}}$	r	0.225	0.190	0.077	0.129	0.225	0.333	0.240	0.056	-0.007	-0.049	0.179	0.156	0.073	0.161	0.204	0.184	0.082	0.090	0.132	0.184	0.185	0.087	0.127
	p-value	0.280	0.363	0.713	0.540	0.280	0.104	0.248	0.792	0.972	0.815	0.393	0.458	0.729	0.441	0.328	0.379	0.696	0.670	0.531	0.379	0.376	0.678	0.546

Notes. The highlighted cells represent the electrodes that showed a significant correlation between the change in substantive EEG feature and mean absolute distance between control and guide points.

Table 6.10: Correlation between the change in substantive EEG features from level 1 to level 5 and the change in root mean square distance between control and guide points from level 1 to level 5.

EEG feature	Pearson's correlation coefficient	FC3	FCz	FC4	C5	C3	C1	Cz	C2	C4	C6	CP3	CPz	CP4	P3	P1	Pz	P2	P4	PO3	PO4	O1	Oz	O2
δ_{relative}	r	0.166	0.083	0.124	0.239	0.220	0.243	0.143	0.124	0.147	0.024	0.197	0.115	0.083	0.157	0.193	0.098	0.086	0.118	0.122	0.171	0.158	0.105	0.135
	p-value	0.428	0.692	0.554	0.249	0.291	0.242	0.497	0.556	0.483	0.908	0.344	0.585	0.693	0.453	0.355	0.641	0.683	0.575	0.560	0.414	0.452	0.617	0.519
α_{relative}	r	-0.245	-0.346	-0.250	-0.222	-0.269	-0.335	-0.311	-0.280	-0.201	-0.031	-0.240	-0.250	-0.165	-0.239	-0.302	-0.253	-0.244	-0.258	-0.260	-0.362	-0.342	-0.372	-0.364
	p-value	0.238	0.090	0.227	0.286	0.193	0.101	0.130	0.176	0.334	0.883	0.249	0.228	0.431	0.251	0.142	0.222	0.239	0.213	0.210	0.075	0.095	0.067	0.074
$(\theta+\alpha)/(\alpha+\beta)$	r	0.371	0.388	0.237	0.128	0.284	0.373	0.358	0.225	0.069	0.008	0.253	0.311	0.226	0.330	0.392	0.415	0.386	0.355	0.337	0.416	0.283	0.192	0.232
	p-value	0.068	0.056	0.253	0.542	0.169	0.066	0.079	0.280	0.744	0.970	0.222	0.130	0.276	0.107	0.053	0.039	0.057	0.082	0.099	0.039	0.171	0.357	0.264
δ/α	r	0.087	0.113	0.076	0.114	0.151	0.218	0.159	0.044	0.035	-0.095	0.113	0.118	0.083	0.027	0.136	0.092	0.061	0.132	0.007	0.182	0.094	0.080	0.146
	p-value	0.679	0.591	0.719	0.586	0.471	0.294	0.446	0.833	0.868	0.653	0.592	0.574	0.695	0.898	0.516	0.661	0.772	0.528	0.975	0.383	0.656	0.704	0.486
Largest Lyapunov exponent	r	0.234	0.162	0.041	0.100	0.147	0.250	0.167	0.005	-0.032	-0.004	0.105	0.066	-0.005	0.114	0.114	0.107	0.027	0.046	0.101	0.190	0.143	0.092	0.117
	p-value	0.261	0.438	0.845	0.633	0.482	0.229	0.426	0.980	0.881	0.985	0.616	0.753	0.980	0.587	0.586	0.610	0.897	0.826	0.630	0.363	0.496	0.662	0.577
$\text{LLyapExp}/\alpha_{\text{relative}}$	r	0.056	0.060	-0.028	0.024	0.046	0.167	0.092	-0.067	-0.120	-0.122	0.048	0.028	-0.027	0.036	0.098	0.083	-0.005	0.027	0.031	0.155	0.148	0.087	0.127
	p-value	0.789	0.777	0.893	0.911	0.826	0.424	0.663	0.750	0.566	0.562	0.819	0.896	0.897	0.864	0.640	0.692	0.980	0.900	0.885	0.460	0.479	0.681	0.545

Notes. The highlighted cells represent the electrodes that showed a significant correlation between the change in substantive EEG feature and root mean square distance between the control and guide points.

with the change in mean absolute distance. Positive correlations were found between the change in mean absolute distance and the change in δ_{relative}, $(\theta+\alpha)/(\alpha+\beta)$, δ/α, largest Lyapunov exponent, respectively on all EEG electrodes around central, parietal and occipital brain regions. Positive correlations were also found on all EEG electrodes around central, parietal and occipital brain regions except on C4 and C6 for LLyapExp$/\alpha_{\text{relative}}$. Among these findings, significant positive correlations were visible on FC3, FCz, C3, C1, Cz, CPz, P3, P1, Pz, P2, P4, PO3, and PO4 electrodes for $(\theta+\alpha)/(\alpha+\beta)$; and on C1 electrode for δ/α. Significant negative correlations, on the other hand, were visible on FCz, C3, C1, Cz, C2, CP3, CPz, P1, Pz, P2, P4, PO4, Oz, and O2 electrodes for α_{relative}. Figure 6.7 shows the correlation between the change in mean absolute distance and the change in α_{relative}, $(\theta+\alpha)/(\alpha+\beta)$, and δ/α on C1 electrode. It was visible that most participants who showed an increase in α_{relative} from level 1 to level 5 also showed either a smaller increase or a decrease in mean absolute distance from level 1 to level 5. Also, most participants who experienced a reduction in $(\theta+\alpha)/(\alpha+\beta)$ and δ/α showed either a smaller increase or a decrease in mean absolute distance. Table 6.10, on the other hand, summarises the findings of Pearson's correlation coefficient (r and p-value) performed on the change in root mean square distance and the change in δ_{relative}, α_{relative}, $(\theta+\alpha)/(\alpha+\beta)$, δ/α, largest Lyapunov exponent, LLyapExp$/\alpha_{\text{relative}}$, respectively. A positive correlation was found between the change in root mean square distance and the change in δ_{relative} and $(\theta+\alpha)/(\alpha+\beta)$ on all EEG electrodes around central, parietal and occipital brain regions. In contrast, a negative correlation was found between the change in mental fatigue level and the change in α_{relative} on all EEG electrodes around central, parietal and occipital brain regions. Significant correlations were only visible on Pz and PO4 electrodes for $(\theta+\alpha)/(\alpha+\beta)$. The above findings showed that the change in δ_{relative}, α_{relative}, $(\theta+\alpha)/(\alpha+\beta)$, δ/α, largest Lyapunov

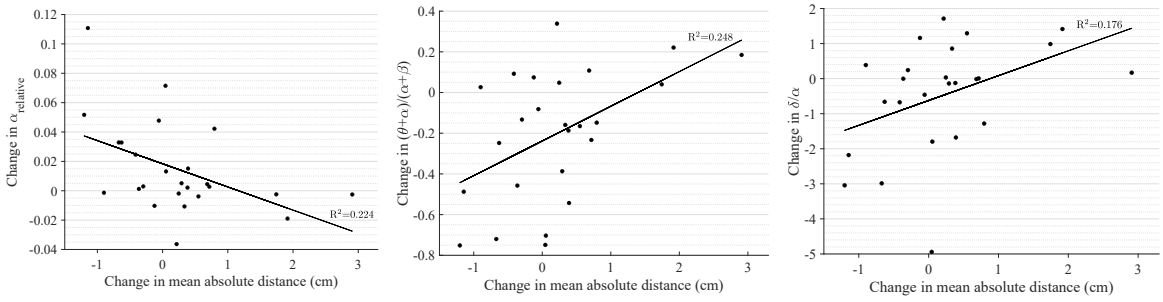

(a) α_{relative} (b) $(\theta+\alpha)/(\alpha+\beta)$ (c) δ/α

Figure 6.7: Correlation between the change in mean absolute distance and the change in (a) α_{relative}, (b) $(\theta+\alpha)/(\alpha+\beta)$, and (c) δ/α from level 1 to level 5 of the robot-mediated visuomotor tracking task on C1 electrode.

exponent, and LLyapExp/α_{relative} around central, parietal and occipital brain regions were mostly associated with the change in mean absolute distance. Therefore, the findings may suggest that participants who maintained better tracking accuracies during the visuomotor tracking task were likely to experience a greater change in δ_{relative}, α_{relative}, $(\theta+\alpha)/(\alpha+\beta)$, δ/α, largest Lyapunov exponent, and LLyapExp/α_{relative}.

6.2.5 Association of the Subjective Measures of the Level of Fatigue with the Movement Variability Measures

Table 6.11 summarises the findings of Pearson's correlation coefficient (r and p-value) performed on the change in mean absolute distance and root mean square distance between control and guide points from level 1 to level 5 and the change in subjective measures of physical and mental fatigue levels, respectively. Negative correlations were visible between the change in mean absolute distance and the change in physical and mental fatigue levels, respectively. Similarly, the change in root mean square distance and the change in physical and mental fatigue levels were also negatively correlated. However, no significant correlations were found between the subjective measures of the level of fatigue and the movement variability measures. Figure 6.8 shows the correlation of the change in physical and mental fatigue level with the change in mean absolute distance and root mean square distance. Negative correlations, although not significant, may suggest that the greater change in the fatigue levels were most likely related to either a decrease or lower increase in the movement variability measures.

Table 6.11: Correlation between the change in mean absolute distance and root mean square distance between control and guide points from level 1 to level 5 of the robot-mediated visuomotor tracking task and the change in subjective measures of physical and mental fatigue levels.

EEG feature	Pearson's correlation coefficient	Physical fatigue level (%)	Mental fatigue level (%)
Mean absolute distance (cm)	r	-0.182	-0.254
	p-value	0.385	0.220
Root mean square distance (cm)	r	-0.082	-0.201
	p-value	0.696	0.336

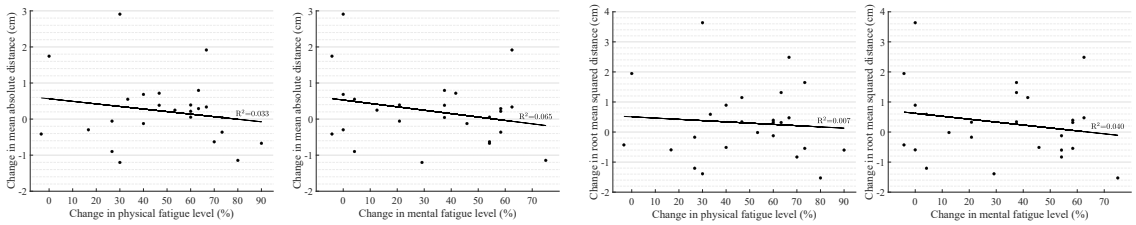

Physical fatigue | Mental fatigue | Physical fatigue | Mental fatigue

(a) Mean absolute distance (b) Root mean square distance

Figure 6.8: Correlation of the change in physical and mental fatigue level with the change in (a) mean absolute distance and (b) root mean square distance between control and guide points from level 1 to level 5 of the robot-mediated visuomotor tracking task.

6.3 Discussion

In this chapter, the association of change in substantive EEG features found in Chapter 5 with the change in subjective measures of fatigue levels and movement variability measures were investigated. As explained in Section 5.1.3, the guide point in the virtual reality environment moves at a constant speed. Participants were instructed to follow the path covered by the guide point while maintaining the speed of the control point (i.e. the speed of the robot arm motion) similar to the speed indicated by the motion of the guide point. Moreover, the damping coefficient were gradually increased from level 1 to level 5, thereby increasing the difficulty level of the task. It was expected that the more attention, focus and physical energy needed to maintain greater tracking accuracies during the robot-mediated visuomotor tracking task may gradually increase the individual fatigue levels.

The findings of this chapter showed a significant increase in physical, mental and global fatigue levels following the robot-mediated interaction. Also, larger effect sizes were visible in these significant changes in fatigue level. Therefore, the subjective measures of the level of fatigue confirmed that the majority of participants experienced an increase in their physical and mental fatigue levels, thereby contributing to an increase in their global fatigue level. Moreover, most participants experienced a comparatively greater increase in their physical fatigue levels than the mental fatigue levels. Also, most participants reported that the task was physically exhausting. Therefore, it can be concluded that the visuomotor tracking task performed using HapticMASTER induced more physical fatigue due to the increase in the physical workload during the task. Although not significant, most participants experienced an increase in the mean absolute distance and root mean square distance when progressing from level 1 to level 5. Huysmans et al. (2008) also found an increase in mean distance to

target at a target tracking task following a fatiguing protocol. Also, some previous studies have reported that a higher movement variability may reflect adaptation strategies followed by an individual to reduce the load on fatiguing tissues (Cignetti et al., 2009; Fuller et al., 2009; Huysmans et al., 2008; Selen et al., 2007; Yang et al., 2018). Therefore, the observed increase in movement variability measures may suggest that either the participants could not trace the guide point's trajectory correctly due to fatigue or followed adaptation strategies to reduce fatigue build-up during the task.

This experiment found a significant decrease in $(\theta+\alpha)/(\alpha+\beta)$ around central, parietal and occipital brain regions from level 1 to level 5 of the visuomotor tracking task. Although, the decrease in $(\theta+\alpha)/(\alpha+\beta)$ found in this experiment is contrary to previous studies (Fan et al., 2015; Jap et al., 2009), the findings were supported by the change in both physical fatigue level and mean absolute distance. In general, the change in $(\theta+\alpha)/(\alpha+\beta)$ were negatively correlated with the change in physical fatigue level and were positively correlated with the change in mean absolute distance on all EEG electrodes around central, parietal and occipital brain regions. Moreover, significant correlations were found on FC3, C3, C1, Cz, CPz, P3, P1, and Pz electrodes for both physical fatigue and mean absolute distance. In addition, significant correlations were also found on C5 and CP3 electrodes for physical fatigue and on FCz, P2, P4, PO3, and PO4 electrodes for mean absolute distance. The findings suggest that the greater decrease in $(\theta+\alpha)/(\alpha+\beta)$ were mostly related to the greater increase in physical fatigue level and the decrease or smaller increase in mean absolute distance. The decrease or smaller increase in mean absolute distance may reflect increased tracking accuracies during the visuomotor tracking task. Therefore, the findings may suggest that more attention, focus and physical energy needed to maintain greater tracking accuracies during the robot-mediated visuomotor tracking task may have gradually increased the physical fatigue level of an individual. Moreover, the decrease in $(\theta+\alpha)/(\alpha+\beta)$ could be considered as the strongest EEG correlate of fatigue induced by a robot-mediated visuomotor tracking task since the above finding was supported by both subjective measures of the level of fatigue and the movement variability measures.

A significant increase in α_{relative} and a significant decrease in largest Lyapunov exponent were also found during the transition to fatigue in the visuomotor tracking task. Previous studies have also reported an increase in α_{relative} and a reduction in largest Lyapunov exponent during the transition from alert to fatigue state (Barwick et al., 2012; Craig et al., 2012; Fan et al., 2015; Käthner et al., 2014; Yao et al., 2009; Zou et al., 2015). It was found that the change in physical fatigue level following the visuomotor tracking task were positively correlated with the change in α_{relative} and negatively correlated with the change in largest Lyapunov exponent on all EEG electrodes around central, parietal and occipital brain regions.

In contrast, the change in mean absolute distance from level 1 to level 5 showed a negative correlation for α_{relative} and a positive correlation for largest Lyapunov exponent on all EEG electrodes around central, parietal and occipital brain regions. Significant correlations were visible on FC3, CP3, and P3 electrodes for the change in largest Lyapunov exponent from level 1 to level 5 and the change in physical fatigue level following the task. Also, significant correlations were visible on FCz, C3, C1, Cz, C2, CP3, CPz, P1, Pz, P2, P4, PO4, Oz, and O2 electrodes for the change in α_{relative} from level 1 to level 5 with the change in mean absolute distance. Therefore, the above findings may also suggest that greater increase in α_{relative} and greater decrease in largest Lyapunov exponent were visible on participants who gained better tracking accuracies, thereby contributing towards an increase in their physical fatigue level.

The new parameter, LLyapExp$/\alpha_{\text{relative}}$, proposed in this experiment also showed a significant reduction mostly around central, parietal and occipital brain regions. The association between the change in LLyapExp$/\alpha_{\text{relative}}$ and physical fatigue level were also similar to the observed negative correlations for $(\theta+\alpha)/(\alpha+\beta)$ and largest Lyapunov exponent on all EEG electrodes around central, parietal and occipital brain regions. Significant negative correlations were found on FC3, C3, C1, Cz, and CP3 electrodes. Although not significant, similar positive correlations were also visible on all except C4 and C6 EEG electrodes around central, parietal and occipital brain regions. Therefore, it can be seen that the reduction in LLyapExp$/\alpha_{\text{relative}}$ were strongly associated with the increase in physical fatigue level.

This experiment also found significant decreases in δ_{relative} and δ/α from level 1 to level 5 of the visuomotor tracking task. The change in both EEG features on all electrodes around central, parietal and occipital brain regions were positively correlated with the mean absolute distance. However, significant correlations were found only for the change in δ/α on C1 electrode. Negative correlations were also found on all electrodes around central, parietal and occipital brain regions between the change in δ/α and physical fatigue level, whereas only all electrodes in the parietal regions were negatively correlated with the change in δ_{relative} and physical fatigue level.

As can be seen in Tables 6.9 and 6.10, widespread significant correlations were only visible for the change in mean absolute distance and the change in α_{relative} and $(\theta+\alpha)/(\alpha+\beta)$. Therefore, this experiment shows that mean absolute distance is better than root mean square distance to quantify the movement variability associated with fatigue in robot-mediated visuomotor tracking tasks. Colombo et al. (2005) also considered mean absolute values of the distance to evaluate the movement accuracy when interacting with a shoulder–elbow rehabilitation device. Moreover, self-rated questionnaires can provide information on the fatigue experienced by an individual. Negative correlations found between the change

in fatigue levels and the change in movement variability measures were not significant. However, significant observations were found on some EEG electrodes between the change in physical fatigue level and the change in $(\theta+\alpha)/(\alpha+\beta)$, largest Lyaounov exponent and LLyapExp/α_{relative}; and between the change in mean absolute distance and the change in α_{relative}, $(\theta+\alpha)/(\alpha+\beta)$ and δ/α. Therefore, this experiment shows that questionnaires cannot be used alone as an indicator of fatigue since the ratings may have a higher individual bias. In a robot-mediated visuomotor tracking task subjective measures of fatigue level and the change in movement variability measures could be used together to confirm whether an individual is fatigued or not following the task.

In summary, this chapter found the associations between the change in substantive EEG features from level 1 to level 5, mean absolute distance from level 1 to level 5 and physical fatigue level following the robot-mediated visuomotor tracking task. Table 6.12 summarises the EEG electrodes that showed significant correlations between the change in substantive EEG features, mean absolute distance and physical fatigue level. Significant associations were found between the change in $(\theta+\alpha)/(\alpha+\beta)$ and physical fatigue level for most EEG electrodes around central and parietal brain regions. Also, most EEG electrodes around central, parietal and occipital brain regions showed significant associations for the change in mean absolute distance. Therefore, $(\theta+\alpha)/(\alpha+\beta)$ could be considered as the most promising EEG feature to describe the underlying changes in the brain due to fatigue in robot-mediated visuomotor tracking tasks. Furthermore, most EEG electrodes around

Table 6.12: Summary of the EEG electrodes that showed significant correlations between the change in substantive EEG features from level 1 to level 5, mean absolute distance from level 1 to level 5 and physical fatigue level following the robot-mediated visuomotor tracking task.

EEG Features	Electrode locations	Significant correlations with the change in EEG feature	
		Change in physical fatigue level	Change in mean absolute distance
δ_{relative}	CP4, P3, P1, Pz, P2, P4, PO3, PO4, O1, Oz, O2	-	-
α_{relative}	C3, C1, Cz, C2, C4, C6, CP3, CPz, CP4, P3, P1, Pz, P2, P4, PO3, PO4, O1, Oz, O2	-	FCz, C3, C1, Cz, C2, CP3, CPz, P1, Pz, P2, P4, PO4, Oz, O2
$(\theta+\alpha)/(\alpha+\beta)$	FC3, FCz, FC4, C5, C3, C1, Cz, C2, C4, C6, CP3, CPz, CP4, P3, P1, Pz, P2, P4, PO3, PO4, O1, Oz	FC3, C5, C3, C1, Cz, CP3, CPz, P3, P1, Pz	FC3, FCz, C3, C1, Cz, CPz, P3, P1, Pz, P2, P4, PO3, PO4
δ/α	Cz, C2, C4, C6, CP3, CPz, CP4, P3, P1, Pz, P2, P4, P03, PO4, O1, Oz, O2	-	C1
Largest Lyapunov exponent	C2, CP3, CPz, CP4, P3, P1, Pz, P2, P4, PO3, PO4, O1, Oz, O2	FC3, CP3, P3	-
LLyapExp/α_{relative}	C2, CP3, CPz, CP4, P3, P1, Pz, P2, P4, PO3, PO4, O1, Oz, O2	FC3, C3, C1, Cz, CP3	-

Notes. The red coloured text represents the EEG electrodes that showed a significant correlation with the change in both physical fatigue level and mean absolute distance. The green coloured text represents the EEG electrodes that showed a significant correlation with the change in both physical fatigue level only. The blue coloured text represents the EEG electrodes that showed a significant correlation with the change in mean absolute distance only.

central, parietal and occipital brain regions that showed a significant increase in α_{relative} were associated with the change in mean absolute distance. The significant decrease in largest Lyapunov exponent observed on CP3 and P3 electrodes and the significant decrease in LLyapExp$/\alpha_{\text{relative}}$ on CP3 electrode also showed significant negative correlations with the change in physical fatigue level. Therefore, the amount of increase in α_{relative} and the amount of decrease in largest Lyapunov exponent and LLyapExp$/\alpha_{\text{relative}}$ could also be used to quantify the progression of fatigue during a robot-mediated visuomotor tracking task. Taken together, EEG electrodes that found significant correlations showed a widespread distribution across central, parietal, and occipital brain regions. Therefore, the findings summarised in this chapter revealed that fatigue induced by robot-mediated visuomotor tracking tasks could be estimated from EEG electrodes placed over the central, parietal and occipital brain regions. The use of fewer electrodes will enable faster setting up time and more comfort and convenience to the user. Therefore, the usage of EEG-based fatigue estimation systems to monitor and control fatigue in rehabilitation sessions may not create additional discomfort to the patients. In addition, the computational complexity and the cost for hardware could also be reduced by using a fewer number of electrodes when designing fatigue detection systems (Min et al., 2017).

6.4 Conclusions

Firstly, this chapter evaluated the changes in physical, mental and global fatigue level percentages using the individual feedback given before and after the robot-mediated interaction. Also, the variations in mean absolute distance and root mean square distance between control and guide points while progressing from level 1 to level 5 of the task were evaluated. Then the association between the modulations in substantive EEG features (i.e., δ_{relative}, α_{relative}, $(\theta+\alpha)/(\alpha+\beta)$, δ/α, largest Lyapunov exponent, and LLyapExp$/\alpha_{\text{relative}}$) around central, parietal, and occipital brain regions, movement variability measures, and subjective measures of fatigue level were examined to identify the EEG features and EEG electrode locations that best describe the underlying changes in the brain due to fatigue induced by robot-mediated visuomotor tracking task.

The experiment found that the greater change in substantive EEG features were mostly associated with either a decrease or a smaller increase in mean absolute distance and a greater increase in physical fatigue level. Therefore, it can be concluded that more attention, focus and physical energy drawn to maintain greater tracking accuracies during the robot-mediated visuomotor tracking task may gradually increase the individual physical fatigue level. As

a consequence, an increase in α_{relative}, and a decrease in δ_{relative}, $(\theta+\alpha)/(\alpha+\beta)$, δ/α, largest Lyapunov exponent, and LLyapExp$/\alpha_{\text{relative}}$ may be visible.

Significant negative correlations were found between the change in $(\theta+\alpha)/(\alpha+\beta)$ and physical fatigue level for most EEG electrodes around central and parietal brain regions. Also, the change in $(\theta+\alpha)/(\alpha+\beta)$ on most EEG electrodes around central, parietal and occipital brain regions were significantly and positively correlated with the change in mean absolute distance. Most EEG electrodes around central, parietal and occipital brain regions also showed significant associations between the change in α_{relative} and the change in mean absolute distance. Moreover, the change in largest Lyapunov exponent and LLyapExp$/\alpha_{\text{relative}}$ were significantly and negatively correlated with the change in physical fatigue level on some EEG electrodes around central and parietal regions (Table 6.12). To conclude, $(\theta+\alpha)/(\alpha+\beta)$ is the most reliable EEG-based index to estimate fatigue induced by robot-mediated visuomotor tracking task. Also, α_{relative}, largest Lyapunov exponent and LLyapExp$/\alpha_{\text{relative}}$ could be used to describe the underlying variations in the processing capacity of sensory information and motor output, and the brain's reduced complexity due to fatigue. EEG electrodes placed over central, parietal and occipital brain regions could be used in future to estimate fatigue accumulated during robot-mediated visuomotor tracking tasks.

Chapter 7

Conclusions and Future Works

The EEG feature modulations associated with fatigue induced by robot-mediated interactions has not yet been comprehensively explored but has been identified as important when designing robot-mediated post-stroke rehabilitation sessions. Personalised rehabilitation sessions that incorporate the knowledge of patient fatigue levels can be beneficial to the treatment and may positively impact on efficiency of the intervention. A thorough investigation of the modulations in both spectral and nonlinear EEG features due to fatigue induced by robot-mediated interactions was conducted in this thesis. Two human-robot interaction experiments, as explained in Chapters 4 and 5 were designed and conducted. In addition to the EEG data recordings, kinematic data and subjective responses reflecting on the fatigue levels before and after the interaction were obtained to further explore the association between fatigue and EEG. This thesis highlights the EEG features that can best describe the effects of fatigue on brain activity patterns. It also proposes the EEG electrode locations to be used in similar future applications. In the following sections, conclusions made, limitations in the present work, and future work related to fatigue assessment in robot-mediated interactions using EEG are discussed.

7.1 Summary of Main Findings

The literature review conducted in this research (Chapter 2) found that previous studies often investigated the modulations in EEG spectral features with fatigue induced by simulated driving tasks, cognitive tasks, voluntary motor tasks and sports-related activities. Although these investigations stated that the linear analysis methods such as frequency domain analysis could not fully describe the underlying complex dynamics of the brain, only a few studies

have evaluated the associations in EEG nonlinear features and fatigue level of an individual. Moreover, to the author's knowledge, EEG correlates of fatigue accumulated during robot-mediated interactions have not yet been comprehensively explored. Therefore, the present research thoroughly investigated the association of both spectral and nonlinear EEG features with fatigue induced by robot-mediated interactions.

In this research work, EEG correlates of fatigue are explored and evaluated when fatigue is induced by three different robot-mediated interactions:

i gross motor interaction with HapticMASTER,

ii fine motor interaction with SCRIPT passive orthosis,

iii visuomotor tracking task with HapticMASTER.

In experiment 1, a comparison between gross motor and fine motor interactions was conducted using EEG spectral features. In experiment 2, an in-depth analysis of both EEG spectral and nonlinear feature variations during a robot-mediated visuomotor tracking task was conducted. The two experiments were designed to address the two research questions derived from the hypothesis of this research, *"EEG correlates of fatigue during robot-mediated interactions are specific to the physical or cognitive nature of the task and the differences in the usage of proximal or distal upper limb"*:

1. Are the EEG spectral feature modulations associated with fatigue localised to different brain regions depending on the type of robotic interaction and the underlying physical and mental workload?
2. Which spectral and nonlinear EEG features and which EEG electrode locations are most capable and reliable in estimating the progression of fatigue during a robot-mediated visuomotor tracking task?

7.1.1 Findings of Experiment 1

Experiment 1 (Chapter 4) was designed and conducted to compare and contrast the modulations in EEG spectral features associated with fatigue induced by robot-mediated gross motor and fine motor interactions. The significant EEG spectral feature modulations found in experiment 1 and their associations with the type of fatigue induced following each interaction is summarised in Table 7.1. It was found that δ_{relative} significantly decreased and α_{relative} significantly increased due to the fatigue induced by both robot-mediated gross motor and fine motor interactions. The gross motor task also showed a significant increase in $(\theta+\alpha)/\beta$ and α/β. The change in α_{relative}, $(\theta+\alpha)/\beta$ and α/β were in agreement with the previous findings. Furthermore, brain regions that showed significant changes were

different between the two tasks. The robot-mediated gross motor interaction mostly changed the EEG activity around central and parietal brain regions whereas the robot-mediated fine motor interaction mostly changed the EEG activity around frontopolar and central brain regions. Most participants reported an increase in their physical fatigue level following the gross motor task, and an increase in their mental fatigue level following the fine motor task. Therefore, the regional differences in the significant EEG spectral features associated with fatigue are most likely due to the differences in the nature of the task (fine/gross motor and distal/proximal upper limb) that may have differently altered an individual's physical and mental fatigue level.

Table 7.1: Results summary of experiment 1: EEG spectral features that showed significant variations following the robot-mediated gross motor and fine motor interactions and their associations with the type of fatigue induced by each interaction.

EEG feature	**Direction of change**	**Brain regions that showed significant differences**		**Associated with the change in fatigue level**	
		Gross motor task	**Fine motor task**	**Physical fatigue in gross motor task**	**Mental fatigue in fine motor task**
δ_{relative}	$\downarrow$	Central	Frontopolar	Yes	Yes
α_{relative}	$\uparrow$	Central, Parietal	Frontopolar, Central	Yes	Yes
$(\theta+\alpha)/\beta$	$\uparrow$	Central	-	Yes	-
α/β	$\uparrow$	Central	-	Yes	-

Notes. $\uparrow$ and $\downarrow$ represents the significant increase and decrease in the corresponding EEG features.

7.1.2 Findings of Experiment 2

Experiment 2 (Chapters 5 and 6) was designed and conducted to investigate the modulations in both spectral and nonlinear EEG features associated with fatigue induced by a robot-mediated visuomotor tracking task. The significant spectral and nonlinear EEG feature modulations found during the robot-mediated visuomotor tracking task, and their associations with the change in mean absolute distance during the task and the change in subjective measures of physical fatigue level obtained before and after the interaction is summarised in Table 7.2.

Modulations in Spectral and Nonlinear EEG Features

It was found that the fatigue induced by the robot-mediated visuomotor tracking task significantly increased α_{relative} and significantly decreased δ_{relative}, $(\theta+\alpha)/(\alpha+\beta)$, δ/α, and largest Lyapunov exponent (LLyapExp). These differences were observed mostly around central, parietal and occipital brain regions. A new EEG feature, LLyapExp$/\alpha_{\text{relative}}$, which shows the combined effect of spectral and nonlinear EEG features is proposed in this ex-

periment. The LLyapExp/α_{relative} also showed a significant decrease during the visuomotor tracking task around central, parietal and occipital brain regions. The variations in α_{relative} and largest Lyapunov exponent were in agreement with previous findings. The significant decrease in δ_{relative} and the significant increase in α_{relative} observed in experiment 2 also support the findings of experiment 1.

Subjective Measures of the Level of Fatigue

A significant increase in the subjective measures of physical and mental fatigue levels was found following the robot-mediated visuomotor tracking task, thereby contributing to a significant increase in the global fatigue level. The participant's feedback also revealed that most participants experienced a comparatively larger increase in the physical fatigue levels than the increase in the mental fatigue levels. The subjective responses may imply that the visuomotor tracking task performed using HapticMASTER caused more physical fatigue than mental fatigue. Therefore, the increase in physical fatigue level during the task may have most likely caused the changes in EEG features.

Measures of Movement Variability

Most participants also showed an increase in the mean absolute distance and root mean squared distance between control and guide points (i.e., movement variability measures) during the robot-mediated visuomotor tracking task. Therefore, the observed increase in movement variability measures may suggest that either the participants could not trace the guide point's trajectory correctly due to fatigue or followed adaptation strategies to reduce fatigue build-up during the task.

Table 7.2: Results summary of experiment 2: Spectral and nonlinear EEG features that showed significant variations following the robot-mediated visuomotor tracking task and their associations with the subjective measures of physical fatigue level following the task and the mean absolute distance during the task.

EEG feature	Direction of change	Brain regions that showed significant differences	Associated with the change in physical fatigue level	Associated with the change in mean absolute distance
δ_{relative}	$\downarrow$	Parietal, Occipital	No	Yes
α_{relative}	$\uparrow$	Central, Parietal, Occipital	Yes	Yes
$(\theta+\alpha)/(\alpha+\beta)$	$\downarrow$	Central, Parietal, Occipital	Yes	Yes
δ/α	$\downarrow$	Central, Parietal, Occipital	Yes	Yes
LLyapExp	$\downarrow$	Parietal, Occipital	Yes	Yes
LLyapExp/α_{relative}	$\downarrow$	Central, Parietal, Occipital	Yes	Yes

Notes. LLyapExp refers to largest Lyapunov exponent. $\uparrow$ and $\downarrow$ represents the significant increase and decrease in the corresponding EEG features.

Associations of the Changes in Substantive EEG Features, Subjective Measures of Physical Fatigue Level and Mean Absolute Distance

Variations in the prominent EEG features in experiment 2 were also supported by the change in subjective measures of physical fatigue level following the task and the change in mean absolute distance during the task. The correlation analysis performed between the change in substantive EEG features and the change in subjective measures of physical fatigue level revealed positive correlations for the change in α_{relative} from level 1 to level 5 of the visuomotor tracking task around central, parietal, and occipital brain regions. Also, the change in $(\theta+\alpha)/(\alpha+\beta)$, δ/α, largest Lyapunov exponent, and LLyapExp$/\alpha_{\text{relative}}$ around central, parietal and occipital brain regions were negatively correlated. Significant negative correlations were found around central and parietal brain regions for $(\theta+\alpha)/(\alpha+\beta)$, largest Lyapunov exponent, and LLyapExp$/\alpha_{\text{relative}}$. In contrast, negative correlations were found between the change in mean absolute distance from level 1 to level 5 and the change α_{relative} from level 1 to level 5 around central, parietal, and occipital brain regions. The change in δ_{relative}, $(\theta+\alpha)/(\alpha+\beta)$, δ/α, largest Lyapunov exponent and LLyapExp$/\alpha_{\text{relative}}$ around central, parietal and occipital brain regions were positively correlated with the change in mean absolute distance. Significant correlations were found around central, parietal, and occipital brain regions for α_{relative} and $(\theta+\alpha)/(\alpha+\beta)$ and around central brain region for δ/α. Taken together, these findings suggest that the greater change in the substantive EEG features was mostly associated with a greater increase in the physical fatigue level and either a decrease or a smaller increase in the mean absolute distance. Therefore, the more attention, focus, and physical energy drawn to maintain increased tracking accuracies during the robot-mediated visuomotor tracking task may have gradually increased the individual fatigue levels. The increased movement variability found in the participants who reported a smaller change in their fatigue levels, on the other hand, suggest that these participants may have followed adaptation strategies to reduce the fatigue build-up during the task. Moreover, $(\theta+\alpha)/(\alpha+\beta)$ could be considered as the most reliable EEG feature to describe the underlying changes in brain activity caused by fatigue in robot-mediated visuomotor tracking tasks. The α_{relative}, largest Lyapunov exponent and LLyapExp$/\alpha_{\text{relative}}$ could also be used to quantify the progression of fatigue during a robot-mediated visuomotor tracking task. EEG electrodes placed over central, parietal and occipital brain regions could be used in future to estimate fatigue accumulated during robot-mediated visuomotor tracking tasks.

7.2 Conclusions

To conclude, two experiments have shown that fatigue was induced during robot-mediated interactions and has differently affected the EEG features and cortical sites. Significant EEG feature modulations were observed around central and parietal brain regions for the robot-mediated gross motor interaction, whereas the frontopolar and central brain regions showed significant variations in EEG features following the robot-mediated fine motor interaction. The robot-mediated visuomotor tracking task revealed significant variations in EEG features mostly localised around central, parietal and occipital brain regions. Also, participant's feedback revealed that both gross motor interaction and visuomotor tracking task performed using HapticMASTER caused more physical fatigue, whereas the fine motor interaction performed using SCRIPT passive orthosis caused more mental fatigue. Therefore, the findings suggest that repetitive gross motor tasks such as arm reach/return exercises that mostly involve the movement and coordination of proximal joints and muscles of the upper limb (shoulder and arm) are likely to induce a more physical fatigue, thereby altering the central and parietal brain regions. Since intensive fine motor tasks require considerable attention and decision-making skills combined with hand, wrist and finger movements, more mental fatigue is likely to occur, and the EEG activity in the frontopolar cortex may also significantly change with fatigue. Premotor, motor, parietal and occipital brain regions are collectively engaged when performing a visuomotor tracking task; thus, fatigue induced by robot-mediated visuomotor tracking tasks may likely to alter central, parietal and occipital brain regions. These findings suggest that the modulations in EEG features and the cortical regions that are mostly affected due to fatigue in robot-mediated interactions are specific to the physical and cognitive nature of the task performed, thereby confirmed the hypothesis of this research. Moreover, since both spectral and nonlinear EEG features showed variations with fatigue, it was most likely that fatigue induced by robot-mediated interactions reduced the capacity for processing sensory information or motor output. Due to cortical inactivation caused by fatigue, lesser neurons are available for information processing; thus, the complexity of the brain is reduced. Therefore, the results of this investigation strongly suggest that both spectral and nonlinear EEG features are reliable indicators of fatigue in robot-mediated interactions. Finally, EEG feature modulations during robot-mediated visuomotor tracking task have shown that fatigue can be estimated from the EEG electrodes placed over the central, parietal and occipital brain regions. Therefore, the use of fewer electrodes in future applications will enable faster setting up time, more comfort and convenience to the user and lesser computational complexity and cost for hardware.

7.3 Contributions to Knowledge

EEG correlates of fatigue in robot-mediated interactions have not been comprehensively explored in the literature. The findings reported in this thesis provide more in-depth insight into the understanding of detecting fatigue during robot-mediated interactions using EEG. Therefore, this thesis contributes to the knowledge by providing further insight on neural correlates of fatigue induced by robot-mediated interactions. This research identified EEG features and electrode locations that can best describe the underlying variations in the processing capacity of sensory information and motor output, and the brain's reduced complexity due to fatigue. This was done by aligning the objectives of the experiments with human-robot interactions that can support the objectives. For example, fine motor tasks performed using a distal robot were considered to inform on neural fatigue correlates of fine motor tasks. This research revealed that $(\theta+\alpha)/(\alpha+\beta)$ is the most capable and reliable EEG feature that can be used to estimate fatigue during a robot-mediated visuomotor tracking task. Also, largest Lyapunov exponent and LLyapExp/α_{relative} could be used to quantify the progression of fatigue during a robot-mediated visuomotor tracking task. The increase in α_{relative} was found to be associated with the fatigue accumulated in robot-mediated gross motor tasks, fine motor tasks and visuomotor tracking tasks. Reductions in δ_{relative} and δ/α were also found in this research. Moreover, the findings of this research contribute to the understanding of EEG nonlinear feature modulations associated with fatigue.

The findings revealed that the modulations in EEG features with fatigue accumulated during robot-mediated interactions are specific to the task's physical or cognitive nature performed using either proximal or distal upper limb. Differences in the topographical distribution may also be visible between different robot-mediated interactions depending on the underlying physical and mental workload. Therefore, when estimating fatigue during robot-mediated interactions, EEG electrodes should be selected depending on the physical and cognitive nature of the task and the usage of the proximal and distal upper limb. This thesis showed that EEG electrodes placed on central, parietal and occipital brain regions could be used to estimate fatigue in robot-mediated visuomotor tracking tasks in future. A limited number of electrodes may reduce the setting up time, computational complexity and cost for hardware.

The research work presented in this thesis has also contributed towards the following publications.

- Dissanayake, U. C., Steuber, V., and Amirabdollahian, F. (2021), 'EEG spectral feature modulations associated with fatigue in robot-mediated upper limb gross motor and fine motor interactions', bioRxiv, doi:10.1101/2021.04.22.440968.

- Dissanayake, U. C., Amirabdollahian, F., and Steuber, V., 'Modulations in EEG spectral and nonlinear features during a visuomotor tracking task performed using the GENTLE/EEG robot-mediated system', [*In preparation*].
- Dissanayake, U. C., Amirabdollahian, F., and Steuber, V., 'Robot-mediated stroke therapy and fatigue [Poster]', *2nd INSPIRE Conference 2017: Identity, Impact and Voice, United Kingdom.*

7.4 Future Works

This research showed that the EEG correlates of fatigue during robot-mediated interactions are specific to the task's physical or cognitive nature and usage of the proximal or distal upper limb. As stated in Chapter 4, the spatial precision of the recordings was limited in experiment 1 since the EEG data acquisition system could only support eight electrode locations. Experiment 1 found differences between the cortical sites that are mostly affected by the type of fatigue (physical/mental) accumulated during the robot-mediated gross motor and fine motor tasks. However, the investigation could not explore whether these variations were localised to specific brain regions or only to a limited number of electrodes within the brain regions. The present research could only suggest EEG electrodes that can best describe the fatigue induced by a robot-mediated visuomotor tracking task. Therefore, future studies can further explore whether the specificity is due to the task nature (physical/cognitive) or the differences in upper limbs' usage (proximal/distal) while utilising a higher number of electrodes.

The present research work has identified EEG features that can best describe the effects of fatigue induced by robot-mediated interactions on brain activity patterns. The investigation has also proposed a new EEG feature, $\mathrm{LLyapExp}/\alpha_{\mathrm{relative}}$. Further studies could implement fatigue countermeasure devices by combining these spectral and nonlinear EEG features with machine learning techniques to detect fatigue in robot-mediated interactions. These fatigue detection algorithms could also be used to adapt the physical behaviour of a robot to mitigate human fatigue and fatigue-related risks during human-robot co-manipulation tasks.

It is more likely that the increased motor/cognitive processing demands required during post-stroke motor retraining exercises may exacerbate stroke patients' fatigue level. Therefore, the findings of this thesis could potentially be used in future to detect and moderate the level of fatigue during robot-mediated post-stroke therapies, acknowledging that stroke patients are more likely to be fatigued than healthy individuals. Future research could also explore whether therapies will induce more recovery in the absence or presence of moderated fatigue.

Moreover, it would be possible to derive more personalised robot-mediated post-stroke rehabilitation regimes that would utilise the individual fatigue levels as a tool to increase the efficacy of upper limb robot-mediated rehabilitation.

References

Abarbanel, H. D. (1996), Choosing the dimension of reconstructed phase space, *in* 'Analysis of observed chaotic data', Springer, pp. 39-67.

Abásolo, D., Hornero, R., Espino, P., Alvarez, D. and Poza, J. (2006), 'Entropy analysis of the EEG background activity in Alzheimer's disease patients', *Physiological measurement* **27**(3), 241.

Abásolo, D., Hornero, R., Espino, P., Poza, J., Sánchez, C. I. and de la Rosa, R. (2005), 'Analysis of regularity in the EEG background activity of Alzheimer's disease patients with approximate entropy', *Clinical Neurophysiology* **116**(8), 1826-1834.

Abbott, J. J., Marayong, P. and Okamura, A. M. (2007), Haptic virtual fixtures for robot-assisted manipulation, *in* 'Robot. Res.', Springer, pp. 49-64.

Acharya, R., Faust, O., Kannathal, N., Chua, T. and Laxminarayan, S. (2005), 'Non-linear analysis of EEG signals at various sleep stages', *Computer methods and programs in biomedicine* **80**(1), 37-45.

Acharya, U. R., Molinari, F., Sree, S. V., Chattopadhyay, S., Ng, K.H. and Suri, J. S. (2012), 'Automated diagnosis of epileptic EEG using entropies', *Biomedical Signal Processing and Control* **7**(4), 401-408.

Adrian, E. D. and Matthews, B. H. C. (1934), 'The interpretation of potential waves in the cortex', *J. Physiol.* **81**(4), 440-471.

Aftanas, L. I., Lotova, N. V., Koshkarov, V. I., Pokrovskaja, V. L., Popov, S. A. and Makhnev, V. P. (1997), 'Non-linear analysis of emotion EEG: Calculation of Kolmogorov entropy and the principal Lyapunov exponent', *Neuroscience letters* **226**(1), 13-16.

Ahmadlou, M., Adeli, H. and Adeli, A. (2010), 'Fractality and a wavelet-chaos-neural network methodology for EEG-based diagnosis of autistic spectrum disorder', *Journal of Clinical Neurophysiology* **27**(5), 328-333.

Ahn, S., Nguyen, T., Jang, H., Kim, J. G. and Jun, S. C. (2016), 'Exploring neuro-physiological correlates of drivers' mental fatigue caused by sleep deprivation using simultaneous EEG, ECG, and fNIRS data', *Frontiers in human neuroscience* **10**, 219.

Alderman, R. B. (1965), 'Influence of local fatigue on speed and accuracy in motor learning', *Res. Quarterly. Am. Assoc. Heal. Phys. Educ. Recreat.* **36**(2), 131-140.

American Clinical Neurophysiology Society (2006), 'Guideline 6: A proposal for standard montages to be used in clinical EEG.', *J. Clin. Neurophysiol. Off. Publ. Am. Electroencephalogr. Soc.* **23**(2), 111.

Amirabdollahian, F., Ates, S., Basteris, A., Cesario, A., Buurke, J., Hermens, H., Hofs, D., Johansson, E., Mountain, G., Nasr, N., Nijenhuis, S., Prange, G., Rahman, N., Sale, P., Schätzlein, F., Van Schooten, B. and Stienen, A. (2014), 'Design, development and deployment of a hand/wrist exoskeleton for home-based rehabilitation after stroke - SCRIPT project', *Robotica* **32**(8), 1331-1346.

Amirabdollahian, F., Loureiro, R., Gradwell, E., Collin, C., Harwin, W. and Johnson, G. (2007), 'Multivariate analysis of the Fugl-Meyer outcome measures assessing the effectiveness of GENTLE/S robot-mediated stroke therapy', *J. Neuroeng. Rehabil.* **4**(1), 4.

Amirabdollahian, F., Loureiro, R. and Harwin, W. (2002), Minimum jerk trajectory control for rehabilitation and haptic applications, *in* 'Robot. Autom. 2002. Proceedings. ICRA'02. IEEE Int. Conf.', Vol. 4, IEEE, pp. 3380-3385.

Arns, M., Conners, C. K. and Kraemer, H. C. (2013), 'A decade of EEG theta/beta ratio research in ADHD: a meta-analysis', *Journal of attention disorders* **17**(5), 374-383.

Arroyo, S., Lesser, R. P., Gordon, B., Uematsu, S., Jackson, D. and Webber, R. (1993), 'Functional significance of the mu rhythm of human cortex: An electrophysiologic study with subdural electrodes', *Electroencephalography and clinical Neurophysiology* **87**(3), 76-87.

Ates, S., Leon, B., Basteris, A., Nijenhuis, S., Nasr, N., Sale, P., Cesario, A., Amirabdollahian, F. and Stienen, A. H. A. (2014), Technical evaluation of and clinical experiences with the SCRIPT passive wrist and hand orthosis, *in* 'Hum. Syst. Interact. (HSI), 2014 7th Int. Conf.', IEEE, pp. 188-193.

Ates, S., Lobo-Prat, J., Lammertse, P., Van Der Kooij, H. and Stienen, A. H. A. (2013), SCRIPT Passive Orthosis: Design and technical evaluation of the wrist and hand orthosis for rehabilitation training at home, *in* 'IEEE Int. Conf. Rehabil. Robot.'.

Aune, T. K., Ingvaldsen, R. and Ettema, G. (2008), 'Effect of physical fatigue on motor control at different skill levels', *Perceptual and motor skills* **106**(2), 371-386.

Bailey, S. P., Hall, E. E., Folger, S. E. and Miller, P. C. (2008), 'Changes in EEG during graded exercise on a recumbent cycle ergometer', *J. Sports Sci. Med.* **7**(4), 505.

Bakshi, R., Miletich, R., Henschel, K., Shaikh, Z., Janardhan, V., Wasay, M., Stengel, L., Ekes, R. and Kinkel, P. (1999), 'Fatigue in multiple sclerosis: Cross-sectional correlation with brain MRI findings in 71 patients', *Neurology* **53**(5), 1151-1151.

Barwick, F., Arnett, P. and Slobounov, S. (2012), 'EEG correlates of fatigue during administration of a neuropsychological test battery', *Clin. Neurophysiol.* **123**(2), 278-284.

Baumeister, J., Reinecke, K., Schubert, M., Schade, J. and Weiss, M. (2012), 'Effects of induced fatigue on brain activity during sensorimotor control', *Eur. J. Appl. Physiol.* **112**(7), 2475-2482.

Bell, A. J. and Sejnowski, T. J. (1995), 'An information-maximization approach to blind separation and blind deconvolution', *Neural Comput.* **7**(6), 1129-1159.

Belouchrani, A., Abed-Meraim, K., Cardoso, J.F. and Moulines, E. (1997), 'A blind source separation technique using second-order statistics', *IEEE Trans. signal Process.* **45**(2), 434-444.

Belza, B. (1995), 'Comparison of self-reported fatigue in rheumatoid arthritis and controls.', *The Journal of Rheumatology* **22**(4), 639-643.

Bendok, B. R., Naidech, A. M., Walker, M. T. and Batjer, H. H. (2011), *Hemorrhagic and ischemic stroke: Medical, imaging, surgical and interventional approaches*, Thieme Medical Publishers, Inc.

Benedek, M., Bergner, S., Könen, T., Fink, A. and Neubauer, A. C. (2011), 'EEG alpha synchronization is related to top-down processing in convergent and divergent thinking', *Neuropsychologia* **49**(12), 3505-3511.

Berndt, I., Franz, V. H., Bülthoff, H. H. and Wascher, E. (2002), 'Effects of pointing direction and direction predictability on event-related lateralizations of the EEG', *Human Movement Science* **21**(3), 75-98.

Bertani, R., Melegari, C., Maria, C., Bramanti, A., Bramanti, P. and Calabrò, R. S. (2017), 'Effects of robot-assisted upper limb rehabilitation in stroke patients: a systematic review with meta-analysis', *Neurol. Sci.* **38**(9), 1561-1569.

Bethel, C. L. and Murphy, R. R. (2010), 'Review of human studies methods in HRI and recommendations'.

Bian, N.Y., Wang, B., Cao, Y. and Zhang, L. (2006), Automatic removal of artifacts from EEG data using ICA and exponential analysis, *in* 'Int. Symp. Neural Networks', Springer, pp. 719-726.

Bigland-Ritchie, B. (1981), 'EMG/force relations and fatigue of human voluntary contractions', *Exerc. Sport Sci. Rev.* .

Bigland-Ritchie, B., Johansson, R., Lippold, O. and Woods, J. (1983), 'Contractile speed and EMG changes during fatigue of sustained maximal voluntary contractions', *Journal of neurophysiology* **50**(1), 313-324.

Blackhart, G. C., Minnix, J. A. and Kline, J. P. (2006), 'Can EEG asymmetry patterns predict future development of anxiety and depression?: A preliminary study', *Biological psychology* **72**(1), 46-50.

Boksem, M. A. S., Meijman, T. F. and Lorist, M. M. (2005), 'Effects of mental fatigue on attention: An ERP study', *Cogn. brain Res.* **25**(1), 107-116.

Borden, N. M., Forseen, S. E. and Stefan, C. (2015), *Imaging Anatomy of the Human Brain: A Comprehensive Atlas Including Adjacent Structures*, Springer Publishing Company.

Borghini, G., Astolfi, L., Vecchiato, G., Mattia, D. and Babiloni, F. (2014), 'Measuring neurophysiological signals in aircraft pilots and car drivers for the assessment of mental workload, fatigue and drowsiness', *Neuroscience & Biobehavioral Reviews* **44**, 58-75.

Boutros, N. N., Arfken, C., Galderisi, S., Warrick, J., Pratt, G. and Iacono, W. (2008), 'The status of spectral EEG abnormality as a diagnostic test for schizophrenia', *Schizophrenia research* **99**(1-3), 225-237.

Branscheidt, M., Kassavetis, P., Anaya, M., Rogers, D., Huang, H. D., Lindquist, M. A. and Celnik, P. (2019), 'Fatigue induces long-lasting detrimental changes in motor-skill learning', *Elife* **8**, e40578.

Brigham, E. O. (1973), 'The fast Fourier transform: An introduction to its theory and application'.

Bruder, G. E., Fong, R., Tenke, C. E., Leite, P., Towey, J. P., Stewart, J. E., McGrath, P. J. and Quitkin, F. M. (1997), 'Regional brain asymmetries in major depression with or without an anxiety disorder: A quantitative electroencephalographic study', *Biological psychiatry* **41**(9), 939-948.

Bruhn, J., Röpcke, H. and Hoeft, A. (2000), 'Approximate entropy as an electroencephalographic measure of anesthetic drug effect during desflurane anesthesia', *Anesthesiology: The Journal of the American Society of Anesthesiologists* **92**(3), 715-726.

Bütefisch, C., Hummelsheim, H., Denzler, P. and Mauritz, K.H. (1995), 'Repetitive training of isolated movements improves the outcome of motor rehabilitation of the centrally paretic hand', *J. Neurol. Sci.* **130**(1), 59-68.

Caldwell, J. A. (2005), 'Fatigue in aviation', *Travel medicine and infectious disease* **3**(2), 85-96.

Caldwell, J. A., Hall, K. K. and Erickson, B. S. (2002), 'EEG data collected from helicopter pilots in flight are sufficiently sensitive to detect increased fatigue from sleep deprivation', *Int. J. Aviat. Psychol.* **12**(1), 19-32.

Cao, L., Wang, Y., Hao, D., Rong, Y., Yang, L., Zhang, S. and Zheng, D. (2017), 'Effects of force load, muscle fatigue, and magnetic stimulation on surface electromyography during side arm lateral raise task: a preliminary study with healthy subjects', *Biomed Res. Int.* .

Cao, T., Wan, F., Wong, C. M., da Cruz, J. N. and Hu, Y. (2014), 'Objective evaluation of fatigue by EEG spectral analysis in steady-state visual evoked potential-based brain-computer interfaces', *Biomed. Eng. Online* **13**(1), 28.

Cardoso, J.F. (1998), 'Blind signal separation: statistical principles', *Proc. IEEE* **86**(10), 2009-2025.

Cardoso, J.F. (1999), 'High-order contrasts for independent component analysis', *Neural Comput.* **11**(1), 157-192.

Cardoso, J.F. and Souloumiac, A. (1993), Blind beamforming for non-gaussian signals, *in* 'IEEE Proc. F (radar signal Process.', Vol. 140, IET, pp. 362-370.

Carignan, C. R. and Akin, D. L. (2003), 'Using robots for astronaut training', *IEEE Control Syst.* **23**(2), 46-59.

Carlson, N. R. (1994), *Physiology of behavior*, Allyn & Bacon.

Carron, A. (1972), 'Motor performance and learning under physical fatigue', *Med. Sci. Sports* **4**(2), 101-106.

Carron, A. V. (1969), 'Physical fatigue and motor learning', *Res. Quarterly. Am. Assoc. Heal. Phys. Educ. Recreat.* **40**(4), 682-686.

Castells, F., Rieta, J. J., Millet, J. and Zarzoso, V. (2005), 'Spatiotemporal blind source separation approach to atrial activity estimation in atrial tachyarrhythmias', *IEEE Trans. Biomed. Eng.* **52**(2), 258-267.

Chalder, T., Berelowitz, G., Pawlikowska, T., Watts, L., Wessely, S., Wright, D. and Wallace, E. (1993), 'Development of a fatigue scale', *Journal of psychosomatic research* **37**(2), 147-

153.

Chang, W. H. and Kim, Y.H. (2013), 'Robot-assisted therapy in stroke rehabilitation', *J. stroke* **15**(3), 174.

Chatrian, G. E., Petersen, M. C. and Lazarte, J. A. (1959), 'The blocking of the rolandic wicket rhythm and some central changes related to movement', *Electroencephalography and clinical neurophysiology* **11**(3), 497-510.

Chemuturi, R., Amirabdollahian, F. and Dautenhahn, K. (2013*a*), 'Adaptive training algorithm for robot-assisted upper-arm rehabilitation, applicable to individualised and therapeutic human-robot interaction', *J. Neuroeng. Rehabil.* **10**(1), 102.

Chemuturi, R., Amirabdollahian, F. and Dautenhahn, K. (2013*b*), 'Performance based upper extremity training: A pilot study evaluation with the GENTLE/A rehabilitation system', *2013 IEEE 13th Int. Conf. Rehabil. Robot.* pp. 1-6.

Chen, A. C. (2001), 'New perspectives in EEG/MEG brain mapping and PET/fMRI neuroimaging of human pain', *International Journal of Psychophysiology* **42**(2), 147-159.

Chen, C., Li, K., Wu, Q., Wang, H., Qian, Z. and Sudlow, G. (2013), 'EEG-based detection and evaluation of fatigue caused by watching 3DTV', *Displays* **34**(2), 81-88.

Cheng, S.Y. and Hsu, H.T. (2011), Mental fatigue measurement using EEG, *in* 'Risk Manag. trends', IntechOpen.

Cheron, G., Petit, G., Cheron, J., Leroy, A., Cebolla, A., Cevallos, C., Petieau, M., Hoellinger, T., Zarka, D., Clarinval, A.M. et al. (2016), 'Brain oscillations in sport: Toward EEG biomarkers of performance', *Frontiers in psychology* **7**, 246.

Cherry, C. (1957), 'On human communication: A review, a survey, and a criticism.'.

Cifrek, M., Medved, V., Tonković, S. and Ostojić, S. (2009), 'Surface EMG based muscle fatigue evaluation in biomechanics', *Clinical biomechanics* **24**(4), 327-340.

Cignetti, F., Schena, F. and Rouard, A. (2009), 'Effects of fatigue on inter-cycle variability in cross-country skiing', *J. Biomech.* **42**(10), 1452-1459.

Cohen, J. (2013), 'Statistical power analysis for the behavioral sciences', Academic press.

Cohen, M. X. (2014), 'Analyzing neural time series data: Theory and practice', MIT press.

Colombo, R., Pisano, F., Micera, S., Mazzone, A., Delconte, C., Chiara Carrozza, M., Dario, P. and Minuco, G. (2005), 'Robotic techniques for upper limb evaluation and rehabilitation of stroke patients', *IEEE Trans. Neural Syst. Rehabil. Eng.* **13**(3), 311-324.

Congedo, M., Gouy-Pailler, C. and Jutten, C. (2008), 'On the blind source separation of human electroencephalogram by approximate joint diagonalization of second order statistics', *Clin. Neurophysiol.* **119**(12), 2677-2686.

Coote, S., Murphy, B., Harwin, W. and Stokes, E. (2008), 'The effect of the GENTLE/S robot-mediated therapy system on arm function after stroke', *Clin. Rehabil.* **22**(5), 395-405.

Cortes, N., Onate, J. and Morrison, S. (2014), 'Differential effects of fatigue on movement variability', *Gait Posture* **39**(3), 888-893.

Côté, J. N., Raymond, D., Mathieu, P. A., Feldman, A. G. and Levin, M. F. (2005), 'Differences in multi-joint kinematic patterns of repetitive hammering in healthy, fatigued and

shoulder-injured individuals', *Clinical Biomechanics* **20**(6), 581-590.

Cotten, D. J., Thomas, J. R., Spieth, W. R. and Biasiotto, J. (1972), 'Temporary fatigue effects in a gross motor skill.', *J. Mot. Behav.* **4**(4), 217-222.

Cowley, J. C. and Gates, D. H. (2017), 'Proximal and distal muscle fatigue differentially affect movement coordination', *PLOS ONE* **12**(2).

Craig, A., Tran, Y., Wijesuriya, N. and Nguyen, H. (2012), 'Regional brain wave activity changes associated with fatigue', *Psychophysiology* **49**(4), 574-582.

Croft, R. J. and Barry, R. J. (2000), 'Removal of ocular artifact from the EEG: A review', *Neurophysiologie Clinique/Clinical Neurophysiology* **30**(1), 5-19.

Dahiya, R. S. and Valle, M. (2012), *Robotic tactile sensing: Technologies and system*, Springer Science & Business Media.

Daly, I., Scherer, R., Billinger, M. and Müller-Putz, G. (2014), 'FORCe: Fully online and automated artifact removal for brain-computer interfacing', *IEEE transactions on neural systems and rehabilitation engineering* **23**(5), 725-736.

De Waard, D. and Brookhuis, K. A. (1991), 'Assessing driver status: A demonstration experiment on the road', *Accid. Anal. Prev.* **23**(4), 297-307.

Debnath, R., Buzzell, G. A., Morales, S., Bowers, M. E., Leach, S. C. and Fox, N. A. (2020), 'The Maryland analysis of developmental EEG (MADE) pipeline', *Psychophysiology* **57**(6), e13580.

Delorme, A., Makeig, S. and Sejnowski, T. (2001), Automatic artifact rejection for EEG data using high-order statistics and independent component analysis, *in* 'Proceedings of the third international ICA conference', pp. 9-12.

Delorme, A., Plamer, J., Oostenveld, R., Onton, J. and Makeig, S. (2007), 'Comparing results of algorithms implementing blind source separation of EEG data', *Swart. Found. NIH Grant* .

Delorme, A., Sejnowski, T. and Makeig, S. (2007), 'Enhanced detection of artifacts in EEG data using higher-order statistics and independent component analysis', *Neuroimage* **34**(4), 1443-1449.

DeLuca, J., Genova, H. M., Hillary, F. G. and Wylie, G. (2008), 'Neural correlates of cognitive fatigue in multiple sclerosis using functional MRI', *Journal of the neurological sciences* **270**(1-2), 28-39.

der Linde, R. Q. and Lammertse, P. (2003), 'HapticMaster - A generic force controlled robot for human interaction', *Ind. Robot An Int. J.* **30**(6), 515-524.

der Linde, R. Q., Lammertse, P., Frederiksen, E. and Ruiter, B. (2002), The HapticMaster, a new high-performance haptic interface, *in* 'Proc. Eurohaptics', pp. 1-5.

Docter, R. F., Naitoh, P. and Smith, J. C. (1966), 'Electroencephalographic changes and vigilance behavior during experimentally induced intoxication with alcoholic subjects.', *Psychosom. Med.* **28**(4), 605-615.

Edwards, S., Steele, J., Cook, J., Purdam, C. and McGhee, D. (2012), Effects of fatigue on movement variability during stretchshortening cycle, *in* 'ISBS-Conference Proc. Arch.', Vol. 1.

El Saddik, A., Orozco, M., Eid, M. and Cha, J. (2011), *Haptics technologies: Bringing touch to multimedia*, Springer Science & Business Media.

Enoka, R. M. and Stuart, D. G. (1992), 'Neurobiology of muscle fatigue', *Journal of applied physiology* **72**(5), 1631-1648.

Eoh, H. J., Chung, M. K. and Kim, S.H. (2005), 'Electroencephalographic study of drowsiness in simulated driving with sleep deprivation', *Int. J. Ind. Ergon.* **35**(4), 307-320.

Epstein, C. M. (2006), 'American Clinical Neurophysiology Society Guideline 5: Guidelines for standard electrode position nomenclature', *J. Clin. Neurophysiol.* **23**(2), 107-110.

Escudero, J., Hornero, R., Abásolo, D., Fernández, A. and López-Coronado, M. (2007), 'Artifact removal in magnetoencephalogram background activity with independent component analysis', *IEEE Trans. Biomed. Eng.* **54**(11), 1965-1973.

Escudero, J., Hornero, R., Poza, J., Abásolo, D. and Fernández, A. (2008), 'Assessment of classification improvement in patients with Alzheimer's disease based on magnetoencephalogram blind source separation', *Artif. Intell. Med.* **43**(1), 75-85.

Fan, X., Zhou, Q., Liu, Z. and Xie, F. (2015), 'Electroencephalogram assessment of mental fatigue in visual search', *Biomed. Mater. Eng.* **26**(s1), S1455-S1463.

Fasoli, S. E., Krebs, H. I. and Hogan, N. (2004), 'Robotic technology and stroke rehabilitation: Translating research into practice', *Top. Stroke Rehabil.* .

Fasoli, S. E., Krebs, H. I., Stein, J., Frontera, W. R. and Hogan, N. (2003), 'Effects of robotic therapy on motor impairment and recovery in chronic stroke', *Arch. Phys. Med. Rehabil.* **84**(4), 477-482.

Fell, J., Röschke, J. and Beckmann, P. (1993), 'Deterministic chaos and the first positive Lyapunov exponent: A nonlinear analysis of the human electroencephalogram during sleep', *Biological cybernetics* **69**(2), 139-146.

Fell, J., Röschke, J., Mann, K. and Schäffner, C. (1996), 'Discrimination of sleep stages: A comparison between spectral and nonlinear EEG measures', *Electroencephalography and clinical Neurophysiology* **98**(5), 401-410.

Ferenets, R., Vanluchene, A., Lipping, T., Heyse, B. and Struys, M. M. (2007), 'Behavior of entropy/complexity measures of the electroencephalogram during propofol-induced sedation: Dose-dependent effects of remifentanil', *The Journal of the American Society of Anesthesiologists* **106**(4), 696-706.

Feys, H. M., De Weerdt, W. J., Selz, B. E., Cox Steck, G. A., Spichiger, R., Vereeck, L. E., Putman, K. D. and Van Hoydonck, G. A. (1998), 'Effect of a therapeutic intervention for the hemiplegic upper limb in the acute phase after stroke: A single-blind, randomized, controlled multicenter trial', *Stroke* **29**(4), 785-792.

Field, A. (2018), *Discovering Statistics Using IBM SPSS Statistics*, 5 edn, Sage Publications Ltd.

Finsterer, J. (2012), 'Biomarkers of peripheral muscle fatigue during exercise', *BMC Musculoskelet. Disord.* **13**(1), 218.

Fisch, B. J. and Spehlmann, R. (1999), *Fisch and Spehlmann's EEG primer: Basic principles of digital and analog EEG*, Elsevier Health Sciences.

Fisk, J. D., Ritvo, P. G., Ross, L., Haase, D. A., Marrie, T. J. and Schlech, W. F. (1994), 'Measuring the functional impact of fatigue: Initial validation of the fatigue impact scale', *Clinical Infectious Diseases* **18**(Supplement_1), S79-S83.

Foong, R., Ang, K. K., Quek, C., Guan, C., Phua, K. S., Kuah, C. W. K., Deshmukh, V. A., Yam, L. H. L., Rajeswaran, D. K., Tang, N. et al. (2019), 'Assessment of the efficacy of EEG-based MI-BCI with visual feedback and EEG correlates of mental fatigue for upper-limb stroke rehabilitation', *IEEE Transactions on Biomedical Engineering* **67**(3), 786-795.

Franceschini, M., Mazzoleni, S., Goffredo, M., Pournajaf, S., Galafate, D., Criscuolo, S., Agosti, M. and Posteraro, F. (2019), 'Upper limb robot-assisted rehabilitation versus physical therapy on subacute stroke patients: A follow-up study', *J. Bodyw. Mov. Ther.* .

Fraser, A. M. and Swinney, H. L. (1986), 'Independent coordinates for strange attractors from mutual information', *Physical review A* **33**(2), 1134.

Frolov, A. A., Mokienko, O., Lyukmanov, R., Biryukova, E., Kotov, S., Turbina, L., Nadareyshvily, G. and Bushkova, Y. (2017), 'Post-stroke rehabilitation training with a motor-imagery-based brain-computer interface (BCI)-controlled hand exoskeleton: A randomized controlled multicenter trial', *Frontiers in neuroscience* **11**, 400.

Fuller, J. R., Lomond, K. V., Fung, J. and Côté, J. N. (2009), 'Posture-movement changes following repetitive motion-induced shoulder muscle fatigue', *Journal of Electromyography and Kinesiology* **19**(6), 1043-1052.

Galka, A. (2000), *Topics in nonlinear time series analysis, with implications for EEG analysis*, Vol. 14, World Scientific.

Gates, D. H. and Dingwell, J. B. (2008), 'The effects of neuromuscular fatigue on task performance during repetitive goal-directed movements', *Experimental Brain Research* **187**(4), 573-585.

Gevins, A. and Smith, M. E. (2007), Electroencephalography (EEG) in neuroergonomics, *in* R. Parasuraman and M. Rizzo, eds, 'Neuroergonomics brain Work', Oxford University Press, pp. 15-31.

Gevins, A., Smith, M. E., McEvoy, L. and Yu, D. (1997), 'High-resolution EEG mapping of cortical activation related to working memory: Effects of task difficulty, type of processing, and practice.', *Cerebral cortex (New York, NY: 1991)* **7**(4), 374-385.

Giannakopoulos, X., Karhunen, J. and Oja, E. (1999), 'An experimental comparison of neural algorithms for independent component analysis and blind separation', *Int. J. Neural Syst.* **9**(02), 99-114.

Gibson, H. and Edwards, R. H. T. (1985), 'Muscular exercise and fatigue', *Sport. Med.* **2**(2), 120-132.

Gilbert, D. G. (1987), 'Effects of smoking and nicotine on EEG lateralization as a function of personality', *Pers. Individ. Dif.* **8**(6), 933-941.

Godwin, M. A. and Schmidt, R. A. (1971), 'Muscular fatigue and learning a discrete motor skill', *Research Quarterly. American Association for Health, Physical Education and Recreation* **42**(4), 374-382.

Goncharova, I. I., McFarland, D. J., Vaughan, T. M. and Wolpaw, J. R. (2003), 'EMG contamination of EEG: Spectral and topographical characteristics', *Clin. Neurophysiol.*

114(9), 1580-1593.

Grabowska, A., Gut, M., Binder, M., Forsberg, L., Rymarczyk, K. and Urbanik, A. (2012), 'Switching handedness: fMRI study of hand motor control in right-handers, left-handers and converted left-handers', *Acta Neurobiol. Exp* **72**(4), 439-451.

Grafton, S. T., Fagg, A. H., Woods, R. P. and Arbib, M. A. (1996), 'Functional anatomy of pointing and grasping in humans', *Cerebral Cortex* **6**(2), 226-237.

Grandjean, E. (1979), 'Fatigue in industry.', *Occup. Environ. Med.* **36**(3), 175-186.

Gruzelier, J. H. (2014), 'EEG-neurofeedback for optimising performance. I: A review of cognitive and affective outcome in healthy participants', *Neuroscience & Biobehavioral Reviews* **44**, 124-141.

g.tec medical engineering GmbH (2014*a*), *g.GAMMACap2 EEG sensor cap: Instructions for use V2.14.00*.

g.tec medical engineering GmbH (2014*b*), *g.GAMMAsys Active Electrode System: Instructions for use V2.14.01*.

g.tec medical engineering GmbH (2016), *Simulink Highspeed On-line Processing: User manual V3.16.00*.

Guger, C., Krausz, G. and Edlinger, G. (2011), *Brain-computer interface control with dry EEG electrodes*, na.

Gut, M., Urbanik, A., Forsberg, L., Binder, M., Rymarczyk, K., Sobiecka, B., Kozub, J. and Grabowska, A. (2007), 'Brain correlates of right-handedness', *Acta Neurobiol. Exp. (Wars).* **67**(1), 43.

Guzzetta, A., Staudt, M., Petacchi, E., Ehlers, J., Erb, M., Wilke, M., Krägeloh-Mann, I. and Cioni, G. (2007), 'Brain representation of active and passive hand movements in children', *Pediatric research* **61**(4), 485-490.

Haas, L. F. (2003), 'Hans Berger (1873-1941), Richard Caton (1842-1926), and electroencephalography', *Journal of Neurology, Neurosurgery & Psychiatry* **74**(1), 9-9.

Halder, S., Bensch, M., Mellinger, J., Bogdan, M., Kübler, A., Birbaumer, N. and Rosenstiel, W. (2007), 'Online artifact removal for brain-computer interfaces using support vector machines and blind source separation', *Comput. Intell. Neurosci.* **2007**.

Hall, E. E., Ekkekakis, P. and Petruzzello, S. J. (2007), 'Regional brain activity and strenuous exercise: Predicting affective responses using EEG asymmetry', *Biol. Psychol.* **75**(2), 194-200.

Hames, E. C. (2014), EEG artifact removal and detection via clustering, PhD thesis.

Hammond, D. C. (2005), 'Neurofeedback treatment of depression and anxiety', *Journal of Adult Development* **12**(2-3), 131-137.

Harmony, T., Fernández, T., Silva, J., Bernal, J., Díiaz-Comas, L., Reyes, A., Marosi, E., Rodríiguez, M. and Rodríiguez, M. (1996), 'EEG delta activity: An indicator of attention to internal processing during performance of mental tasks', *Int. J. Psychophysiol.* **24**(1-2), 161-171.

Hart, S. G. (1986), 'NASA TLX Paper/Pencil Version'.

Haufler, A. J., Spalding, T. W., Santa Maria, D. and Hatfield, B. D. (2000), 'Neuro-cognitive activity during a self-paced visuospatial task: Comparative EEG profiles in marksmen and novice shooters', *Biological psychology* **53**(2-3), 131-160.

Hayward, V., Astley, O. R., Cruz-Hernandez, M., Grant, D. and Robles-De-La-Torre, G. (2004), 'Haptic interfaces and devices', *Sens. Rev.* **24**(1), 16-29.

Hesse, S., Schulte-Tigges, G., Konrad, M., Bardeleben, A. and Werner, C. (2003), 'Robot-assisted arm trainer for the passive and active practice of bilateral forearm and wrist movements in hemiparetic subjects', *Arch. Phys. Med. Rehabil.* **84**(6), 915-920.

Hirshkowitz, M., Whiton, K., Albert, S. M., Alessi, C., Bruni, O., DonCarlos, L., Hazen, N., Herman, J., Katz, E. S., Kheirandish-Gozal, L. and Others (2015), 'National Sleep Foundation's sleep time duration recommendations: Methodology and results summary', *Sleep Heal. J. Natl. Sleep Found.* **1**(1), 40-43.

Hoffmann, U., Vesin, J.M., Ebrahimi, T. and Diserens, K. (2008), 'An efficient P300-based brain-computer interface for disabled subjects', *Journal of Neuroscience methods* **167**(1), 115-125.

Hogan, N. (1985), 'Impedance control: An approach to manipulation: Part I - Theory, Part II – implementation, Part III – Applications', *J. Dyn. Syst. Meas. Control* **107**(1), 1-24.

Hosseinifard, B., Moradi, M. H. and Rostami, R. (2013), 'Classifying depression patients and normal subjects using machine learning techniques and nonlinear features from EEG signal', *Computer methods and programs in biomedicine* **109**(3), 339-345.

Hu, J. (2017), 'Automated detection of driver fatigue based on adaboost classifier with EEG signals', *Frontiers in computational neuroscience* **11**, 72.

Hu, J. and Min, J. (2018), 'Automated detection of driver fatigue based on EEG signals using gradient boosting decision tree model', *Cognitive neurodynamics* **12**(4), 431-440.

Hu, S. and Zheng, G. (2009), 'Driver drowsiness detection with eyelid related parameters by support vector machine', *Expert Systems with Applications* **36**(4), 7651-7658.

Huang, Y., Su, S. W. and Song, R. (2020), Voluntary intention-driven rehabilitation robots for the upper limb, *in* 'Intelligent Biomechatronics in Neurorehabilitation', Elsevier, pp. 111-130.

Huffenus, A.F., Amarantini, D. and Forestier, N. (2006), 'Effects of distal and proximal arm muscles fatigue on multi-joint movement organization', *Experimental brain research* **170**(4), 438-447.

Hurt, E., Arnold, L. E. and Lofthouse, N. (2014), 'Quantitative EEG neurofeedback for the treatment of pediatric attention-deficit/hyperactivity disorder, autism spectrum disorders, learning disorders, and epilepsy', *Child and Adolescent Psychiatric Clinics* **23**(3), 465-486.

Huysmans, M. A., Hoozemans, M. J. M., der Beek, A. J., De Looze, M. P. and Van Dieën, J. H. (2008), 'Fatigue effects on tracking performance and muscle activity', *J. Electromyogr. Kinesiol.* **18**(3), 410-419.

Hyvarinen, A. (1999), 'Fast and robust fixed-point algorithms for independent component analysis', *IEEE Trans. Neural Networks* **10**(3), 626-634.

Hyvärinen, A. and Oja, E. (2000), 'Independent component analysis: Algorithms and applications', *Neural networks* **13**(4-5), 411-430.

Iwasaki, M., Kellinghaus, C., Alexopoulos, A. V., Burgess, R. C., Kumar, A. N., Han, Y. H., Lüders, H. O. and Leigh, R. J. (2005), 'Effects of eyelid closure, blinks, and eye movements on the electroencephalogram', *Clin. Neurophysiol.* **116**(4), 878-885.

Jackson, C. (2014), 'The Chalder fatigue scale (CFQ 11)', *Occup. Med. (Chic. Ill).* **65**(1), 86.

Jap, B. T., Lal, S., Fischer, P. and Bekiaris, E. (2009), 'Using EEG spectral components to assess algorithms for detecting fatigue', *Expert Syst. Appl.* **36**(2), 2352-2359.

Jasper, H. H. (1958), 'The Ten-Twenty Electrode System of the International Federation', *Electroencephalogr Clin Neurophysiol* **10**, 371-375.

Javed, K. and Lui, F. (2019), Neuroanatomy, cerebral cortex, *in* 'StatPearls [Internet]', StatPearls Publishing.

Jensen, O. and Tesche, C. D. (2002), 'Frontal theta activity in humans increases with memory load in a working memory task', *Eur. J. Neurosci.* **15**(8), 1395-1399.

Jiang, X., Bian, G.B. and Tian, Z. (2019), 'Removal of artifacts from EEG signals: A review', *Sensors* **19**(5), 987.

Johansson, B. B. (2000), 'Brain plasticity and stroke rehabilitation: The Willis lecture', *Stroke* .

Jones Jr, H. R., Burns, T., Aminoff, M. J. and Pomeroy, S. (2013), *The Netter Collection of Medical Illustrations: Nervous System, Part 1-Brain*, 2 edn, Elsevier Health Sciences.

Jordan, D., Schneider, G., Hock, A., Hensel, T., Stockmanns, G. and Kochs, E. F. (2006), 'EEG parameters and their combination as indicators of depth of anaesthesia', *Biomedical Engineering/Biomedizinische Technik* **51**(2), 89-94.

Jung, T.P., Humphries, C., Lee, T.W., Makeig, S., McKeown, M. J., Iragui, V. and Sejnowski, T. J. (1998), Extended ICA removes artifacts from electroencephalographic recordings, *in* 'Advances in neural information processing systems', pp. 894-900.

Jung, T.P., Makeig, S., Humphries, C., Lee, T.W., Mckeown, M. J., Iragui, V. and Sejnowski, T. J. (2000), 'Removing electroencephalographic artifacts by blind source separation', *Psychophysiology* **37**(2), 163-178.

Kachenoura, A., Albera, L., Senhadji, L. and Comon, P. (2007), 'ICA: A potential tool for BCI systems', *IEEE Signal Processing Magazine* **25**(1), 57-68.

Kanda, P. A. d. M., Anghinah, R., Smidth, M. T. and Silva, J. M. (2009), 'The clinical use of quantitative EEG in cognitive disorders', *Dement. Neuropsychol.* **3**(3), 195-203.

Kane, N., Acharya, J., Benickzy, S., Caboclo, L., Finnigan, S., Kaplan, P. W., Shibasaki, H., Pressler, R. and van Putten, M. J. A. M. (2017), 'A revised glossary of terms most commonly used by clinical electroencephalographers and updated proposal for the report format of the EEG findings. Revision 2017', *Clin. Neurophysiol. Pract.* **2**, 170.

Kannathal, N., Choo, M. L., Acharya, U. R. and Sadasivan, P. (2005), 'Entropies for detection of epilepsy in EEG', *Computer methods and programs in biomedicine* **80**(3), 187-194.

Kantz, H. and Schreiber, T. (2004), *Nonlinear time series analysis*, Vol. 7, Cambridge university press.

Kar, S., Bhagat, M. and Routray, A. (2010), 'EEG signal analysis for the assessment and quantification of driver's fatigue', *Transportation research part F: Traffic psychology and behaviour* **13**(5), 297-306.

Käthner, I., Wriessnegger, S. C., Müller-Putz, G. R., Kübler, A. and Halder, S. (2014), 'Effects of mental workload and fatigue on the P300, alpha and theta band power during operation of an ERP (P300) brain-computer interface', *Biol. Psychol.* **102**, 118-129.

Keith, R. A. (1997), 'Treatment strength in rehabilitation', *Arch. Phys. Med. Rehabil.* **78**(12), 1298-1304.

Kim, D.J., Jeong, J., Chae, J.H., Park, S., Kim, S. Y., Go, H. J., Paik, I.H., Kim, K.S. and Choi, B. (2000), 'An estimation of the first positive Lyapunov exponent of the EEG in patients with schizophrenia', *Psychiatry Research: Neuroimaging* **98**(3), 177-189.

Kirschstein, T. and Köhling, R. (2009), 'What is the Source of the EEG?', *Clin. EEG Neurosci.* **40**(3), 146-149.

Klem, G. H., LuÈders, H. O., Jasper, H. H., Elger, C. and Others (1999), 'The ten-twenty electrode system of the International Federation', *Electroencephalogr Clin Neurophysiol* **52**(3), 3-6.

Klimesch, W. (1996), 'Memory processes, brain oscillations and EEG synchronization', *Int. J. Psychophysiol.* **24**(1-2), 61-100.

Klimesch, W. (1997), 'EEG-alpha rhythms and memory processes', *Int. J. Psychophysiol.* **26**(1-3), 319-340.

Klimesch, W. (1999), 'EEG alpha and theta oscillations reflect cognitive and memory performance: A review and analysis', *Brain research reviews* **29**(2-3), 169-195.

Klimesch, W., Doppelmayr, M., Russegger, H., Pachinger, T. and Schwaiger, J. (1998), 'Induced alpha band power changes in the human EEG and attention', *Neuroscience letters* **244**(2), 73-76.

Kokkinakis, K. and Loizou, P. C. (2008), 'Using blind source separation techniques to improve speech recognition in bilateral cochlear implant patients', *J. Acoust. Soc. Am.* **123**(4), 2379-2390.

Kong, W., Zhou, Z., Hu, S., Zhang, J., Babiloni, F. and Dai, G. (2013), 'Automatic and direct identification of blink components from scalp EEG', *Sensors* **13**(8), 10783-10801.

Krakauer, J. W. (2005), Arm function after stroke: From physiology to recovery, *in* 'Semin. Neurol.', Vol. 25, Copyright©2005 by Thieme Medical Publishers, Inc., 333 Seventh Avenue, New York, NY 10001, USA, pp. 384-395.

Krebs, H. I., Hogan, N., Aisen, M. L. and Volpe, B. T. (1998), 'Robot-aided neurorehabilitation', *IEEE Trans. Rehabil. Eng.* **6**(1), 75-87.

Krebs, H. I., Volpe, B. T., Williams, D., Celestino, J., Charles, S. K., Lynch, D. and Hogan, N. (2007), 'Robot-aided neurorehabilitation: A robot for wrist rehabilitation', *IEEE Trans. neural Syst. Rehabil. Eng.* **15**(3), 327-335.

Krishnaveni, V., Jayaraman, S., Aravind, S., Hariharasudhan, V. and Ramadoss, K. (2006), 'Automatic identification and removal of ocular artifacts from EEG using wavelet transform', *Measurement science review* **6**(4), 45-57.

Kropotov, J. D. (2010), *Quantitative EEG, event-related potentials and neurotherapy*, Academic Press.

Krupp, L. B., LaRocca, N. G., Muir-Nash, J. and Steinberg, A. D. (1989), 'The fatigue severity scale: Application to patients with multiple sclerosis and systemic lupus erythematosus', *Archives of neurology* **46**(10), 1121-1123.

Kubitz, K. A. and Mott, A. A. (1996), 'EEG power spectral densities during and after cycle ergometer exercise', *Res. Q. Exerc. Sport* **67**(1), 91-96.

Kwakkel, G. (2006), 'Impact of intensity of practice after stroke: Issues for consideration', *Disabil. Rehabil.* **28**(13-14), 823-830.

Kwakkel, G., Kollen, B. J., van der Grond, J. and Prevo, A. J. H. (2003), 'Probability of regaining dexterity in the flaccid upper limb: Impact of severity of paresis and time since onset in acute stroke', *Stroke* **34**(9), 2181-2186.

Lacquaniti, F., Caminiti, R. et al. (1998), 'Visuo-motor transformations for arm reaching', *European Journal of Neuroscience* **10**, 195-203.

Lagopoulos, J., Xu, J., Rasmussen, I., Vik, A., Malhi, G. S., Eliassen, C. F., Arntsen, I. E., Sæther, J. G., Hollup, S., Holen, A. and Others (2009), 'Increased theta and alpha EEG activity during nondirective meditation', *J. Altern. Complement. Med.* **15**(11), 1187-1192.

Lahiri, R., Rakshit, P. and Konar, A. (2017), 'Evolutionary perspective for optimal selection of EEG electrodes and features', *Biomedical Signal Processing and Control* **36**, 113-137.

Lal, S. K. L. and Craig, A. (2001), 'A critical review of the psychophysiology of driver fatigue', *Biol. Psychol.* **55**(3), 173-194.

Lal, S. K. L. and Craig, A. (2002), 'Driver fatigue: Electroencephalography and psychological assessment', *Psychophysiology* **39**(3), 313-321.

Laszlo, S., Ruiz-Blondet, M., Khalifian, N., Chu, F. and Jin, Z. (2014), 'A direct comparison of active and passive amplification electrodes in the same amplifier system', *J. Neurosci. Methods* **235**, 298-307.

Laureiro-Martinez, D., Canessa, N., Brusoni, S., Zollo, M., Hare, T., Alemanno, F. and Cappa, S. F. (2014), 'Frontopolar cortex and decision-making efficiency: Comparing brain activity of experts with different professional background during an exploration-exploitation task', *Frontiers in human neuroscience* **7**, 927.

Lawrence, E. S., Coshall, C., Dundas, R., Stewart, J., Rudd, A. G., Howard, R. and Wolfe, C. D. A. (2001), 'Estimates of the prevalence of acute stroke impairments and disability in a multiethnic population', *Stroke* **32**(6), 1279-1284.

Leon, B., Basteris, A., Infarinato, F., Sale, P., Nijenhuis, S., Prange, G. and Amirabdollahian, F. (2014), 'Grasps recognition and evaluation of stroke patients for supporting rehabilitation therapy', *Biomed Res. Int.* **2014**.

Lerdal, A., Bakken, L. N., Kouwenhoven, S. E., Pedersen, G., Kirkevold, M., Finset, A. and Kim, H. S. (2009), 'Poststroke fatigue - A review', *J. Pain Symptom Manage.* **38**(6), 928-

949.

Li, W., Gu, F., Ball, A. D., Leung, A. Y. T. and Phipps, C. E. (2001), 'A study of the noise from diesel engines using the independent component analysis', *Mech. Syst. Signal Process.* **15**(6), 1165-1184.

Li, Y., Ma, Z., Lu, W. and Li, Y. (2006), 'Automatic removal of the eye blink artifact from EEG using an ICA-based template matching approach', *Physiol. Meas.* **27**(4), 425.

Li, Y., Tong, S., Liu, D., Gai, Y., Wang, X., Wang, J., Qiu, Y. and Zhu, Y. (2008), 'Abnormal EEG complexity in patients with schizophrenia and depression', *Clinical Neurophysiology* **119**(6), 1232-1241.

Lin, C.T., Liao, L.D., Liu, Y.H., Wang, I.J., Lin, B.S. and Chang, J.Y. (2011), 'Novel dry polymer foam electrodes for long-term EEG measurement', *IEEE Trans. Biomed. Eng.* **58**(5), 1200-1207.

Liu, C., Yao, R., Wang, Z. and Zhou, R. (2014), 'N450 as a candidate neural marker for interference control deficits in children with learning disabilities', *International journal of psychophysiology* **93**(1), 70-77.

Liu, J. Z., Dai, T. H., Sahgal, V., Brown, R. W. and Yue, G. H. (2002), 'Nonlinear cortical modulation of muscle fatigue: A functional MRI study', *Brain research* **957**(2), 320-329.

Liu, J. Z., Shan, Z. Y., Zhang, L. D., Sahgal, V., Brown, R. W. and Yue, G. H. (2003), 'Human brain activation during sustained and intermittent submaximal fatigue muscle contractions: An fMRI study', *J. Neurophysiol.* **90**(1), 300-312.

Liu, J., Zhang, C. and Zheng, C. (2010), 'EEG-based estimation of mental fatigue by using KPCA-HMM and complexity parameters', *Biomed. Signal Process. Control* **5**(2), 124-130.

Liu, Y., Sourina, O. and Nguyen, M. K. (2011), Real-time EEG-based emotion recognition and its applications, *in* 'Transactions on computational science XII', Springer, pp. 256-277.

Lohse, K. R., Lang, C. E. and Boyd, L. A. (2014), 'Is more better? Using metadata to explore dose-response relationships in stroke rehabilitation', *Stroke* **45**(7), 2053-2058.

Lopez-Gordo, M. A., Sanchez-Morillo, D. and Valle, F. P. (2014), 'Dry EEG electrodes', *Sensors* **14**(7), 12847-12870.

Lorenz, E. N. (1963), 'Deterministic nonperiodic flow', *Journal of atmospheric sciences* **20**(2), 130-141.

Lorist, M. M., Boksem, M. A. and Ridderinkhof, K. R. (2005), 'Impaired cognitive control and reduced cingulate activity during mental fatigue', *Cognitive Brain Research* **24**(2), 199-205.

Lorist, M. M., Klein, M., Nieuwenhuis, S., De Jong, R., Mulder, G. and Meijman, T. F. (2000), 'Mental fatigue and task control: Planning and preparation', *Psychophysiology* **37**(5), 614-625.

Loureiro, R., Amirabdollahian, F., Coote, S., Stokes, E. and Harwin, W. (2001), Using haptics technology to deliver motivational therapies in stroke patients: Concepts and initial pilot studies, *in* 'Proceedings of EuroHaptics', Vol. 2001, p. 6.

Loureiro, R., Amirabdollahian, F., Topping, M., Driessen, B. and Harwin, W. (2003), 'Upper limb robot mediated stroke therapy - GENTLE/S approach', *Auton. Robots* **15**(1), 35-51.

Luengo-Fernandez, R., Leal, J. and Gray, A. (2015), 'UK research spend in 2008 and 2012: Comparing stroke, cancer, coronary heart disease and dementia', *BMJ Open* **5**(4), e006648.

Lum, P. S., Burgar, C. G., Shor, P. C., Majmundar, M. and der Loos, M. (2002), 'Robot-assisted movement training compared with conventional therapy techniques for the rehabilitation of upper-limb motor function after stroke', *Arch. Phys. Med. Rehabil.* **83**(7), 952-959.

Lum, P. S., Burgar, C. G., Van der Loos, M., Shor, P. C., Majmundar, M. and Yap, R. (2006), 'MIME robotic device for upper-limb neurorehabilitation in subacute stroke subjects: A follow-up study', *Journal of rehabilitation research and development* **43**(5), 631.

Maciejasz Paweł and Eschweiler, J., Gerlach-Hahn, K., Jansen-Troy, A. and Leonhardt, S. (2014), 'A survey on robotic devices for upper limb rehabilitation', *J. Neuroeng. Rehabil.* **11**(1), 3.

Mackay, J., with Shanthi Mendis, G. M. . and Greenland., K. (2004), 'The atlas of heart disease and stroke'. **URL:** *https://apps.who.int/iris/handle/10665/43007*

MacKenzie, I. S., Kauppinen, T. and Silfverberg, M. (2001), Accuracy measures for evaluating computer pointing devices, *in* 'Proc. SIGCHI Conf. Hum. factors Comput. Syst. - CHI '01', pp. 9-16. **URL:** *http://portal.acm.org/citation.cfm?doid=365024.365028*

Madeleine, P. and Madsen, T. M. T. (2009), 'Changes in the amount and structure of motor variability during a deboning process are associated with work experience and neck-shoulder discomfort', *Appl. Ergon.* .

Mahajan, R. and Morshed, B. I. (2014), 'Unsupervised eye blink artifact denoising of EEG data with modified multiscale sample entropy, kurtosis, and wavelet-ICA', *IEEE journal of Biomedical and Health Informatics* **19**(1), 158-165.

Makeig, S., Bell, A. J., Jung, T.P. and Sejnowski, T. J. (1996), Independent component analysis of electroencephalographic data, *in* 'Advances in neural information processing systems', pp. 145-151.

Malmivuo, J. and Plonsey, R. (1995), *Bioelectromagnetism: principles and applications of bioelectric and biomagnetic fields*, Oxford University Press, USA.

Mammone, N. and Morabito, F. C. (2008), 'Enhanced automatic artifact detection based on independent component analysis and renyi's entropy', *Neural networks* **21**(7), 1029-1040.

Mandal, B., Li, L., Wang, G. S. and Lin, J. (2016), 'Towards detection of bus driver fatigue based on robust visual analysis of eye state', *IEEE Transactions on Intelligent Transportation Systems* **18**(3), 545-557.

Mannan, M. M. N., Kamran, M. A. and Jeong, M. Y. (2018), 'Identification and removal of physiological artifacts from electroencephalogram signals: A review', *IEEE Access* **6**, 30630-30652.

Marcora, S. M., Staiano, W. and Manning, V. (2009), 'Mental fatigue impairs physical performance in humans', *Journal of applied physiology* **106**(3), 857-864.

Masiero, S., Armani, M., Rosati, G. and Others (2011), 'Upper-limb robot-assisted therapy in rehabilitation of acute stroke patients: Focused review and results of new randomized controlled trial', *J Rehabil Res Dev* **48**(4), 355-366.

Masiero, S., Celia, A., Rosati, G. and Armani, M. (2007), 'Robotic-assisted rehabilitation of the upper limb after acute stroke', *Arch. Phys. Med. Rehabil.* **88**(2), 142-149.

Masumoto, Y., Morinushi, T., Kawasaki, H., Ogura, T. and Takigawa, M. (1999), 'Effects of three principal constituents in chewing gum on electroencephalographic activity', *Psychiatry Clin. Neurosci.* **53**(1), 17-23.

Mehta, R. K. and Parasuraman, R. (2014), 'Effects of mental fatigue on the development of physical fatigue: A neuroergonomic approach', *Hum. Factors* .

Michielsen, H. J., De Vries, J. and Van Heck, G. L. (2003), 'Psychometric qualities of a brief self-rated fatigue measure: The Fatigue Assessment Scale', *J. Psychosom. Res.* .

Min, J., Wang, P. and Hu, J. (2017), 'Driver fatigue detection through multiple entropy fusion analysis in an EEG-based system', *PLOS ONE* **12**(12), e0188756.

Miyakoshi, M. (n.d.), 'Makoto's useful EEGlab code', https://sccn.ucsd.edu/wiki/Makoto's_useful_EEGLAB_code. Accessed: 2018-10-26.

Mognon, A., Jovicich, J., Bruzzone, L. and Buiatti, M. (2011), 'ADJUST: An automatic EEG artifact detector based on the joint use of spatial and temporal features', *Psychophysiology* **48**(2), 229-240.

Molier, B. I., Prange, G. B., Krabben, T., Buurke, J., Hermens, H. J. and Tong, R. (2011), 'Upper extremity rehabilitation systems and augmented feedback', *Biomechatronics Med. Heal. Care* pp. 143-156.

Molla, M. K., Tanaka, T., Rutkowski, T. M. and Cichocki, A. (2010), Separation of EOG artifacts from EEG signals using bivariate EMD, *in* '2010 IEEE International Conference on Acoustics, Speech and Signal Processing', IEEE, pp. 562-565.

Morris, T. and Miller, J. C. (1996), 'Electrooculographic and performance indices of fatigue during simulated flight', *Biological psychology* **42**(3), 343-360.

Mu, Z., Hu, J. and Min, J. (2017), 'Driver fatigue detection system using electroencephalography signals based on combined entropy features', *Applied Sciences* **7**(2), 150.

Mulholland, T. (1995), 'Human EEG, behavioral stillness and biofeedback', *Int. J. Psychophysiol.* **19**(3), 263-279.

Murphy, M., Bruno, M.A., Riedner, B. A., Boveroux, P., Noirhomme, Q., Landsness, E. C., Brichant, J.F., Phillips, C., Massimini, M., Laureys, S. et al. (2011), 'Propofol anesthesia and sleep: A high-density EEG study', *Sleep* **34**(3), 283-291.

Muthukumaraswamy, S. (2013), 'High-frequency brain activity and muscle artifacts in MEG/EEG: A review and recommendations', *Front. Hum. Neurosci.* **7**, 138.

Myers, J. B., Guskiewicz, K. M., Schneider, R. A. and Prentice, W. E. (1999), 'Proprioception and neuromuscular control of the shoulder after muscle fatigue', *Journal of athletic training* **34**(4), 362.

Naik, G. R. and Kumar, D. K. (2011), 'An overview of independent component analysis and its applications', *Informatica* **35**(1).

Naranjo, J., Brovelli, A., Longo, R., Budai, R., Kristeva, R. and Battaglini, P. P. (2007), 'EEG dynamics of the frontoparietal network during reaching preparation in humans', *Neuroimage* **34**(4), 1673-1682.

Natarajan, K., Acharya, R., Alias, F., Tiboleng, T. and Puthusserypady, S. K. (2004), 'Non-linear analysis of EEG signals at different mental states', *Biomedical engineering online* **3**(1), 7.

Nef, T., Guidali, M. and Riener, R. (2009), 'ARMin III - arm therapy exoskeleton with an ergonomic shoulder actuation', *Appl. Bionics Biomech.* **6**(2), 127-142.

Neuberger, G. B. (2003), 'Measures of fatigue: The fatigue questionnaire, fatigue severity scale, multidimensional assessment of fatigue scale, and short form-36 vitality (energy/fatigue) subscale of the short form health survey', *Arthritis Care Res. (Hoboken).* **49**(S5).

Neuper, C. and Pfurtscheller, G. (2001), 'Event-related dynamics of cortical rhythms: Frequency-specific features and functional correlates', *Int. J. Psychophysiol.* **43**(1), 41-58.

Ng, S. C. and Raveendran, P. (2007), EEG peak alpha frequency as an indicator for physical fatigue, *in* '11th Mediterranean Conference on Medical and Biomedical Engineering and Computing 2007', Springer, pp. 517-520.

Nijenhuis, S. M., Prange-Lasonder, G. B., Amirabdollahian, F., Infarinato, F., Buurke, J. H. and Rietman, J. S. (2016), Feasibility of a second iteration wrist and hand supported training system for self-administered training at home in chronic stroke, *in* 'eighth Int. Conf. eHealth, telemedicine, Soc. Med. Venice, Italy. eTELEMED'.

Nolan, H., Whelan, R. and Reilly, R. B. (2010), 'FASTER: Fully automated statistical thresholding for EEG artifact rejection', *J. Neurosci. Methods* **192**(1), 152-162.

Norouzi-Gheidari, N., Archambault, P. S. and Fung, J. (2012), 'Effects of robot-assisted therapy on stroke rehabilitation in upper limbs: Systematic review and meta-analysis of the literature.', *Journal of Rehabilitation Research & Development* **49**(4).

Nuwer, M. (1997), 'Assessment of digital EEG, quantitative EEG, and EEG brain mapping: Report of the American Academy of Neurology and the American Clinical Neurophysiology Society', *Neurology* **49**(1), 277-292.

Ofori, E., Coombes, S. A. and Vaillancourt, D. E. (2015), '3D Cortical electrophysiology of ballistic upper limb movement in humans', *Neuroimage* **115**, 30-41.

Oh, S. L., Hagiwara, Y., Raghavendra, U., Yuvaraj, R., Arunkumar, N., Murugappan, M. and Acharya, U. R. (2018), 'A deep learning approach for parkinson's disease diagnosis from EEG signals', *Neural Computing and Applications* pp. 1-7.

Okogbaa, O. G., Shell, R. L. and Filipusic, D. (1994), 'On the investigation of the neurophysiological correlates of knowledge worker mental fatigue using the EEG signal', *Appl. Ergon.* **25**(6), 355-365.

Onton, J., Westerfield, M., Townsend, J. and Makeig, S. (2006), 'Imaging human EEG dynamics using independent component analysis', *Neurosci. Biobehav. Rev.* **30**(6), 808-822.

Ortner, R., Grünbacher, E. and Guger, C. (2013), 'State of the art in sensors, signals and signal processing', *Guger Technol. OG, Graz, Austria* .

Osowski, S., Swiderski, B., Cichocki, A. and Rysz, A. (2007), 'Epileptic seizure characterization by Lyapunov exponent of EEG signal', *COMPEL - The international journal for computation and mathematics in electrical and electronic engineering* .

Otaduy, M. A. and Lin, M. C. (2006), 'High fidelity haptic rendering', *Synth. Lect. Comput. Graph. Animat.* **1**(1), 1-112.

Oujamaa, L., Relave, I., Froger, J., Mottet, D. and Pelissier, J.Y. (2009), 'Rehabilitation of arm function after stroke. Literature review', *Ann. Phys. Rehabil. Med.* **52**(3), 269-293.

Pedroni, A., Bahreini, A. and Langer, N. (2019), 'Automagic: Standardized preprocessing of big EEG data', *Neuroimage* **200**, 460-473.

Pellouchoud, E., Smith, M. E., McEvoy, L. and Gevins, A. (1999), 'Mental effort-related EEG modulation during video-game play: Comparison between juvenile subjects with epilepsy and normal control subjects', *Epilepsia* **40**, 38-43.

Peterson, D. A., Knight, J. N., Kirby, M. J., Anderson, C. W. and Thaut, M. H. (2005), 'Feature selection and blind source separation in an EEG-based brain-computer interface', *EURASIP J. Adv. Signal Process.* **2005**(19), 218613.

Pfurtscheller, G. (1997), 'EEG event-related desynchronization (ERD) and synchronization (ERS)', *Electroencephalography and Clinical Neurophysiology* **1**(103), 26.

Pfurtscheller, G., Stancak Jr, A. and Neuper, C. (1996), 'Event-related synchronization (ERS) in the alpha band — an electrophysiological correlate of cortical idling: A review', *International journal of psychophysiology* **24**(1-2), 39-46.

Phothisonothai, M., Tsubomi, H., Kondo, A., Kikuchi, M., Yoshimura, Y., Minabe, Y. and Watanabe, K. (2012), Linear and nonlinear features for automatic artifacts removal from meg data based on ICA, *in* 'Proceedings of The 2012 Asia Pacific Signal and Information Processing Association Annual Summit and Conference', IEEE, pp. 1-9.

Pignolo, L. (2009), Robotics in neuro-rehabilitation, *in* 'J. Rehabil. Med.'.

Pincus, S. (1995), 'Approximate entropy (ApEn) as a complexity measure', *Chaos: An Interdisciplinary Journal of Nonlinear Science* **5**(1), 110-117.

Pincus, S. M. (1991), 'Approximate entropy as a measure of system complexity.', *Proceedings of the National Academy of Sciences* **88**(6), 2297-2301.

Pincus, S. M. and Viscarello, R. R. (1992), 'Approximate entropy: A regularity measure for fetal heart rate analysis', *Obstet Gynecol* **79**(2), 249-255.

Pinegger, A., Wriessnegger, S. C., Faller, J. and Müller-Putz, G. R. (2016), 'Evaluation of different EEG acquisition systems concerning their suitability for building a brain-computer interface: Case studies', *Frontiers in neuroscience* **10**, 441.

Pion-Tonachini, L., Kreutz-Delgado, K. and Makeig, S. (2019), 'ICLabel: An automated electroencephalographic independent component classifier, dataset, and website', *NeuroImage* **198**, 181-197.

Pradhan, N. and Sadasivan, P. (1996), 'The nature of dominant Lyapunov exponent and attractor dimension curves of EEG in sleep', *Computers in biology and medicine* **26**(5), 419-428.

Prange, G. B., Jannink, M. J. A., Groothuis-Oudshoorn, C. G. M., Hermens, H. J. and IJzerman, M. J. (2006), 'Systematic review of the effect of robot-aided therapy on recovery of the hemiparetic arm after stroke', *J. Rehabil. Res. Dev.* **43**(2), 171.

Prasad, G., Herman, P., Coyle, D., McDonough, S. and Crosbie, J. (2010), 'Applying a brain-computer interface to support motor imagery practice in people with stroke for upper limb recovery: A feasibility study', *Journal of neuroengineering and rehabilitation* **7**(1), 60.

Purves, D., Augustine, G. J., Fitzpatrick, D., Hall, W. C., Lamantia, A.S., Mcnamara, J. O. and Williams, S. M. (2004), *Neuroscience*, 3 edn, Sinauer Associates, Inc.

Qin, J., Lin, J.H., Faber, G. S., Buchholz, B. and Xu, X. (2014), 'Upper extremity kinematic and kinetic adaptations during a fatiguing repetitive task', *Journal of Electromyography and Kinesiology* **24**(3), 404-411.

Qin, Y., Rahman, N. and Amirabdollahian, F. (2014), 'Asymmetrical performance and abnormal synergies of the post-stroke patient wearing SCRIPT passive orthosis in calibration, exercise and energy evaluation', *Adv Robot Autom* **3**(122), 2.

Rahbar, K. and Reilly, J. P. (2005), 'A frequency domain method for blind source separation of convolutive audio mixtures', *IEEE Trans. Speech Audio Process.* **13**(5), 832-844.

Ramachandran, V. S. (2002), *Encyclopedia of the Human Brain, Four-Volume Set.*, Academic Press.

Reinkensmeyer, D. J., Dewald, J. P. A. and Rymer, W. Z. (1999), 'Guidance-based quantification of arm impairment following brain injury: A pilot study', *IEEE Trans. Rehabil. Eng.* **7**(1), 1-11.

Rhodes, C. and Morari, M. (1997), 'False-nearest-neighbors algorithm and noise-corrupted time series', *Physical Review E* **55**(5), 6162.

Richardson, J. T. (2011), 'Eta squared and partial eta squared as measures of effect size in educational research', *Educational Research Review* **6**(2), 135-147.

Richman, J. S. and Moorman, J. R. (2000), 'Physiological time-series analysis using approximate entropy and sample entropy', *Am. J. Physiol. Circ. Physiol.* **278**(6), H2039-H2049.

Roan, M. J., Erling, J. G. and Sibul, L. H. (2002), 'A new, non-linear, adaptive, blind source separation approach to gear tooth failure detection and analysis', *Mech. Syst. Signal Process.* **16**(5), 719-740.

Rosati, G., Gallina, P. and Masiero, S. (2007), 'Design, implementation and clinical tests of a wire-based robot for neurorehabilitation', *IEEE Trans. Neural Syst. Rehabil. Eng.* **15**(4), 560-569.

Röschke, J., Fell, J. and Beckmann, P. (1993), 'The calculation of the first positive Lyapunov exponent in sleep EEG data', *Electroencephalography and clinical neurophysiology* **86**(5), 348-352.

Röschke, J., Fell, J. and Beckmann, P. (1995*a*), 'Nonlinear analysis of sleep EEG data in schizophrenia: Calculation of the principal Lyapunov exponent', *Psychiatry research* **56**(3), 257-269.

Röschke, J., Fell, J. and Beckmann, P. (1995*b*), 'Nonlinear analysis of sleep EEG in depression: Calculation of the largest Lyapunov exponent', *European archives of psychiatry and clinical neuroscience* **245**(1), 27-35.

Rosenstein, M. T., Collins, J. J. and De Luca, C. J. (1993), 'A practical method for calculating largest Lyapunov exponents from small data sets', *Physica D: Nonlinear Phenomena* **65**(1-2), 117-134.

Ruiter, B. A. (2003), *HapticAPI Programming Manual*, FCS Control Systems.

Sabes, P. N. (2000), 'The planning and control of reaching movements', *Current opinion in neurobiology* **10**(6), 740-746.

Safieddine, D., Kachenoura, A., Albera, L., Birot, G., Karfoul, A., Pasnicu, A., Biraben, A., Wendling, F., Senhadji, L. and Merlet, I. (2012), 'Removal of muscle artifact from EEG data: Comparison between stochastic (ICA and CCA) and deterministic (EMD and wavelet-based) approaches', *EURASIP Journal on Advances in Signal Processing* **2012**(1), 127.

Sahonero-Alvarez, G. and Calderón, H. (2017), A comparison of SOBI, FastICA, JADE and Infomax algorithms, *in* 'Proc. 8th Int. Multi-Conference Complexity, Informatics Cybern', Vol. 17, p. 22.

Sanchez, R., Reinkensmeyer, D., Shah, P., Liu, J., Rao, S., Smith, R., Cramer, S., Rahman, T. and Bobrow, J. (2004), Monitoring functional arm movement for home-based therapy after stroke, *in* '26th Annu. Int. Conf. IEEE Eng. Med. Biol. Soc.', Vol. 2, IEEE, pp. 4787-4790.

Sanei, S. and Chambers, J. A. (2013*b*), *EEG signal processing*, John Wiley & Sons.

Santamaria, J. and Chiappa, K. H. (1987), 'The EEG of drowsiness in normal adults', *Journal of clinical Neurophysiology* **4**(4), 327-382.

Sarnthein, J., Stern, J., Aufenberg, C., Rousson, V. and Jeanmonod, D. (2006), 'Increased EEG power and slowed dominant frequency in patients with neurogenic pain', *Brain* **129**(1), 55-64.

Schacter, D. L. (1977), 'EEG theta waves and psychological phenomena: A review and analysis', *Biol. Psychol.* **5**(1), 47-82.

Schalk, G., McFarland, D. J., Hinterberger, T., Birbaumer, N. and Wolpaw, J. R. (2004), 'BCI2000: A general-purpose brain-computer interface (BCI) system', *IEEE Transactions on biomedical engineering* **51**(6), 1034-1043.

Schomer, D. L. and Da Silva, F. L. (2012), *Niedermeyer's electroencephalography: Basic principles, clinical applications, and related fields*, Lippincott Williams & Wilkins.

Schwartz, J., Janford, L. and Krupp, L. (1993), 'The assessment of fatigue: A new measurement', *Journal of Psychosomatic Researches* **37**(7), 753-762.

Selen, L. P. J., Beek, P. J. and Van Dieën, J. H. (2007), 'Fatigue-induced changes of impedance and performance in target tracking', *Exp. Brain Res.* .

Shahid, A., Shen, J. and Shapiro, C. M. (2010), 'Measurements of sleepiness and fatigue', *J. Psychosom. Res.* **69**(1), 81-89.

Shan, H., Xu, H., Zhu, S. and He, B. (2015), 'A novel channel selection method for optimal classification in different motor imagery BCI paradigms', *Biomedical engineering online* **14**(1), 1-18.

Siepmann, M. and Kirch, W. (2002), 'Effects of caffeine on topographic quantitative EEG', *Neuropsychobiology* **45**(3), 161-166.

Singh, N. B., Arampatzis, A., Duda, G., Heller, M. O. and Taylor, W. R. (2010), 'Effect of fatigue on force fluctuations in knee extensors in young adults', *Philosophical Transactions of the Royal Society A: Mathematical, Physical and Engineering Sciences* **368**(1920), 2783-2798.

Smith, M. R., Coutts, A. J., Merlini, M., Deprez, D., Lenoir, M. and Marcora, S. M. (2016), 'Mental fatigue impairs soccer-specific physical and technical performance', *Medicine & Science in Sports & Exercise* **48**(2), 267-276.

Snyder, S. M. and Hall, J. R. (2006), 'A meta-analysis of quantitative EEG power associated with attention-deficit hyperactivity disorder', *Journal of Clinical Neurophysiology* **23**(5), 441-456.

Sommer, D. and Golz, M. (2010), Evaluation of PERCLOS based current fatigue monitoring technologies, *in* '2010 Annual International Conference of the IEEE Engineering in Medicine and Biology', IEEE, pp. 4456-4459.

Song, R., Tong, K.y., Hu, X. and Li, L. (2008), 'Assistive control system using continuous myoelectric signal in robot-aided arm training for patients after stroke', *IEEE transactions on neural systems and rehabilitation engineering* **16**(4), 371-379.

Srinivasan, D. and Mathiassen, S. E. (2012), 'Motor variability in occupational health and performance'.

Staines, W. R., McIlroy, W. E. and Brooks, D. (2009), 'Functional impairments following stroke: Implications for rehabilitation', *Curr Issues Card. Rehab Prev.* **17**(1), 5-8.

Stam, C., Jelles, B., Achtereekte, H., Rombouts, S., Slaets, J. and Keunen, R. (1995), 'Investigation of EEG non-linearity in dementia and parkinson's disease', *Electroencephalography and clinical neurophysiology* **95**(5), 309-317.

Stam, K. J., Tavy, D. L., Jelles, B., Achtereekte, H. A., Slaets, J. P. and Keunen, R. W. (1994), 'Non-linear dynamical analysis of multichannel EEG: Clinical applications in dementia and parkinson's disease', *Brain topography* **7**(2), 141-150.

Staub, F. and Bogousslavsky, J. (2001), 'Fatigue after stroke: A major but neglected issue', *Cerebrovascular Diseases* **12**(2), 75-81.

Stergiou, N. (2018), *Nonlinear analysis for human movement variability*, CRC press.

Stergiou, N. and Decker, L. M. (2011), 'Human movement variability, nonlinear dynamics, and pathology: Is there a connection?', *Hum. Mov. Sci.* .

Stergiou, N., Harbourne, R. T. and Cavanaugh, J. T. (2006), 'Optimal movement variability: A new theoretical perspective for neurologic physical therapy', *J. Neurol. Phys. Ther.* .

Sterr, A. and Furlan, L. (2015), 'A case to be made: Theoretical and empirical arguments for the need to consider fatigue in post-stroke motor rehabilitation', *Neural Regen. Res.* **10**(8), 1195.

Strogatz, S. H. (2018), *Nonlinear dynamics and chaos: With applications to physics, biology, chemistry, and engineering*, CRC press.

Stroke Association (2018), 'State of the nation: Stroke statistics - February 2018'.

Sullivan, G. M. and Feinn, R. (2012), 'Using effect size - or why the P value is not enough', *J. Grad. Med. Educ.* .

Tanaka, M., Ishii, A. and Watanabe, Y. (2015), 'Effects of mental fatigue on brain activity and cognitive performance: A magnetoencephalography study', *Anat Physiol* **4**, 1-5.

Tanaka, M., Shigihara, Y., Ishii, A., Funakura, M., Kanai, E. and Watanabe, Y. (2012), 'Effect of mental fatigue on the central nervous system: An electroencephalography study', *Behav. brain Funct.* **8**(1), 48.

Thickbroom, G., Phillips, B., Morris, I., Byrnes, M. and Mastaglia, F. (1998), 'Isometric force-related activity in sensorimotor cortex measured with functional MRI', *Experimental brain research* **121**(1), 59-64.

Thomas, J. R., Cotten, D. J., Spieth, W. R. and Abraham, N. L. (1975), 'Effects of fatigue on stabilometer performance and learning of males and females.', *Medicine and science in sports* **7**(3), 203-206.

Ting, P.H., Hwang, J.R., Doong, J.L. and Jeng, M.C. (2008), 'Driver fatigue and highway driving: A simulator study', *Physiology & behavior* **94**(3), 448-453.

Tong, S. and Thakor, N. V. (2009), Chapter 3: Single-Channel EEG Analysis, *in* H. Al-Nashash, ed., 'Quant. EEG Anal. methods Clin. Appl.', Artech House, pp. 51-107.

Torsvall, L. and Others (1987), 'Sleepiness on the job: Continuously measured EEG changes in train drivers', *Electroencephalogr. Clin. Neurophysiol.* **66**(6), 502-511.

Tran, Y., Craig, A., Craig, R., Chai, R. and Nguyen, H. (2020), 'The influence of mental fatigue on brain activity: Evidence from a systematic review with meta-analyses', *Psychophysiology* **57**(5), e13554.

Tran, Y., Thuraisingham, R. A., Wijesuriya, N., Nguyen, H. T. and Craig, A. (2007), Detecting neural changes during stress and fatigue effectively: A comparison of spectral analysis and sample entropy, *in* '2007 3rd Int. IEEE/EMBS Conf. Neural Eng.', IEEE, pp. 350-353.

Tran, Y., Wijesuryia, N., Thuraisingham, R. A., Craig, A. and Nguyen, H. T. (2008), Increase in regularity and decrease in variability seen in electroencephalography (EEG) signals from alert to fatigue during a driving simulated task, *in* '2008 30th Annu. Int. Conf. IEEE Eng. Med. Biol. Soc.', IEEE, pp. 1096-1099.

Trejo, L. J., Kubitz, K., Rosipal, R., Kochavi, R. L. and Montgomery, L. D. (2015), 'EEG-based estimation and classification of mental fatigue', *Psychology* **6**(05), 572.

Turner, D. L., Murguialday, A. R., Birbaumer, N., Hoffmann, U. and Luft, A. (2013), 'Neurophysiology of robot-mediated training and therapy: A perspective for future use in clinical populations', *Front. Neurol.* **4**, 184.

Ullsperger, M. and Debener, S. (2010), Using ICA for the analysis of multi-channel EEG data, *in* F. C. Viola, S. Debener, J. Thorne and T. R. Schneider, eds, 'Simultaneous EEG fMRI Rec. Anal. Appl. Rec. Anal. Appl.', Oxford Univ. Press, pp. 121-133.

Urigüen, J. A. and Garcia-Zapirain, B. (2015), 'EEG artifact removal - state-of-the-art and guidelines', *Journal of neural engineering* **12**(3), 031001.

Van Cutsem, J., Marcora, S., De Pauw, K., Bailey, S., Meeusen, R. and Roelands, B. (2017), 'The effects of mental fatigue on physical performance: A systematic review', *Sports medicine* **47**(8), 1569-1588.

Van der Linden, D., Frese, M. and Meijman, T. F. (2003), 'Mental fatigue and the control of cognitive processes: Effects on perseveration and planning', *Acta psychologica* **113**(1), 45-65.

Vázquez, R. R., Velez-Perez, H., Ranta, R., Dorr, V. L., Maquin, D. and Maillard, L. (2012), 'Blind source separation, wavelet denoising and discriminant analysis for EEG artefacts and noise cancelling', *Biomed. Signal Process. Control* **7**(4), 389-400.

Veerbeek, J. M., van Wegen, E., van Peppen, R., van der Wees, P. J., Hendriks, E., Rietberg, M. and Kwakkel, G. (2014), 'What is the evidence for physical therapy poststroke? A systematic review and meta-analysis', *PLOS ONE* **9**(2), e87987.

Vercoulen, J. H., Swanink, C. M., Fennis, J. F., Galama, J. M., van der Meer, J. W. and Bleijenberg, G. (1994), 'Dimensional assessment of chronic fatigue syndrome', *Journal of psychosomatic research* **38**(5), 383-392.

Volpe, B. T., Ferraro, M., Krebs, H. I. and Hogan, N. (2002), 'Robotics in the rehabilitation treatment of patients with stroke', *Curr. Atheroscler. Rep.* **4**(4), 270-276.

Volpe, B. T., Krebs, H. I., Hogan, N., Edelstein, L., Diels, C. and Aisen, M. (2000*a*), 'A novel approach to stroke rehabilitation: Robot-aided sensorimotor stimulation', *Neurology* **54**(10), 1938-1944.

Vorobyov, S. and Cichocki, A. (2002), 'Blind noise reduction for multisensory signals using ICA and subspace filtering, with application to EEG analysis', *Biol. Cybern.* **86**(4), 293-303.

Vuckovic, A., Radivojevic, V., Chen, A. C. and Popovic, D. (2002), 'Automatic recognition of alertness and drowsiness from EEG by an artificial neural network', *Medical engineering & physics* **24**(5), 349-360.

Wade, D. T., Langton-Hewer, R., Wood, V. A., Skilbeck, C. E. and Ismail, H. M. (1983), 'The hemiplegic arm after stroke: Measurement and recovery.', *J. Neurol. Neurosurg. Psychiatry* **46**(6), 521-524.

Wang, F., Wang, H. and Fu, R. (2018), 'Real-time ECG-based detection of fatigue driving using sample entropy', *Entropy* **20**(3), 196.

Wang, F., Wu, S., Zhang, W., Xu, Z., Zhang, Y. and Chu, H. (2020), 'Multiple nonlinear features fusion based driving fatigue detection', *Biomedical Signal Processing and Control* **62**, 102075.

Wang, H., Wu, C., Li, T., He, Y., Chen, P. and Bezerianos, A. (2019), 'Driving fatigue classification based on fusion entropy analysis combining EOG and EEG', *IEEE Access* **7**, 61975-61986.

Wang, J., Wu, Y., Qu, H. and Xu, G. (2014), 'EEG-based fatigue driving detection using correlation dimension', *J. Vibroengineering* **16**(1), 407-413.

Wang, Q., Yang, J., Ren, M. and Zheng, Y. (2006), Driver fatigue detection: A survey, *in* '2006 6th world congress on intelligent control and automation', Vol. 2, IEEE, pp. 8587-8591.

Wang, Y., Cao, L., Hao, D., Rong, Y., Yang, L., Zhang, S., Chen, F. and Zheng, D. (2017), 'Effects of force load, muscle fatigue and extremely low frequency magnetic stimulation on EEG signals during side arm lateral raise task', *Physiol. Meas.* **38**(5), 745.

Waser, M. and Garn, H. (2013), Removing cardiac interference from the electroencephalogram using a modified pan-tompkins algorithm and linear regression, *in* '2013 35th Annual International Conference of the IEEE Engineering in Medicine and Biology Society (EMBC)', IEEE, pp. 2028-2031.

Watson, C., Kirkcaldie, M. and Paxinos, G. (2010), *The brain: An introduction to functional neuroanatomy*, Academic Press.

Welch, P. (1967), 'The use of fast Fourier transform for the estimation of power spectra: A method based on time averaging over short, modified periodograms', *IEEE Trans. audio Electroacoust.* **15**(2), 70-73.

Wen, K., Necsulescu, D. and Sasiadek, J. (2008), 'Haptic force control based on impedance/admittance control aided by visual feedback', *Multimed. Tools Appl.* **37**(1), 39-52.

Widmann, A., Schröger, E. and Maess, B. (2015), 'Digital filter design for electrophysiological data - A practical approach', *Journal of neuroscience methods* **250**, 34-46.

Wilcox, R. R. (2012), *Introduction to Robust Estimation and Hypothesis Testing*, Academic press.

Williams, J. D. and Gruzelier, J. H. (2001), 'Differentiation of hypnosis and relaxation by analysis of narrow band theta and alpha frequencies', *Int. J. Clin. Exp. Hypn.* **49**(3), 185-206.

Williams, J. and Singer, R. N. (1975), 'Muscular fatigue and the learning and performance of a motor control task', *Journal of motor behavior* **7**(4), 265-269.

Woestenburg, J., Verbaten, M. and Slangen, J. (1983), 'The removal of the eye-movement artifact from the EEG by regression analysis in the frequency domain', *Biological psychology* **16**(1-2), 127-147.

Wolf, A., Swift, J. B., Swinney, H. L. and Vastano, J. A. (1985), 'Determining Lyapunov exponents from a time series', *Physica D: Nonlinear Phenomena* **16**(3), 285-317.

Wolpaw, J. R., Birbaumer, N., Heetderks, W. J., McFarland, D. J., Peckham, P. H., Schalk, G., Donchin, E., Quatrano, L. A., Robinson, C. J. and Vaughan, T. M. (2000), 'Brain-computer interface technology: A review of the first international meeting', *IEEE transactions on rehabilitation engineering* **8**(2), 164-173.

Wolpaw, J. R., McFarland, D. J., Neat, G. W. and Forneris, C. A. (1991), 'An EEG-based brain-computer interface for cursor control', *Electroencephalography and clinical neurophysiology* **78**(3), 252-259.

Wu, D.Y., Cai, G., Yuan, Y., Liu, L., Li, G.Q., Song, W.Q. and Wang, M.B. (2011), 'Application of nonlinear dynamics analysis in assessing unconsciousness: A preliminary study', *Clinical Neurophysiology* **122**(3), 490-498.

Xiong, Y., Gao, J., Yang, Y., Yu, X. and Huang, W. (2016), 'Classifying driving fatigue based on combined entropy measure using EEG signals', *International Journal of Control and Automation* **9**(3), 329-338.

Xu, R., Zhang, C., He, F., Zhao, X., Qi, H., Zhou, P., Zhang, L. and Ming, D. (2018), 'How physical activities affect mental fatigue based on EEG energy, connectivity, and complexity', *Front. Neurol.* **9**.

Yamaguchi, S., Tsuchiya, H. and Kobayashi, S. (1994), 'Electrooencephalographic activity associated with shifts of visuospatial attention', *Brain* **117**(3), 553-562.

Yang, C., Bouffard, J., Srinivasan, D., Ghayourmanesh, S., Cantú, H., Begon, M. and Côtéa, J. N. (2018), 'Changes in movement variability and task performance during a fatiguing repetitive pointing task', *J. Biomech.* **76**, 212-219.

Yao, B., Liu, J. Z., Brown, R. W., Sahgal, V. and Yue, G. H. (2009), 'Nonlinear features of surface EEG showing systematic brain signal adaptations with muscle force and fatigue', *Brain Res.* **1272**, 89-98.

Yockey, R. D. (2016), *SPSS demystified: A simple guide and reference*, Routledge.

Zarzoso, V., Nandi, A. K. and Bacharakis, E. (1997), 'Maternal and foetal ECG separation using blind source separation methods', *Math. Med. Biol. A J. IMA* **14**(3), 207-225.

Zhang, C., Wang, H. and Fu, R. (2013), 'Automated detection of driver fatigue based on entropy and complexity measures', *IEEE Transactions on Intelligent Transportation Systems* **15**(1), 168-177.

Zhao, C., Zhao, M., Liu, J. and Zheng, C. (2012), 'Electroencephalogram and electrocardiograph assessment of mental fatigue in a driving simulator', *Accid. Anal. Prev.* **45**, 83-90.

Zhao, D., Wang, Y., Wang, Q. and Wang, X. (2019), 'Comparative analysis of different characteristics of automatic sleep stages', *Computer methods and programs in biomedicine* **175**, 53-72.

Zhu, D.H., Tong, J.J. and Chen, Y.Q. (2008), An ICA-based method for automatic eye blink artifact correction in multi-channel EEG, *in* '2008 International Conference on Information Technology and Applications in Biomedicine', IEEE, pp. 338-341.

Zoefel, B., Huster, R. J. and Herrmann, C. S. (2011), 'Neurofeedback training of the upper alpha frequency band in EEG improves cognitive performance', *Neuroimage* **54**(2), 1427-1431.

Zou, B., Liu, Y., Guo, M. and Wang, Y. (2015), 'EEG-based assessment of stereoscopic 3D visual fatigue caused by vergence-accommodation conflict', *J. Disp. Technol.* **11**(12), 1076-1083.

Appendix A

Supplementary Materials and Results of the Experiment 1

A.1 Paired Samples *t*-test Results of the Robot-Mediated Gross Motor and Fine Motor Interactions

The following sections summarise the results of the paired samples *t*-tests of each EEG spectral feature performed on all eight electrodes under both eyes opened and closed conditions following the robot-mediated gross motor and fine motor interactions.

A.1.1 Modulations in the Relative Delta Band Power

Table A.1: Paired samples *t*-test results for relative delta band power before ('baseline') and after ('recovery') the robot-mediated gross motor interaction with the eyes opened.

Electrode Location	Sample mean ± std		Paired samples *t*-test				Direction of change if significant
	Baseline	Recovery	*t*	*df*	*p*-value	Effect size *r*	
FP1	0.525 ± 0.153	0.497 ± 0.099	0.933	9	0.375	0.297	-
F3	0.542 ± 0.133	0.498 ± 0.064	1.356	9	0.208	0.412	-
FC3	0.555 ± 0.131	0.504 ± 0.073	1.543	9	0.157	0.457	-
C3	0.542 ± 0.109	0.476 ± 0.067	2.593	9	0.029	0.654	↓
C4	0.543 ± 0.138	0.508 ± 0.107	1.285	9	0.231	0.394	-
P3	0.487 ± 0.068	0.445 ± 0.115	2.119	9	0.063	0.577	-
O1	0.497 ± 0.158	0.490 ± 0.158	0.193	9	0.852	0.064	-
T7	0.530 ± 0.201	0.539 ± 0.130	-0.205	9	0.842	0.068	-

Notes. ↓ = significant decrease.

Table A.2: Paired samples *t*-test results for relative delta band power before ('baseline') and after ('recovery') the robot-mediated fine motor interaction with the eyes opened.

Electrode Location	Sample mean ± std		Paired samples *t*-test				Direction of change if significant
	Baseline	Recovery	*t*	*df*	*p*-value	Effect size *r*	
FP1	0.550 ± 0.096	0.504 ± 0.106	3.066	9	0.013	0.715	↓
F3	0.542 ± 0.105	0.533 ± 0.085	0.707	9	0.497	0.229	-
FC3	0.520 ± 0.149	0.499 ± 0.129	1.115	9	0.294	0.348	-
C3	0.546 ± 0.160	0.505 ± 0.106	1.632	9	0.137	0.478	-
C4	0.525 ± 0.117	0.506 ± 0.099	0.518	9	0.617	0.170	-
P3	0.499 ± 0.141	0.480 ± 0.122	0.674	9	0.517	0.219	-
O1	0.490 ± 0.143	0.473 ± 0.116	0.466	9	0.652	0.153	-
T7	0.539 ± 0.100	0.530 ± 0.090	0.300	9	0.771	0.100	-

Notes. ↓ = significant decrease.

Table A.3: Paired samples *t*-test results for relative delta band power before ('baseline') and after ('recovery') the robot-mediated gross motor interaction with the eyes closed.

Electrode Location	Sample mean ± std		Paired samples *t*-test				Direction of change if significant
	Baseline	Recovery	*t*	*df*	*p*-value	Effect size *r*	
FP1	0.361 ± 0.156	0.329 ± 0.111	0.879	9	0.402	0.281	-
F3	0.405 ± 0.174	0.363 ± 0.159	0.785	9	0.453	0.253	-
FC3	0.357 ± 0.151	0.355 ± 0.126	0.122	9	0.906	0.041	-
C3	0.351 ± 0.189	0.337 ± 0.117	0.331	9	0.748	0.110	-
C4	0.346 ± 0.165	0.321 ± 0.126	1.214	9	0.255	0.375	-
P3	0.263 ± 0.133	0.268 ± 0.134	-0.153	9	0.882	0.051	-
O1	0.299 ± 0.147	0.298 ± 0.142	0.021	9	0.984	0.007	-
T7	0.384 ± 0.144	0.379 ± 0.180	0.110	9	0.915	0.037	-

Table A.4: Paired samples *t*-test results for relative delta band power before ('baseline') and after ('recovery') the robot-mediated fine motor interaction with the eyes closed.

Electrode Location	Sample mean ± std		Paired samples *t*-test				Direction of change if significant
	Baseline	Recovery	*t*	*df*	*p*-value	Effect size *r*	
FP1	0.456 ± 0.126	0.443 ± 0.144	0.585	9	0.573	0.191	-
F3	0.462 ± 0.104	0.464 ± 0.134	-0.071	9	0.945	0.024	-
FC3	0.441 ± 0.134	0.467 ± 0.146	-0.892	9	0.395	0.285	-
C3	0.421 ± 0.118	0.431 ± 0.133	-0.323	9	0.754	0.107	-
C4	0.439 ± 0.092	0.430 ± 0.111	0.334	9	0.746	0.111	-
P3	0.346 ± 0.152	0.347 ± 0.158	-0.034	9	0.974	0.011	-
O1	0.356 ± 0.172	0.343 ± 0.197	0.417	9	0.686	0.138	-
T7	0.463 ± 0.122	0.457 ± 0.134	0.279	9	0.786	0.093	-

A.1.2 Modulations in the Relative Theta Band Power

Table A.5: Paired samples *t*-test results for relative theta band power before ('baseline') and after ('recovery') the robot-mediated gross motor interaction with the eyes opened.

Electrode Location	Sample mean ± std		Paired samples *t*-test				Direction of change if significant
	Baseline	Recovery	*t*	*df*	*p*-value	Effect size *r*	
FP1	0.187 ± 0.065	0.193 ± 0.054	-0.330	9	0.749	0.109	-
F3	0.195 ± 0.065	0.217 ± 0.044	-1.245	9	0.245	0.383	-
FC3	0.196 ± 0.057	0.202 ± 0.044	-0.391	9	0.705	0.129	-
C3	0.193 ± 0.049	0.199 ± 0.050	-0.458	9	0.658	0.151	-
C4	0.185 ± 0.059	0.181 ± 0.042	0.360	9	0.727	0.119	-
P3	0.175 ± 0.027	0.163 ± 0.043	1.228	9	0.251	0.379	-
O1	0.160 ± 0.046	0.165 ± 0.050	-0.247	9	0.811	0.082	-
T7	0.155 ± 0.048	0.162 ± 0.036	-0.740	9	0.478	0.239	-

Table A.6: Paired samples *t*-test results for relative theta band power before ('baseline') and after ('recovery') the robot-mediated fine motor interaction with the eyes opened.

Electrode Location	Sample mean ± std		Paired samples *t*-test				Direction of change if significant
	Baseline	Recovery	*t*	*df*	*p*-value	Effect size *r*	
FP1	0.212 ± 0.037	0.222 ± 0.039	-1.886	9	0.092	0.532	-
F3	0.233 ± 0.052	0.235 ± 0.036	-0.202	9	0.844	0.067	-
FC3	0.214 ± 0.044	0.220 ± 0.042	-0.461	9	0.656	0.152	-
C3	0.205 ± 0.059	0.218 ± 0.045	-0.941	9	0.371	0.299	-
C4	0.193 ± 0.033	0.226 ± 0.039	-3.507	9	0.007	0.760	↑
P3	0.199 ± 0.055	0.210 ± 0.050	-0.776	9	0.457	0.250	-
O1	0.207 ± 0.034	0.211 ± 0.044	-0.255	9	0.805	0.085	-
T7	0.185 ± 0.041	0.201 ± 0.045	-1.404	9	0.194	0.424	-

Notes. ↑ = significant increase.

Table A.7: Paired samples *t*-test results for relative theta band power before ('baseline') and after ('recovery') the robot-mediated gross motor interaction with the eyes closed.

Electrode Location	Sample mean ± std		Paired samples *t*-test				Direction of change if significant
	Baseline	Recovery	*t*	*df*	*p*-value	Effect size *r*	
FP1	0.169 ± 0.086	0.176 ± 0.080	-0.532	9	0.608	0.175	-
F3	0.186 ± 0.086	0.185 ± 0.079	0.076	9	0.941	0.025	-
FC3	0.188 ± 0.067	0.184 ± 0.071	0.485	9	0.639	0.160	-
C3	0.165 ± 0.053	0.180 ± 0.067	-1.180	9	0.268	0.366	-
C4	0.168 ± 0.058	0.169 ± 0.068	-0.102	9	0.921	0.034	-
P3	0.145 ± 0.056	0.148 ± 0.056	-0.378	9	0.714	0.125	-
O1	0.132 ± 0.051	0.146 ± 0.064	-1.867	9	0.095	0.528	-
T7	0.158 ± 0.044	0.156 ± 0.064	0.313	9	0.761	0.104	-

Table A.8: Paired samples *t*-test results for relative theta band power before ('baseline') and after ('recovery') the robot-mediated fine motor interaction with the eyes closed.

Electrode Location	Sample mean ± std		Paired samples *t*-test				Direction of change if significant
	Baseline	Recovery	*t*	*df*	*p*-value	Effect size *r*	
FP1	0.222 ± 0.077	0.207 ± 0.051	1.094	9	0.302	0.343	-
F3	0.245 ± 0.088	0.228 ± 0.054	1.129	9	0.288	0.352	-
FC3	0.230 ± 0.098	0.211 ± 0.052	1.071	9	0.312	0.336	-
C3	0.232 ± 0.095	0.212 ± 0.060	1.334	9	0.215	0.406	-
C4	0.220 ± 0.060	0.218 ± 0.056	0.169	9	0.870	0.056	-
P3	0.187 ± 0.081	0.187 ± 0.076	0.055	9	0.958	0.018	-
O1	0.178 ± 0.066	0.182 ± 0.071	-0.660	9	0.526	0.215	-
T7	0.214 ± 0.099	0.198 ± 0.047	0.712	9	0.494	0.231	-

A.1.3 Modulations in the Relative Alpha Band Power

Table A.9: Paired samples *t*-test results for relative alpha band power before ('baseline') and after ('recovery') the robot-mediated gross motor interaction with the eyes opened.

Electrode Location	Sample mean ± std		Paired samples *t*-test				Direction of change if significant
	Baseline	Recovery	*t*	*df*	*p*-value	Effect size *r*	
FP1	0.212 ± 0.095	0.236 ± 0.093	-1.339	9	0.213	0.408	-
F3	0.187 ± 0.069	0.210 ± 0.057	-1.426	9	0.188	0.429	-
FC3	0.180 ± 0.068	0.225 ± 0.069	-2.378	9	0.041	0.621	↑
C3	0.198 ± 0.070	0.259 ± 0.095	-3.148	9	0.012	0.724	↑
C4	0.211 ± 0.094	0.249 ± 0.091	-2.163	9	0.059	0.585	-
P3	0.271 ± 0.094	0.330 ± 0.154	-2.646	9	0.027	0.661	↑
O1	0.259 ± 0.136	0.277 ± 0.171	-0.556	9	0.592	0.182	-
T7	0.212 ± 0.116	0.222 ± 0.085	-0.430	9	0.677	0.142	-

Notes. ↑ = significant increase.

Table A.10: Paired samples *t*-test results for relative alpha band power before ('baseline') and after ('recovery') the robot-mediated fine motor interaction with the eyes opened.

Electrode Location	Sample mean ± std		Paired samples *t*-test				Direction of change if significant
	Baseline	Recovery	*t*	*df*	*p*-value	Effect size *r*	
FP1	0.179 ± 0.075	0.211 ± 0.104	-2.871	9	0.018	0.691	↑
F3	0.171 ± 0.078	0.175 ± 0.082	-0.569	9	0.583	0.186	-
FC3	0.183 ± 0.089	0.190 ± 0.089	-0.776	9	0.457	0.250	-
C3	0.202 ± 0.127	0.227 ± 0.117	-2.555	9	0.031	0.648	↑
C4	0.202 ± 0.066	0.207 ± 0.106	-0.227	9	0.826	0.075	-
P3	0.242 ± 0.107	0.259 ± 0.137	-0.782	9	0.454	0.252	-
O1	0.223 ± 0.109	0.251 ± 0.142	-1.065	9	0.315	0.335	-
T7	0.187 ± 0.067	0.194 ± 0.077	-0.455	9	0.660	0.150	-

Notes. ↑ = significant increase.

Table A.11: Paired samples *t*-test results for relative alpha band power before ('baseline') and after ('recovery') the robot-mediated gross motor interaction with the eyes closed.

Electrode Location	Sample mean ± std		Paired samples *t*-test				Direction of change if significant
	Baseline	Recovery	*t*	*df*	*p*-value	Effect size *r*	
FP1	0.419 ± 0.199	0.450 ± 0.168	-0.967	9	0.359	0.307	-
F3	0.361 ± 0.198	0.406 ± 0.199	-0.959	9	0.363	0.304	-
FC3	0.400 ± 0.185	0.404 ± 0.167	-0.159	9	0.877	0.053	-
C3	0.427 ± 0.188	0.429 ± 0.166	-0.043	9	0.967	0.014	-
C4	0.436 ± 0.174	0.463 ± 0.160	-1.115	9	0.294	0.348	-
P3	0.543 ± 0.170	0.536 ± 0.184	0.188	9	0.855	0.063	-
O1	0.506 ± 0.181	0.500 ± 0.182	0.202	9	0.845	0.067	-
T7	0.379 ± 0.152	0.397 ± 0.170	-0.448	9	0.664	0.148	-

Table A.12: Paired samples *t*-test results for relative alpha band power before ('baseline') and after ('recovery') the robot-mediated fine motor interaction with the eyes closed.

Electrode Location	Sample mean ± std		Paired samples *t*-test				Direction of change if significant
	Baseline	Recovery	*t*	*df*	*p*-value	Effect size *r*	
FP1	0.278 ± 0.142	0.303 ± 0.150	-0.835	9	0.425	0.268	-
F3	0.250 ± 0.112	0.263 ± 0.135	-0.390	9	0.706	0.129	-
FC3	0.245 ± 0.107	0.246 ± 0.124	-0.017	9	0.987	0.006	-
C3	0.304 ± 0.103	0.311 ± 0.140	-0.206	9	0.841	0.069	-
C4	0.297 ± 0.112	0.306 ± 0.133	-0.350	9	0.734	0.116	-
P3	0.420 ± 0.169	0.427 ± 0.178	-0.175	9	0.865	0.058	-
O1	0.416 ± 0.212	0.428 ± 0.212	-0.353	9	0.732	0.117	-
T7	0.254 ± 0.098	0.281 ± 0.131	-1.103	9	0.299	0.345	-

A.1.4 Modulations in the Relative Beta Band Power

Table A.13: Paired samples *t*-test results for relative beta band power before ('baseline') and after ('recovery') the robot-mediated gross motor interaction with the eyes opened.

Electrode Location	Sample mean ± std		Paired samples *t*-test				Direction of change if significant
	Baseline	Recovery	*t*	*df*	*p*-value	Effect size *r*	
FP1	0.077 ± 0.047	0.074 ± 0.040	0.216	9	0.834	0.072	-
F3	0.076 ± 0.043	0.075 ± 0.034	0.164	9	0.873	0.055	-
FC3	0.069 ± 0.044	0.069 ± 0.033	-0.023	9	0.982	0.008	-
C3	0.067 ± 0.041	0.066 ± 0.033	0.178	9	0.862	0.059	-
C4	0.061 ± 0.037	0.062 ± 0.035	-0.112	9	0.914	0.037	-
P3	0.067 ± 0.038	0.062 ± 0.035	0.967	9	0.359	0.307	-
O1	0.083 ± 0.050	0.069 ± 0.026	1.089	9	0.305	0.341	-
T7	0.103 ± 0.091	0.077 ± 0.038	1.189	9	0.265	0.368	-

Table A.14: Paired samples *t*-test results for relative beta band power before ('baseline') and after ('recovery') the robot-mediated fine motor interaction with the eyes opened.

Electrode Location	Sample mean ± std		Paired samples *t*-test				Direction of change if significant
	Baseline	Recovery	*t*	*df*	*p*-value	Effect size *r*	
FP1	0.060 ± 0.019	0.062 ± 0.032	-0.184	9	0.858	0.061	-
F3	0.054 ± 0.022	0.057 ± 0.024	-0.480	9	0.643	0.158	-
FC3	0.083 ± 0.090	0.091 ± 0.113	-0.942	9	0.371	0.300	-
C3	0.047 ± 0.021	0.050 ± 0.013	-0.495	9	0.633	0.163	-
C4	0.080 ± 0.072	0.061 ± 0.029	0.821	9	0.433	0.264	-
P3	0.061 ± 0.036	0.052 ± 0.015	1.016	9	0.336	0.321	-
O1	0.079 ± 0.061	0.065 ± 0.023	0.812	9	0.438	0.261	-
T7	0.089 ± 0.059	0.074 ± 0.039	0.946	9	0.369	0.301	-

Table A.15: Paired samples *t*-test results for relative beta band power before ('baseline') and after ('recovery') the robot-mediated gross motor interaction with the eyes closed.

Electrode Location	Sample mean ± std		Paired samples *t*-test				Direction of change if significant
	Baseline	Recovery	*t*	*df*	*p*-value	Effect size *r*	
FP1	0.051 ± 0.032	0.044 ± 0.022	1.559	9	0.153	0.461	-
F3	0.048 ± 0.029	0.046 ± 0.025	0.400	9	0.699	0.132	-
FC3	0.055 ± 0.032	0.058 ± 0.036	-0.638	9	0.539	0.208	-
C3	0.057 ± 0.037	0.054 ± 0.028	0.674	9	0.517	0.219	-
C4	0.050 ± 0.027	0.047 ± 0.023	1.442	9	0.183	0.433	-
P3	0.050 ± 0.026	0.048 ± 0.027	0.427	9	0.679	0.141	-
O1	0.063 ± 0.043	0.056 ± 0.033	0.873	9	0.405	0.279	-
T7	0.079 ± 0.051	0.068 ± 0.055	0.838	9	0.424	0.269	-

Table A.16: Paired samples *t*-test results for relative beta band power before ('baseline') and after ('recovery') the robot-mediated fine motor interaction with the eyes closed.

Electrode Location	Sample mean ± std		Paired samples *t*-test				Direction of change if significant
	Baseline	Recovery	*t*	*df*	*p*-value	Effect size *r*	
FP1	0.044 ± 0.015	0.047 ± 0.017	-0.982	9	0.352	0.311	-
F3	0.042 ± 0.013	0.044 ± 0.016	-1.061	9	0.316	0.333	-
FC3	0.083 ± 0.123	0.077 ± 0.100	0.803	9	0.443	0.259	-
C3	0.043 ± 0.014	0.046 ± 0.017	-1.010	9	0.339	0.319	-
C4	0.045 ± 0.011	0.046 ± 0.014	-0.452	9	0.662	0.149	-
P3	0.046 ± 0.027	0.039 ± 0.019	1.619	9	0.140	0.475	-
O1	0.050 ± 0.024	0.047 ± 0.022	1.304	9	0.224	0.399	-
T7	0.068 ± 0.033	0.065 ± 0.028	0.517	9	0.618	0.170	-

A.1.5 Modulations in the $(\theta+\alpha)/\beta$ Power Ratio

Table A.17: Paired samples *t*-test results for $(\theta+\alpha)/\beta$ power ratio before ('baseline') and after ('recovery') the robot-mediated gross motor interaction with the eyes opened.

Electrode Location	Sample mean ± std		Paired samples *t*-test				Direction of change if significant
	Baseline	Recovery	*t*	*df*	*p*-value	Effect size *r*	
FP1	7.548 ± 5.060	7.850 ± 5.015	-0.467	9	0.652	0.154	-
F3	6.851 ± 3.852	7.350 ± 3.936	-0.900	9	0.392	0.287	-
FC3	7.751 ± 4.308	7.714 ± 3.420	0.071	9	0.945	0.024	-
C3	8.151 ± 4.349	8.923 ± 4.167	-2.787	9	0.021	0.681	↑
C4	8.564 ± 4.450	8.910 ± 4.183	-0.666	9	0.522	0.217	-
P3	9.292 ± 5.588	11.021 ± 7.652	-1.784	9	0.108	0.511	-
O1	7.362 ± 5.148	8.060 ± 7.137	-0.546	9	0.598	0.179	-
T7	6.861 ± 4.868	6.603 ± 3.832	0.449	9	0.664	0.148	-

Notes. ↑ = significant increase.

Table A.18: Paired samples *t*-test results for $(\theta+\alpha)/\beta$ power ratio before ('baseline') and after ('recovery') the robot-mediated fine motor interaction with the eyes opened.

Electrode Location	Sample mean ± std		Paired samples *t*-test				Direction of change if significant
	Baseline	Recovery	*t*	*df*	*p*-value	Effect size *r*	
FP1	7.379 ± 2.699	8.633 ± 4.328	-1.434	9	0.185	0.431	-
F3	8.743 ± 3.452	8.516 ± 4.333	0.212	9	0.837	0.070	-
FC3	7.168 ± 2.927	7.640 ± 4.172	-0.559	9	0.590	0.183	-
C3	9.528 ± 2.618	9.372 ± 2.468	0.203	9	0.844	0.068	-
C4	7.154 ± 3.332	8.441 ± 3.909	-1.422	9	0.189	0.428	-
P3	9.815 ± 6.243	9.904 ± 4.316	-0.078	9	0.940	0.026	-
O1	7.859 ± 4.842	8.232 ± 4.491	-0.519	9	0.616	0.170	-
T7	5.967 ± 3.064	6.675 ± 4.070	-0.647	9	0.534	0.211	-

Table A.19: Paired samples *t*-test results for $(\theta+\alpha)/\beta$ power ratio before ('baseline') and after ('recovery') the robot-mediated gross motor interaction with the eyes closed.

Electrode Location	Sample mean ± std		Paired samples *t*-test				Direction of change if significant
	Baseline	Recovery	*t*	*df*	*p*-value	Effect size *r*	
FP1	19.145 ± 17.619	19.070 ± 12.484	0.038	9	0.970	0.013	-
F3	16.755 ± 14.749	17.519 ± 12.660	-0.499	9	0.629	0.164	-
FC3	16.218 ± 13.607	16.239 ± 12.963	-0.020	9	0.985	0.007	-
C3	15.497 ± 11.232	16.378 ± 11.932	-1.071	9	0.312	0.336	-
C4	16.460 ± 11.264	17.479 ± 10.113	-0.654	9	0.529	0.213	-
P3	18.711 ± 11.593	20.291 ± 13.516	-1.621	9	0.139	0.475	-
O1	14.799 ± 11.778	17.310 ± 13.476	-1.729	9	0.118	0.499	-
T7	9.988 ± 6.230	12.761 ± 8.061	-2.077	9	0.068	0.569	-

Table A.20: Paired samples *t*-test results for $(\theta+\alpha)/\beta$ power ratio before ('baseline') and after ('recovery') the robot-mediated fine motor interaction with the eyes closed.

Electrode Location	Sample mean ± std		Paired samples *t*-test				Direction of change if significant
	Baseline	Recovery	*t*	*df*	*p*-value	Effect size *r*	
FP1	12.887 ± 5.788	12.058 ± 4.940	1.291	9	0.229	0.395	-
F3	12.968 ± 4.134	12.209 ± 3.598	1.660	9	0.131	0.484	-
FC3	11.381 ± 5.876	10.642 ± 4.874	1.031	9	0.329	0.325	-
C3	14.359 ± 6.668	12.844 ± 4.036	1.001	9	0.343	0.317	-
C4	12.657 ± 5.045	13.012 ± 4.444	-0.530	9	0.609	0.174	-
P3	18.999 ± 14.295	19.802 ± 10.852	-0.530	9	0.609	0.174	-
O1	18.301 ± 16.783	18.489 ± 14.232	-0.157	9	0.879	0.052	-
T7	9.487 ± 6.754	8.993 ± 3.930	0.270	9	0.793	0.090	-

A.1.6 Modulations in the α/β Power Ratio

Table A.21: Paired samples *t*-test results for α/β power ratio before ('baseline') and after ('recovery') the robot-mediated gross motor interaction with the eyes opened.

Electrode Location	Sample mean ± std		Paired samples *t*-test				Direction of change if significant
	Baseline	Recovery	*t*	*df*	*p*-value	Effect size *r*	
FP1	4.189 ± 3.587	4.408 ± 3.819	-0.447	9	0.665	0.147	-
F3	3.459 ± 2.346	3.679 ± 2.324	-0.589	9	0.570	0.193	-
FC3	3.706 ± 2.348	4.121 ± 2.231	-1.045	9	0.323	0.329	-
C3	4.213 ± 2.612	4.997 ± 2.812	-2.403	9	0.040	0.625	↑
C4	4.593 ± 3.012	5.290 ± 3.208	-1.690	9	0.125	0.491	-
P3	5.900 ± 4.482	7.735 ± 7.199	-1.803	9	0.105	0.515	-
O1	4.638 ± 4.408	5.410 ± 7.098	-0.692	9	0.506	0.225	-
T7	3.363 ± 1.964	3.559 ± 1.762	-0.620	9	0.550	0.202	-

Notes. ↑ = significant increase.

Table A.22: Paired samples *t*-test results for α/β power ratio before ('baseline') and after ('recovery') the robot-mediated fine motor interaction with the eyes opened.

Electrode Location	Sample mean ± std		Paired samples *t*-test				Direction of change if significant
	Baseline	Recovery	*t*	*df*	*p*-value	Effect size *r*	
FP1	3.271 ± 1.538	4.074 ± 2.410	-1.877	9	0.093	0.530	-
F3	3.585 ± 1.637	3.499 ± 2.128	0.171	9	0.868	0.057	-
FC3	3.158 ± 1.699	3.396 ± 2.134	-0.649	9	0.532	0.211	-
C3	4.391 ± 1.905	4.602 ± 1.909	-0.694	9	0.505	0.225	-
C4	3.579 ± 1.988	3.854 ± 2.363	-0.632	9	0.543	0.206	-
P3	5.276 ± 3.570	5.354 ± 2.984	-0.132	9	0.898	0.044	-
O1	4.021 ± 3.108	4.432 ± 3.055	-0.993	9	0.347	0.314	-
T7	2.818 ± 1.469	3.021 ± 1.774	-0.478	9	0.644	0.157	-

Table A.23: Paired samples *t*-test results for α/β power ratio before ('baseline') and after ('recovery') the robot-mediated gross motor interaction with the eyes closed.

Electrode Location	Sample mean ± std		Paired samples *t*-test				Direction of change if significant
	Baseline	Recovery	*t*	*df*	*p*-value	Effect size *r*	
FP1	15.147 ± 16.815	14.551 ± 12.086	0.329	9	0.750	0.109	-
F3	12.151 ± 14.170	12.581 ± 12.422	-0.285	9	0.782	0.095	-
FC3	11.808 ± 12.969	11.997 ± 12.168	-0.180	9	0.862	0.060	-
C3	11.104 ± 10.346	12.224 ± 11.022	-1.279	9	0.233	0.392	-
C4	12.282 ± 10.396	13.160 ± 9.158	-0.599	9	0.564	0.196	-
P3	15.001 ± 10.818	16.461 ± 12.554	-1.578	9	0.149	0.466	-
O1	12.208 ± 11.258	14.047 ± 12.914	-1.671	9	0.129	0.487	-
T7	7.223 ± 5.388	9.182 ± 6.898	-1.601	9	0.144	0.471	-

Table A.24: Paired samples *t*-test results for α/β power ratio before ('baseline') and after ('recovery') the robot-mediated fine motor interaction with the eyes closed.

Electrode Location	Sample mean ± std		Paired samples *t*-test				Direction of change if significant
	Baseline	Recovery	*t*	*df*	*p*-value	Effect size *r*	
FP1	7.379 ± 4.900	7.100 ± 4.183	0.451	9	0.662	0.149	-
F3	6.672 ± 3.429	6.294 ± 2.882	0.629	9	0.545	0.205	-
FC3	5.913 ± 3.638	5.543 ± 2.955	0.756	9	0.469	0.244	-
C3	8.069 ± 3.847	7.462 ± 3.397	0.733	9	0.482	0.237	-
C4	7.417 ± 4.081	7.488 ± 3.879	-0.124	9	0.904	0.041	-
P3	13.360 ± 11.187	13.745 ± 9.110	-0.310	9	0.763	0.103	-
O1	13.742 ± 14.542	13.464 ± 12.315	0.244	9	0.813	0.081	-
T7	4.845 ± 2.716	4.988 ± 2.465	-0.268	9	0.795	0.089	-

A.1.7 Modulations in the $(\theta+\alpha)/(\alpha+\beta)$ Power Ratio

Table A.25: Paired samples *t*-test results for $(\theta+\alpha)/(\alpha+\beta)$ power ratio before ('baseline') and after ('recovery') the robot-mediated gross motor interaction with the eyes opened.

Electrode Location	Sample mean ± std		Paired samples *t*-test				Direction of change if significant
	Baseline	Recovery	*t*	*df*	*p*-value	Effect size *r*	
FP1	1.490 ± 0.248	1.481 ± 0.317	0.107	9	0.917	0.036	-
F3	1.553 ± 0.246	1.562 ± 0.274	-0.115	9	0.911	0.038	-
FC3	1.649 ± 0.327	1.520 ± 0.266	1.712	9	0.121	0.496	-
C3	1.579 ± 0.298	1.517 ± 0.304	0.916	9	0.384	0.292	-
C4	1.585 ± 0.303	1.467 ± 0.252	1.925	9	0.086	0.540	-
P3	1.392 ± 0.247	1.337 ± 0.251	1.277	9	0.234	0.392	-
O1	1.345 ± 0.296	1.377 ± 0.243	-0.402	9	0.697	0.133	-
T7	1.451 ± 0.546	1.390 ± 0.291	0.611	9	0.557	0.200	-

Table A.26: Paired samples *t*-test results for $(\theta+\alpha)/(\alpha+\beta)$ power ratio before ('baseline') and after ('recovery') the robot-mediated fine motor interaction with the eyes opened.

Electrode Location	Sample mean ± std		Paired samples *t*-test				Direction of change if significant
	Baseline	Recovery	*t*	*df*	*p*-value	Effect size *r*	
FP1	1.749 ± 0.344	1.715 ± 0.355	0.444	9	0.667	0.146	-
F3	1.944 ± 0.469	1.920 ± 0.417	0.420	9	0.684	0.139	-
FC3	1.717 ± 0.451	1.696 ± 0.499	0.294	9	0.775	0.098	-
C3	1.868 ± 0.467	1.756 ± 0.324	1.201	9	0.260	0.372	-
C4	1.531 ± 0.330	1.788 ± 0.364	-1.988	9	0.078	0.552	-
P3	1.532 ± 0.251	1.633 ± 0.296	-1.139	9	0.284	0.355	-
O1	1.564 ± 0.375	1.576 ± 0.274	-0.146	9	0.887	0.049	-
T7	1.498 ± 0.442	1.613 ± 0.361	-1.080	9	0.308	0.339	-

Table A.27: Paired samples *t*-test results for $(\theta+\alpha)/(\alpha+\beta)$ power ratio before ('baseline') and after ('recovery') the robot-mediated gross motor interaction with the eyes closed.

Electrode Location	Sample mean ± std		Paired samples *t*-test				Direction of change if significant
	Baseline	Recovery	*t*	*df*	*p*-value	Effect size *r*	
FP1	1.359 ± 0.378	1.400 ± 0.422	-0.853	9	0.416	0.273	-
F3	1.479 ± 0.435	1.497 ± 0.476	-0.224	9	0.828	0.074	-
FC3	1.420 ± 0.370	1.384 ± 0.365	0.728	9	0.485	0.236	-
C3	1.384 ± 0.414	1.346 ± 0.292	0.392	9	0.704	0.130	-
C4	1.326 ± 0.298	1.328 ± 0.304	-0.038	9	0.970	0.013	-
P3	1.226 ± 0.264	1.225 ± 0.215	0.026	9	0.980	0.009	-
O1	1.137 ± 0.096	1.198 ± 0.130	-1.458	9	0.179	0.437	-
T7	1.242 ± 0.275	1.311 ± 0.349	-1.014	9	0.337	0.320	-

Table A.28: Paired samples *t*-test results for $(\theta+\alpha)/(\alpha+\beta)$ power ratio before ('baseline') and after ('recovery') the robot-mediated fine motor interaction with the eyes closed.

Electrode Location	Sample mean ± std		Paired samples *t*-test				Direction of change if significant
	Baseline	Recovery	*t*	*df*	*p*-value	Effect size *r*	
FP1	1.664 ± 0.344	1.610 ± 0.407	0.531	9	0.608	0.174	-
F3	1.817 ± 0.404	1.787 ± 0.439	0.260	9	0.800	0.086	-
FC3	1.621 ± 0.558	1.602 ± 0.489	0.168	9	0.870	0.056	-
C3	1.619 ± 0.366	1.596 ± 0.362	0.266	9	0.796	0.088	-
C4	1.608 ± 0.325	1.632 ± 0.390	-0.293	9	0.776	0.097	-
P3	1.371 ± 0.246	1.441 ± 0.350	-1.012	9	0.338	0.320	-
O1	1.331 ± 0.173	1.359 ± 0.227	-0.804	9	0.442	0.259	-
T7	1.524 ± 0.420	1.513 ± 0.357	0.094	9	0.927	0.031	-

A.1.8 Modulations in the θ/β Power Ratio

Table A.29: Paired samples *t*-test results for θ/β power ratio before ('baseline') and after ('recovery') the robot-mediated gross motor interaction with the eyes opened.

Electrode Location	Sample mean ± std		Paired samples *t*-test				Direction of change if significant
	Baseline	Recovery	*t*	*df*	*p*-value	Effect size *r*	
FP1	3.359 ± 1.742	3.442 ± 1.899	-0.243	9	0.813	0.081	-
F3	3.392 ± 1.664	3.670 ± 1.895	-0.840	9	0.423	0.270	-
FC3	4.045 ± 2.219	3.593 ± 1.485	1.395	9	0.196	0.422	-
C3	3.938 ± 1.962	3.926 ± 1.986	0.046	9	0.964	0.015	-
C4	3.971 ± 1.875	3.620 ± 1.386	1.086	9	0.306	0.340	-
P3	3.392 ± 1.701	3.286 ± 1.512	0.473	9	0.648	0.156	-
O1	2.724 ± 1.638	2.650 ± 1.018	0.187	9	0.856	0.062	-
T7	3.498 ± 3.193	3.044 ± 2.268	1.173	9	0.271	0.364	-

Table A.30: Paired samples *t*-test results for θ/β power ratio before ('baseline') and after ('recovery') the robot-mediated fine motor interaction with the eyes opened.

Electrode Location	Sample mean ± std		Paired samples *t*-test				Direction of change if significant
	Baseline	Recovery	*t*	*df*	*p*-value	Effect size *r*	
FP1	4.108 ± 1.610	4.559 ± 2.294	-0.900	9	0.392	0.287	-
F3	5.158 ± 2.427	5.017 ± 2.525	0.234	9	0.820	0.078	-
FC3	4.010 ± 1.629	4.244 ± 2.317	-0.457	9	0.659	0.151	-
C3	5.137 ± 1.899	4.770 ± 1.552	0.693	9	0.506	0.225	-
C4	3.575 ± 1.599	4.587 ± 1.959	-1.856	9	0.096	0.526	-
P3	4.538 ± 2.882	4.550 ± 2.013	-0.017	9	0.987	0.006	-
O1	3.838 ± 2.023	3.800 ± 1.972	0.079	9	0.939	0.026	-
T7	3.149 ± 1.815	3.654 ± 2.442	-0.719	9	0.490	0.233	-

Table A.31: Paired samples *t*-test results for θ/β power ratio before ('baseline') and after ('recovery') the robot-mediated gross motor interaction with the eyes closed.

Electrode Location	Sample mean ± std		Paired samples *t*-test				Direction of change if significant
	Baseline	Recovery	*t*	*df*	*p*-value	Effect size *r*	
FP1	3.998 ± 1.584	4.519 ± 1.671	-1.869	9	0.094	0.529	-
F3	4.604 ± 1.888	4.938 ± 2.237	-1.456	9	0.179	0.437	-
FC3	4.410 ± 2.029	4.242 ± 2.041	0.754	9	0.470	0.244	-
C3	4.392 ± 2.711	4.154 ± 1.922	0.446	9	0.666	0.147	-
C4	4.179 ± 1.955	4.319 ± 2.027	-0.562	9	0.588	0.184	-
P3	3.710 ± 2.135	3.830 ± 1.974	-0.547	9	0.598	0.179	-
O1	2.591 ± 1.212	3.264 ± 1.640	-1.442	9	0.183	0.433	-
T7	2.764 ± 1.425	3.579 ± 2.108	-2.225	9	0.053	0.596	-

Table A.32: Paired samples *t*-test results for θ/β power ratio before ('baseline') and after ('recovery') the robot-mediated fine motor interaction with the eyes closed.

Electrode Location	Sample mean ± std		Paired samples *t*-test				Direction of change if significant
	Baseline	Recovery	*t*	*df*	*p*-value	Effect size *r*	
FP1	5.508 ± 2.073	4.958 ± 1.830	1.159	9	0.276	0.360	-
F3	6.296 ± 2.266	5.916 ± 2.156	0.869	9	0.407	0.278	-
FC3	5.468 ± 3.332	5.099 ± 2.653	0.578	9	0.577	0.189	-
C3	6.290 ± 4.223	5.381 ± 2.160	0.962	9	0.361	0.305	-
C4	5.240 ± 1.859	5.524 ± 2.315	-0.615	9	0.554	0.201	-
P3	5.639 ± 4.446	6.058 ± 3.607	-0.721	9	0.489	0.234	-
O1	4.560 ± 3.346	5.025 ± 3.516	-1.882	9	0.093	0.531	-
T7	4.641 ± 4.577	4.005 ± 2.371	0.466	9	0.652	0.153	-

Appendix B

Supplementary Materials and Results of the Experiment 2

B.1 Target Point Locations in the Virtual 3D Room

The target points that were used for the visuomotor tracking task explained in Section 5.1.3 is given in Table B.1.

Table B.1: Target point locations and reaching order

Loop	Point reach order	Point No	x/m	y/m	z/m
Forward Loop	1	1	0.12	0	-0.19
	2	2	-0.01	-0.125	0.015
	3	3	-0.14	0	-0.19
	4	4	0.028	-0.11	-0.005
	5	5	0.172	0.05	-0.173
	6	6	-0.017	-0.113	-0.062
	7	7	-0.151	0.102	-0.165
	8	8	-0.056	-0.123	-0.043
	9	9	0.048	0.079	-0.195
	10	10	0.156	-0.102	-0.021
	11	11	-0.018	-0.218	0.155
	12	12	-0.146	-0.053	-0.021
	13	13	0	0.099	-0.195
Reverse Loop	14	12	-0.146	-0.053	-0.021
	15	11	-0.018	-0.218	0.155
	16	10	0.156	-0.102	-0.021
	17	9	0.048	0.079	-0.195
	18	8	-0.056	-0.123	-0.043
	19	7	-0.151	0.102	-0.165
	20	6	-0.017	-0.113	-0.062
	21	5	0.172	0.05	-0.173
	22	4	0.028	-0.11	-0.005
	23	3	-0.14	0	-0.19
	24	2	-0.01	-0.125	0.015
	25	1	0.12	0	-0.19

B.2 Complete Analysis of the Two-way Repeated Measures ANOVA Performed on All EEG Features

Table B.2 summarises the two-way repeated measures ANOVA results of all EEG feature considered in this experiment (δ_{relative}, θ_{relative}, α_{relative}, β_{relative}, $(\theta+\alpha)/\beta$, α/β, $(\theta+\alpha)/(\alpha+\beta)$, θ/β, δ/α, largest Lyapunov exponent and approximate entropy). In general, significant main effect of the electrode locations and significant interaction between measurement time and electrode locations were observed on all EEG features. The measurement time effects were significant only on δ_{relative}, α_{relative}, $(\theta+\alpha)/\beta$, α/β, $(\theta+\alpha)/(\alpha+\beta)$, δ/α and largest Lyapunov exponent values. Table B.3 summarises the pairwise comparison of the EEG features that showed a significant measurement time effect. In general, δ_{relative}, α_{relative}, $(\theta+\alpha)/\beta$, α/β, $(\theta+\alpha)/(\alpha+\beta)$, δ/α showed a significant difference between baseline and level 1, and between level 5 and recovery, thereby suggesting that there is a significant change in the EEG features at the onset of the task and when moving to the resting state following the robot-mediated interaction. Furthermore, the majority of the features (i.e., δ_{relative}, α_{relative}, $(\theta+\alpha)/(\alpha+\beta)$, δ/α and largest Lyapunov exponent) showed significant variations between level 1 and level 5.

Comparison of the sample mean of each EEG feature across all measurement times and EEG electrodes are shown in Figures B.1 to B.12, respectively in Section B.2.13. Tables B.4 to B.15 in Section B.2.14 summarise the p-values obtained from the pairwise comparison of the interaction between measurement time and electrode locations of all EEG features. The topographical distribution of the significant differences of all EEG features before, during and after the visuomotor tracking task are shown in Figures B.13 to B.23, respectively in Section B.2.15. The following sections discuss the analysis of EEG feature variations in detail.

B.2.1 Modulations in δ_{relative} Before, During and After the Robot-Mediated Visuomotor Tracking Task

Two-way repeated measures ANOVA on δ_{relative} indicated that there was a significant main effect in measurement time (F(6, 144) = 24.055, p = 0.000, ε = 0.352, η_P^2 = 0.501, power = 1.000) and electrode location (F(31, 744) = 8.379, p = 0.000, ε = 0.134, η_P^2 = 0.259, power = 0.999) with a larger effect size and a sufficient power (i.e, over 80%) to find the statistical differences in the main effects. It was visible that the sample mean of δ_{relative} on all electrodes increased following the onset of robot-mediated interaction (i.e., from baseline to level 1) and decreased following the interaction (i.e., from level 5 to recovery). The δ_{relative} during

Table B.2: Two-way repeated measures ANOVA results of the EEG feature modulations with fatigue in robot-mediated visuomotor tracking task.

EEG Features	Measurement time						Electrode location						Measurement time x Electrode location					
	df	F	ε	p-value	η_p^2	Observed power	df	F	ε	p-value	η_p^2	Observed power	df	F	ε	p-value	η_p^2	Observed power
Relative δ band power	6	24.055	0.352	0.000	0.501	1.000	31	8.379	0.134	0.000	0.259	0.999	186	4.900	0.046	0.000	0.170	0.999
Relative θ band power	6	1.505	0.324	0.233	0.059	0.301	31	27.613	0.057	0.000	0.535	1.000	186	2.458	0.039	0.018	0.093	0.874
Relative α band power	6	26.613	0.291	0.000	0.526	1.000	31	11.870	0.148	0.000	0.331	1.000	186	6.182	0.026	0.000	0.205	0.995
Relative β band power	6	0.317	0.347	0.738	0.013	0.099	31	12.473	0.108	0.000	0.342	1.000	186	2.304	0.040	0.026	0.088	0.852
$(\theta+\alpha)/\beta$	6	6.350	0.259	0.007	0.209	0.812	31	11.810	0.117	0.000	0.330	1.000	186	5.920	0.018	0.001	0.198	0.962
α/β	6	12.596	0.235	0.000	0.344	0.974	31	8.502	0.097	0.000	0.262	0.991	186	6.563	0.014	0.001	0.215	0.947
$(\theta+\alpha)/(\alpha+\beta)$	6	20.602	0.427	0.000	0.462	1.000	31	32.172	0.086	0.000	0.573	1.000	186	2.310	0.048	0.017	0.088	0.900
θ/β	6	0.937	0.415	0.415	0.038	0.225	31	24.893	0.093	0.000	0.509	1.000	186	2.336	0.040	0.023	0.089	0.860
δ/α	6	32.673	0.475	0.000	0.577	1.000	31	6.945	0.128	0.000	0.224	0.992	186	2.248	0.064	0.010	0.086	0.950
Largest Lyapunov exponent	6	21.790	0.445	0.000	0.476	1.000	31	24.050	0.127	0.000	0.501	1.000	186	2.660	0.053	0.005	0.100	0.958
Approximate entropy	6	2.112	0.368	0.126	0.081	0.436	31	13.955	0.167	0.000	0.368	1.000	186	6.620	0.041	0.000	0.216	1.000
LLyapExp/α_{Relative}	6	21.284	0.520	0.000	0.470	1.000	31	12.912	0.080	0.000	0.350	0.999	186	2.336	0.057	0.010	0.089	0.941

Notes. Cell colours blue, green and red represents p-values < 0.05, < 0.01, and < 0.001, respectively.

Table B.3: Pairwise comparison of the significant measurement time effect on EEG features.

Measurement time		$\delta_{relative}$	$\alpha_{relative}$	$(\theta+\alpha)/\beta$	α/β	$(\theta+\alpha)/(\alpha+\beta)$	δ/α	Largest Lyapunov Exponent	LLyapExp/$\alpha_{relative}$
Baseline	**Level 1**	0.000	0.000	0.028	0.001	0.000	0.000	0.000	0.000
Level 1	**Level 2**	0.369	0.153	0.834	0.125	0.016	0.056	0.189	0.086
	Level 3	0.299	0.063	0.626	0.062	0.032	0.063	0.088	0.094
	Level 4	0.117	0.013	0.273	0.018	0.006	0.039	0.076	0.068
	Level 5	0.040	0.006	0.840	0.072	0.010	0.004	0.035	0.014
Level 5	**Recovery**	0.000	0.000	0.003	0.001	0.000	0.000	0.000	0.000
Baseline	**Recovery**	0.240	0.196	0.151	0.117	0.043	0.042	0.049	0.000

Notes. Cell colours blue, green and red represents p-values < 0.05, < 0.01, and < 0.001, respectively.

recovery was lower than baseline on electrodes belonging to central, parietal, and occipital regions. Furthermore, a decrease in $\delta_{relative}$ on the majority of electrodes was visible when progressing to level 5 (i.e., from level 1 to level 5) (Figure B.1). The pairwise comparison on measurement time main effect revealed that there was a significant increase in $\delta_{relative}$ from baseline to level 1, and then a significant decrease from level 1 to level 5 and from level 5 to recovery. There was a statistically significant interaction between measurement time and electrode locations as well (F(186,4464) = 4.90, $p = 0.000$, $\varepsilon = 0.046$, $\eta_P^2 = 0.170$, power = 0.999). The interaction also had a larger effect size and the power to find differences was also high. The pairwise comparison of interaction between measurement time and electrode locations (Table B.4) revealed a significant increase in $\delta_{relative}$ from baseline to level 1 on all electrode locations and a significant decrease from level 1 to level 3 on P7; from level 1 to level 4 on CP4, P4, PO4, Oz, and O2; from level 1 to level 5 on CP4, P3, P1, Pz, P2, P4, PO3, PO4, O1, Oz, O2, and P8; from level 5 to recovery on all electrode locations; and from baseline to recovery on P3, PO3, and Oz electrodes. The topographical distribution of significant differences between visuomotor tracking task interaction levels (i.e., level 1 to level 2, level 1 to level 3, level 1 to level 4, and level 1 to level 5) showed that significant variations in $\delta_{relative}$ was localised to parietal and occipital regions (Figure B.13). Furthermore, variation in sample mean and standard deviation of these significant electrodes revealed that $\delta_{relative}$ on parietal and occipital regions significantly decreased following the robotic interaction.

B.2.2 Modulations in $\theta_{relative}$ Before, During and After the Robot-Mediated Visuomotor Tracking Task

Two-way repeated measures ANOVA on $\theta_{relative}$ revealed a significant main effect in electrode location (F(31, 744) = 27.613, $p = 0.000$, $\varepsilon = 0.057$, $\eta_P^2 = 0.535$, power = 1.000) and a

significant interaction between measurement time and electrode locations (F(186, 4464) = 2.458, p = 0.018, ε = 0.039, η_P^2 = 0.093, power = 0.874). The significant main effect in electrode location had a larger effect size whereas the interaction had a medium effect size. However, both had sufficient power (i.e, over 80%) to find the statistical differences in the main effects. There was no significant main effect in the measurement time (F(6, 144) = 1.505, p = 0.233, ε = 0.324, η_P^2 = 0.059, power = 0.301). The pairwise comparison of interaction between measurement time and electrode locations (Table B.5) revealed a significant increase in θ_{relative} from baseline to level 1 on C3, P2, PO4, Oz, O2, and T7 electrodes, whereas a significant decrease was visible from level 5 to recovery on FP1, FP2, PO4, and O2 electrodes. Furthermore, a significant reduction in θ_{relative} was observed from level 1 to level 2 on C3, P1, P2, PO3, PO4, and O2; level 1 to level 3 on FC3, C5, C3, C1, Cz, C2, CP3, and CPz; level 1 to level 4 on FC3, C3, C1, Cz, C2, C4, and CP3; level 1 to level 5 on FC3, C3, C1, Cz and CP3 electrodes. The topographical distribution of the significant differences show that the significant changes in θ_{relative} is localised mostly around the central region (Figure B.14).

B.2.3 Modulations in α_{relative} Before, During and After the Robot-Mediated Visuomotor Tracking Task

A reduction in α_{relative} after the onset of robot-mediated interaction (i.e., from baseline to level 1) was visible on all electrodes, followed by an increase α_{relative} on all electrodes from level 1 to 5. Following the completion of the robotic interaction, there was again a rise in the α_{relative} from level 5 to recovery. In comparison to the α_{relative} during baseline, a larger increase were visible during recovery on electrodes belonging to central, parietal, and occipital regions (Figure B.3). Two-way repeated measures ANOVA on α_{relative} indicated that there was a significant main effect in the measurement time (F(6, 144) = 26.613, p = 0.000, ε = 0.291 , η_P^2 = 0.526, power = 1.000) and electrode location (F(31, 744) = 11.87, p = 0.000, ε = 0.148, η_P^2 = 0.331, power = 1.000). The power to find differences in both conditions was high and the effect sizes were large. Pairwise comparison of measurement time effect showed that there was a significant decrease in α_{relative} from baseline to level 1 of the robotic interaction, a significant increase from level 1 to level 4, from level 1 to level 5, and from level 5 to recovery. The interaction between measurement time and electrode locations was also statistically significant with a larger effect size (F(186, 4464) = 6.182, p = 0.000, ε = 0.026, η_P^2 = 0.205, power = 0.995). The power analysis also showed that the interaction between measurement time and electrode locations of α_{relative} had sufficient power to find statistical differences in the interaction. The pairwise comparison showed that

there was a significant increase between level 1 to level 2 on O1, Oz, and P8; level 1 to level 3 on FP1, Pz, P4, O1, Oz, T7, and P7; level 1 to level 4 on FCz, C3, C1, Cz, C2, C4, C6, CP3, CPz, CP4, P3, P1, Pz, P2, P4, PO3, PO4, O1, Oz, O2, and P8; level 1 to level 5 on C3, C1, Cz, C2, C4, C6, CP3, CPz, CP4, P3, P1, Pz, P2, P4, PO3, PO4, O1, Oz, O2, T8, P7, and P8 electrodes (Table B.6 and Figure B.3). The topographical distribution of the significant differences shows that these variations shows a widespread distribution across the posterior brain regions, including central, parietal, occipital and temporal brain regions (Figure B.15).

B.2.4 Modulations in β_{relative} Before, During and After the Robot-Mediated Visuomotor Tracking Task

Two-way repeated measures ANOVA on β_{relative} also revealed a significant main effect in electrode location (F(31, 744) = 12.473, $p = 0.000$, $\varepsilon = 0.108$, $\eta_P^2 = 0.342$, power = 1.000) and a significant interaction between measurement time and electrode locations (F(186, 4464) = 2.304, $p = 0.026$, $\varepsilon = 0.040$, $\eta_P^2 = 0.088$, power = 0.852). The significant main effect in electrode location had a larger effect size whereas the interaction had a medium effect size. However, both had sufficient power (i.e, over 80%) to find the statistical differences in the main effects. The pairwise comparison of the interaction effect showed significant differences on only a few electrode locations (Table B.7 and Figure B.16). There was a significant decrease in β_{relative} on FC3, FCz, C5, C1, and Cz from baseline to level 1; a significant increase on O1 and P7 from level 1 to level 2, on P7 from level 1 to level 3, on T8 from level 1 to level 5, on FCz from level 5 to recovery.

B.2.5 Modulations in $(\theta + \alpha)/\beta$ Before, During and After the Robot-Mediated Visuomotor Tracking Task

Two-way repeated measures ANOVA on $(\theta + \alpha)/\beta$ found that there was a significant main effect in measurement time (F(6, 144) = 6.350, $p = 0.007$, $\varepsilon = 0.259$, $\eta_P^2 = 0.209$, power = 0.812) and electrode location (F(31, 744) = 11.810, $p = 0.000$, $\varepsilon = 0.117$, $\eta_P^2 = 0.330$, power = 1.000) with a larger effect size and a sufficient power (i.e., over 80%) to find the statistical differences in the main effects. The pairwise comparison on measurement time main effect showed that the significant differences were only visible from baseline to level 1 and from level 5 to recovery. The interaction between measurement time and electrode locations was also significant (F(186, 4464) = 5.920, $p = 0.001$, $\varepsilon = 0.018$, $\eta_P^2 = 0.198$, power = 0.962) and showed a larger effect size and a higher power to find differences. As shown in Table B.8, the significant differences were visible only on CP3, CPz, CP4, P3, P1, Pz,

P2, P4, PO3, PO4, O1, Oz, O2, T8, P7, and P8 electrodes from baseline to level 1 and on FC4, C5, C3, C1, Cz, C2, C4, C6, CP3, CPz, CP4, P3, P1, Pz, P2, P4, PO3, PO4, O1, Oz, O2, P7, and P8 electrodes from baseline to recovery. There was no significant difference in the interaction between the robot-mediated visuomotor tracking task interaction levels and electrode locations. However, as can be seen in B.5, there was an increase in $(\theta+\alpha)/\beta$ around the parietal region.

B.2.6 Modulations in α/β Before, During and After the Robot-Mediated Visuomotor Tracking Task

Two-way repeated measures ANOVA on α/β showed a significant main effect in measurement time (F(6, 144) = 12.596, p = 0.000, ε = 0.235, η_P^2 = 0.344, power = 0.974), electrode location (F(31, 744) = 8.502, p = 0.000, ε = 0.097, η_P^2 = 0.262, power = 0.991) and a significant interaction between measurement time and electrode locations (F(186, 4464) = 6.563, p = 0.001, ε = 0.014, η_P^2 = 0.215, power = 0.947). Both main effects and the interaction showed a larger effect size and had sufficient power to find statistical differences in the main effects. The pairwise comparison of the main effect in measurement time revealed a significant decrease in α/β from baseline to level 1, a significant increase from level 1 to level 4 and from level 5 to recovery. As can be seen in Figure B.6, α/β also increased in all EEG electrodes from level 1 to level 5. The pairwise comparison of the interaction between measurement time and electrode locations (Table B.9) showed a significant differences on all electrodes from baseline to level 1 and from level 5 to recovery. Also, there was a significant increase in α/β from baseline to recovery on CP3. The comparison between the robot-mediated interaction levels showed a significant increase from level 1 to level 2 on F3, FC3, FCz, C1, Cz, C2, CPz, and CP4 electrodes; from level 1 to level 3 on Cz, CPz, CP4, and T8 electrodes; from level 1 to level 4 on Fz, FC3, FCz, FC4, C3, C1, Cz, C2, C4, CP3, CPz, CP4, P3, P1, Pz, P2, P4, and P8 electrodes; and from level 1 to level 5 on CPz and P8. From the topographical distribution of the significant differences of α/β between the task interaction levels, it was observed that α/β around central and parietal regions were significantly changed from level 1 to 4 (Figure B.17).

B.2.7 Modulations in $(\theta+\alpha)/(\alpha+\beta)$ Before, During and After the Robot-Mediated Visuomotor Tracking Task

Comparison of the sample mean of $(\theta+\alpha)/(\alpha+\beta)$ on all 32 electrodes between measurement times is shown in Figure B.7. The $(\theta+\alpha)/(\alpha+\beta)$ on all electrodes were increased

from baseline to level 1 and then decreased from level 5 to recovery. Also a larger decrease is visible from baseline to recovery on the electrodes places over the central, parietal and occipital brain regions. The $(\theta+\alpha)/(\alpha+\beta)$ also showed a decreasing trend from level 1 to level 5, thereby suggesting that fatigue induced during the robot-mediated interaction decreased the $(\theta+\alpha)/(\alpha+\beta)$ band power ratio. Two-way repeated measures ANOVA also resulted in a significant main effect in measurement time (F(6, 144) = 20.602, p = 0.000, ε = 0.427, η_P^2 = 0.462, power = 1.000), electrode location (F(31, 744) = 32.172, p = 0.000, ε = 0.086, η_P^2 = 0.573, power = 1.000) and a significant interaction between measurement time and electrode locations (F(186, 4464) = 2.310, p = 0.017, ε = 0.048, η_P^2 = 0.088, power = 0.900). Both main effects showed a larger effect size and had sufficient power to find statistical differences in the main effects. The interaction effect, on the other hand, showed a medium effect size, and the power to find differences was high. The pairwise comparison of the main effect in measurement time showed significant differences from baseline to level 1, level 1 to level 2, level 1 to level 3, level 1 to level 4, level 1 to level 5, level 5 to recovery and baseline to recovery. The pairwise comparison of the interaction between measurement time and electrode locations (Table B.10) revealed significant differences from baseline to level 1 on all electrodes and from level 5 to recovery on all electrodes except T8. Furthermore, a significant decrease from baseline to recovery was also found on FCz, C3, C1, Cz, CP3, CPz, P3, P1, Pz, and T8 electrodes. The $(\theta+\alpha)/(\alpha+\beta)$ around the central, parietal, and occipital regions are found to be significantly altered during the robot-mediated interactions (Figure B.18). There was a significant decrease in $(\theta+\alpha)/(\alpha+\beta)$ from level 1 to level 2 on C5, C3, CP3, CPz, CP4, P3, P1, Pz, P2, P4, PO3, PO4, O1, Oz, O2, T7, and P7 electrodes; from level 1 to level 3 on FC3, C5, C3, C1, Cz, CP3, CPz, P3, P1, PO3, O1, T7, and P7 electrodes; from level 1 to level 4 on FC3, FCz, C5, C3, C1, Cz, C2, C4, C6, CP3, CPz, CP4, P3, P1, Pz, P2, P4, PO3, PO4, and P7 electrodes; from level 1 to level 5 on FC3, FCz, FC4, C5, C3, C1, Cz, C2, C4, C6, CP3, CPz, CP4, P3, P1, Pz, P2, P4, PO3, PO4, O1, Oz, and P7 electrode.

B.2.8 Modulations in θ/β Before, During and After the Robot-Mediated Visuomotor Tracking Task

Two-way repeated measures ANOVA on θ/β showed a significant main effect on electrode location (F(31,744) = 24.893, p = 0.000, ε = 0.093, η_P^2 = 0.509, power = 1.000) and a significant interaction between measurement time and electrode locations (F(186, 4464) = 2.336, p = 0.023, ε = 0.040, η_P^2 = 0.089, power = 0.860). The main effect on electrode location had a larger effect size while the interaction effect had a medium effect size. Also,

both had sufficient power to find statistical differences. There was no significant main effect on measurement time (F(6, 144) = 0.937, $p = 0.415$, $\varepsilon = 0.415$, $\eta_P^2 = 0.038$, power = 0.225). The pairwise comparison of the interaction between measurement time and electrode locations (Table B.11) showed a significant increase from baseline to level 1 on F3, Fz, F4, FC3, FCz, C5, C3, C1, Cz, and C2 electrodes and a significant decrease from level 5 to recovery on FP1, F3, and FCz electrodes. Also, θ/β was not much affected during the robot-mediated interaction. The significant differences were only visible on P7 electrode from level 1 to level 2, 3, 4, and 5, PO3 and PO4 electrodes from level 1 to level 2, on CP4 electrode from level 1 to level 4, on CP4 electrode from level 1 to level 4, on C5 electrode from level 1 to level 5 (Figure B.19).

B.2.9 Modulations in δ/α Before, During and After the Robot-Mediated Visuomotor Tracking Task

As can be seen in Figure B.9, δ/α on all electrodes showed a decreasing trend from level 1 to level 5 during the robot-mediated interaction and from baseline to recovery. Furthermore, two-way repeated measures ANOVA showed a significant main effect in measurement time (F(6, 144) = 32.673, $p = 0.000$, $\varepsilon = 0.475$, $\eta_P^2 = 0.577$, power = 1.000), electrode location (F(31, 744) = 6.945, $p = 0.000$, $\varepsilon = 0.128$, $\eta_P^2 = 0.224$, power = 0.992) and a significant interaction between measurement time and electrode locations (F(186, 4464) = 2.248, $p = 0.010$, $\varepsilon = 0.064$, $\eta_P^2 = 0.086$, power = 0.950). Larger effect sizes were also found on measurement time and electrode location whereas medium effect size was found on the interaction between measurement time and electrode locations. The power to find the statistical differences were high in all conditions and in the interaction. The pairwise comparison of the main effect of measurement time showed significant differences from baseline to level 1, level 1 to level 4, level 1 to level 5, level 5 to recovery and baseline to recovery. In additions, the pairwise comparison of the interaction between measurement time and electrode locations (Table B.12) found a significant increase in δ/α from baseline to recovery on all electrodes and a significant decrease from level 5 to recovery on all electrodes. Moreover, a significant decrease in δ/α was visible from level 1 to level 2 on Cz, C2, CPz, CP4, Pz, P2, P4, PO3, PO4, O1, O2, P7, and P8 electrodes; from level 1 to level 3 on CPz CP4 P3 Pz P2 P4 PO4 O1 Oz O2, and P7 electrodes; from level 1 to level 4 on C2, CPz, CP4, P3, P1, Pz, P2, P4, PO4, and O2 electrodes; from level 1 to level 5 on Cz, C2, C4, C6, CP3, CPz, CP4, P3, P1, Pz, P2, P4, PO3, PO4, O1, Oz, O2, P7, and P8 electrodes. The topographical distribution of the significant differences showed that the changes in δ/α were localised around central, parietal, occipital and temporal brain regions (Figure B.20).

B.2.10 Modulations in the EEG Largest Lyapunov Exponent Before, During and After the Robot-Mediated Visuomotor Tracking Task

Comparison of the sample mean of largest Lyapunov exponent on all 32 electrodes between measurement times is illustrated in Figure B.10. The largest Lyapunov exponent values on all electrodes were increased from baseline to level 1 and decreased from level 5 to recovery. Also, in the majority of electrodes larger differences were observed between level 1 and level 5 of the robot-mediate interaction that may have caused due to the development of fatigue during the task. Two-way repeated measures ANOVA on largest Lyapunov exponent showed that there was a significant main effect in measurement time ($F(6, 144) = 21.790$, $p = 0.000$, $\varepsilon = 0.445$, $\eta_P^2 = 0.476$, power = 1.000) and in electrode location ($F(31, 744) = 24.050$, $p = 0.000$, $\varepsilon = 0.127$, $\eta_P^2 = 0.501$, power = 1.000). Also, the effect sizes were large and the power to find the statistical differences were high in all conditions. The pairwise comparison of the main effect of measurement time revealed that there was a significant difference from baseline to level 1, level 1 to level 5, level 5 to recovery and baseline to recovery. The interaction between measurement time and electrode locations was also significant with a medium effect size and a larger power to find the statistical differences ($F(186, 4464) = 2.660$, $p = 0.005$, $\varepsilon = 0.053$, $\eta_P^2 = 0.100$, power = 0.958). The interaction had a medium effect size and a larger power to find the statistical differences. Table B.13 summarises the p-values obtained from the pairwise comparison of the interaction between measurement time and electrode locations. There were significant differences from baseline to level 1 and from level 5 to recovery on all electrode locations. Also, a significant decrease in the largest Lyapunov exponent from baseline to recovery on C3, C1, CP3, CPz, P3, P1, Pz, PO3, O1, and Oz electrodes was visible. The largest Lyapunov exponent values from level 1 to level 2 on PO3, PO4, O1, Oz, O2, and P7 electrodes, from level 1 to level 3 on P3, P1, Pz, P4, PO3, PO4, O1, Oz, and P7 electrodes, from level 1 to level 4 on CPz, CP4, P3, P1, Pz, P2, P4, PO4, and P7 electrodes, from level 1 to level 5 on C2, CP3, CPz, CP4, P3, P1, Pz, P2, P4, PO3, PO4, O1, Oz, O2, and P7 electrodes also decreased significantly, thereby suggesting a decreasing trend in the largest Lyapunov exponent with fatigue. The topographical distribution of the significant differences between visuomotor tracking task interaction levels showed that the changes in the largest Lyapunov exponent were mostly localised around parietal and occipital brain regions (Figure B.21).

B.2.11 Modulations in the EEG Approximate Entropy Before, During and After the Robot-Mediated Visuomotor Tracking Task

Two-way repeated measures ANOVA on approximate entropy showed a significant main effect in electrode location (F(31, 744) = 13.955, $p = 0.000$, $\varepsilon = 0.167$, $\eta_P^2 = 0.368$, power = 1.000) and a significant interaction between measurement time and electrode locations (F(186, 4464) = 6.620, $p = 0.000$, $\varepsilon = 0.041$, $\eta_P^2 = 0.216$, power = 1.000). Also, both had larger effect sizes and larger power to find the statistical differences. The pairwise comparison of the interaction between measurement time and electrode locations found a significant increase in the approximate entropy from baseline to level 1 on P3, P1, Pz, P2, P4, PO3, PO4, O1, Oz, O2, T7, P7 and P8 electrodes. Furthermore, a significant decrease was visible from level 1 to level 3 on FC3 and C3 electrodes; from level 1 to level 4 on C1 electrode; from level 1 to level 5 on F3, FC3, C5, C3, C1, and T7 electrodes; and from level 5 to recovery on P2, P4, PO3, PO4, O1, Oz, O2, P7 and P8 electrodes (Table B.14). The topographical distribution of the significant differences showed that the changes in approximate entropy were mostly localised around the central brain region (Figure B.22).

B.2.12 Modulations in the $\mathrm{LLyapExp}/\alpha_{\mathrm{relative}}$ Before, During and After the Robot-Mediated Visuomotor Tracking Task

As can be seen in Figure B.12, $\mathrm{LLyapExp}/\alpha_{\mathrm{relative}}$ on all EEG electrodes increased from baseline to level 1 and then decreased from level 5 to recovery. Also, a decreasing trend was visible from baseline to recovery. The $\mathrm{LLyapExp}/\alpha_{\mathrm{relative}}$ during the robot-mediated interaction showed a decrease in all EEG electrodes from level 1 to level 5. Two-way repeated measures ANOVA on $\mathrm{LLyapExp}/\alpha_{\mathrm{relative}}$ indicated that there was a significant main effect in measurement time (F(6, 144) = 21.284, $p = 0.000$, $\varepsilon = 0.520$, $\eta_P^2 = 0.470$, power = 1.000) and electrode location (F(31, 744) = 12.912, $p = 0.000$, $\varepsilon = 0.080$, $\eta_P^2 = 0.350$, power = 0.999) with a larger effect size and a sufficient power to find the statistical differences in the main effects. The pairwise comparison on measurement time main effect revealed that there were significant differences from baseline to level 1, level 1 to level 5, level 5 to recovery, and baseline to recovery. Furthermore, there was a statistically significant interaction between measurement time and electrode locations (F(186, 4464) = 2.336, $p = 0.010$, $\varepsilon = 0.057$, η_P^2 = 0.089, power = 0.941). The interaction had a medium effect size and the power to find differences was also high. The pairwise comparison of interaction between measurement time and electrode locations is summarised in Table B.15. There was a significant increase in $\mathrm{LLyapExp}/\alpha_{\mathrm{relative}}$ from baseline to level 1 and a significant decrease from level 5 to recovery on all electrode locations. A significant decrease was also found from baseline to recovery

on C5, C3, C1, Cz, CP3, CPz, P3, P1, Pz, PO3, O1, and Oz electrodes. When compared with level 1 of the robot-mediated interaction, significant decrease in LLyapExp/α_{relative} were found on P1, Pz, P2, P4, PO3, PO4, O1, Oz, O2, and P7 electrodes during level 2, on P3, P1, Pz, P2, P4, PO3, PO4, O1, Oz, O2, and P7 electrodes during level 3, on C2, CPz, CP4, P3, P1, Pz, P2, P4, PO3, and PO4 electrodes during level 4 and on Cz, C2, C6, CP3, CPz, CP4, P3, P1, Pz, P2, P4, PO3, PO4, O1, Oz, O2, and P7 electrodes during level 5. The topographical distribution of significant differences between visuomotor tracking task interaction levels showed that significant variations in LLyapExp/α_{relative} was mostly localised to parietal and occipital regions (Figure B.23).

B.2.13 Comparison of the Sample Mean of EEG Features on 32 Electrodes Between Measurement Times of the Robot-Mediated Interaction

Figures B.1 to B.12, respectively show the comparison of the sample mean of each EEG feature across all measurement times and EEG electrodes. Connecting lines in the figures do not imply a linear relationship between electrode locations but merely for the ease of identifying the numerical changes between baseline, level 1, level 2, level 3, level 4, level 5 and recovery states.

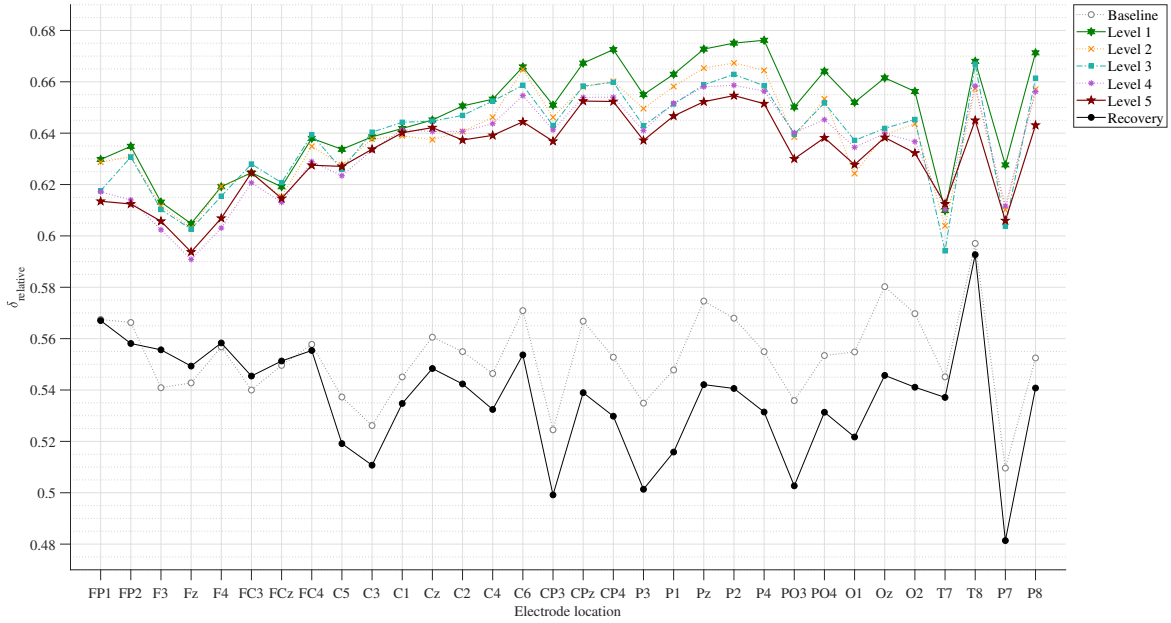

Figure B.1: Comparison of the sample mean of δ_{relative} on all 32 electrodes between measurement times (baseline, level 1, level 2, level 3, level 4, level 5 and recovery) of the robot-mediated interaction.

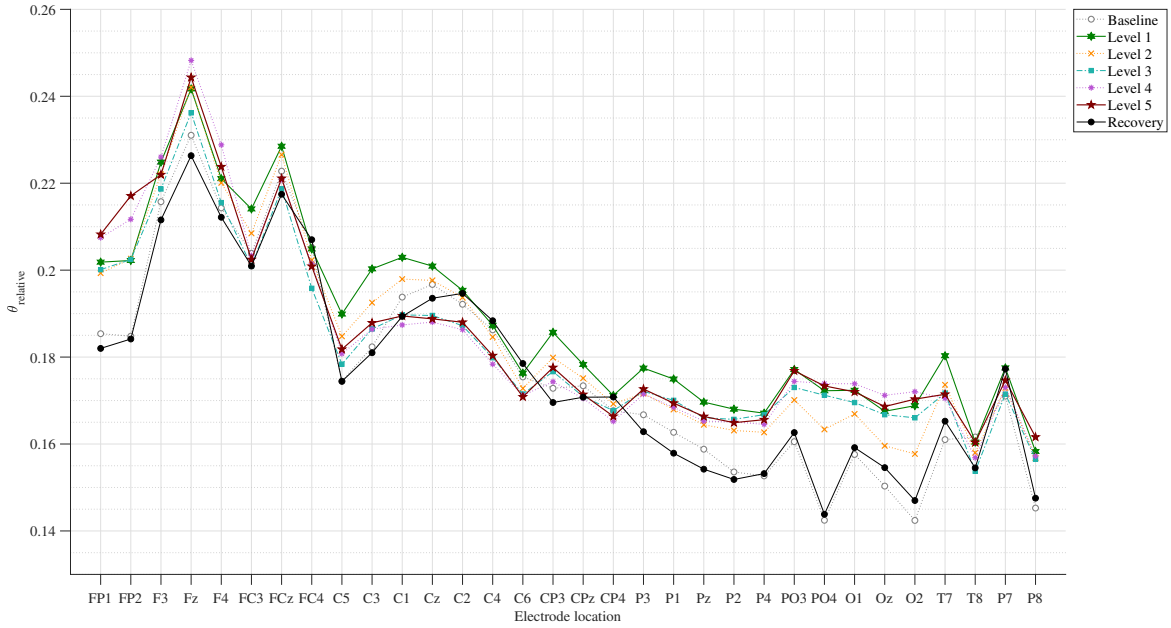

Figure B.2: Comparison of the sample mean of θ_{relative} on all 32 electrodes between measurement times (baseline, level 1, level 2, level 3, level 4, level 5 and recovery) of the robot-mediated interaction.

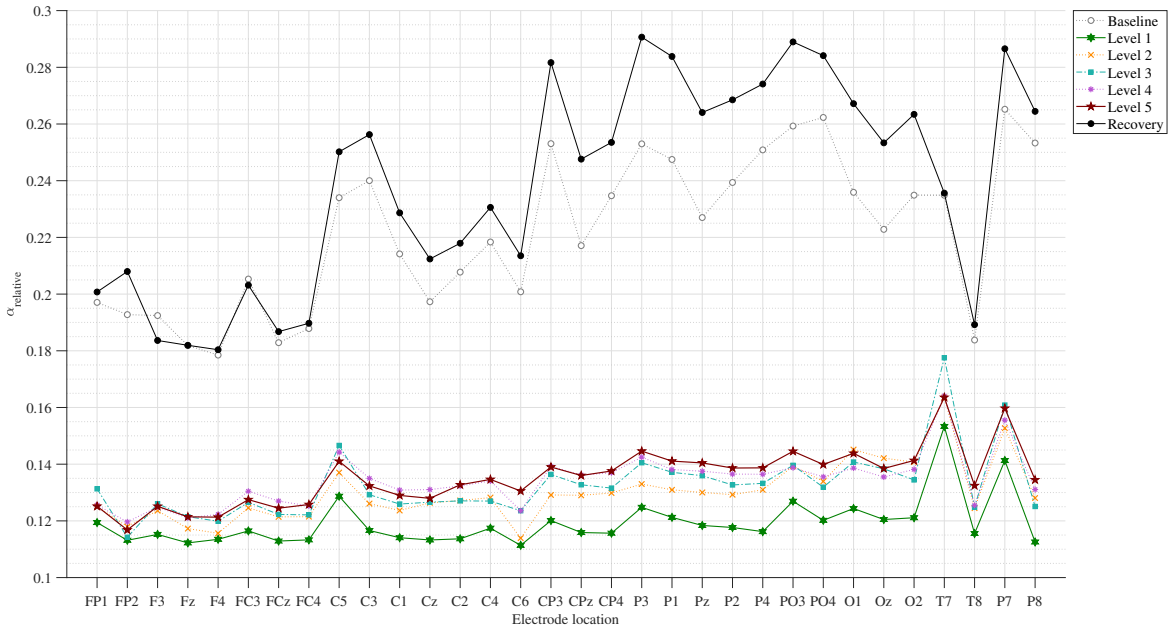

Figure B.3: Comparison of the sample mean of α_{relative} on all 32 electrodes between measurement times (baseline, level 1, level 2, level 3, level 4, level 5 and recovery) of the robot-mediated interaction.

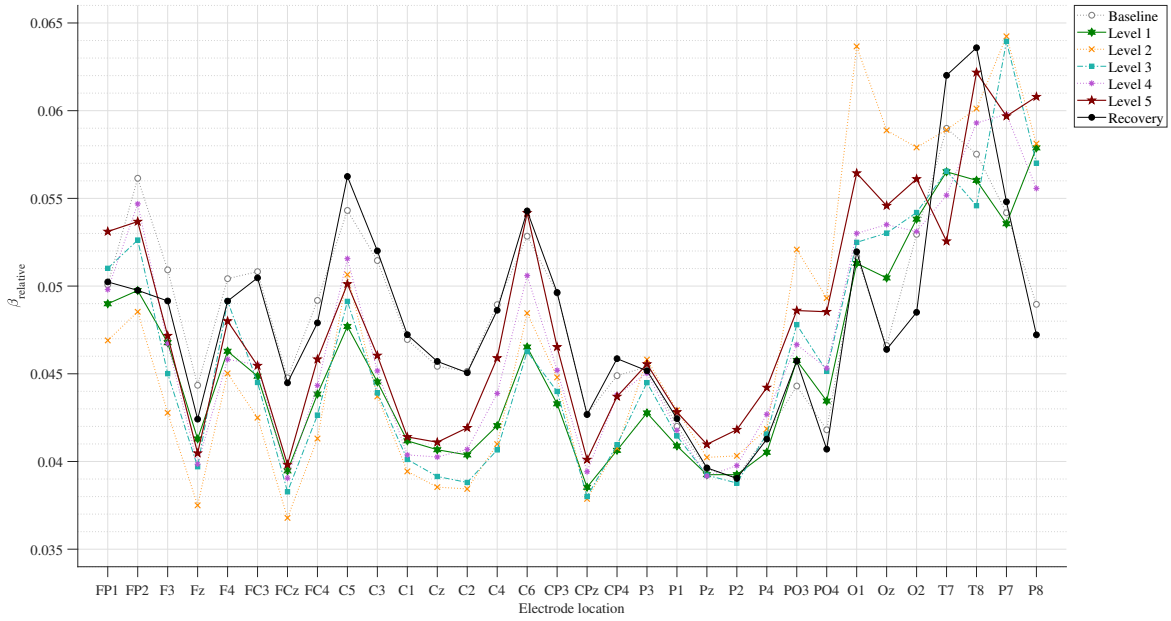

Figure B.4: Comparison of the sample mean of β_{relative} on all 32 electrodes between measurement times (baseline, level 1, level 2, level 3, level 4, level 5 and recovery) of the robot-mediated interaction.

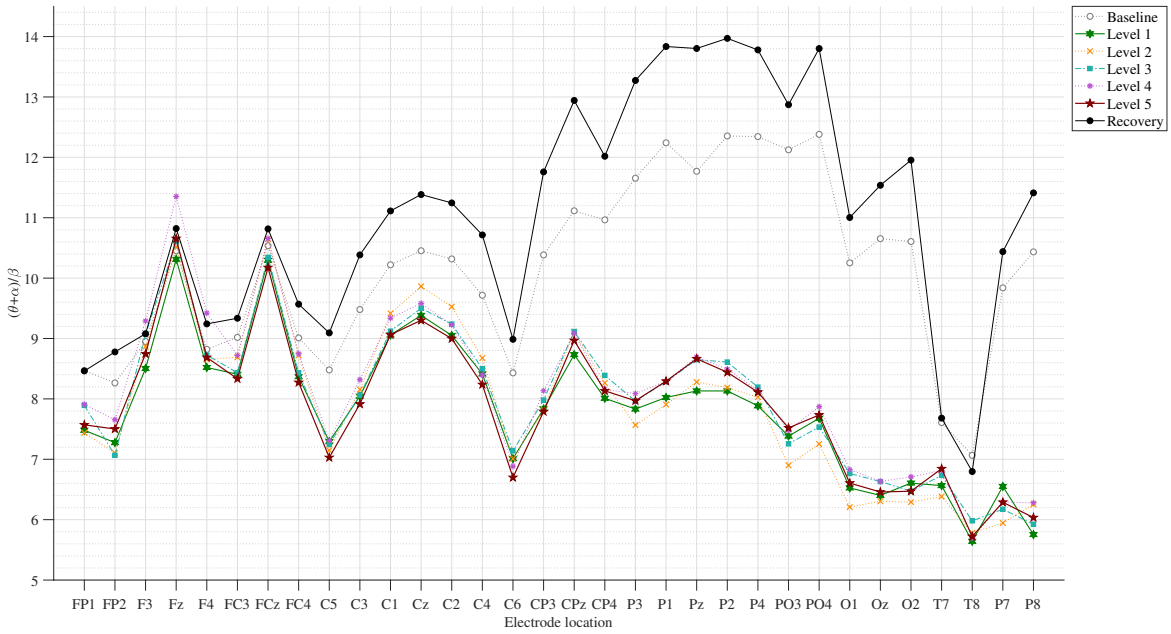

Figure B.5: Comparison of the sample mean of $(\theta + \alpha)/\beta$ on all 32 electrodes between measurement times (baseline, level 1, level 2, level 3, level 4, level 5 and recovery) of the robot-mediated interaction.

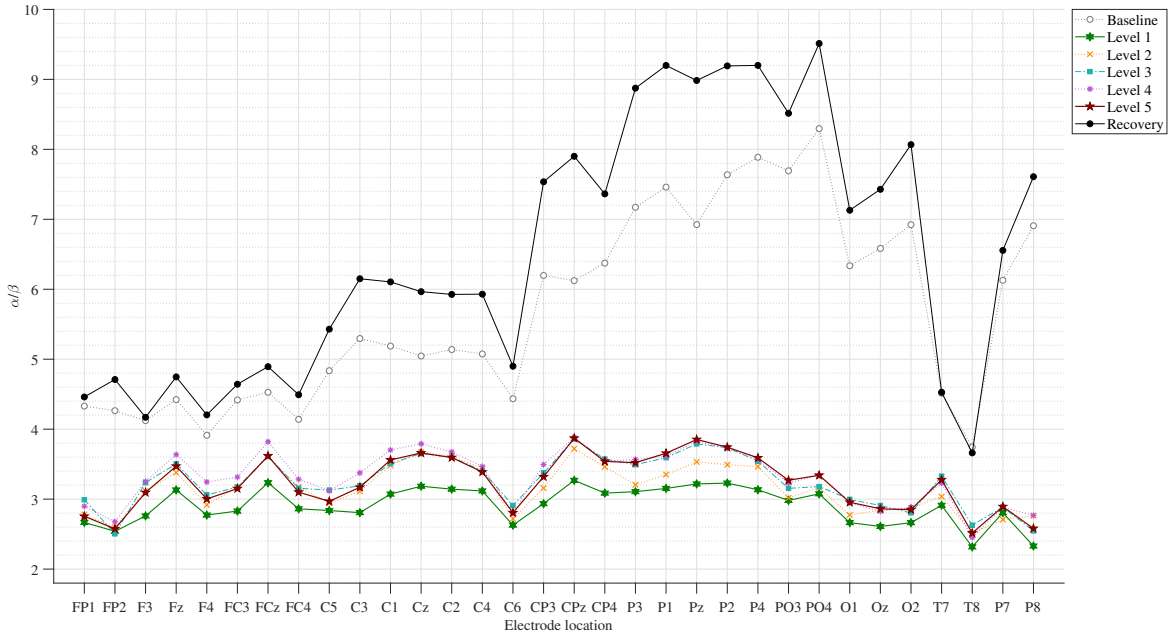

Figure B.6: Comparison of the sample mean of α/β on all 32 electrodes between measurement times (baseline, level 1, level 2, level 3, level 4, level 5 and recovery) of the robot-mediated interaction.

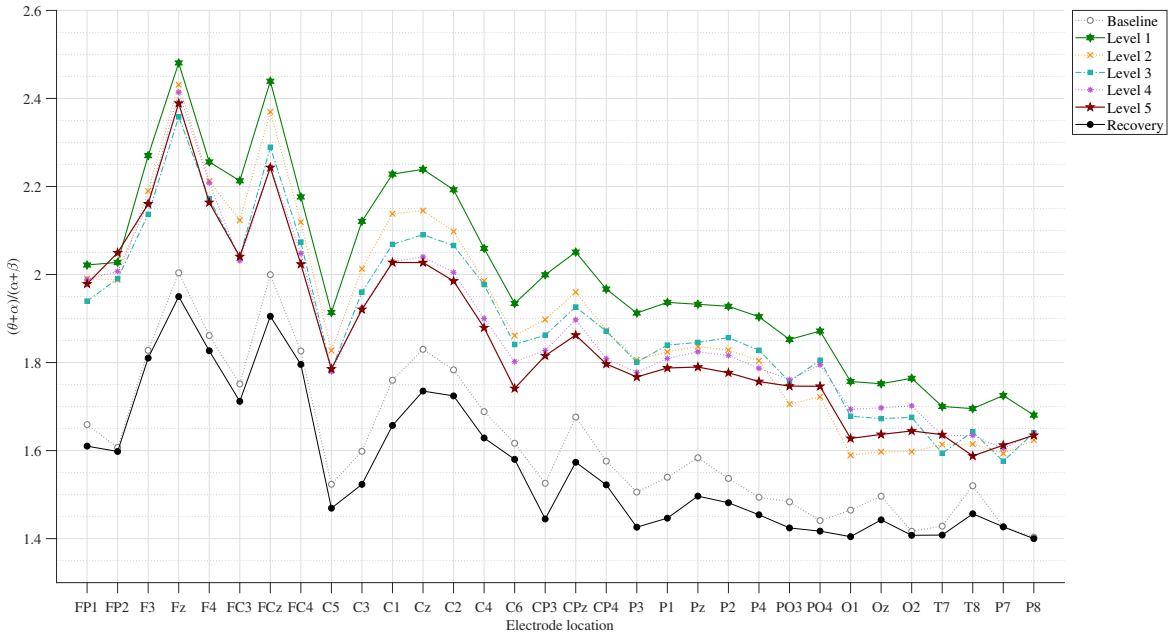

Figure B.7: Comparison of the sample mean of $(\theta+\alpha)/(\alpha+\beta)$ on all 32 electrodes between measurement times (baseline, level 1, level 2, level 3, level 4, level 5 and recovery) of the robot-mediated interaction.

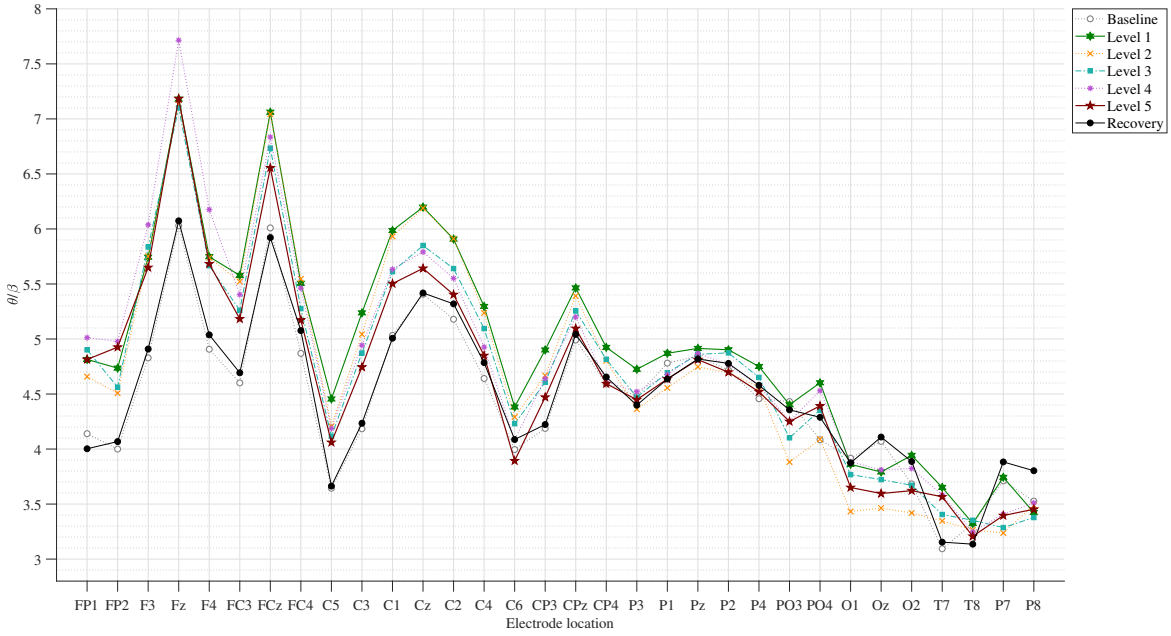

Figure B.8: Comparison of the sample mean of θ/β on all 32 electrodes between measurement times (baseline, level 1, level 2, level 3, level 4, level 5 and recovery) of the robot-mediated interaction.

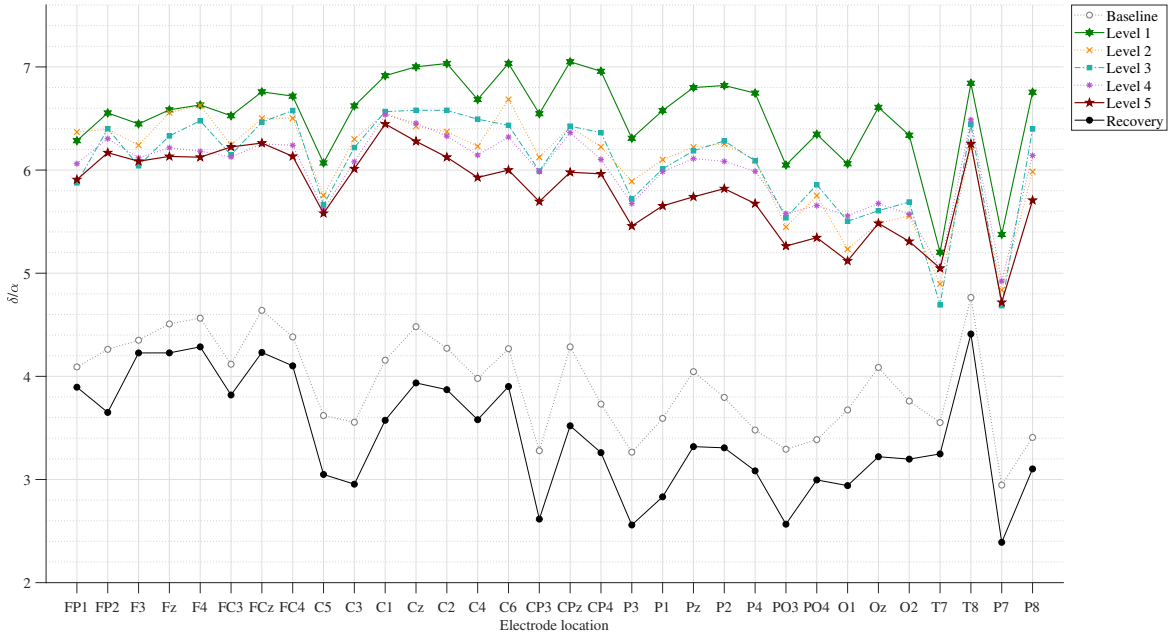

Figure B.9: Comparison of the sample mean of δ/α on all 32 electrodes between measurement times (baseline, level 1, level 2, level 3, level 4, level 5 and recovery) of the robot-mediated interaction.

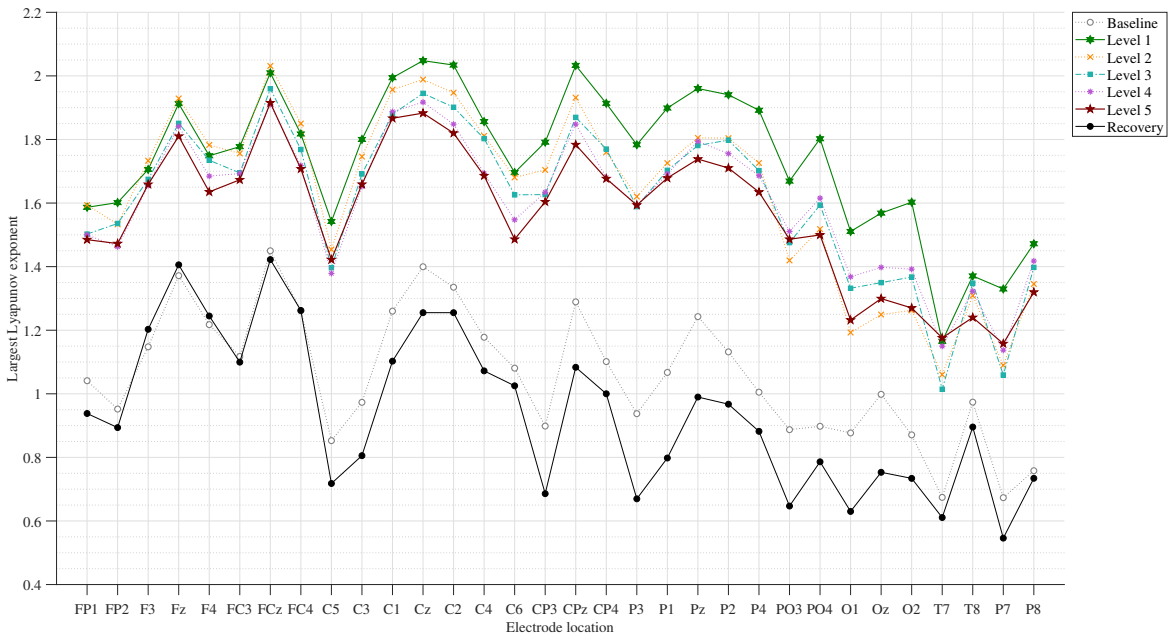

Figure B.10: Comparison of the sample mean of largest Lyapunov exponent on all 32 electrodes between measurement times (baseline, level 1, level 2, level 3, level 4, level 5 and recovery) of the robot-mediated interaction.

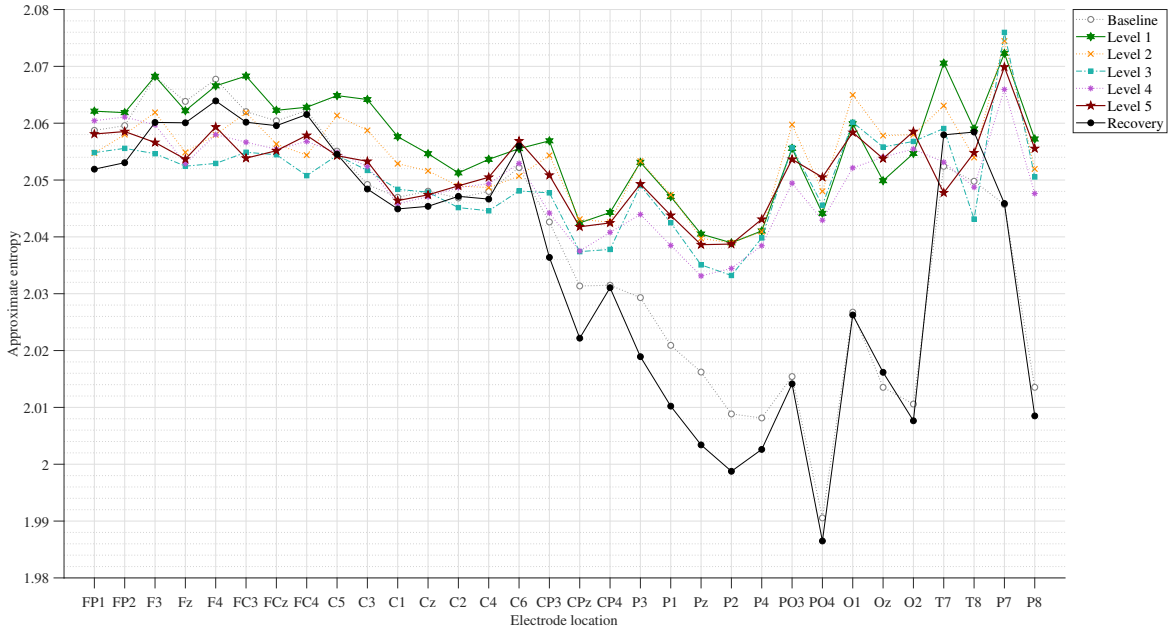

Figure B.11: Comparison of the sample mean of approximate entropy on all 32 electrodes between measurement times (baseline, level 1, level 2, level 3, level 4, level 5 and recovery) of the robot-mediated interaction.

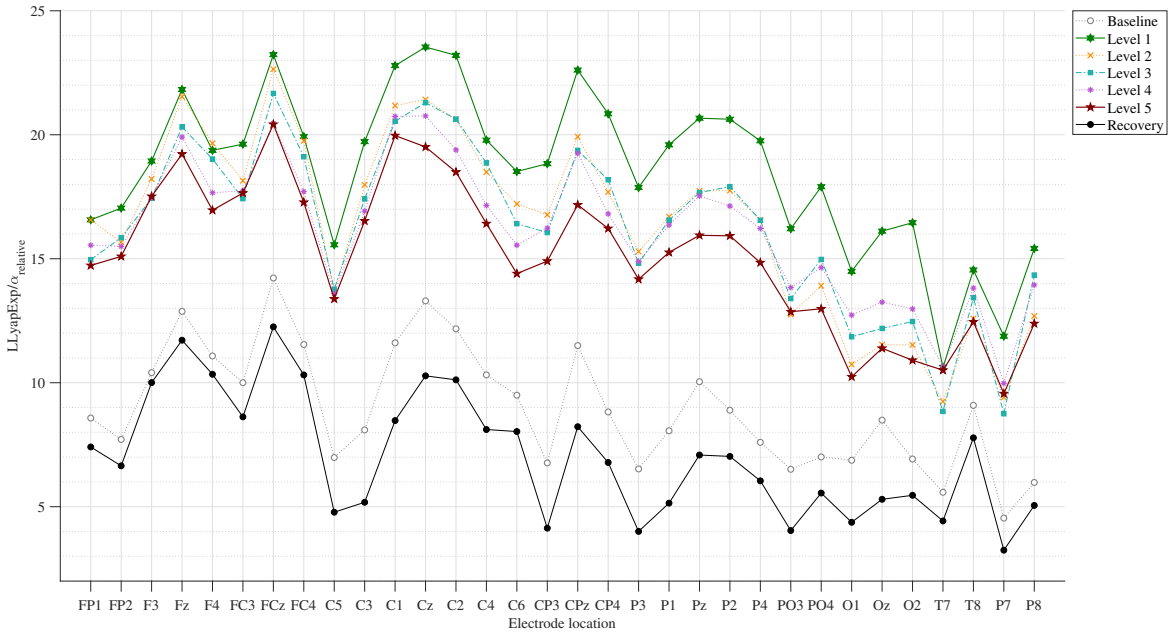

Figure B.12: Comparison of the sample mean of LLyapExp/α_{relative} on all 32 electrodes between measurement times (baseline, level 1, level 2, level 3, level 4, level 5 and recovery) of the robot-mediated interaction.

B.2.14 Pairwise Comparison of the Interaction Between Measurement Time and Electrode Locations on All EEG Features

Tables B.4 to B.15 summarise the *p*-values obtained from the pairwise comparison of the interaction between measurement time and electrode locations of all EEG features.

Table B.4: Pairwise comparison of the interaction between measurement time and electrode locations on δ_{relative}.

Measurement time		FP1	FP2	F3	Fz	F4	FC3	FCz	FC4	C5	C3	C1	Cz	C2	C4	C6	CP3	CPz	CP4	P3	P1	Pz	P2	P4	PO3	PO4	O1	Oz	O2	T7	T8	P7	P8
Baseline	Level 1	0.001	0.000	0.001	0.001	0.001	0.001	0.001	0.000	0.000	0.000	0.000	0.000	0.000	0.000	0.000	0.000	0.000	0.000	0.000	0.000	0.000	0.000	0.000	0.000	0.000	0.001	0.000	0.006	0.005	0.000	0.000
Level 1	Level 2	0.924	0.690	0.878	0.865	0.992	0.985	0.619	0.746	0.611	0.930	0.740	0.369	0.261	0.421	0.903	0.631	0.306	0.180	0.574	0.622	0.441	0.418	0.253	0.300	0.335	0.058	0.161	0.438	0.632	0.290	0.154	0.168
	Level 3	0.270	0.651	0.717	0.795	0.717	0.667	0.834	0.868	0.538	0.851	0.772	0.960	0.683	0.941	0.501	0.439	0.352	0.190	0.203	0.238	0.176	0.201	0.072	0.271	0.164	0.105	0.078	0.362	0.249	0.914	0.013	0.377
	Level 4	0.284	0.149	0.297	0.201	0.101	0.685	0.499	0.309	0.330	0.586	0.957	0.582	0.254	0.350	0.246	0.318	0.157	0.049	0.133	0.214	0.134	0.067	0.036	0.242	0.014	0.106	0.047	0.047	0.970	0.406	0.164	0.128
	Level 5	0.250	0.055	0.485	0.224	0.104	0.999	0.618	0.232	0.536	0.588	0.826	0.681	0.110	0.159	0.060	0.097	0.064	0.040	0.044	0.048	0.024	0.021	0.011	0.039	0.005	0.025	0.016	0.025	0.848	0.104	0.050	0.018
Level 5	Recovery	0.002	0.000	0.000	0.001	0.000	0.000	0.000	0.000	0.000	0.000	0.000	0.000	0.000	0.000	0.000	0.000	0.000	0.000	0.000	0.000	0.000	0.000	0.000	0.000	0.000	0.000	0.000	0.000	0.000	0.001	0.000	0.000
Baseline	Recovery	0.974	0.515	0.321	0.616	0.900	0.726	0.898	0.860	0.240	0.328	0.527	0.394	0.380	0.317	0.234	0.111	0.092	0.108	0.047	0.068	0.067	0.119	0.141	0.038	0.211	0.051	0.040	0.082	0.591	0.787	0.082	0.462

Notes. Cell colours blue, green and red represents p-values < 0.05, < 0.01, and < 0.001, respectively.

Table B.5: Pairwise comparison of the interaction between measurement time and electrode locations on θ_{relative}.

Measurement time		FP1	FP2	F3	Fz	F4	FC3	FCz	FC4	C5	C3	C1	Cz	C2	C4	C6	CP3	CPz	CP4	P3	P1	Pz	P2	P4	PO3	PO4	O1	Oz	O2	T7	T8	P7	P8
Baseline	Level 1	0.142	0.166	0.238	0.273	0.371	0.202	0.439	0.963	0.066	0.021	0.226	0.589	0.672	0.899	0.926	0.099	0.503	0.660	0.192	0.112	0.096	0.044	0.081	0.060	0.000	0.061	0.030	0.000	0.010	0.899	0.482	0.120
Level 1	Level 2	0.573	0.952	0.625	0.946	0.869	0.132	0.654	0.496	0.274	0.015	0.084	0.294	0.580	0.334	0.368	0.099	0.263	0.382	0.053	0.025	0.080	0.032	0.058	0.043	0.003	0.145	0.070	0.004	0.105	0.664	0.240	0.738
	Level 3	0.794	0.974	0.313	0.446	0.493	0.008	0.099	0.099	0.038	0.001	0.000	0.006	0.049	0.072	0.352	0.009	0.028	0.331	0.086	0.121	0.279	0.487	0.926	0.213	0.788	0.462	0.877	0.461	0.121	0.232	0.064	0.713
	Level 4	0.453	0.325	0.859	0.463	0.299	0.014	0.184	0.476	0.087	0.004	0.001	0.006	0.028	0.039	0.338	0.032	0.095	0.127	0.210	0.171	0.335	0.501	0.561	0.586	0.742	0.788	0.516	0.485	0.052	0.558	0.308	0.797
	Level 5	0.405	0.105	0.652	0.762	0.721	0.028	0.288	0.457	0.102	0.004	0.001	0.006	0.089	0.110	0.311	0.048	0.088	0.233	0.227	0.150	0.409	0.448	0.714	0.948	0.830	0.950	0.850	0.787	0.109	0.992	0.531	0.502
Level 5	Recovery	0.014	0.023	0.190	0.180	0.322	0.812	0.640	0.418	0.280	0.337	0.989	0.553	0.389	0.316	0.250	0.255	0.936	0.587	0.239	0.121	0.082	0.075	0.113	0.188	0.001	0.182	0.094	0.003	0.389	0.338	0.823	0.068
Baseline	Recovery	0.527	0.912	0.457	0.465	0.688	0.582	0.349	0.712	1.000	0.781	0.418	0.536	0.607	0.655	0.531	0.528	0.629	0.456	0.474	0.398	0.440	0.756	0.914	0.706	0.807	0.751	0.391	0.317	0.475	0.125	0.287	0.631

Notes. Cell colours blue, green and red represents p-values < 0.05, < 0.01, and < 0.001, respectively.

Table B.6: Pairwise comparison of the interaction between measurement time and electrode locations on α_{relative}.

Measurement time		FP1	FP2	F3	Fz	F4	FC3	FCz	FC4	C5	C3	C1	Cz	C2	C4	C6	CP3	CPz	CP4	P3	P1	Pz	P2	P4	PO3	PO4	O1	Oz	O2	T7	T8	P7	P8
Baseline	Level 1	0.000	0.000	0.001	0.000	0.001	0.001	0.000	0.000	0.000	0.000	0.000	0.000	0.000	0.000	0.000	0.000	0.000	0.000	0.000	0.000	0.000	0.000	0.000	0.000	0.000	0.000	0.000	0.002	0.000	0.000	0.000
Level 1	Level 2	0.550	0.463	0.298	0.464	0.776	0.320	0.192	0.255	0.414	0.290	0.228	0.082	0.079	0.168	0.592	0.291	0.118	0.081	0.311	0.227	0.160	0.175	0.093	0.158	0.115	0.048	0.047	0.095	0.345	0.062	0.228	0.044
	Level 3	0.040	0.842	0.106	0.112	0.390	0.155	0.161	0.273	0.084	0.137	0.130	0.085	0.101	0.274	0.092	0.075	0.052	0.059	0.060	0.060	0.047	0.075	0.042	0.105	0.095	0.035	0.026	0.059	0.026	0.108	0.023	0.068
	Level 4	0.335	0.389	0.133	0.141	0.145	0.071	0.037	0.051	0.063	0.019	0.023	0.010	0.005	0.028	0.047	0.011	0.008	0.004	0.012	0.013	0.011	0.006	0.004	0.046	0.003	0.042	0.015	0.005	0.193	0.290	0.063	0.003
	Level 5	0.478	0.548	0.191	0.108	0.130	0.118	0.067	0.054	0.079	0.016	0.026	0.018	0.006	0.033	0.011	0.005	0.004	0.006	0.004	0.004	0.003	0.004	0.003	0.014	0.001	0.006	0.004	0.002	0.227	0.039	0.019	0.004
Level 5	Recovery	0.000	0.000	0.000	0.000	0.000	0.000	0.000	0.000	0.000	0.000	0.000	0.000	0.000	0.000	0.000	0.000	0.000	0.000	0.000	0.000	0.000	0.000	0.000	0.000	0.000	0.000	0.000	0.000	0.000	0.000	0.000	0.000
Baseline	Recovery	0.769	0.137	0.505	0.994	0.841	0.877	0.711	0.864	0.286	0.289	0.355	0.274	0.439	0.352	0.266	0.079	0.073	0.168	0.042	0.052	0.055	0.099	0.148	0.108	0.181	0.089	0.087	0.062	0.952	0.635	0.225	0.446

Notes. Cell colours blue, green and red represents p-values < 0.05, < 0.01, and < 0.001, respectively.

Table B.7: Pairwise comparison of the interaction between measurement time and electrode locations on β_{relative}.

Measurement time		FP1	FP2	F3	Fz	F4	FC3	FCz	FC4	C5	C3	C1	Cz	C2	C4	C6	CP3	CPz	CP4	P3	P1	Pz	P2	P4	PO3	PO4	O1	Oz	O2	T7	T8	P7	P8
Baseline	Level 1	0.747	0.270	0.097	0.235	0.196	0.018	0.006	0.062	0.047	0.051	0.029	0.035	0.086	0.068	0.148	0.129	0.160	0.263	0.518	0.776	0.925	0.965	0.797	0.771	0.699	0.950	0.458	0.877	0.569	0.743	0.902	0.175
Level 1	Level 2	0.379	0.632	0.086	0.110	0.577	0.194	0.089	0.132	0.272	0.636	0.307	0.214	0.263	0.559	0.543	0.508	0.673	0.942	0.229	0.322	0.562	0.551	0.546	0.052	0.192	0.019	0.104	0.516	0.451	0.317	0.019	0.945
	Level 3	0.720	0.492	0.331	0.257	0.610	0.807	0.387	0.506	0.446	0.639	0.442	0.327	0.379	0.427	0.917	0.590	0.700	0.875	0.171	0.668	0.985	0.744	0.471	0.228	0.531	0.648	0.500	0.946	0.990	0.655	0.006	0.793
	Level 4	0.786	0.273	0.988	0.516	0.894	0.803	0.832	0.849	0.258	0.824	0.646	0.800	0.859	0.376	0.128	0.514	0.562	0.152	0.320	0.534	0.941	0.644	0.129	0.559	0.494	0.582	0.351	0.859	0.662	0.373	0.069	0.568
	Level 5	0.376	0.239	0.875	0.582	0.495	0.734	0.798	0.364	0.276	0.435	0.885	0.782	0.393	0.154	0.109	0.145	0.294	0.095	0.140	0.296	0.350	0.183	0.059	0.203	0.172	0.195	0.318	0.687	0.269	0.045	0.072	0.484
Level 5	Recovery	0.510	0.340	0.539	0.380	0.780	0.075	0.020	0.554	0.139	0.146	0.069	0.098	0.307	0.566	0.987	0.514	0.494	0.648	0.936	0.933	0.721	0.497	0.537	0.562	0.155	0.484	0.117	0.170	0.091	0.849	0.391	0.083
Baseline	Recovery	0.954	0.167	0.381	0.234	0.624	0.867	0.883	0.549	0.506	0.805	0.896	0.896	0.971	0.898	0.612	0.991	0.991	0.639	0.915	0.824	0.970	0.972	0.877	0.504	0.508	0.932	0.934	0.262	0.421	0.180	0.811	0.350

Notes. Cell colours blue and green represents p-values < 0.05 and < 0.01, respectively.

Table B.8: Pairwise comparison of the interaction between measurement time and electrode locations on $(\theta+\alpha)/\beta$.

Measurement time		FP1	FP2	F3	Fz	F4	FC3	FCz	FC4	C5	C3	C1	Cz	C2	C4	C6	CP3	CPz	CP4	P3	P1	Pz	P2	P4	PO3	PO4	O1	Oz	O2	T7	T8	P7	P8
Baseline	Level 1	0.227	0.318	0.494	0.814	0.629	0.307	0.686	0.240	0.126	0.083	0.130	0.137	0.092	0.121	0.091	0.044	0.035	0.024	0.034	0.020	0.009	0.015	0.022	0.015	0.009	0.016	0.010	0.028	0.143	0.044	0.017	0.003
Level 1	Level 2	0.923	0.683	0.382	0.645	0.731	0.418	0.394	0.339	0.724	0.734	0.338	0.236	0.189	0.437	0.996	0.972	0.235	0.392	0.359	0.681	0.617	0.845	0.620	0.119	0.256	0.430	0.822	0.535	0.660	0.665	0.060	0.276
	Level 3	0.406	0.660	0.349	0.662	0.668	0.952	0.920	0.873	0.885	0.961	0.878	0.782	0.665	0.835	0.770	0.689	0.377	0.340	0.717	0.468	0.263	0.273	0.395	0.659	0.663	0.510	0.534	0.732	0.643	0.295	0.187	0.646
	Level 4	0.414	0.597	0.279	0.214	0.207	0.481	0.501	0.352	0.953	0.422	0.475	0.590	0.599	0.943	0.626	0.361	0.323	0.600	0.400	0.417	0.120	0.293	0.408	0.766	0.573	0.408	0.431	0.755	0.346	0.838	0.285	0.186
	Level 5	0.852	0.683	0.613	0.553	0.753	0.854	0.806	0.808	0.344	0.731	0.992	0.854	0.908	0.675	0.462	0.911	0.624	0.738	0.737	0.550	0.311	0.532	0.597	0.772	0.910	0.897	0.916	0.784	0.402	0.824	0.280	0.401
Level 5	Recovery	0.266	0.121	0.587	0.790	0.274	0.081	0.208	0.010	0.022	0.013	0.032	0.014	0.007	0.010	0.009	0.006	0.009	0.010	0.006	0.005	0.004	0.003	0.006	0.003	0.002	0.003	0.001	0.004	0.242	0.097	0.002	0.001
Baseline	Recovery	0.987	0.376	0.703	0.347	0.272	0.465	0.543	0.230	0.268	0.137	0.208	0.178	0.176	0.145	0.314	0.071	0.077	0.141	0.097	0.116	0.134	0.148	0.109	0.375	0.127	0.428	0.337	0.114	0.864	0.564	0.254	0.287

Notes. Cell colours blue and green represents p-values < 0.05 and < 0.01, respectively.

Table B.9: Pairwise comparison of the interaction between measurement time and electrode locations on α/β.

Measurement time		FP1	FP2	F3	Fz	F4	FC3	FCz	FC4	C5	C3	C1	Cz	C2	C4	C6	CP3	CPz	CP4	P3	P1	Pz	P2	P4	PO3	PO4	O1	Oz	O2	T7	T8	P7	P8
Baseline	Level 1	0.005	0.016	0.007	0.007	0.012	0.004	0.006	0.003	0.004	0.001	0.003	0.003	0.002	0.004	0.004	0.002	0.003	0.002	0.005	0.003	0.001	0.002	0.004	0.003	0.001	0.003	0.004	0.007	0.008	0.004	0.002	0.001
Level 1	Level 2	0.633	0.749	0.036	0.103	0.388	0.047	0.023	0.100	0.654	0.098	0.030	0.016	0.013	0.114	0.671	0.193	0.022	0.041	0.517	0.225	0.084	0.140	0.084	0.825	0.693	0.612	0.324	0.484	0.627	0.242	0.561	0.069
	Level 3	0.106	0.846	0.050	0.076	0.210	0.107	0.081	0.185	0.167	0.082	0.058	0.038	0.052	0.242	0.198	0.073	0.038	0.045	0.115	0.074	0.063	0.071	0.065	0.310	0.513	0.098	0.102	0.384	0.083	0.046	0.636	0.165
	Level 4	0.318	0.615	0.084	0.048	0.058	0.043	0.022	0.019	0.111	0.008	0.014	0.010	0.007	0.041	0.262	0.018	0.019	0.023	0.033	0.034	0.017	0.035	0.038	0.147	0.125	0.130	0.114	0.126	0.075	0.492	0.565	0.026
	Level 5	0.659	0.845	0.169	0.092	0.177	0.122	0.083	0.114	0.350	0.060	0.059	0.053	0.060	0.196	0.383	0.088	0.047	0.052	0.096	0.069	0.051	0.085	0.075	0.272	0.282	0.378	0.359	0.400	0.061	0.175	0.536	0.041
Level 5	Recovery	0.008	0.001	0.020	0.005	0.004	0.006	0.005	0.001	0.003	0.002	0.006	0.005	0.003	0.002	0.002	0.001	0.005	0.002	0.002	0.002	0.003	0.001	0.002	0.000	0.000	0.001	0.000	0.001	0.031	0.007	0.000	0.000
Baseline	Recovery	0.661	0.125	0.810	0.115	0.104	0.403	0.165	0.234	0.197	0.079	0.106	0.086	0.110	0.103	0.259	0.038	0.062	0.105	0.065	0.069	0.117	0.128	0.105	0.273	0.158	0.331	0.319	0.149	0.960	0.793	0.334	0.383

Notes. Cell colours blue, green and red represents p-values < 0.05, < 0.01, and < 0.001, respectively.

Table B.10: Pairwise comparison of the interaction between measurement time and electrode locations on $(\theta+\alpha)/(\alpha+\beta)$.

Measurement time		FP1	FP2	F3	Fz	F4	FC3	FCz	FC4	C5	C3	C1	Cz	C2	C4	C6	CP3	CPz	CP4	P3	P1	Pz	P2	P4	PO3	PO4	O1	Oz	O2	T7	T8	P7	P8
Baseline	Level 1	0.002	0.001	0.001	0.001	0.002	0.000	0.000	0.001	0.000	0.000	0.000	0.000	0.000	0.000	0.000	0.000	0.000	0.000	0.000	0.000	0.000	0.000	0.000	0.000	0.000	0.001	0.000	0.000	0.014	0.000	0.001
Level 1	Level 2	0.611	0.587	0.356	0.542	0.568	0.150	0.300	0.280	0.048	0.045	0.099	0.067	0.060	0.147	0.162	0.023	0.030	0.040	0.006	0.003	0.010	0.008	0.008	0.001	0.000	0.001	0.003	0.003	0.015	0.001	0.272
	Level 3	0.234	0.611	0.098	0.156	0.378	0.012	0.073	0.158	0.024	0.010	0.019	0.025	0.051	0.157	0.130	0.007	0.016	0.070	0.008	0.024	0.050	0.104	0.081	0.011	0.119	0.024	0.106	0.093	0.029	0.001	0.433
	Level 4	0.635	0.798	0.163	0.449	0.608	0.012	0.017	0.073	0.014	0.003	0.002	0.001	0.002	0.006	0.013	0.002	0.001	0.001	0.001	0.001	0.001	0.001	0.000	0.016	0.041	0.134	0.184	0.126	0.115	0.002	0.305
	Level 5	0.608	0.813	0.198	0.345	0.329	0.017	0.025	0.039	0.010	0.002	0.005	0.002	0.002	0.007	0.004	0.002	0.000	0.002	0.002	0.001	0.001	0.001	0.001	0.015	0.011	0.008	0.033	0.059	0.177	0.083	0.428
Level 5	Recovery	0.001	0.000	0.004	0.004	0.011	0.001	0.001	0.020	0.000	0.000	0.000	0.000	0.001	0.002	0.027	0.000	0.000	0.000	0.000	0.000	0.000	0.000	0.000	0.000	0.000	0.002	0.005	0.000	0.000	0.056	0.025	0.001
Baseline	Recovery	0.300	0.869	0.687	0.244	0.442	0.259	0.032	0.433	0.087	0.030	0.007	0.014	0.096	0.110	0.215	0.025	0.006	0.107	0.028	0.014	0.014	0.090	0.178	0.134	0.237	0.091	0.102	0.772	0.565	0.032	0.998	0.857

Notes. Cell colours blue, green and red represents p-values < 0.05, < 0.01, and < 0.001, respectively.

Table B.11: Pairwise comparison of the interaction between measurement time and electrode locations on θ/β.

Measurement time		FP1	FP2	F3	Fz	F4	FC3	FCz	FC4	C5	C3	C1	Cz	C2	C4	C6	CP3	CPz	CP4	P3	P1	Pz	P2	P4	PO3	PO4	O1	Oz	O2	T7	T8	P7	P8
Baseline	Level 1	0.123	0.117	0.020	0.008	0.031	0.005	0.010	0.072	0.009	0.003	0.011	0.029	0.039	0.077	0.288	0.076	0.182	0.385	0.612	0.846	0.837	0.629	0.478	0.954	0.186	0.895	0.511	0.561	0.092	0.990	0.942	0.806
Level 1	Level 2	0.572	0.447	0.980	0.911	0.976	0.829	0.960	0.874	0.281	0.391	0.842	0.973	0.988	0.798	0.723	0.231	0.722	0.535	0.056	0.079	0.341	0.202	0.265	0.010	0.008	0.062	0.166	0.053	0.132	0.753	0.009	0.798
	Level 3	0.811	0.612	0.836	0.886	0.833	0.275	0.402	0.448	0.112	0.132	0.200	0.252	0.380	0.454	0.590	0.161	0.383	0.655	0.185	0.349	0.806	0.898	0.637	0.078	0.247	0.633	0.759	0.285	0.212	0.895	0.008	0.849
	Level 4	0.557	0.617	0.545	0.398	0.408	0.531	0.547	0.884	0.099	0.185	0.146	0.089	0.113	0.072	0.111	0.138	0.141	0.042	0.183	0.246	0.771	0.382	0.226	0.446	0.703	0.912	0.923	0.561	0.663	0.647	0.025	0.697
	Level 5	1.000	0.655	0.776	0.991	0.880	0.163	0.194	0.288	0.044	0.059	0.105	0.058	0.097	0.130	0.068	0.080	0.135	0.142	0.200	0.290	0.670	0.396	0.308	0.523	0.444	0.506	0.514	0.305	0.662	0.645	0.034	0.905
Level 5	Recovery	0.044	0.064	0.048	0.054	0.118	0.067	0.045	0.752	0.104	0.059	0.069	0.433	0.773	0.850	0.541	0.435	0.877	0.876	0.898	0.999	0.985	0.829	0.887	0.819	0.791	0.601	0.193	0.494	0.115	0.815	0.317	0.412
Baseline	Recovery	0.593	0.841	0.725	0.871	0.604	0.702	0.747	0.366	0.924	0.831	0.924	0.965	0.634	0.563	0.615	0.895	0.860	0.769	0.763	0.617	0.922	0.824	0.585	0.789	0.246	0.883	0.868	0.242	0.783	0.281	0.512	0.133

Notes. Cell colours blue and green represents p-values < 0.05 and < 0.01, respectively.

Table B.12: Pairwise comparison of the interaction between measurement time and electrode locations on δ/α.

Measurement time		FP1	FP2	F3	Fz	F4	FC3	FCz	FC4	C5	C3	C1	Cz	C2	C4	C6	CP3	CPz	CP4	P3	P1	Pz	P2	P4	PO3	PO4	O1	Oz	O2	T7	T8	P7	P8
Baseline	Level 1	0.000	0.000	0.000	0.000	0.000	0.000	0.000	0.000	0.000	0.000	0.000	0.000	0.000	0.000	0.000	0.000	0.000	0.000	0.000	0.000	0.000	0.000	0.000	0.000	0.000	0.001	0.000	0.001	0.001	0.000	0.000
Level 1	Level 2	0.798	0.537	0.474	0.929	0.989	0.292	0.320	0.557	0.377	0.228	0.177	0.037	0.033	0.151	0.310	0.104	0.016	0.026	0.106	0.066	0.034	0.044	0.029	0.046	0.038	0.026	0.059	0.039	0.289	0.068	0.036	0.035
	Level 3	0.163	0.614	0.193	0.385	0.606	0.213	0.337	0.655	0.303	0.252	0.317	0.197	0.154	0.544	0.102	0.097	0.045	0.044	0.040	0.060	0.034	0.043	0.016	0.069	0.037	0.015	0.030	0.031	0.121	0.268	0.008	0.380
	Level 4	0.563	0.517	0.291	0.178	0.174	0.254	0.105	0.175	0.241	0.133	0.263	0.077	0.042	0.152	0.050	0.092	0.039	0.011	0.024	0.033	0.022	0.014	0.011	0.053	0.008	0.115	0.086	0.029	0.598	0.437	0.127	0.071
	Level 5	0.349	0.291	0.315	0.071	0.051	0.391	0.099	0.067	0.135	0.056	0.153	0.014	0.005	0.036	0.008	0.004	0.001	0.006	0.003	0.001	0.000	0.001	0.001	0.008	0.001	0.002	0.001	0.001	0.700	0.214	0.029	0.006
Level 5	Recovery	0.000	0.000	0.000	0.000	0.000	0.000	0.000	0.000	0.000	0.000	0.000	0.000	0.000	0.000	0.000	0.000	0.000	0.000	0.000	0.000	0.000	0.000	0.000	0.000	0.000	0.000	0.000	0.000	0.000	0.000	0.000	0.000
Baseline	Recovery	0.444	0.019	0.695	0.307	0.287	0.346	0.116	0.340	0.033	0.035	0.051	0.058	0.151	0.171	0.228	0.013	0.009	0.107	0.009	0.007	0.005	0.068	0.131	0.015	0.113	0.022	0.005	0.099	0.207	0.306	0.045	0.196

Notes. Cell colours blue, green and red represents p-values < 0.05, < 0.01, and < 0.001, respectively.

Table B.13: Pairwise comparison of the interaction between measurement time and electrode locations on largest Lyapunov exponent.

Measurement time		FP1	FP2	F3	Fz	F4	FC3	FCz	FC4	C5	C3	C1	Cz	C2	C4	C6	CP3	CPz	CP4	P3	P1	Pz	P2	P4	PO3	PO4	O1	Oz	O2	T7	T8	P7	P8
Baseline	Level 1	0.001	0.000	0.001	0.001	0.001	0.001	0.001	0.001	0.000	0.000	0.000	0.000	0.000	0.000	0.001	0.000	0.000	0.000	0.000	0.000	0.000	0.000	0.000	0.000	0.000	0.000	0.003	0.001	0.004	0.025	0.000	0.000
Level 1	Level 2	0.943	0.441	0.796	0.872	0.747	0.820	0.811	0.729	0.405	0.578	0.678	0.502	0.341	0.657	0.885	0.343	0.272	0.146	0.113	0.081	0.109	0.154	0.098	0.035	0.007	0.020	0.039	0.023	0.173	0.491	0.021	0.216
	Level 3	0.366	0.439	0.715	0.410	0.875	0.313	0.542	0.584	0.214	0.230	0.195	0.241	0.153	0.563	0.539	0.089	0.076	0.135	0.023	0.027	0.046	0.084	0.027	0.023	0.014	0.009	0.049	0.054	0.093	0.834	0.001	0.502
	Level 4	0.456	0.232	0.651	0.461	0.599	0.411	0.290	0.381	0.139	0.179	0.239	0.129	0.051	0.152	0.163	0.129	0.045	0.026	0.049	0.025	0.049	0.032	0.012	0.055	0.010	0.131	0.140	0.081	0.854	0.664	0.044	0.570
	Level 5	0.430	0.290	0.645	0.177	0.268	0.269	0.291	0.329	0.221	0.145	0.172	0.053	0.032	0.145	0.078	0.048	0.005	0.032	0.038	0.015	0.018	0.012	0.007	0.047	0.003	0.006	0.025	0.017	0.915	0.220	0.048	0.201
Level 5	Recovery	0.000	0.000	0.002	0.002	0.007	0.000	0.000	0.004	0.000	0.000	0.000	0.000	0.000	0.000	0.002	0.000	0.000	0.000	0.000	0.000	0.000	0.000	0.000	0.000	0.000	0.000	0.000	0.000	0.000	0.019	0.000	0.000
Baseline	Recovery	0.233	0.500	0.510	0.632	0.742	0.821	0.722	0.989	0.076	0.030	0.045	0.101	0.277	0.166	0.382	0.009	0.017	0.124	0.005	0.006	0.006	0.054	0.104	0.024	0.162	0.019	0.024	0.191	0.489	0.316	0.176	0.714

Notes. Cell colours blue, green and red represents p-values < 0.05, < 0.01, and < 0.001, respectively.

Table B.14: Pairwise comparison of the interaction between measurement time and electrode locations on approximate entropy.

Measurement time		FP1	FP2	F3	Fz	F4	FC3	FCz	FC4	C5	C3	C1	Cz	C2	C4	C6	CP3	CPz	CP4	P3	P1	Pz	P2	P4	PO3	PO4	O1	Oz	O2	T7	T8	P7	P8
Baseline	Level 1	0.666	0.798	0.993	0.778	0.858	0.385	0.777	0.932	0.250	0.122	0.257	0.416	0.580	0.477	0.733	0.204	0.277	0.217	0.046	0.031	0.028	0.017	0.019	0.003	0.001	0.013	0.015	0.009	0.006	0.446	0.017	0.007
Level 1	Level 2	0.216	0.531	0.238	0.198	0.138	0.121	0.179	0.112	0.592	0.141	0.228	0.450	0.569	0.194	0.379	0.540	0.861	0.660	0.966	0.942	0.850	1.000	0.975	0.424	0.458	0.399	0.393	0.643	0.181	0.465	0.639	0.378
	Level 3	0.282	0.352	0.065	0.119	0.135	0.044	0.187	0.100	0.153	0.043	0.106	0.238	0.338	0.181	0.332	0.185	0.452	0.361	0.452	0.404	0.455	0.436	0.843	0.972	0.786	0.953	0.469	0.734	0.136	0.091	0.340	0.397
	Level 4	0.786	0.909	0.171	0.078	0.221	0.058	0.194	0.355	0.154	0.055	0.035	0.140	0.663	0.518	0.745	0.052	0.435	0.596	0.066	0.095	0.251	0.461	0.643	0.102	0.791	0.138	0.630	0.884	0.006	0.292	0.205	0.170
	Level 5	0.550	0.573	0.012	0.056	0.149	0.002	0.124	0.310	0.049	0.024	0.011	0.093	0.650	0.561	0.835	0.193	0.895	0.739	0.381	0.444	0.731	0.969	0.698	0.537	0.207	0.619	0.428	0.467	0.002	0.568	0.491	0.781
Level 5	Recovery	0.474	0.495	0.629	0.272	0.500	0.369	0.482	0.588	0.979	0.652	0.885	0.827	0.841	0.682	0.910	0.287	0.192	0.364	0.084	0.058	0.050	0.022	0.022	0.013	0.002	0.025	0.011	0.003	0.333	0.650	0.033	0.002
Baseline	Recovery	0.263	0.241	0.080	0.357	0.393	0.721	0.838	0.896	0.946	0.915	0.809	0.740	0.968	0.848	0.546	0.507	0.444	0.956	0.408	0.411	0.383	0.405	0.559	0.905	0.733	0.963	0.791	0.784	0.503	0.225	0.982	0.632

Notes. Cell colours blue, and green represents p-values < 0.05, and < 0.01, respectively.

Table B.15: Pairwise comparison of the interaction between measurement time and electrode locations on LLyapExp/α_{relative}.

Measurement time		FP1	FP2	F3	Fz	F4	FC3	FCz	FC4	C5	C3	C1	Cz	C2	C4	C6	CP3	CPz	CP4	P3	P1	Pz	P2	P4	PO3	PO4	O1	Oz	O2	T7	T8	P7	P8
Baseline	Level 1	0.003	0.001	0.001	0.002	0.002	0.000	0.002	0.001	0.000	0.000	0.000	0.000	0.000	0.000	0.000	0.000	0.000	0.000	0.000	0.000	0.000	0.000	0.000	0.000	0.001	0.004	0.000	0.002	0.027	0.000	0.000
Level 1	Level 2	0.998	0.346	0.645	0.864	0.866	0.281	0.707	0.919	0.262	0.240	0.278	0.154	0.113	0.394	0.472	0.136	0.051	0.062	0.058	0.040	0.035	0.047	0.032	0.022	0.004	0.017	0.045	0.014	0.141	0.191	0.026	0.072
	Level 3	0.323	0.420	0.364	0.338	0.836	0.179	0.378	0.641	0.366	0.190	0.242	0.232	0.168	0.560	0.275	0.100	0.054	0.106	0.021	0.035	0.042	0.048	0.027	0.027	0.021	0.003	0.027	0.022	0.179	0.537	0.003	0.575
	Level 4	0.626	0.416	0.412	0.219	0.370	0.295	0.106	0.250	0.254	0.142	0.245	0.095	0.045	0.152	0.107	0.124	0.046	0.024	0.035	0.023	0.030	0.021	0.018	0.041	0.010	0.178	0.168	0.070	0.977	0.698	0.095	0.286
	Level 5	0.348	0.321	0.399	0.071	0.118	0.236	0.100	0.143	0.153	0.060	0.113	0.015	0.012	0.061	0.034	0.015	0.001	0.012	0.011	0.004	0.003	0.004	0.003	0.014	0.002	0.002	0.008	0.004	0.941	0.204	0.042	0.065
Level 5	Recovery	0.000	0.000	0.001	0.001	0.003	0.000	0.000	0.002	0.000	0.000	0.000	0.000	0.000	0.000	0.001	0.000	0.000	0.000	0.000	0.000	0.000	0.000	0.000	0.000	0.000	0.001	0.001	0.002	0.000	0.008	0.000	0.000
Baseline	Recovery	0.176	0.151	0.613	0.210	0.429	0.185	0.052	0.288	0.016	0.020	0.027	0.021	0.072	0.057	0.095	0.013	0.007	0.074	0.010	0.006	0.004	0.069	0.084	0.014	0.051	0.020	0.002	0.288	0.182	0.142	0.143	0.121

Notes. Cell colours blue and green represents p-values < 0.05 and < 0.01, respectively.

B.2.15 The Topographical Distribution of the Significant Differences of EEG Features Between Level 1-2, Level 1-3, Level 1-4, Level 1-5, and Between Baseline-Recovery.

The topographical distribution of the significant differences of all EEG features before, during and after the visuomotor tracking task are shown in Figures B.13 to B.23, respectively.

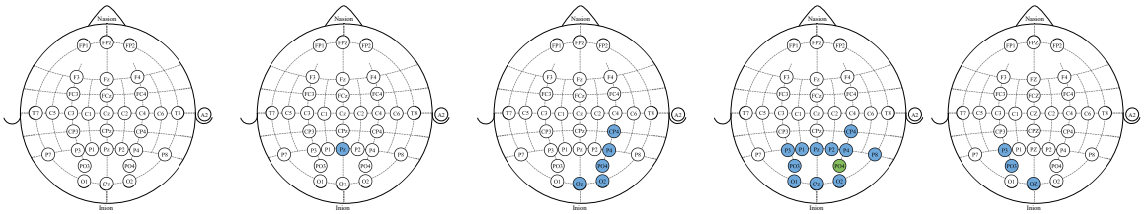

(a) Level 1-2 (b) Level 1-3 (c) Level 1-4 (d) Level 1-5 (e) Baseline-Recovery

Figure B.13: The topographical distribution of the significant differences in δ_{relative} between (a) level 1-2, (b) level 1-3, (c) level 1-4, (d) level 1-5, (e) baseline-recovery. Circle colours blue and green represents p-values < 0.05 and < 0.01, respectively.

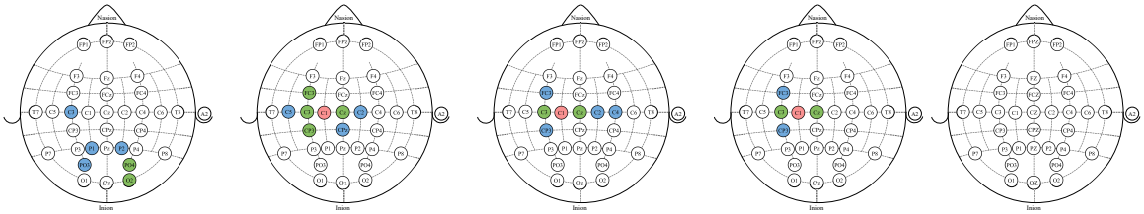

(a) Level 1-2 (b) Level 1-3 (c) Level 1-4 (d) Level 1-5 (e) Baseline-Recovery

Figure B.14: The topographical distribution of the significant differences in θ_{relative} between (a) level 1-2, (b) level 1-3, (c) level 1-4, (d) level 1-5, (e) baseline-recovery. Circle colours blue, green and red represents p-values < 0.05, < 0.01, and < 0.001, respectively.

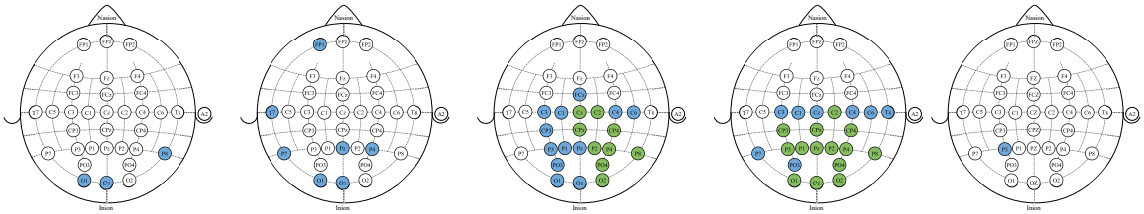

(a) Level 1-2 (b) Level 1-3 (c) Level 1-4 (d) Level 1-5 (e) Baseline-Recovery

Figure B.15: The topographical distribution of the significant differences in α_{relative} between (a) level 1-2, (b) level 1-3, (c) level 1-4, (d) level 1-5, (e) baseline-recovery. Circle colours blue and green represents p-values < 0.05 and < 0.01, respectively.

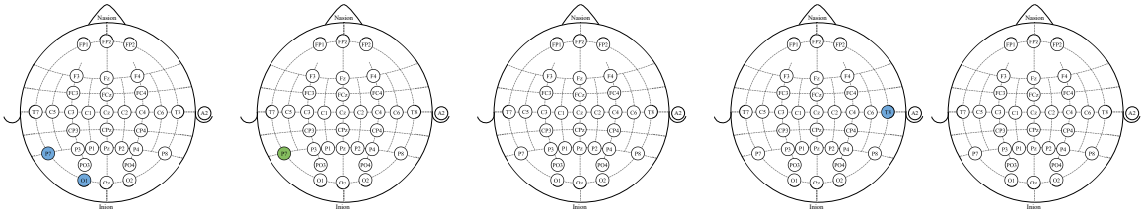

(a) Level 1-2 (b) Level 1-3 (c) Level 1-4 (d) Level 1-5 (e) Baseline-Recovery

Figure B.16: The topographical distribution of the significant differences in β_{relative} between (a) level 1-2, (b) level 1-3, (c) level 1-4, (d) level 1-5, (e) baseline-recovery. Circle colours blue and green represents p-values < 0.05 and < 0.01, respectively.

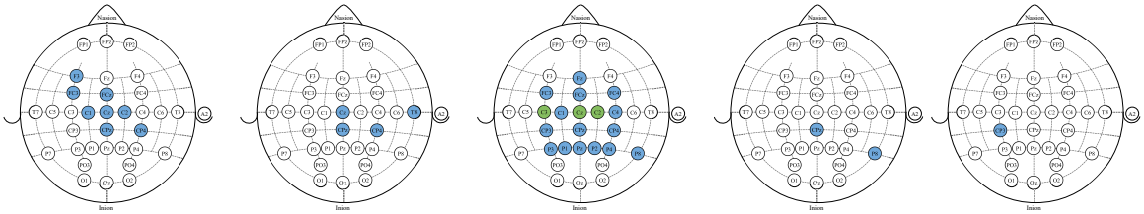

(a) Level 1-2 (b) Level 1-3 (c) Level 1-4 (d) Level 1-5 (e) Baseline-Recovery

Figure B.17: The topographical distribution of the significant differences in α/β between (a) level 1-2, (b) level 1-3, (c) level 1-4, (d) level 1-5, (e) baseline-recovery. Circle colours blue and green represents p-values < 0.05 and < 0.01, respectively.

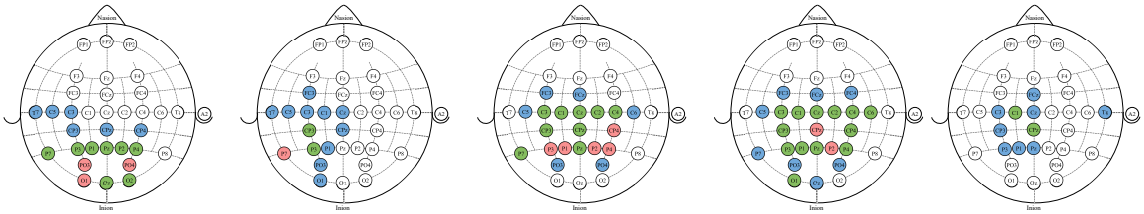

(a) Level 1-2 (b) Level 1-3 (c) Level 1-4 (d) Level 1-5 (e) Baseline-Recovery

Figure B.18: The topographical distribution of the significant differences in $(\theta+\alpha)/(\alpha+\beta)$ between (a) level 1-2, (b) level 1-3, (c) level 1-4, (d) level 1-5, (e) baseline-recovery. Circle colours blue, green and red represents p-values < 0.05, < 0.01, and < 0.001, respectively.

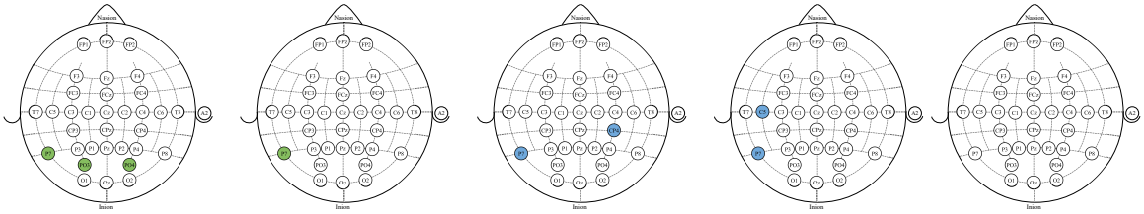

(a) Level 1-2 (b) Level 1-3 (c) Level 1-4 (d) Level 1-5 (e) Baseline-Recovery

Figure B.19: The topographical distribution of the significant differences in θ/β between (a) level 1-2, (b) level 1-3, (c) level 1-4, (d) level 1-5, (e) baseline-recovery. Circle colours blue and green represents p-values < 0.05 and < 0.01, respectively.

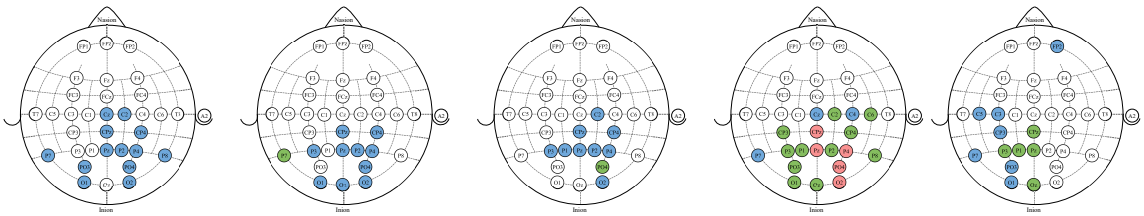

(a) Level 1-2 (b) Level 1-3 (c) Level 1-4 (d) Level 1-5 (e) Baseline-Recovery

Figure B.20: The topographical distribution of the significant differences in δ/α between (a) level 1-2, (b) level 1-3, (c) level 1-4, (d) level 1-5, (e) baseline-recovery. Circle colours blue, green and red represents p-values < 0.05, < 0.01, and < 0.001, respectively.

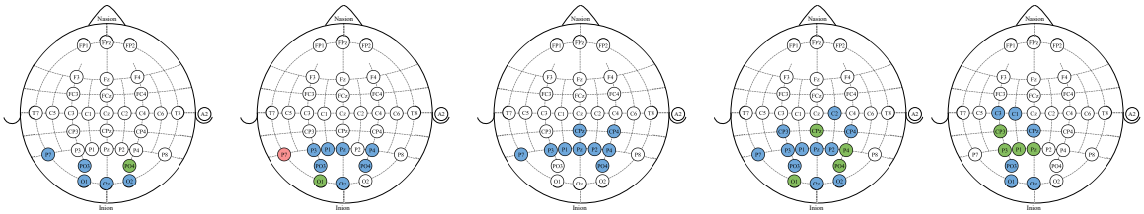

(a) Level 1-2 (b) Level 1-3 (c) Level 1-4 (d) Level 1-5 (e) Baseline-Recovery

Figure B.21: The topographical distribution of the significant differences in largest Lyapunov exponent between (a) level 1-2, (b) level 1-3, (c) level 1-4, (d) level 1-5, (e) baseline-recovery. Circle colours blue, green and red represents p-values < 0.05, < 0.01, and < 0.001, respectively.

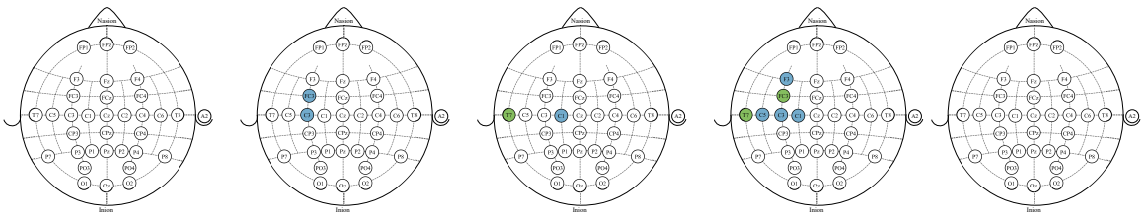

(a) Level 1-2 (b) Level 1-3 (c) Level 1-4 (d) Level 1-5 (e) Baseline-Recovery

Figure B.22: The topographical distribution of the significant differences in approximate entropy between (a) level 1-2, (b) level 1-3, (c) level 1-4, (d) level 1-5, (e) baseline-recovery. Circle colours blue and green represents p-values < 0.05 and < 0.01, respectively.

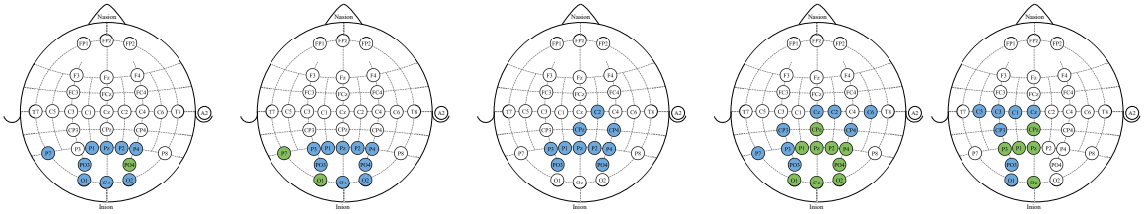

(a) Level 1-2 (b) Level 1-3 (c) Level 1-4 (d) Level 1-5 (e) Baseline-Recovery

Figure B.23: The topographical distribution of the significant differences in LLyapExp/α_{relative} between (a) level 1-2, (b) level 1-3, (c) level 1-4, (d) level 1-5, (e) baseline-recovery. Circle colours blue and green represents p-values < 0.05 and < 0.01, respectively.

Appendix C

Questionnaires Used in the Experiments

C.1 Experiment 1

The two questionnaires given before and after the robot-mediated interactions in experiment 1 are shown in this section. The questionnaire given before the robotic interactions (Questionnaire 1) gathered information about the participant's demographics and a subjective measure of their physical and mental fatigue level before performing the assigned robot-mediated interaction. The questionnaire given after the interaction (Questionnaire 2) was used to obtain a subjective measure of the physical and mental fatigue levels following the robotic interaction, the subjective evaluation of physical and mental workload across the robotic interaction, and the session's comfortability.

Subject ID: xxxx Ethics protocol number: COM/PG/UH/00100 and aCOM/PG/UH/00100

Questionnaire 1

Thank you for deciding to participate in the study. Please place a 'X' mark in the corresponding box of your answer or write your answer in the provided space. The answers will be anonymous and will only be used for the experimental result analysis.

Section A: Personal Details

1. How old are you? : .....
2. Are you? : ☐ Male ☐ Female
3. Are you? : ☐ Left-handed ☐ Right-handed
4. What is your occupation? : .....

Section B: Medical History

5. Have you ever had a head/brain injury? : ☐ Yes ☐ No

   If yes, please provide a detailed description.

   .....

6. Have you ever had an injury to the right hand? : ☐ Yes ☐ No

   If yes, please provide a detailed description.

   .....

7. Are you wearing glasses or contacts now? : ☐ Yes ☐ No

   If yes, please provide a detailed description about your weakness.

   .....

8. Do you currently take any prescription medications? : ☐ Yes ☐ No

   If yes, did you take any medicine during the last 5 hours? : ☐ Yes ☐ No

Section C: Gaming History

9. Do you often play video games? : ☐ Yes ☐ No

   If yes,

   i. How many hours, on the average, do you play during a day? : .....

   ii. How many days, on the average, do you play during a week? : .....

10. Have you ever played any games with external robotic interfaces before? : ☐ Yes ☐ No

Subject ID: xxxx Ethics protocol number: COM/PG/UH/00100 and aCOM/PG/UH/00100

Section D: Other Details

11. How many hours, on the average, did you sleep last night?

☐ Less than 3 ☐ 4 ☐ 5 ☐ 6 ☐ 7 ☐ 8 ☐ 9 ☐ more than 9

12. How long ago did you last drink a caffeinated beverage (tea, coffee, energy drinks etc.)?

☐ Within the last 30 minutes
☐ Between 30 minutes and 1 hour ago
☐ Between 1 hour and 3 hours ago
☐ Between 3 hours and 5 hours ago
☐ More than 5 hours ago

13. How many drinks of alcohol, on the average, did you take during the last 24 hours?

☐ 0 ☐ 1-2 ☐ 3-4 ☐ 5-6 ☐ 7-9 ☐ more than 9

14. Do you currently use any tobacco or nicotine products (for example cigarettes, pipe tobacco, snuff, chewing tobacco etc.) : ☐ Yes ☐ No

If yes,

i. How often, on the average, do you take these products?

☐ Every day
☐ At least once or twice a week, but not all the days
☐ At least few days a month

ii. How long is it since you last used any of these products?

☐ Within the last 30 minutes
☐ Between 30 minutes and 1 hour ago
☐ Between 1 hour and 3 hours ago
☐ Between 3 hours and 5 hours ago
☐ More than 5 hours ago

Section E: Current Physical and Mental States

15. We would like to know how you feel right now. Please circle a number which closely indicates how you are feeling right now.

i. How would you rate your current physical fatigue level?

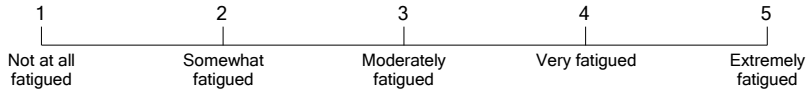

ii. How would you rate your current mental fatigue level?

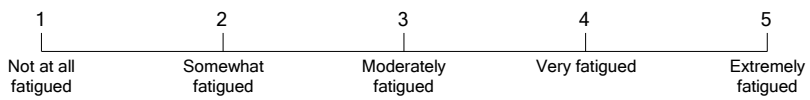

Subject ID: xxxx Ethics protocol number: COM/PG/UH/00100 and aCOM/PG/UH/00100

Questionnaire 2

Thank you for completing the study. We would like to know your views about this study and how you feel after completing the task. The answers will be anonymous and will only be used to compare the experimental results.

Please circle the number that most closely indicates your response

16. How physically demanding was the task?

1	2	3	4	5
Not at all demanding	Somewhat demanding	Moderately demanding	Very demanding	Extremely demanding

17. How would you rate your current physical fatigue level?

1	2	3	4	5
Not at all fatigued	Somewhat fatigued	Moderately fatigued	Very fatigued	Extremely fatigued

18. How mentally demanding was the task?

1	2	3	4	5
Not at all demanding	Somewhat demanding	Moderately demanding	Very demanding	Extremely demanding

19. How would you rate your current physical fatigue level?

1	2	3	4	5
Not at all fatigued	Somewhat fatigued	Moderately fatigued	Very fatigued	Extremely fatigued

20. How would you rate your current eye strain level?

1	2	3	4	5
Not at all strained	Somewhat strained	Moderately strained	Very strained	Extremely strained

21. How comfortable were you with wearing the EEG headset?

1	2	3	4	5
Not at all comfortable	Somewhat comfortable	Moderately comfortable	Very comfortable	Extremely comfortable

22. How would you think that wearing the EEG headset affected your fatigue state?

1	2	3	4	5
Not at all	Slightly	Moderately	Largely	Extremely

23. How would you think that using the robotic interface affected your fatigue state?

1	2	3	4	5
Not at all	Slightly	Moderately	Largely	Extremely

C.2 Experiment 2

The two questionnaires given before and after the robot-mediated interactions in experiment 2 are shown in this section. The questionnaire given before the robotic interactions (Questionnaire 1) gathered information about the participant's demographics and a subjective measure of their physical and mental fatigue level before performing the robot-mediated visuomotor tracking task. The questionnaire given after the task (Questionnaire 2) was used to obtain a subjective measure of the physical and mental fatigue levels following the robot-mediated visuomotor tracking task and feedback on the underlying comfortability of the experiment.

Subject ID: C..... *UH Ethics Protocol No: COM/PGR/UH/02973*

Questionnaire 1

Thank you for deciding to take part in the research study, GENTLE/EEG rehabilitation system: EEG based fatigue estimation of arm reaching and returning exercise.

We would like to know about you. Please answer ALL the questions.

Section A: Personal Details

1. **How old are you?** _____
2. **What is your gender?** ☐ Male ☐ Female
3. **What is your handedness type?**
   ☐ Right-handedness ☐ Left-handedness ☐ Mixed-handedness ☐ Ambidexterity
4. **What is your occupation?** _____

Section B: Medical History

5. **Have you had any injuries to the right hand previously that caused arm functional difficulties (for example dislocated shoulders)?** ☐ Yes ☐ No
6. **Have you had any brain or head injury previously?** ☐ Yes ☐ No
7. **Do you suffer from epilepsy?** ☐ Yes ☐ No
8. **Are you currently taking any medication (prescription/non-prescription)?** ☐ Yes ☐ No

   If yes, did you take any medicine during the last 5 hours? ☐ Yes ☐ No
9. **Are you wearing glasses or contact lenses now?** ☐ Yes ☐ No
   If you are wearing contact lenses, please remove them before the experiment as was mentioned in the participant information sheet and replace them with glasses if required.

Section C: General Information

10. **On average, how many hours did you sleep last night?**
    ☐ Less than 3 ☐ 4 ☐ 5 ☐ 6 ☐ 7 ☐ 8 ☐ More than 9
11. **How long ago did you have your last caffeinated beverage (tea, coffee, energy drinks etc.)?**
    ☐ Within the last 1 hour ☐ Between 1 hour and 2 hours ago
    ☐ Between 2 hours and 4 hours ago ☐ More than 4 hours ago
12. **On average, how many drinks of alcohol have you taken during the last 24 hours?**
    ☐ 0 ☐ 1-2 ☐ 3-4 ☐ 5-6 ☐ 7-8 ☐ More than 9

13. Do you currently use any tobacco or nicotine products (for example cigarettes, pipe tobacco, snuff, chewing tobacco etc.)? ☐ Yes ☐ No

If yes,

a. On average, how often do you take these products?
- ☐ Every day
- ☐ At least once or twice a week, but not all the days
- ☐ At least few days a month

b. How long since you last used any of these products?
- ☐ Within the last 1 hour
- ☐ Between 1 hour and 2 hours ago
- ☐ Between 2 hours and 4 hours ago
- ☐ More than 4 hours ago

14. Have you interacted with the HapticMaster robot before? ☐ Yes ☐ No

15. Have you previously participated in a EEG data acquisition session? ☐ Yes ☐ No

Section D: Fatigue Level Before the Robotic Interaction

We would like to know how you feel right now.

On a scale of 1 to 7, with 1 being not at all and 7 being extremely, please cross the number that best describes your current mental and physical states.

	Not at all						Extremely
16. Physically, do you feel exhausted?	①	②	③	④	⑤	⑥	⑦
17. Do you feel sleepy or drowsy?	①	②	③	④	⑤	⑥	⑦
18. Mentally, do you feel exhausted?	①	②	③	④	⑤	⑥	⑦
19. Do you feel less strength in your muscles?	①	②	③	④	⑤	⑥	⑦
20. Do you have difficulties in concentrating?	①	②	③	④	⑤	⑥	⑦
21. Do you need to rest?	①	②	③	④	⑤	⑥	⑦
22. Are you motivated?	①	②	③	④	⑤	⑥	⑦
23. Do you feel tired?	①	②	③	④	⑤	⑥	⑦
24. How alert do you feel?	①	②	③	④	⑤	⑥	⑦

Subject ID: C..... *UH Ethics Protocol No: COM/PGR/UH/02973*

Questionnaire 2

Section E: Fatigue Level After the Robotic Interaction

We would like to know how you feel after interacting with the GENTLE/EEG rehabilitation system.

On a scale of 1 to 7, with 1 being not at all and 7 being extremely, please cross the number that best describes your current mental and physical states.

	Not at all						Extremely
25. Physically, do you feel exhausted?	(1)	(2)	(3)	(4)	(5)	(6)	(7)
26. Do you feel sleepy or drowsy?	(1)	(2)	(3)	(4)	(5)	(6)	(7)
27. Mentally, do you feel exhausted?	(1)	(2)	(3)	(4)	(5)	(6)	(7)
28. Do you feel less strength in your muscles?	(1)	(2)	(3)	(4)	(5)	(6)	(7)
29. Do you have difficulties in concentrating?	(1)	(2)	(3)	(4)	(5)	(6)	(7)
30. Do you need to rest?	(1)	(2)	(3)	(4)	(5)	(6)	(7)
31. Are you motivated?	(1)	(2)	(3)	(4)	(5)	(6)	(7)
32. Do you feel tired?	(1)	(2)	(3)	(4)	(5)	(6)	(7)
33. How alert do you feel?	(1)	(2)	(3)	(4)	(5)	(6)	(7)

Section F: General Information About the Study

On a scale of 1 to 7, with 1 being not at all and 7 being extremely, please cross the number which you feel best fits the following statements.

	Not at all						Extremely
34. Performing the task was physically exhausting.	(1)	(2)	(3)	(4)	(5)	(6)	(7)
35. Performing the task was mentally exhausting.	(1)	(2)	(3)	(4)	(5)	(6)	(7)
36. It was difficult to move the robot arm in early stages of the interaction.	(1)	(2)	(3)	(4)	(5)	(6)	(7)
37. It was difficult to move the robot arm in latter stages of the interaction.	(1)	(2)	(3)	(4)	(5)	(6)	(7)
38. Eye strain was experienced during the task.	(1)	(2)	(3)	(4)	(5)	(6)	(7)

Appendix D

Ethics Approval Notifications

University of Hertfordshire UH

UNIVERSITY OF HERTFORDSHIRE
SCIENCE & TECHNOLOGY

ETHICS APPROVAL NOTIFICATION

TO Udeshika Dissanayake

CC Dr Farshid Amirabdollahian

FROM Dr Simon Trainis, Science and Technology ECDA Chairman

DATE 20/07/2015

Protocol number: COM/PG/UH/00100

Title of study: Estimation of fatigue induced by robot-mediated interactions using quantitative EEG

Your application for ethics approval has been accepted and approved by the ECDA for your school.

This approval is valid:

From: 20/07/2015

To: 20/12/2015

Please note:

Approval applies specifically to the research study/methodology and timings as detailed in your Form EC1. Should you amend any aspect of your research, or wish to apply for an extension to your study, you will need your supervisor's approval and must complete and submit form EC2. In cases where the amendments to the original study are deemed to be substantial, a new Form EC1 may need to be completed prior to the study being undertaken.

Should adverse circumstances arise during this study such as physical reaction/harm, mental/emotional harm, intrusion of privacy or breach of confidentiality this must be reported to the approving Committee immediately. Failure to report adverse circumstance/s would be considered misconduct.

Ensure you quote the UH protocol number and the name of the approving Committee on all paperwork, including recruitment advertisements/online requests, for this study.

Students must include this Approval Notification with their submission.

University of Hertfordshire UH

UNIVERSITY OF HERTFORDSHIRE
HEALTH AND HUMAN SCIENCES

ETHICS APPROVAL NOTIFICATION

TO Udeshika Dissanayake

CC Dr Farshid Amirabdollahian

FROM Dr Simon Trainis, Science and Technology ECDA Chairman

DATE 06/08/15

Protocol number: **aCOM/PG/UH/00100**

Title of study: Estimation of fatigue induced by robot-mediated interactions using quantitative EEG

Your application to modify the existing protocol **COM/PG/UH/00100** as detailed below has been accepted and approved by the ECDA for your school.

Modification: Correcting a typo error in Questionnaire 2

This approval is valid:

From: 06/08/15

To: 20/12/15

Please note:

Any conditions relating to the original protocol approval remain and must be complied with.

Approval applies specifically to the research study/methodology and timings as detailed in your Form EC1 or as detailed in the EC2 request. Should you amend any further aspect of your research, or wish to apply for an extension to your study, you will need your supervisor's approval and must complete and submit a further EC2 request. In cases where the amendments to the original study are deemed to be substantial, a new Form EC1 may need to be completed prior to the study being undertaken.

Should adverse circumstances arise during this study such as physical reaction/harm, mental/emotional harm, intrusion of privacy or breach of confidentiality this must be reported to the approving Committee immediately. Failure to report adverse circumstance/s would be considered misconduct.

Ensure you quote the UH protocol number and the name of the approving Committee on all paperwork, including recruitment advertisements/online requests, for this study.

Students must include this Approval Notification with their submission.

University of Hertfordshire UH

SOCIAL SCIENCES, ARTS AND HUMANITIES ECDA

ETHICS APPROVAL NOTIFICATION

TO Udeshika Dissanayake

CC Dr Farshid Amirabdollahian

FROM Dr Simon Trainis, Health, Science, Engineering & Technology ECDA Chairman

DATE 17/10/17

Protocol number: COM/PGR/UH/02973

Title of study: GENTLE/EEG rehabilitation system: EEG based fatigue estimation of arm reaching and returning exercise

Your application for ethics approval has been accepted and approved by the ECDA for your School and includes work undertaken for this study by the named additional workers below:

This approval is valid:

From: 17/10/17

To: 27/01/18

Additional workers: no additional workers named

Please note:

If your research involves invasive procedures you are required to complete and submit an EC7 Protocol Monitoring Form, and your completed consent paperwork to this ECDA once your study is complete. You are also required to complete and submit an EC7 Protocol Monitoring Form if you are a member of staff.

Approval applies specifically to the research study/methodology and timings as detailed in your Form EC1A. Should you amend any aspect of your research, or wish to apply for an extension to your study, you will need your supervisor's approval (if you are a student) and must complete and submit form EC2. In cases where the amendments to the original study are deemed to be substantial, a new Form EC1A may need to be completed prior to the study being undertaken.

Should adverse circumstances arise during this study such as physical reaction/harm, mental/emotional harm, intrusion of privacy or breach of confidentiality this must be reported to the approving Committee immediately. Failure to report adverse circumstance/s would be considered misconduct.

Ensure you quote the UH protocol number and the name of the approving Committee on all paperwork, including recruitment advertisements/online requests, for this study.

Students must include this Approval Notification with their submission.